INVESTIGATION OF OXYRESVERATROL CYTOTOXICITY

SARAYUT RADAPONG

A Thesis submitted in partial fulfilment of the requirements of the Liverpool John Moores University for the degree of

Doctor of Philosophy

February 2021

ACKNOWLEDGEMENTS

ABSTRACT

Oxyresveratrol (OXY) belongs to the group of phytochemicals known as hydroxystilbenoids, and has a molecular structure similar to the well-known phytochemical resveratrol. It is found to be particularly concentrated in the heartwood of *Artocarpus lakoocha* Wall. ex Roxb. (Family: Moraceae), an indigenous plant in Thailand. This species has been used as a Thai traditional medicine for the treatment of various parasitic diseases. Previous studies have also reported that it may exhibit pro-oxidative properties, which associated with the amount of the main compound in the extracts. OXY may share biological activities with resveratrol and be developed as an anticancer agent. This thesis aimed to investigate the cytotoxicity of OXY, consequently. The heartwood was ground, dried and extracted. The chromatographic and spectroscopic analyses were carried out and OXY was identified as the major component in the extracts (33.55%, 37.81% and 64.23 % w/w in water, ethanol and ethyl acetate, respectively). Resveratrol was quantified as a minor compound, (0.37%, 0.45% and 0.65% w/w in water, ethanol and ethyl acetate extracts, respectively). The pro-oxidant activity was investigated using DNA–nick, reactive oxygen species (ROS), copper reducing and glutathione depletion assays. The results showed that OXY induced DNA damage dose-dependently in the presence of copper (II) ions. It was also found to generate ROS in a dose-dependent manner, reduce copper (II) to copper (I) and depleting glutathione. OXY was able to show higher capability than resveratrol at the same doses, while the *trans–* stilbene did not show the activities. The three *A. lakoocha* extracts also showed damaged DNA consistent with the amount of OXY presented. The cytotoxicity of OXY to different kinds of cancer cell lines including Human Caucasian lung carcinoma cells (A549), human colorectal cancer cells (CACO–2), Human Caucasian hepatocyte carcinoma cells (HepG2), Human breast cancer cells (MCF7), Caucasian prostate adenocarcinoma cells

(PC–3), Mouse macrophage cells (RAW 264.7) and the two non-transformed cell lines including Human foetal lung cells (MRC–5) and normal human breast cells (MCF10A), was investigated using MTT (3-(4,5-dimethylthiazol-2-yl)-2,5-diphenyltetrazolium bromide). Cells were either pre-treated with 50µM $Cu(OAc)_2$ for 24 h, or OXY in the medium supplemented with 50µM $Cu(OAc)_2$ then exposed to OXY for 48 h compared to the control with no $Cu(OAc)_2$. More than 80% of the cells treated with OXY in the presence of copper showed less toxicity than the condition without copper. MCF7 cell was the most susceptible to the compound and therefore chosen to be a model studying molecular effects. The cells that OXY caused toxicity (IC_{50}) to were MCF7 (30.64±4.79 µM), HepG2 (104.47±0.82 µM), PC–3 (106.90±8.63 µM), RAW 264.7 (115.95±11.28 µM) and A549 (148.63±4.48 µM). Whereas, the compound was not toxic to non-transformed cells (MRC–5 and MCF10A). Moreover, OXY and OXY–copper (II) did not increase intracellular ROS and damage the DNA in MCF7 at the concentration investigated. MCF7 was chosen to be a cell line model for gene expression investigation. The gene-level expression of more than 20,000 human well-annotated genes was determined using Clariom Affymetrix microarray under two different OXY treatments (50 µM and 100 µM) for 24 h. A total of 686 genes were found to have altered mRNA expression levels of two-fold or more in the 50 µM OXY-treated group (262 upregulated and 424 downregulated genes). Total 2,338 genes were differentially expressed in the 100 µM-treated group (907 upregulated and 1,431 downregulated genes). The relevant visualized global expression patterns of genes and pathways were generated; genes involved in cell cycle control, apoptosis and autophagy, as well as DNA repair, showed the greatest differences in expression relative to controls. Gene expression was validated by quantitative PCR and western blot protein analysis. OXY induced apoptosis in MCF7 and HepG2 cells. The cascade events were activated through extrinsic and intrinsic pathways through various genes including caspase 3. The final stage was activated

resulting in losing cell membrane integrity, losing mitochondrial membrane potential, chromatin condensation and eventually cell death. However, OXY did not cause TP53 activation, ROS generation and severe cellular DNA breakage. OXY also down-regulated genes controlling cell migration and metastasis, especially genes in the non–canonical pathway (SMAD–independent) such as PI3K/AKT, CXCR4 and its ligand (CXCL12) which may consequently affect cell growth, proliferation and cell survival. Interestingly, OXY inhibited the gene expression in the cancer DNA repair pathway; the most significantly affected were RAD51 ($P < 0.0001$) and genes in homologous recombination. These results indicated that OXY could overcome drug resistance, enhance the efficacy of chemotherapy drugs and could be developed as chemotherapy or chemosensitising agent.

TABLE OF CONTENTS

LIST OF FIGURES

LIST OF TABLES

LIST OF ABBREVIATIONS

μL	Microlitre
^{1}H–NMR	Proton nuclear magnetic resonance
AKT	v–akt murine thymoma viral oncogene homolog
AMPK	5' AMP-activated protein kinase
APAF	Apoptotic peptidase activating factor
Atg	Autophagy signal transduction
BAK	BCL2-antagonist/killer
BAX	BCL2 Associated X
BBC3	BCL2 binding component 3
BCL–2	B cell lymphoma–2
BRCA	Breast cancer gene
CASP	Caspase , apoptosis–related cysteine peptidase
CDK	Cyclin–dependent kinase
Ct	Cycle threshold
Cu(OAc)$_2$	Copper(II) acetate
CXCR4	Chemokine receptor type 4
DIABLO	Diablo, IAP–binding mitochondrial
DMEM	Dulbecco's modified eagle medium
DMSC	Department of Medical Sciences
DMSO	Dimethyl sulfoxide
DNA	Deoxyribonucleic acid
E2F	E2 promoter binding factor
EDTA	Ethylenediaminetetraacetic acid
EGF	Epidermal growth factor
ERK	Extracellular receptor kinase
ESR	Estrogen receptor
EtOAc	Ethyl acetate
FasL	Fas ligand
FasR	Fas receptor
FBS	Fetal bovine serum
g	Gram
GABARAPL2	Receptor–associated protein like 2

GADD45A	Growth arrest and DNA damage-inducible 45 alpha
GAPDH	Glyceraldehyde 3–phosphate dehydrogenase
GSH	Glutathione
h	Hour
H_2DCFDA	2',7'–dichlorodihydrofluorescein diacetate
HEPES	4–(2–hydroxyethyl)–1–piperazineethanesulfonic acid
HIV	Human immunodeficiency virus
HPLC	High–performance liquid chromatography
IC_{50}	Inhibitory concentration
j	Coupling constant
JNK	c-Jun N-terminal kinase
JUNB	JunB proto-oncogene
LC/MS	Liquid chromatography–mass spectrometry
M	Molar (concentration)
M.W.	Molecular weight
MAP1LC3B or LC3	Microtubule-associated proteins 1A/1B light chain 3B
MAP2K, MEK, MAPKK, p38	Mitogen-activated protein kinase
MeOH	Methanol
mg	Milligram
min	Minute
mL	Millilitre
MS	Mass spectroscopy
mTOR	Mammalian target of rapamycin
MTT	3–(4,5–Dimethylthiazol–2–yl)–2,5–Diphenyltetrazolium bromide
NF–κB	Nuclear factor kappa-light-chain-enhancer of activated B cells
NMR	Nuclear magnetic resonance spectroscopy
OD	Optical density
p15INK4B	Cyclin-dependent kinase inhibitor protein
p21 or Cip1or CDKN1A	Cyclin–dependent kinase inhibitor 1A
p27(kip1) or CDKN1B	Cyclin-dependent kinase inhibitor 1B
PARP	Poly(ADP–ribose) polymerase
PBS	Phosphate buffered saline

PI3K	Phosphoinositide–3–kinase
pRB	Retinoblastoma protein
qPCR	Quantitative polymerase chain reaction
RAD	RAD Recombinase
RFU	Reactive fluorescence units
RNA	Ribonucleic acid
ROS	Reactive oxygen species
RT	Retention time
Smad	Signal transducers for receptors of TGF–β
SQSTM1	Sequestosome 1
TGF–β	Transforming growth factor–beta
TMS	Tetramethylsilane
TNFR1	The tumour necrosis factor receptor 1
TNFRSF10B	Tumour necrosis factor receptor superfamily, member 10b
TNF–α	Tumour necrosis factor alpha
TP53	Tumour protein p53
TRAIL	TNF-related apoptosis-inducing ligand
UV	Ultraviolet
VEGF	Vascular endothelial growth factor
Wnt	Wingless-related integration site

CHAPTER 1 INTRODUCTION

1.1 Cancer and its hallmarks

Cancer is one of the leading causes of death globally; 9.6 million deaths are estimated to occur in 2018 and the new incident number is projected to increase from 18 million in 2018 to 29.5 million cases in 2040 (WHO, 2020). The most common types of cancer in men are lung and prostate cancers while in women are breast, colorectal and cervical cancers. The cancer burden continues to grow exerting physical, emotional and financial strain on individuals, communities and countries globally.

Cancer is a multi–step process in which cells proliferate in an excessive and uncontrolled manner. Cancer causes major alterations in genetics and epigenetics (Merlo *et al.*, 2006). The genetic change is the alteration that modifies the DNA sequence; several thousand of the genes (3,000–5,000) encode proteins involved in genetic programmes deregulated in cancer. The causes of DNA sequence's change are point mutations on a genome–wide basis, insertions and deletions, copy number changes and genomic rearrangements (Stratton *et al.*, 2009). These changes arise through the accumulation of modifications in the genetic programmes that control the molecular and cellular activities including cell proliferation, cellular defence mechanism, self–repair, cell differentiation, migration, relationships with neighbouring cells, and capacity to escape the immune system. This process results in the formation of a mass of deregulated cells, which can cause cells to become unstable and uncontrollable. For example, a mutation in a gene called Kirsten rat sarcoma viral oncogene homolog (KRAS), one of the oncogenes, can promote uncontrollable cell division and cell proliferation or the dysfunction of TP53, the cancer suppressor gene, which becomes unable to stop the proliferation of cells when needed. The other way is epigenetics, which changes the programme of cells such as modifying the conformation of chromatin or DNA strands, micro RNA, copying and repairing machinery (Figure 1).
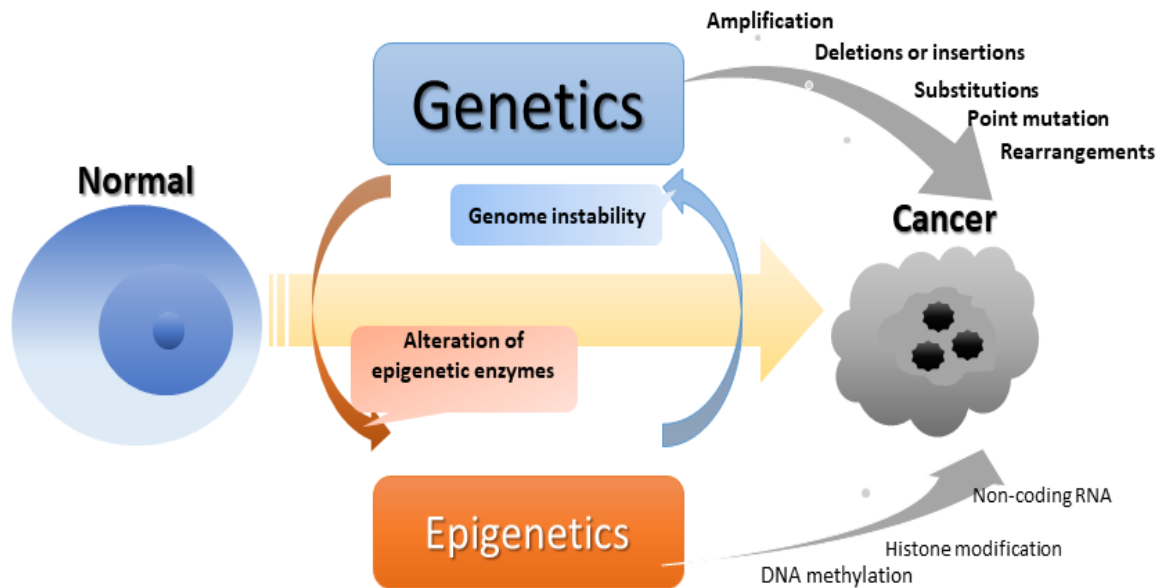
Figure 1 Genetics and epigenetics changes cause a normal cell to be a cancer cell because of genome instability and alteration of epigenetic enzymes (Chen *et al*., 2014).

The causes of genetic and epigenetic changes are numerous. The genome contains 3 billion base pairs and there may be affected and modified by reactions with a variety of chemical, physical and toxicological agents. For instance, some chemicals classified as carcinogens can cause changes in DNA bases, bind to them and modify the DNA sequence resulting in the mistranslation of the enzymes. UV light can form the pyrimidine dimer, called double mutations, which are the signature of mutagenesis by UV light of skin cancers. The ionising radiations also induce single or double DNA strand breaks. Each time there is a perfect proofreading and repair reading systems. However, the error may occur and remain unrepaired, leading to mutation and malignant tumour development (Chen *et al.*, 2014).

In general, cancer cells have defects in the regulation of cell proliferation and homeostasis. Cell genotypes manifest the essential alterations in cell physiology

collectively dictating malignant growth including evasion of programmed cell death (apoptosis), self–sufficiency in growth signals, insensitivity to growth–inhibitory (antigrowth), limitless replicative potential, sustainment of angiogenesis, and tissue invasion and metastasis (Figure 2).
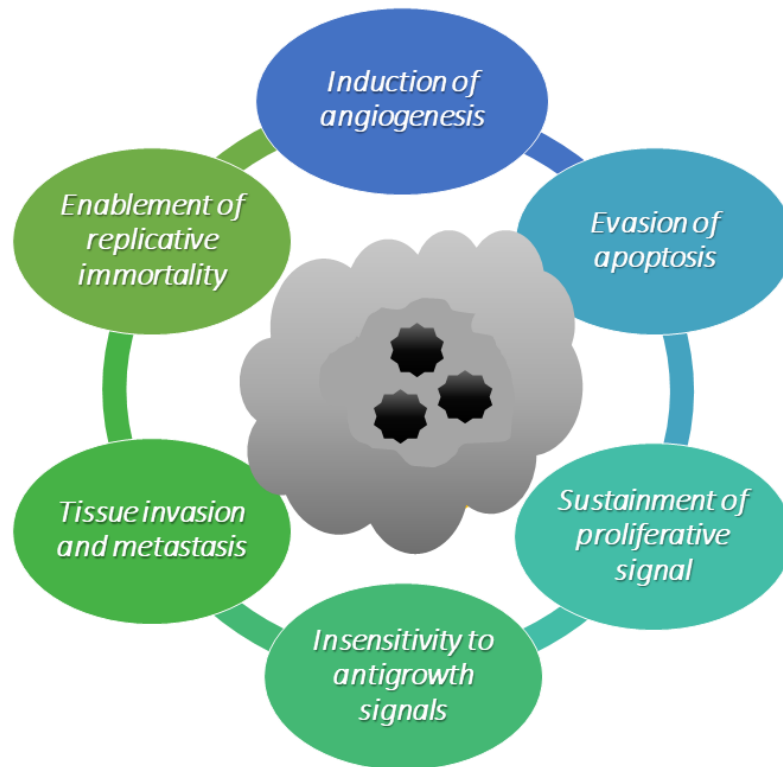
Figure 2 The hallmarks of cancer associated with the six major biological processes adapted from Hanahan and Weinberg (2000)

Evasion of apoptosis: The evasion of apoptosis is a key mechanism by which cancer develops oncogenes such as BCL–2 are anti–apoptotic activity e.g. BCL-2, BCL-XL, BCL-W, MCL-1, BFL-1/A1. The expression of BCL–2 promoted the survival of B–lymphoid tumours in mice and the co cooperation with c–myc promoted proliferation of B–cell precursors, some of which became tumourigenic (Suvarna *et al.*, 2019). One of the most common losses of pro–apoptotic activity involved the mutation of TP53 tumour suppressor gene resulting in resistance to apoptosis in more than 50% of human cancers.

The p53 protein has been known to be the DNA damage sensor that induces apoptotic cascade (Aubrey *et al.*, 2018).

Sustainment of proliferative signal: Normal cells maintain their cellular quiescence state and homeostasis by receiving growth inhibitors and immobilized inhibitors embedded in the extracellular matrix and on the surfaces of nearby cells. The extracellular signals couple with transmembrane receptors and then induce the cells from active proliferative cycle into G0 phase of the cell cycle. The other mechanism is that the cells are forced to stop proliferative potential by being induced to enter into post–mitotic states (Matson and Cook, 2017).

Retinoblastoma protein (pRb) is one of the enzymes playing the crucial role in anti–proliferative that can block and alter E2F transcription factor that controls the expression of many enzymes in the procession of G1 to S phase of the cell cycle (Farra *et al.*, 2019).

The transforming growth factor–beta family (TGF–β) is a multifunctional cytokine this protein can be competitive to pRb by preventing the phosphorylation and inactivating the enzyme. Therefore, the cells are blocked through G1 phase. Moreover, TGF–β also causes synthesis p15INK4B and p21 proteins, which blocks the reaction of cyclin: CDK and then sequentially effects to the pRb phosphorylation (Datto *et al.*, 1997; Principe *et al.*, 2017).

Insensitivity to antigrowth signals: Cancer cells deregulate the production and release of growth–promoting signals to control the progression of cell cycle and growth (Matson and Cook, 2017).

Tissue invasion and metastasis: Metastasis is the process of cancers travelling into the other sites and settles new colonies, which the cause of more than 90% human cancer deaths (Guan, 2015). Several classes of proteins are involved in this process. The main proteins affected are in the cell–cell adhesion molecules (CAMs) including the

immunoglobulin and calcium–dependent cadherin and integrin protein, which mediates the cell–to–cell interaction and link the cells to extracellular substrates (Basu *et al.*, 2018).

Enablement of replicative immortality: The immortal property of cancers means that they could overcome cell senescence to unlimited proliferation. Human cancer cells can counter the erosion or shortening of telomeres and losing telomere–binding proteins by expressing the significantly vast majority (∼90%) of telomerase enzyme compared to normal cells. Mice that lack telomerase activity and are more resistant to cancer (Shay and Wright, 2000; Blasco, 2005).

Induction of angiogenesis: Tumour–associated neovasculature is a process to sustain nutrient and oxygen for neoplastic growths. The molecular mechanism of angiogenesis is controlled by the inducer or inhibitor, which are vascular endothelial growth factor–A (VEGF–A) and thrombospondin–1 (TSP–1), respectively (Hanahan and Weinberg, 2011).

According to the knowledge of the cancer hallmarks, this brings about the subsequent evolution of cancer treatment; the therapy targeting actionable alterations oncogenes–driven cancers. Technology such as gene sequencing or human genome project acquire tumour molecular profiling and the discovery of predictive molecular targets (Zugazagoitia *et al.*, 2016).

Cancer treatment has become more effective. The combination of gene-targeted therapy with immune-targeted approaches to overcome the complexity of tumour biology has been developed such as checkpoint blockade, personalized vaccines and/or chimeric antigen receptor T-cells), hormonal therapy, chemotherapy and/or novel agents (Tsimberidou *et al.*, 2020). However, it found that cancer treatment practically based on the broad use of cytotoxic chemotherapies in patients reaching therapeutic a plateau,

worsen side effects and drug resistance. There are mainly five types of chemotherapeutics including alkylating agents, antimetabolites, anti–microtubule agents, topoisomerase inhibitors and cytotoxic antibiotics, of which the mechanism of actions interfere with DNA, RNA or proteins regarding blocking DNA synthesis and cell proliferation without specificity to cancer cells (Figure 3).
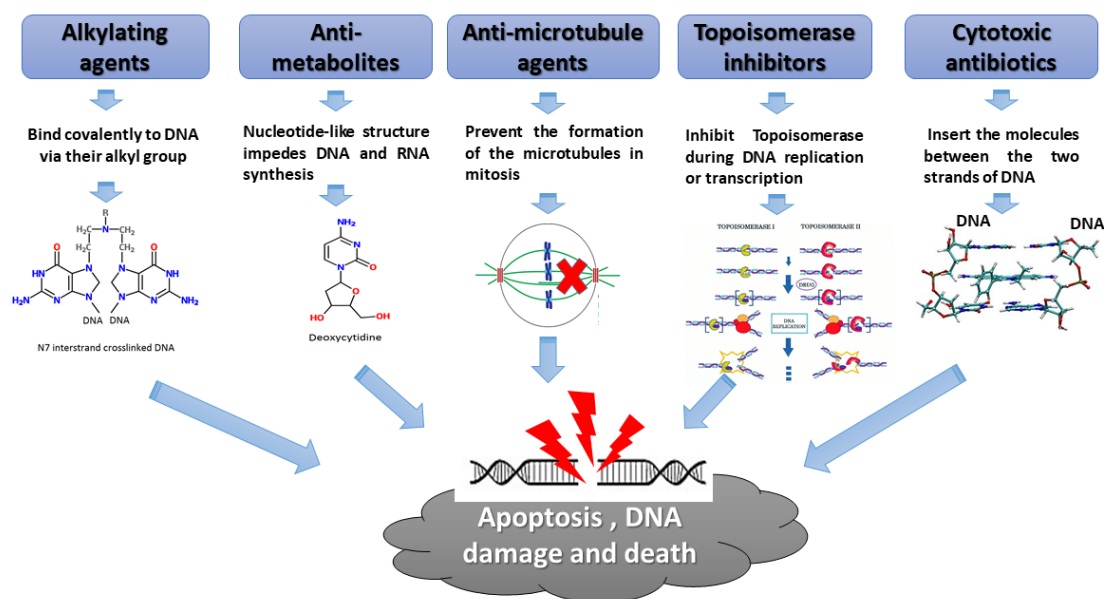
Figure 3 Chemotherapeutics and mechanisms of action; there are five types of chemotherapeutics including alkylating agents, anti-metabolites, anti-microtubule agents, topoisomerase inhibitors and cytotoxic antibiotics that cause DNA damage through apoptosis pathway (Huang *et al.*, 2017).

1.2 Cancer drugs from medicinal plants

Herbal medicines have been used mostly in developing countries as the primary sources of medical treatment for human diseases including cancer. They are considered effective, less toxic side effects and less cost consuming compared to current chemotherapy (Desai *et al.*, 2008). Currently, many studies and research report that the phytochemicals

presenting in plants such as polyphenols, flavonoids, protein and stilbenoids show beneficial health effects and may reduce cancer incidence (Greenwell and Rahman, 2015). The biological activities of encounter the hallmarks of cancer cells without or less toxic effect to normal cells via the various mechanism of actions including reduction of cell cycle progression, anti–proliferative effects, inhibition of tumour growth and progression, inhibition of cyclin–dependent kinases, immunomodulatory activity, anti–angiogenesis, migration, invasion and metastasis, inhibition of DNA repair and induction of apoptosis (Schnekenburger *et al.*, 2014).

Numerous phytochemicals, some already in clinical use and others in clinical trials as anticancer agents, encounter intracellular targets of cancer cells reported. For instance, vincristine is one of the first plant-derived anticancer drugs approved by The United States Food and Drug Administration (USFDA) in 1963. It is the alkaloid extracted from the leaves of *Catharanthus roseus* (L.) G.Don, which has been effectively used as chemotherapy for acute lymphoblastic leukemia, rhabdomyosarcoma, neuroblastoma, lymphomas and nephroblastoma. The mechanism of action involves the interaction with the spindle tubulins during mitosis, which leads to the dismissal of cell proliferation (Seca and Pinto, 2018). Paclitaxel is the blockbuster of the plant-derived anticancer agent, which has a tremendous impact on the pharmaceutical industry. This compound was isolated from the bark of *Taxus brevifolia* Nutt. (Pacific Yew) and then sold under the commercial name as Taxol® since 1993. The mechanism of action is tubulin-assembly promotion and inhibition of cell proliferation and DNA repair that showed great success in the treatment of breast, ovarian and lung cancers (Weaver, 2014; Bernabeu *et al.*, 2017). Because of the development for the last few decades, there has been generated several derivatives such as Lipusu®, Abraxane®, Taxotere® and Jevtana®, which increased its effectiveness and reduced side effects (Seca and Pinto, 2018). Another well–known antioxidant, resveratrol, mostly found in grapes and berries was intensively reported the

molecular mechanisms and pathways against cancer cells by inducing cell cycle arrest, autophagy, apoptosis, angiogenesis and invasion/metastasis mediated through PI3K/Akt/mTOR, Wnt, ROS, NF–κB, BAX/Bcl–2, AMPK, ERK, MAPK signalling pathways (Figure 4) (Kim and Kim, 2018). These phytochemicals have been studied both in preclinical and clinical trials. Therefore, further active experimental research on these molecules or chemical structure–related compounds can give us a deeper understanding of their mechanisms of action and therapeutic effects on cancer or other human diseases.
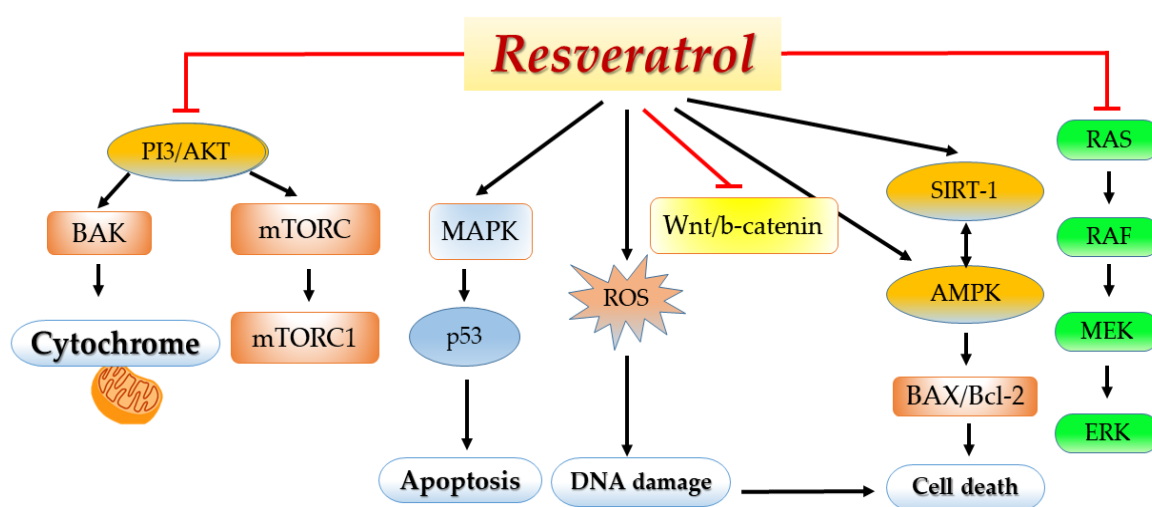
Figure 4 Effect of resveratrol on signalling pathways, Black arrows indicate activation cascade, while red lines indicate the inhibition cascade (Kim and Kim, 2018).

Apoptosis is the central mechanism of chemotherapeutics and of most of plant–derived anticancer drugs (Cragg and Pezzuto, 2016). Moreover, some polyphenolic compounds have been already investigated to have the DNA breakage activity in the presence of only themselves or oxidized metal ions. For example, Fe^{3+}, Cu^{2+}, Zn^{2+} or Ni^{2+} could trigger the Fenton–mediated ROS generation. The pro–oxidant property of phytochemicals was also considered one of the mechanisms against cancer cells (Yamada *et al.*, 1985; Lopes *et al.*, 1999; Subramanian *et al.*, 2004; Azmi *et al.*, 2005). Therefore, the DNA damaging

property of phytochemicals could be used for pre–screening the compounds anti–cancer activity (Figure 5).
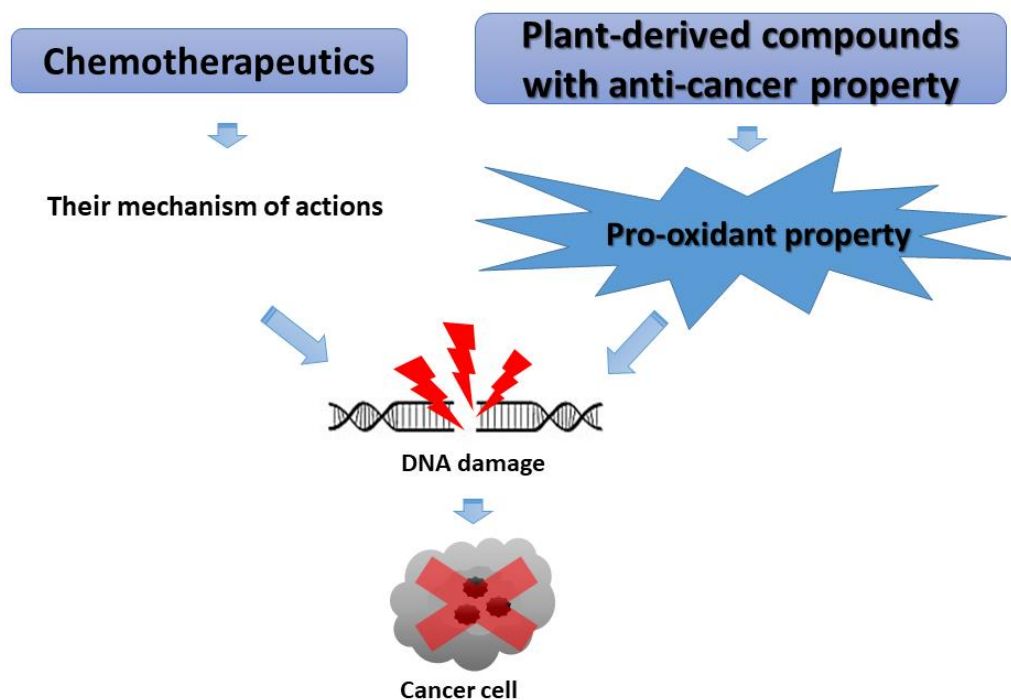
Figure 5 DNA damage causing cell death is the central mechanism of chemotherapeutics (Huang *et al*., 2017). Plant-derived compounds with the pro-oxidant property may consequently damage the DNA.

1.3 DNA damage caused by phytochemicals

Some phytochemicals have antioxidant property. However, they can behave like pro–oxidants in some conditions such as high concentration, the high partial pressure of dioxygen(pO_2) or with transition metals such as Cu^{2+}, Fe^{3+} or Cr^{3+} by generating ROS such as superoxide ($\cdot O_2^-$), hydroxyl ($\cdot OH$) or peroxyl ($ROO\cdot$) radicals (Valko *et al*., 2004). All ROS are likely to interact with the cellular components including DNA or RNA to produce the damaged bases or strand breaks (Cadet and Wagner, 2013). For

example, carotenoid presents itself as a pro–oxidant at a higher pO_2 condition. Carotenoid radical (Carotenoid•) reacts to oxygen generating carotenoid–peroxy radical (Carotenoid–OO˙), at this stage the radical acts as a pro–oxidant by promoting the oxidation of unsaturated lipid (RH). Finally, the lipid radical (R˙) reacts to O_2 and generates peroxy radicals (ROO˙); the reactions shown in *Scheme 1* (Valko *et al.*, 2004).

$$Carotenoid˙ + O_2 \rightarrow Carotenoid\ –OO˙$$

$$Carotenoid\ –OO• + RH \rightarrow Carotenoid\ –OOH + R˙$$

$$R˙ + O_2 \rightarrow ROO˙$$
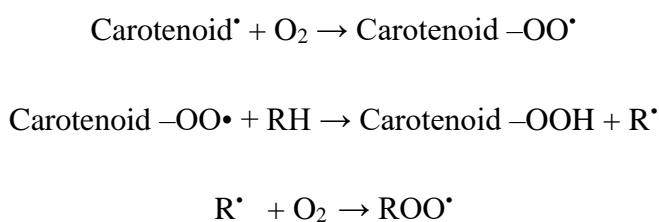
Scheme 1 The mechanism of ROS production by carotenoids

Ascorbic acid is a reducing agent that can also act as a pro–oxidant. Ascorbate in aqueous solution is oxidised by ferric (III) or cupric (II) into ascorbyl radicals. Then the reduced metals produce the hydroxyl radicals by using hydrogen peroxide through the Fenton reaction; the reactions shown in *Scheme 2* (Carr and Frei, 1999).

$$Ascorbate^- + Fe^{3+} \rightarrow Ascorbyl\ radical + Fe^{2+} + H^+$$

$$Ascorbate^- + Cu^{2+} \rightarrow Ascorbyl\ radical + Cu^{1+} + H^+$$

$$H_2O_2 + Fe^{2+} \rightarrow •OH + Fe^{3+} + {}^-OH$$

$$H_2O_2 + Cu^{1+} \rightarrow •OH + Cu^{2+} + {}^-OH$$
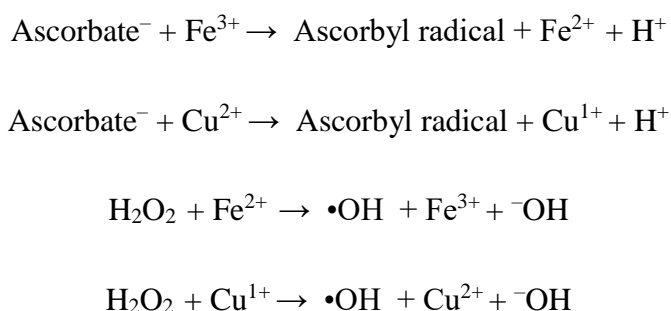
Scheme 2 The mechanism of ROS production by ascorbic acid

Another well–known phytochemical; resveratrol in the presence of transition metals can also generate ROS. Resveratrol reduces cupric (II) into cuprous (I), then the cuprous reacts with O_2 generating superoxide radical ($\cdot O_2^-$), the radical causes directly oxidative stress or reacts to hydrogen ions presenting hydrogen peroxide (H_2O_2). Lastly, the cupric ion and hydrogen peroxide in the reaction generate Cu^{1+}Oxo–species complex, which damages DNA; the reactions are shown in *Scheme 3* (Subramanian *et al.*, 2004).

$$Resveratrol + Cu^{2+} \rightarrow Cu^{1+} + Resveratrol^{\cdot+}$$

$$Cu^{1+} + O_2 \rightarrow Cu^{2+} + \cdot O_2^-$$

$$\cdot 2O_2^- + 4H^+ \rightarrow 2H_2O_2 + O_2$$

$$Cu^{1+} + 2H_2O_2 \rightarrow Cu^{1+} \; Oxo\text{–species}$$
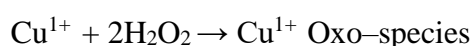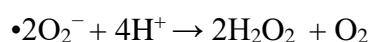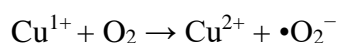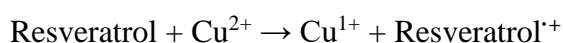
Scheme 3 The mechanism of ROS production by resveratrol

The scavenging of ROS in the presence of copper by hydroxystilbenoids, such as resveratrol, is thought to be an important mechanism of action against carcinogenesis (Alarcon de la lastra and Villegas, 2007; Galindo *et al.*, 2011).

1.4 Copper ions in cancer cells

Copper plays an important role in biological functions (Kalinowski *et al.*, 2016). However, the excess copper also is found to be a potent catalyst of ROS generation and DNA damage (Theophanides and Anastassopoulou, 2002). It has also been reported that significantly elevated levels of copper have been found in both serum and tissue of cancer

patients. The amount of copper in serum and tissues of cancer patients has been reviewed; the data shown were from the different age group of patients (10–50 years old), male and female and different geographical locations in a wide spectrum of tumours including acute lymphocytic leukaemia, breast cancer, colorectal cancer, lung cancer, ovarian cancer and prostate cancer (Gupte and Mumper, 2009). The copper level in serum in all kinds of the tumours was significantly higher than in normal patients. The highest elevated serum copper was found in acute lymphocytic leukaemia, roughly three times higher than the normal (around 100 µg/dL). Breast and colorectal cancer were raised to 173 and 165 µg/dL, respectively. While in lung, ovarian and prostate cancers were increased to lower than 150 µg/dL. In tissues, the amount of copper in all types of cancer collected was also higher than in normal tissues. In leukemic cells were also found to present around three times higher than the normal (15 µg/10^6 cells) (Carpentieri et al., 1986). In the solid tumours, breast cancer tissues gave the highest at 21 µg/g compared to the others, which were raised to lower than 5 µg/g. Indeed, the level of copper also was investigated in the different progression stages of tumours with later stages if tumour progression being associated with higher amounts of serum copper.

Interestingly, serum copper levels have also been observed to be linked to drug resistance in cancer (Majumder et al., 2009). Indeed, cancer patients that did not respond to drug treatment demonstrated 130–160% higher levels of copper in their serum than treatment responsive patients (Majumder et al., 2009). Moreover, ceruloplasmin (Cp), the major copper–carrying protein, was reported to elevate in lung, breast, colon and gastrointestinal cancer patients (Linder et al., 1981). In addition, copper has associated with numerous angiogenic factors such as basic fibroblast growth factor (bFGF), tumour necrosis factor–alpha (TNF–α), interleukin 1, IL–6, IL–8 and fibronectin (Carmeliet and Jain, 2000). This obvious evidence of raising copper levels in cancers triggers the cancer hallmarks to be targeted for anti–cancer phytochemicals.

1.5 *Artocarpus lakoocha*

A. lakoocha Wall. ex Roxb. (Family: Moraceae), an indigenous plant in Thailand known as Ma–Haad, is widely distributed in the southeast and south Asia. There are different common names such as Monkey Jack (English), Dahu or Lakoocha (Hindi). There are more than 50 plant species in this genus, which are evergreen and deciduous trees. Different parts of the tree such as leaves, bark, stem or fruits contain different kinds and proportions of main compounds, which have been shown to possess various biological activities such as antibacterial, antiviral, antimalarial, antifungal, antidiabetic, antioxidant and anticancer (Jagtap and Bapat, 2010).

Figure 6 Fruits and heartwood of *A. lakoocha* (Homhual, S., 2021)

A. lakoocha have been used in Thai traditional medicine, an aqueous extracted product of its heartwood called Puag–Haad, is used for antihelminthic treatment. It has been effectively used to treat Taeniasis and other human and cattle parasitic tapeworms and also blood and liver fluke infection (Preyavichyapugdee *et al.*, 2016). Moreover, it has been found to have strong tyrosinase inhibition activity over kojic acid and liquorice extract, and can be used as a potent skin whitening agent (Tengamnuay *et al.*, 2006). The water– extracted compound also shows antibacterial activity to *Enterococcus faecalis* (Singhatong *et al.*, 2010; Teanpaisan *et al.*, 2013). The tree bark containing high tannin is used to treat skin ailments. Recently, it has been reported to be a valuable resource of phenolic compounds including flavonoids, tannins and stilbenoids (Maneechai *et al.*, 2009; Singhatong *et al.*, 2010). More importantly, stilbenoids, especially OXY, seems to be the promising active compound in this natural resource.

1.6 OXY

OXY (OXY)($C_{14}H_{12}O_4$, M.W. 244.24 g/mol) is one of the small structure phytochemicals belonging to the group of the stilbenoids, which was richest in *A. lakoocha* heartwood. The amount of OXY (182,000 µg/g) and resveratrol (90,000 µg/g) were higher than resveratrol presenting in other plants such as grapes (0.5 µg/g), itadori (523 µg/g) or peanuts (5.1 µg/g) (Burns *et al.*, 2002; Maneechai *et al.*, 2009; Borah *et al.*, 2017). Recently, these compounds have been extensively studied for their efficacy. The chemical structure of OXY, resveratrol and *trans*–stilbene are shown in Figure 7.
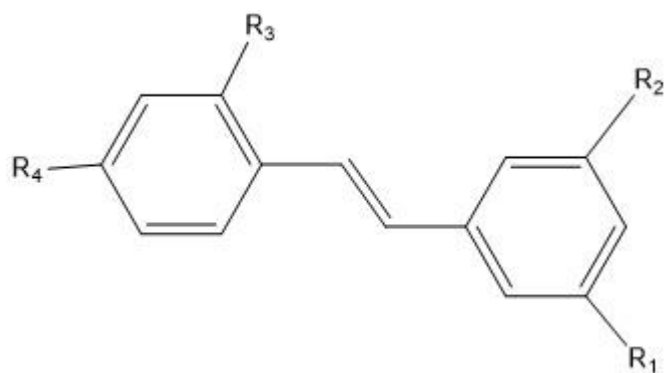
	R_1	R_2	R_3	R_4
OXY	OH	OH	OH	OH
Resveratrol	OH	OH	H	OH
Trans–stilbene	H	H	H	H

Figure 7 Chemical structure of OXY, resveratrol and *trans*–stilbene

OXY has been shown to possess various potent bioactivities with the main property being an antioxidant (Lorenz *et al.*, 2003). With other reported properties being anti–inflammatory (Lee *et al.*, 2015), anti–herpes, varicella–zoster virus, human immunodeficiency virus (HIV) and swine flu virus (Chuanasa *et al.*, 2008; Galindo *et al.*, 2011), anti–cancer (Rahman *et al.*, 2017), hepatoprotective (Choi *et al.*, 2016), neuroprotective and anti–stroke (Andrabi *et al.*, 2004; Weber *et al.*, 2012), DNA protective (Hu *et al.*, 2015), anti–diabetes (Tan *et al.*, 2015), antiglycation (Povichit *et al.*, 2010) and tyrosinase inhibition (Likhitwitayawuid *et al.*, 2006). In consideration of these traditional uses, this compound provides opportunities for the development of dietary supplements, functional foods and cosmetics or even pharmaceuticals.

However, concerns have been raised over the toxicity of the tree's crude extract and OXY. It has been previously reported these compounds might act as pro–oxidants causing lipid peroxidation to human blood at the concentration 50 and 100 µg/mL (Singhatong *et al.*, 2010). Moreover, it has been reported that the chemically related resveratrol and some hydroxystilbenes could cause DNA breakage in normal human lymphocyte cells in the presence of Cu^{2+} ion and oxygen (Subramanian *et al.*, 2004).

1.7 Molecular targets of OXY and *trans*– stilbenoids in cancer cells

Stilbenoids, such as resveratrol, pterostilbene and piceatannol, has been intensively studied for cytotoxicity against cancers and some molecular targets have been identified (Varoni *et al.*, 2016). These compounds share a common backbone structure but differ in the nature and position of substituents. Therefore, they may share biological activities including anticancer properties. At clinical trial resveratrol has been found to have several molecular targets, with its efficacy depending upon the type and stage of cancers, dosage levels and treatment periods. Moreover, there have been a number of investigations on stilbenoids focusing on their cellular mechanism of action (Berman *et al.*, 2017). In consideration of the cancer hallmarks mentioned previously. OXY has been shown to affect several hallmarks. In particular, it has been found to be a selective target multiple a cancer hallmark capabilities, some of them shown in Figure 8.
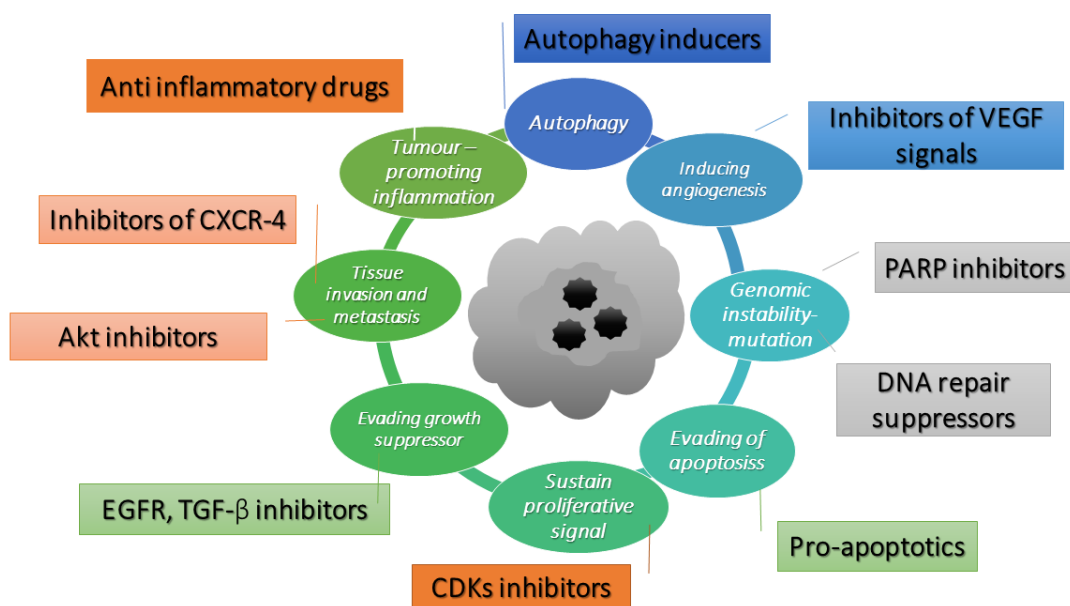
Figure 8 Potential molecular targets of anti-cancer compounds adapted from Hanahan and Weinberg (2000).

1.7.1 pro–apoptotic

Apoptosis is the mechanism of programmed cell death activated through two different intracellular signals; the intrinsic and extrinsic pathways, which referred to the mitochondrial and death receptor signalling, respectively. Cancer therapy targeting apoptosis is effective to all types of cancer because apoptosis evasion is one of the important hallmarks of cancer (Pfeffer and Singh, 2018).

OXY has been reported to induce the intrinsic pathway of apoptosis in neuroblastoma cells (Rahman *et al.*, 2017). Rahman *et al*. (2017) have provided the supporting evidence of the apoptotic cell morphology changes that the OXY–treated cells shrank and became rounded with membrane blebbing and apoptotic vacuoles. The molecular targets of this pathway included Bax and Bcl–2 proteins, which triggered the cascade proteins through

mitochondrial apoptosis, resulting in significant changes in the Bax/Bcl–2 ratio and the mitochondria membrane potential of neuroblastoma cells was greatly depolarized by OXY. Likewise, resveratrol has been intensively investigated for the property of apoptotic activation in several cancer cells. For instance, it also increased the expression of proapoptotic proteins such as Bax, Bcl–2 –antagonist/killer–1 (Bak), p53 upregulated modulator of apoptosis, the Bcl–2 Homology (BH)$_3$–containing proteins, TRAIL death receptors (Fulda and Debatin, 2005). Whereas anti–apoptotic proteins including Bcl–2, B-cell lymphoma-extra large (Bcl–XL), survivin, and X-linked inhibitor of apoptosis protein (XIAP) were downregulated (Shankar *et al.*, 2007). Other stilbenoids derivatives including deoxyrhaponticin, rhaponticin, pterostilbene, and piceatannol have also been confirmed to exhibit apoptosis induction in human acute promyelocytic leukaemia and acute lymphoblastic leukaemia cell lines (Czop *et al.*, 2019). Other phenolic compounds including stilbenoids also showed an anti–TRAIL expression property, which could be a promising approach to kill resistant cancer cells (Jacquemin *et al.*, 2010).

1.7.2 Anti–proliferative signalling

Several phytochemicals inhibit cancer cell proliferation by modulating the genes that control several aspects of the cell cycle. Cyclin–dependent kinases (CDKs) and E3 ubiquitin ligases mainly play a crucial role throughout the process (Duronio and Xiong, 2013).

OXY inhibited Human SH–SY5Y neuroblastoma cell growth dose–dependently and found to arrest G2/M phase. The molecular target was investigated to reduce cyclin D1, CDK3 and CDK4 expression (Rahman *et al.*, 2017).

Resveratrol also caused the growth inhibition of human epidermoid carcinoma (A431) cells via cell cycle arrest and apoptosis induction. Treatment with resveratrol (1–50 μM for 24 h) causes an induction of WAF1/p21 that inhibits cyclin D1/D2–CDK6, cyclin D1/D2– CDK4, and cyclin E–CDK2 complexes, thereby imposing an artificial checkpoint at the G1→S transition of the cell cycle (Ahmad *et al.*, 2001). More evidence of cell cycle arrest property was investigated via pRb–E2F/DP pathway; hyperphosphorylated was decreased with hypophosphorylated pRb was relatively increased and E2F protein expression was downregulated (Adhami *et al.*, 2001).

1.7.3 Growth suppression

Generally, epidermal growth factor (EGF) and related receptor (EGF–R) stimulate cell growth and differentiation while transforming growth factor–beta (TGF–β) functions as a potent cell proliferation inhibitor (Plaut, 1993). Resveratrol shows antigrowth signalling activity by inhibiting EGF and related receptor (EGF–R), a transmembrane tyrosine kinase activated by ligands and TGF–β. In breast cancer cells, TGF–β promotes the migration and invasion abilities of breast cancer cells, along with the increase in EGFR expression through Smad3 signalling pathway (Zhao *et al.*, 2018). Some studies illustrated that TGF–β, IGF1 and EGF signalling inhibitors could be the key mechanism of cancer therapeutics (Yingling *et al.*, 2004). Resveratrol also showed the growth inhibition in SKOV–3 and OVCAR–8 ovarian cancer cells by the cleaving PARP–1, reducing the phosphorylation of human epidermal growth factor receptor 2 (Her–2), EGFR and expressing extracellular signal–regulated kinases (Hogg *et al.*, 2015).

1.7.4 Anti–migration, anti–invasion and metastasis

OXY suppressed cell migration of Jurkat T cells in response to stromal cell-derived factor 1 (SDF–1). The mechanistic study indicated that OXY diminished CXCR4 –mediated T–cell migration via inhibition of the MEK/ERK signalling cascade (Chen *et al.*, 2013). Resveratrol showed anti–migration and invasion by down–regulating and inactivating Akt. Moreover, the compound also showed its efficacy in *in vivo* experiment by oral administration of 1 mg resveratrol in the malignant mouse model in three weeks. Interestingly, the tumour volume was inhibited more than 60% (p=0.001) compared to the control group. The study was concluded that resveratrol could reduce the malignant properties of highly invasive melanoma cells by inactivating Akt (Bhattacharya *et al.*, 2011). The other stilbene, Pterostilbene suppressed AKT/ERK–regulated assembly on suspended Lewis lung carcinoma cells and pulmonary metastasis. The compound also possessed potency in both preventing and treating metastasis of lung cancer cells in apoptosis–independent and apoptosis–dependent manners, respectively (Wang *et al.*, 2017).

1.7.6 Autophagy

Autophagy meaning, "self–eating", is an evolutionarily conserved catabolic pathway in eukaryotes and it plays a significant role in the recycling of cellular components as part of a housekeeping function. A compound–triggered cell via this pathway was described to be a promising, novel mechanism for enhancing anticancer treatments and overcoming current challenges such as chemotherapy resistance (Duffy *et al.*, 2015). During autophagy, some autophagy–related proteins were activated such as Beclin1, Atg5, Atg6, Atg12 and LC3 and played an essential role in mediating autophagosome initiation and expansion stages (Geng and Klionsky, 2008). OXY has been reported to exhibit

autophagy independently from apoptosis in neuroblastoma cells. The molecular targets were mostly via inhibition of PI3K/AKT/mTOR/pS6 signalling and activation of p38 MAPK pathway (Rahman *et al.*, 2017).

1.7.7 PARP and other DNA repair inhibitors

Poly (ADP–ribose) polymerases (PARPs) are enzymes involved in DNA–damage repair. Recently, inhibition of PARP is a promising strategy for targeting cancers with defective DNA–damage repair, including BRCA1 and BRCA2 mutation–associated breast and ovarian cancers (Livraghi and Garber, 2015). The original concept of the activity of PARP inhibitors was that they acted through synthetic lethality by targeting the base excision repair pathway (BER) in BRCA–deficient tumour. Therefore, disruption of the two pathways led to cell death (Iglehart and Silver, 2009). Resveratrol has been reported to show cleavage induction of PARP1 (Demoulin *et al.*, 2015). The compound also reduced the expression of genes in homologous recombination (HR) of the DNA damage repair pathway including RAD51 in MCF7 cells, which enhance the antiproliferative effect of cisplatin (Leon-Galicia *et al.*, 2018). RAD51 is an important part of the mechanism and has been observed that the gene was overexpressed in chemoresistant cancers (Slupianek *et al.*, 2001; Hannay *et al.*, 2007).

1.7.8 Inhibitors of VEGF signalling (angiogenesis)

The vascular endothelial growth factor (VEGF) and its receptor (VEGFR) have been shown to play major roles not only in physiological but also in most pathological angiogenesis such as cancers. The major VEGF–A ligand is a single gene product and it utilizes only two receptors (VEGFR–1 and VEGFR–2) involved in pathological angiogenesis in tumour vasculature (Shibuya, 2011). OXY decreased micro–blood and

micro–lymphatic vessel density in the lymph node metastasis by inhibiting the expression of CD31, VEGFR3, and VEGF–C (Liu *et al.*, 2018). More evidence from resveratrol, it also has the synergised effect of paclitaxel on EBC–1 cells through p27kip1, E–cadherin, EGFR and Bcl–2 expression (Kubota *et al.*, 2003).

1.7.9 Anti–inflammatory

Epidemiological studies have revealed that chronic inflammation predisposes to different forms of cancer. Molecular and cellular pathways linking inflammation and cancer have been identified. The main pathway linking to inflammation and cancer includes transcription factors (e.g. nuclear factor kappa–B (NFκB)), cytokines (e.g. TNF), and chemokines (Mantovani *et al.*, 2010). OXY showed anti-inflammatory properties in murine macrophage cell line RAW 264.7 by inhibiting the nitric oxide synthase (iNOS) and cyclooxygenase-2 (COX-2) expression through down-regulation of NF-kB binding activity (Chung *et al.*, 2003).

There have been studies that have identified the molecular targets of stilbenoids on various kinds of cancer. The molecular targets and pathways in cancer cells of OXY are shown in Table 1.

Table 1 Molecular targets of OXY

Target in carcinogenetic processes	Cancer cells	Molecular pathways	References
1.1 Anti–proliferative, cell growth	Neuroblastoma	G2/M phase arrest, cyclin D1, CDK3 and CDK4 reduction expression, p38 activation, ERK1/2, and JNK inactivation	(Rahman *et al.*, 2017)
	Prostate cancer cells	p27(kip1) inhibition	(Kim *et al.*, 2008)
1.2 Anti–invasion and migration	Acute T cell leukemia	CXCR4–mediated T–cell migration via inhibition of the MEK/ERK signalling cascade	(Chen *et al.*, 2013)
1.3 Proapoptotic	Neuroblastoma	Procaspase–9 decrease, active cleaved caspase–9 and –3 up–regulation, p38 MAPK activation, Bax/Bcl–2 up–regulation	(Rahman *et al.*, 2017)
1.4 Angiogenesis	Lymph node tumour	CD31, VEGFR3, and VEGF–C expression inhibition	(Liu *et al.*, 2018)
1.5 Autophagy	Neuroblastoma	Beclin–1, LC3, Atg5 and Atg7 increase, p38 MAPK activation, PI3K/AKT/mTOR signalling decrease	(Rahman *et al.*, 2017)
1.6 anti–inflammatory	Murine macrophage cell line	Inducible nitric oxide synthase (iNOS) and NF-kB and cyclooxygenase-2 (COX-2) inhibition	(Chung *et al.*, 2003)

1.8 Aims & Objectives

The aim of this research was to investigate the cytotoxicity of OXY and its effects on the expression of genes associated with the hallmarks of cancer.

Objectives

- Investigate and verify the phytochemical profile of *A. lakoocha* heartwood as a major source of OXY (Chapter 3).

- Investigate the pro–oxidant activities of OXY and other stilbenoids in the presence and absence of copper (cell–free) (Chapter 4).

- Identify a cell line model (transformed and non–transformed) in which cytotoxicity is demonstrated in response to OXY (with and without copper) (Chapter 5).

- Elucidate gene–level expression profile, and assess changes in key genes and pathways that involved in the biological response to OXY using microarray and quantitative polymerase chain reaction analysis (Chapter 6).

- Investigate the expression of key genes in apoptosis, cell proliferation, metastasis and DNA repair pathways following treatment with OXY (Chapter 7 and 8).

CHAPTER 2 MATERIALS & METHODS

The materials and methods utilised in this research are listed in this chapter, along with the procedures and protocols.

2.1 General chemicals

Table 2 General chemicals and suppliers

Chemicals	Company	City/ Country
2′,7′ dichlorodihydrofluorescein diacetate (H_2DCFDA)	Sigma–Aldrich	Jerusalem, Israel
5,5′–dithiobis (2–nitrobenzoic acid)	Sigma–Aldrich	Saint Louis, MO, USA
Acetic acid	Thermo Fisher Scientific	Waltham, MA, USA
Acetonitrile, HPLC grade	Thermo Fisher Scientific	New York, NY, USA
Bathocuproinedisulfonic acid disodium salt hydrate	Sigma–Aldrich	New South Wales, Australia
Copper acetate ($CuOAc_2$) (99.99%)	Sigma–Aldrich	Darmstadt, Germany
Dimethyl sulfoxide anhydrous, ≥99.9%	Thermo Fisher Scientific	New York, NY, USA
Ethanol	Sigma–Aldrich	Saint Louis, MO, USA

Table 2 *Continue*

Ethyl acetate	Sigma–Aldrich	Darmstadt, Germany
Ethylene diamine tetraacetic acid, anhydrous (≥99%)	Sigma–Aldrich	Darmstadt, Germany
Glutathione reduced	Sigma–Aldrich	Tokyo, Japan
Hoechst 33342	Thermo Fisher Scientific	New York, NY, USA
Hydrogen Peroxide (30% in Water)	Thermo Fisher Scientific	New York, NY, USA
Iron (III) chloridehexahydrate ($FeCl_3 \cdot 6H_2O$) (≥99%)	Sigma–Aldrich	Saint Louis, MO, USA
Methanol	Fisher Scientific	Loughborough, UK
NMR solvents including water (D_2O), methanol (CD_3OD), dimethyl sulfoxide (DMSO–d6) and acetone (acetone–d_6)	Cambridge Isotope Laboratories	Tewksbury, MA, USA
OXY (>97%)	Sigma–Aldrich	Buchs, Switzerland
Resveratrol (>99%)	Sigma–Aldrich	Saint Louis, MO, USA
Trans–stilbene (96%)	Sigma–Aldrich	Milan, Italy
Zinc chloride ($ZnCl_2$) (≥98%)	Sigma–Aldrich	Saint Louis, MO, USA

2.2 Cell lines, media and reagents

Names and tissues of origin of each cell lines used in this study are listed in Table 3 and media and reagents regarding cell culture work listed in Table 4. CACO–2, MCF7 were purchased from European Collection of Authenticated Cell Cultures (ECACC) (Salisbury, UK); while HCC1937 and MCF10A were from the American Type Culture Collection (ATCC) (Manassas, VA, USA); and the other cells were obtained from Dr Kenneth Ritchie cells bank (LJMU, Liverpool, UK).

Table 3 Name and origin of the cell lines

Name	Origin
A549	Adenocarcinoma human alveolar basal epithelial cells
CACO–2	Human colorectal cancer cells
HCC1937	Human breast cancer cell line (invasive cells)
HepG2	Human Caucasian hepatocyte carcinoma cells
MCF7	Human breast adenocarcinoma cells
PC–3	Human prostate cancer cell line
RAW 264.7	Mouse blood cells
MRC–5	Human foetal lung cells
MCF10A	Human breast cells

Table 4 Media, reagents and suppliers

Media/ reagents	Company	City/ Country
0.25% trypsin/EDTA	Sigma–Aldrich	Saint louis, MO, USA
0.4%Trypan blue stain	Thermo Fisher Scientific	New York, NY, USA
1 M HEPES solution, pH 7.0–7.6	Sigma–Aldrich	Darmstadt, Germany
Agarose BioReagent, low EEO	Sigma–Aldrich	Saint Louis, MO, USA
Cholera toxin	Sigma–Aldrich	Darmstadt, Germany
Doxorubicin	Sigma–Aldrich	Saint Louis, MO, USA
Dulbecco's modified eagles (DMEM, high glucose)	Biosera Europe	Nuaille, France
Dulbecco's modified eagle medium: Nutrient mixture F–12 (DMEM/F12)	Thermo Fisher Scientific	New York, NY, USA
Foetal Bovine Serum (FBS)	Thermo Fisher Scientific	New York, NY, USA
Horse serum	Thermo Fisher Scientifi	North Shore City, New Zealand
Lamda DNA Hind III digest	Sigma–Aldrich	Saint louis, MO, USA

Table 4 *Continue*

Mammary Epithelial Cell Growth Kit	ATCC	Manassas, VA, USA
Minimum Essential Medium (MEM)	Thermo Fisher Scientific	New York, NY, USA
Non–essential amino acids (NEAA)	Thermo Fisher Scientific	New York, NY, USA
pBR322 Supercoid plasmid DNA	Thermo Fisher Scientific	Vilnius, Lithunia
Penicillin–Streptomycin (100X)	Biosera	Boussens , France
Phosphate buffer saline (PBS)	Sigma–Aldrich	Saint louis, MO, USA
Sodium Pyruvate (100 mM)	Thermo Fisher Scientifi	Paisley, UK
Thiazolyl blue tetrazolium bromide (MTT) (98%)	Sigma–Aldrich	Saint Louis, MO, USA
Tris–Borate–EDTA buffer	Sigma–Aldrich	Darmstadt, Germany

2.3 Equipment

Table 5 Equipment and suppliers

Equipment	Company	City/ Country
High-Performance Liquid Chromatography (HPLC); the analysis was performed on a Phenomenex liquid chromatography system consisting of a Chomeleon system, WPS–3000TSL Autosampler and DAD–3000 detector	Thermo Fisher Scientific	New York, NY, USA
Luna@ C18 column (4.6 mm×15cm, 5 μm)	Phenomenex	Torrance, CA, USA
Biosafety cabinet class II, Envair laboratory equipment	Monmouth Scientific	Somerset, UK
Refrigerated centrifuge, 810R	Eppendorf	Hamburg, Germany
Inverted microscope, Olympus CKX41, with Cellsens Entry 1.16 software	Olympus Corporation	Manila, Philip
Microplate reader, Clariostar	MBG Labtech GmBH	Ortenberg, Germany
Gel documentation imaging system	Bio–Rad	Hercules, CA, USA
Flow cytometer	BD Biosciences	San Jose, CA, USA

2.4 Methods

All statistical analysis was carried out using Microsoft excel 2016 or GraphPad Prism 8 (GraphPad Software, La Jolla, CA, USA).

2.4.1. Investigate and verify the phytochemical profiles of *A. lakoocha* heartwood

2.4.1.1 Plant collection

A. lakoocha heartwood was collected from Chanthaburi province of Thailand seen in Figure 9, in June 2018. The voucher specimens were identified as DMSC 5237 and deposited voucher specimens at DMSC International Herbarium, Department of Medical Sciences, Ministry of Public Health, Thailand.

Figure 9 Map showing Thailand geographical position and Chanthaburi province where the plant samples were collected

2.4.1.2. Plant extraction

2.4.1.2.1 Reflux extraction

The heartwood was ground into a powder and dried until constant weight. The dried powder was extracted with two different solvents including distilled water and ethanol using reflux extraction method modified from Borah *et al.* (2017) as briefly described; 250 g of the powder was filled in a round–bottomed flask containing 3,000 mL of solvent and connected to a reflux condenser. Constant boiling temperature and agitation were maintained throughout the 1.5 h. Afterwards, the solvent was collected and then the plant particles were further extracted with the fresh solvent and repeated twice the same procedure. All of the extracted solvents were pooled, filtered and dried by rotary evaporation or lyophilization. The Reflux extraction and its accessories are shown in Figure 10.
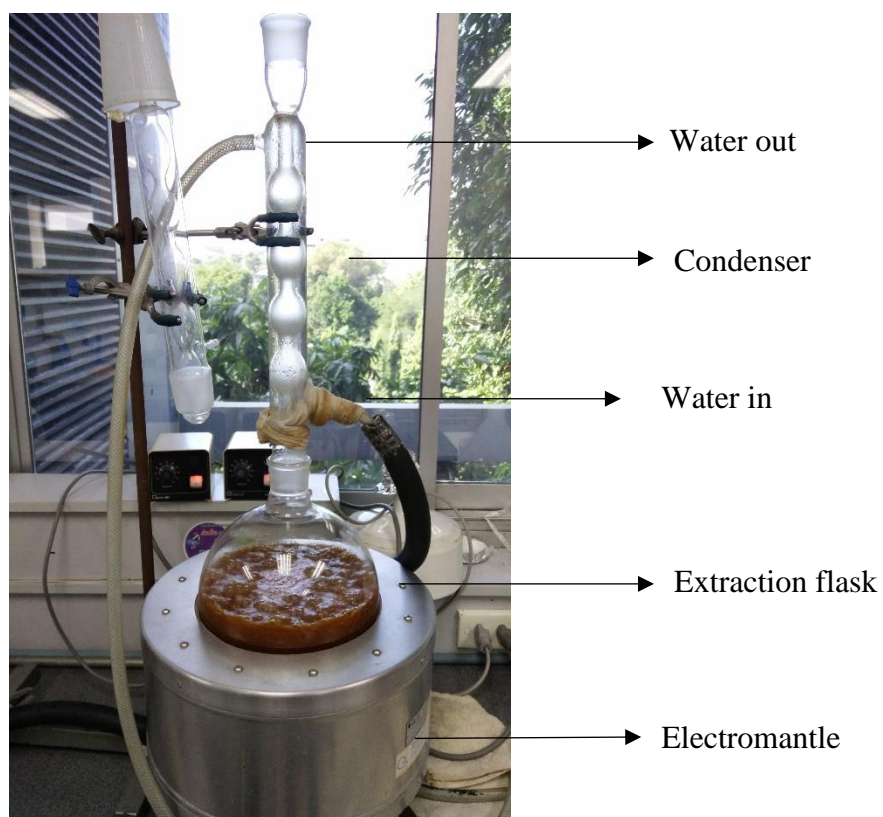
Figure 10 Reflux extraction

2.4.1.2.2 Soxhlet Apparatus

Ethyl acetate fraction extracted by Soxhlet apparatus (showed in Figure 11) as briefly described; 800 g of dried powder was extracted with 4,500 mL ethyl acetate using Soxhlet apparatus constant boiling temperature and agitation were maintained for 18–h extraction period. Afterwards, the solvent was collected and filtered. Finally, the extract was concentrated and dried under a fume hood.
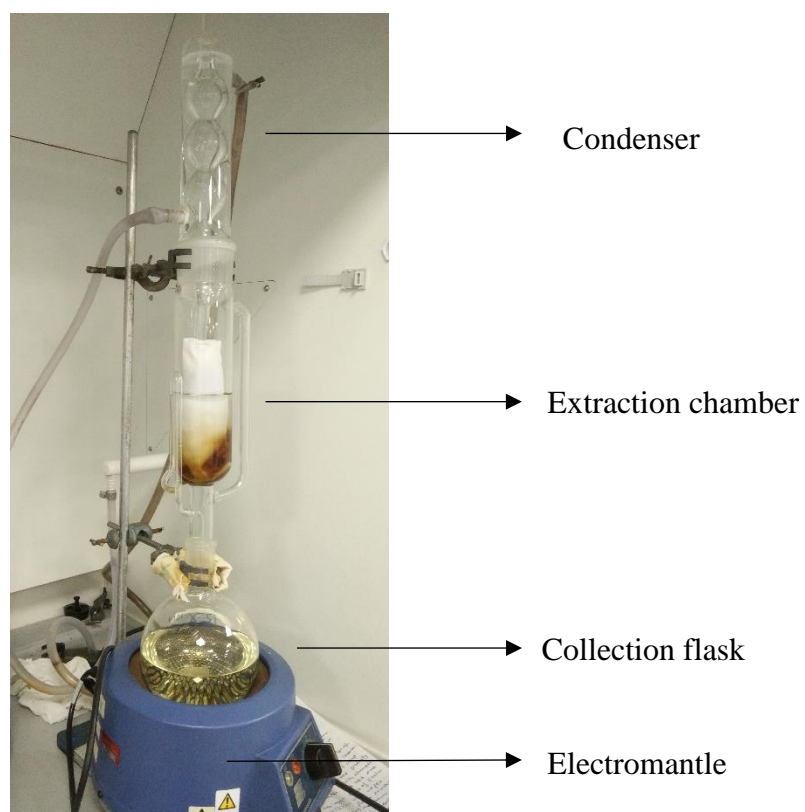
Figure 11 Soxhlet apparatus

2.4.1.3 Preparation of standard solutions and quality control samples.

Standard stock solutions of OXY and resveratrol were prepared at the concentration of 1000 µg/mL in methanol. Then the stock solution was subsequently 2–fold diluted to obtain 5 different concentrations of working solution in the ranges 12.20–200.00 µg/mL for OXY and 1.25–20.00 µg/mL for resveratrol. All the solutions were freshly prepared in the vessel protected from light in the day of analysis.

The sample solutions of the extracts were prepared at the concentration 1000 µg/mL in methanol by weighing 5.00 g of each dried powder. Then, they were diluted with

methanol and sonicated for 1 min. The volume was adjusted to reach 5 mL in volume metric flasks. Finally, the solutions were filtered by the solid phase extraction before analysing by HPLC.

2.4.1.4 High–performance liquid chromatography

HPLC was performed to analyse the amount of OXY and resveratrol. The standard curves of the two compounds were created to qualify the total content in *A. lakoocha*'s extracts. The phytochemical profiles of the three extracts were generated based on their retention times and UV spectra. The mobile phase was (A) water (0.5% acetic acid) and (B) acetonitrile using a gradient elution of 10–50% (v/v) B at 0–30 min, 50–100 % (v/v) B at 30–33 min, 100 % B (v/v) at 33–35 min and 100–10 % (v/v) B at 35–37 min. The flow–rate and injection volume were set at 1.0 mL/min and 20 μL, respectively.

2.4.1.5 Nuclear magnetic resonance

^{1}H–NMR (600 MH$_z$) spectra were used to investigate the configuration (*cis–* or *trans–*), purity of the compound and configuration stability of the compounds using TMS (for ^{1}H–NMR) as an internal standard at 25°C. OXY was dissolved in four different solvents including water–d$_2$, methanol–d$_4$, dimethyl sulfoxide–d$_6$ and acetone–d$_6$ and then all solutions were transferred to 5 mm NMR sample tubes and then measured ^{1}H–NMR.

2.4.1.6 In–Line Liquid Chromatography/ Mass Spectrometry

Analyses were performed using an inline Liquid Chromatography–Ultraviolet–Mass Spectroscopy (LC–UV–MS) system equipped with an electrospray ion source. All of the LC separations were carried out at room temperature and in the gradient mode using a

Waters 2695 series Alliance quaternary pump (Waters, Milford, MA, USA) equipped with model Waters 2487 dual λ absorbance detector. Injection volume was 20 μL. The LC column was 150 x 4.6 mm Luna C18 packed with 5 μm particles. A Luna C18 cartridge C18 was used as the pre–column. The mobile phase consisted of aqueous formic (A) and acid acetonitrile (B) at the flow rate of 1 mL/min. The solvent delivered to the ESI interface was split in a 1:3 ratio, delivering 300 μL/min to the interface. Waters Micromass LCT instrument (Micromass, Manchester, UK) equipped with a pneumatically assisted electrospray interface. The system was controlled by Masslynx software version 3.4 (Micromass). The nebulizing gas (nitrogen, 99.999% purity) and the desolvation gas (nitrogen, 99.999% purity) were delivered at flow rates of 20 and 700 L/h, respectively. Infusion experiments were conducted by infusing the standard solution of OXY (100 μg/mL) with a Harvard syringe pump (Harvard Apparatus, South Natick, MA, USA) at the flow rate of 20 μL/min. Full scan LC–MS analyses were carried out in positive ion mode. Optimized conditions of the interface were as follows: capillary voltage, 3 kV; cone voltage, 30 V; rf lens, 300 V; source temperature, 100 °C; desolvation temperature, 200°C. Full–scan mass spectra were acquired over the scan range m/z 150–1000.

2.4.2 Investigate the pro–oxidant of OXY and other stilbenes in the presence and absence of copper in a cell–free environment

2.4.2.1 DNA nicking assay

The reaction mixture (total volume 20 μL) contained 10 μL pBR322 plasmid DNA (200 ng) and $Cu(OAc)_2$ (50 μM) or 50 μM $FeCl_3$ or 50 μM $ZnCl_2$ in 10 μL of 10 mM HEPES buffer pH 7.2. The stock solutions of OXY, resveratrol and *trans*–stilbene were prepared at the concentration of 1000 μM in 1% (v/v) DMSO/Milli–Q water. *A. lakoocha*

heartwood extracts were prepared at the concentration of 1.00 mg/mL, total volume 5 mL, in 1% (v/v) DMSO/Milli–Q water.

To study the effect of OXY to cause nicks in DNA; the stock compound was diluted to six different concentrations including 1000, 500, 250, 50, 10 and 2 µM, respectively. The reactions were initiated by adding 5 µL of each dilution into 20 µL of the reaction mixture so that the final concentrations were 200, 100, 50, 10, 2 and 0.40 µM, respectively. After the addition of the compound, the tubes were incubated at 37 °C for 15 min.

To study the effect of chelating metals to cause nicks in DNA; the three chelating metals including $Cu(OAc)_2$, $FeCl_3 \cdot 6H_2O$ and $ZnCl_2$ were prepared at the concentration of 50 µM in 10 mM HEPES buffer pH 7.2. OXY at the concentration of 50 µM was chosen to test. The reactions were initiated by adding 5 µL of OXY into each of the reaction mixtures and incubated at 37 °C.

To study the effect of the amount of Cu(II) to cause nicks in DNA in the presence of a fixed concentration of OXY. The six different doses of Cu (II) were diluted including 200, 100, 50, 10, 2 and 0.40 µM, respectively. OXY was chosen at the dose of 50 µM contained 200 ng of the plasmid DNA as the reaction mixture. The 10 µL of each diluted concentration was mixed with 10 µL of OXY. All tubes were spun down and incubated at 37 °C.

To study the effect of other stilbenes to cause nicks in DNA; resveratrol and *trans–stilbene* were prepared at the concentration of 50 µM in 10 mM HEPES buffer pH 7.2. Additionally, the three *A. lakoocha* heartwood extracts including water, ethanol and ethyl acetate fractions were also investigated and prepared at the concentration of 1.00 mg/mL in the presence and absence of $Cu(OAc)_2$. The other two stilbenes were added into the reaction mixture the same volume as OXY. While each fraction of the *A. lakoocha*'s extract was 8–fold serially diluted to the three tested concentrations at 200.00, 25.00 and

39

3.13 µg/mL, respectively. The reaction was initiated by adding 5 µL of each compound into 20 µL of the reaction mixture and incubated at 37 °C for 15 min.

After the incubation, the reaction was terminated by placing the tubes on ice and adding DNA gel loading dye before loading to 0.8% agarose gel, which was consisted of 2 µL of Gelred. The samples were loaded in the gel and subjected to electrophoresis at 75 V for 1.50 h. After the running period, the gel was removed and visualized under UV light. The image of the gel was quantified by Bio–Rad documentation imaging system.

2.4.2.2 Reactive oxygen species assay

DCFH$_2$ preparation

Total 2.5 mg of 2',7'–dichlorodihydrofluorescein diacetate (H$_2$DCFDA) was weighed and dissolved in 5 mL methanol, then 500 µL of the solution was added to 2 mL of 0.01 N sodium hydroxide (NaOH). The mixed solution was incubated for 30 min at room temperature. After that 8 mL of 10 mM HEPES buffer pH 7.2 was added. In this experiments, 50 µL of this solution was added to the reaction solutions in 96–well plate format so that the final concentration of H$_2$DCFDA was 10 µM as previously described (Cohn *et al.*, 2008). The chemical reaction shows in Figure 12.
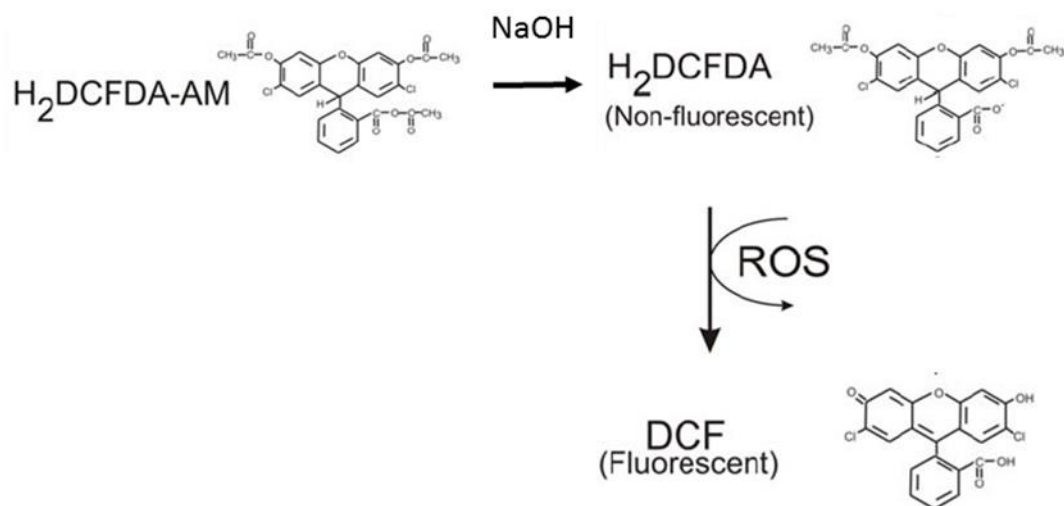
Figure 12 H₂DCFDA transformation to DCF (Fluorescent)

ROS assay of OXY, stilbenes and the extracts

The stock solution of OXY was freshly prepared at the concentration of 1000 µM in 1% DMSO/Milli–Q water, volume 5.00 mL. Then, it was 2–fold serially diluted for different eight concentrations of 3.13–400.00 µM. Total 100 µL of each concentration was pipetted into each well of the 96–well plate for triplicates. The reaction was initiated by adding 50 µL of 200 µM Cu(II) or HEPES buffer into each well to make 200 µL total volume so that the final concentration of OXY were 200, 100, 50, 25, 12.50, 6.25, 3.13 and 1.56 µM, respectively. After addition, the tubes were incubated at 37 °C for 15 min. DCF, the fluorescence product of the reaction, was quantitated spectrofluorimetrically with excitation and emission wavelengths of 492 nm and 525 nm, respectively.

Resveratrol and *trans*–stilbene were also prepared at the concentration of 1000 µM in 1% DMSO/HEPES buffer. Then the experiment was carried out in the same protocol as OXY.

Moreover, the thee solutions of *A. lakoocha* heartwood extracts were prepared at the concentration of 1.00 mg/mL in 1% DMSO /HEPES buffer and was investigated the ROS production at the concentration of 1.56–200 µg/mL.

2.4.2.3 Copper reducing assay

Cu(II) reduction by OXY was determined colourimetrically using the Cu(I)–stabilizing reagent bathocuproine disulfonic acid adapted from Subramanian *et al*. (2004). The stock solution of OXY (resveratrol or *trans*–stilbene) was prepared at the concentration of 1000 µg/mL and diluted to eight different concentrations between 3.13–400 µg/mL in 10 mM HEPES buffer pH 7.0. The reaction mixture (total volume for each tested concentration 200 µL) contained 50 µL of 2,000 mM bathocuproine disulfonic acid and 100 µL of OXY in 10 mM HEPES buffer. The reaction was initiated by adding 50 µL of 200 mM $Cu(OAc)_2$ in the sample tubes and the absorbance of the mixture at 484 nm was read at the end of 5 min. Appropriate blanks, without OXY, were used in each experiment. The chemical reaction shows in Figure 13.
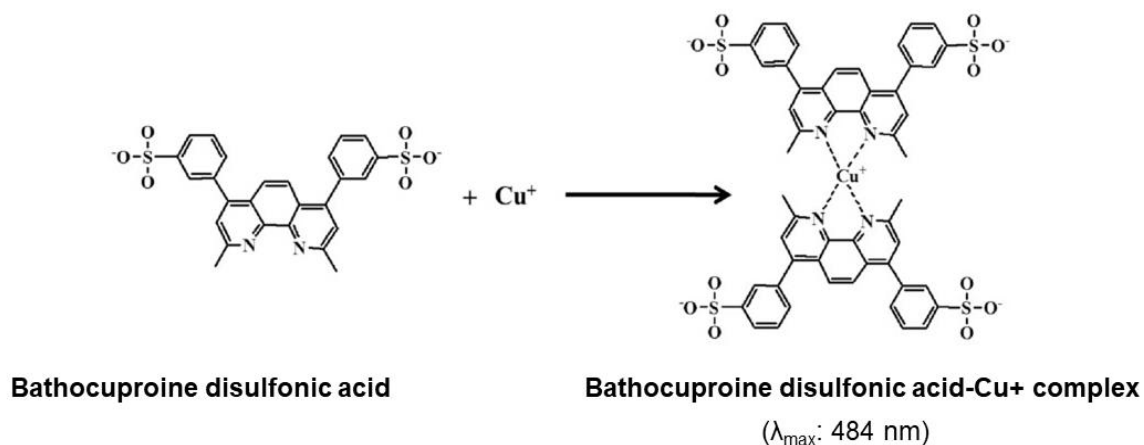
Figure 13 Formation of Cu(I)–stabilizing reagent bathocuproine disulfonic acid

2.4.2.4 Glutathione (GSH) assay

Standard curve of glutathione

Glutathione stock solution was prepared at 4,000 nmol/mL, volume 5.00 mL in phosphate buffer–EDTA. Then it was diluted to different ten concentrations between 7.51–100 nmol/mL of 200 μL total volume. The triplicates of each concentration were measured by adding 20 μL of 2.5 mM solution of 5,5′–dithiobis (2–nitrobenzoic acid) (DTNB) in phosphate buffer/EDTA (pH 7.0). The yellow reaction product of 5′–dithiobenzoic acid (TNB) was measured spectrophotometrically at 412 nm. The chemical reaction shows in Figure 14.
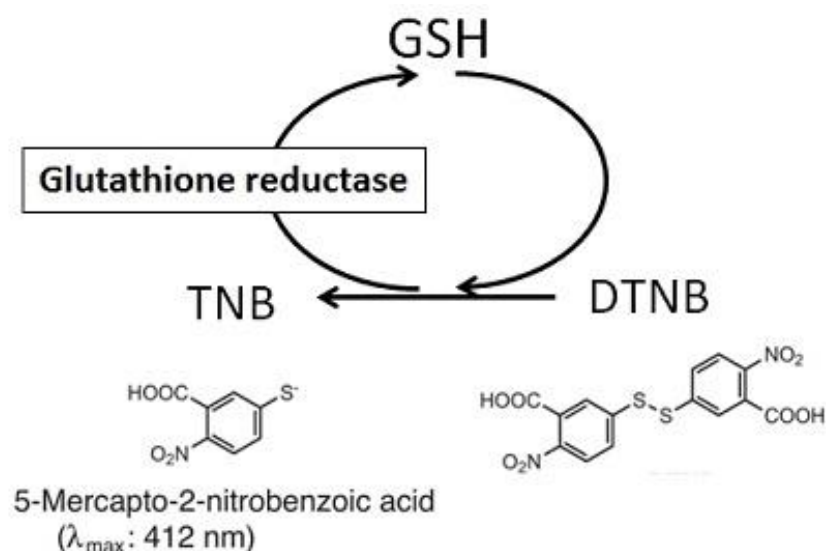
Figure 14 Transformation of 5,5′–dithiobis (2–nitrobenzoic acid) (DTNB) to 5′–dithiobenzoic acid (TNB)

GSH assay of OXY, resveratrol and trans–stilbene

OXY was prepared at the concentration of 1000 µM and was diluted to seven different concentrations in phosphate buffer (pH 7.0) with and without 100 µM Cu(OAc)$_2$. Each concentration of OXY (50 µL) was initiated by adding 50 µL Cu(II)(50 µM) or PBS. The mixtures were incubated at 37ºC for 30 min. After that, 100 µL of 100 nmol/mL GSH in PBS–EDTA was added to 96–well microliter plates and continued incubation for 1 h. The GSH was detected by adding 20 µL of 2.5 mM solution of 5,5′–dithiobis (2–nitrobenzoic acid) (DTNB) in phosphate buffer/EDTA (pH 7.0) by spectrophotometry at the absorbance 412 nm.

2.4.3. *In-vitro* cytotoxicity assays

2.4.3.1. Growth curve study

The growth of cells in a 96–well plate was studied to ensure that cells number was suitable and cells were grown in the log phase of the growth by counting the cell under the microscope. CACO–2, HepG2, MCF7, and MRC–5 cells were cultured in EMEM. While, A549, PC–3 and RAW 264.7 cells were maintained in DMEM; both EMEM and DMEM media were supplemented with 2 mM glutamine, 1% (v/v) NEAA and 10% (v/v) FBS in cell culture incubator at 37°C and 5% CO_2. Whereas, MCF10A cells were cultured in DMEM/F12 medium supplemented with 5% horse serum, 20 ng/mL Epithelial growth factor, 0.5 mg/mL hydrocortisone, 100 ng/mL cholera toxin, 10 µg/mL insulin and 1X penicillin–streptomycin. All cells were maintained in growth media. On the day of the experiment, the cells were trypsinised, resuspended with the medium and centrifuged to collect the cells. After receiving the cell pellet, the medium solution was discarded and resuspended the pellet with fresh growth medium. The viable cells were counted using a haemocytometer and trypan blue stain. The non–viable cells would be stained in blue. The viable cells were counted and the cell density was recorded. The cell suspension volumes were calculated to make the initial cell density at $5x10^3$, $7 x10^3$, $1x10^4$ and $2 x10^4$ cells per well. Each cell group was seeded in duplicated wells to be counted daily for four consecutive days. The cell number was counted each day and average±SD cells were calculated.

2.4.3.2 Cell viability using MTT assay

Total 1.2 mg of OXY was dissolved in 5 mL 1% DMSO/growth medium to reach 1000 µM and then diluted to 200 µM as a working solution. It was serially 2–fold diluted for seven concentrations for cell treatment. Doxorubicin was used as a standard drug in the experiment (Chatsumpun *et al.*, 2016). The stock solution was prepared at 2 mg/mL and then was diluted to 10 µg/mL as a working solution. It was serially 2–fold diluted for seven concentrations for cell treatment. Total 0.5 mg/mL MTT solution was prepared by dissolving 50 mg in 10 mL PBS. It then was diluted 10 times before incubating with cells. Cells were seeded at 5×10^3 cells (1×10^4 cells for MCF7 and PC–3) (optimal growth) in 100 µL medium per well of 96–well plates and left in the incubator for 24 h. The medium was removed and the cells were treated with eight different concentrations of OXY in triplicate and then incubated for 48 h. The medium was removed and 200–µL MTT reagent was added in each well, and then continued to incubate for 4 h. The MTT solution was discarded and 100 µL DMSO was added to each well to dissolve the purple formazan product. The cell control did not add the tested chemical and the blank wells were no seeded cells used for determining background absorbance. The absorbance of the formazan product of viable cells was read using the microplate reader at 570 nm. The mean absorbance and standard deviation were calculated for each concentration of OXY, controlled cells and blank. The background absorbance was reduced by the blank. The mean % cell viability was calculated as follows;

% cell viability = (absorbance sample/ absorbance control) x 100%

The 50% inhibitory concentration (IC_{50}) was calculated using GraphPad software. The chemical reaction of MTT shows in Figure 15.
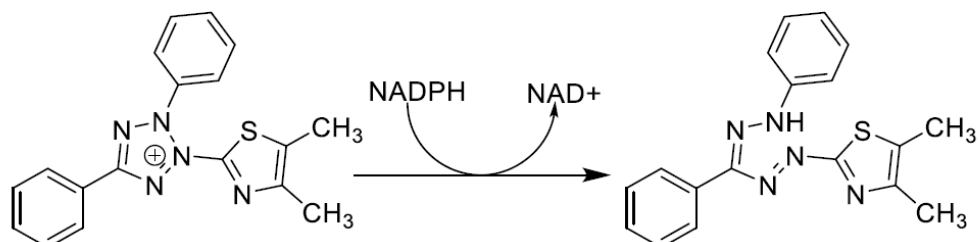
Figure 15 MTT transformation to formazan

2.4.3.3 Toxicity of OXY to cancer cells in the presence or absence of copper

Copper (II) acetate was diluted with cell media to between 1–200 µM and then cells treated the cells using an MTT assay described above. The non–toxic concentration of copper for each cell was chosen to investigate the toxicity of OXY in the presence and absence of copper; the investigation was separated into two procedures. The first, cells were pre–incubated with 50 µM $Cu(OAc)_2$ (OXY–Pre–Cu^{2+}) for 24 h in 96–well plate, after that the cells were rinsed with the culture medium and replaced with different concentrations of OXY for 48 h. The other procedure was that the cells were treated for 48 h with different concentrations of OXY (without copper pre–incubation), which was diluted with medium supplemented with 50 µM $Cu(OAc)_2$(OXY–Cu^{2+}). Cell viability was detected using MTT assay.

The cell lines which had demonstrated OXY toxicity ($IC_{50} \leq$ or around 100 µM) were chosen to investigate further (pre–treatment with different concentrations of copper). Four different concentrations of copper at 25, 50, 100 and 200 µM were used for pre–treatment. Then they were treated with OXY for 48 h. The cell viability was detected using MTT assay.

The intracellular ROS production was also investigated. Cells were pre–treated with different concentrations of copper at the dosed of 25, 50 and 100 µM, and then treated with OXY. They were determined intracellular ROS levels generated at the time 2, 6, 24 and 48 h of the incubation followed the protocol described by (Panich *et al.*, 2012). The cells were washed twice with 100 µL PBS and then incubated with 5µM $DCFH_2DA$ for 1 h at 37ºC. DCF fluorescence intensity of ROS formation was evaluated by spectrofluorometry at the excitation/emission wavelength of 485/530 nm. The data were expressed as the percentage of intracellular oxidant formation (relative fluorescence units, RFUs) of the control cells.

2.4.4 Investigation of the mechanisms of action

2.4.4.1 Microarray gene expression assay

RNA extraction

Total RNA was extracted using the RNeasy Mini Kit (Qiagen, Hilden, Germany) pre–treated with on–column DNase digestion with RNase–free DNase set (Qiagen, Hilden, Germany) according to the manufacturer's protocol. RNA was recovered in 30 µL of nuclease–free water and stored at −80°C until further analysis. The amount and quality of the RNA samples were analysed by NanoDrop2000 Thermo Fisher Scientific (New York, NY, USA) and the samples were run on an Agilent RNA 6000 Pico chip to assess

RNA integrity using the 2100 Expert Software (Agilent Technologies, Palo Alto, CA, USA). RNA integrity numbers were measured from 8.1 to 9.0.

Amplification and labelling process

Total RNA was processed using GeneChip^{TM} WT PLUS Reagents (Thermo Fisher Scientific, Palo Alto, CA, USA) containing WT amplification kit module 1, WT amplification kit module 2, Poly–A RNA Control Kit, WT Terminal Labelling Kit and Hybridisation Control Kit. The workflow step of the amplification and labelling process is shown in Figure 16.
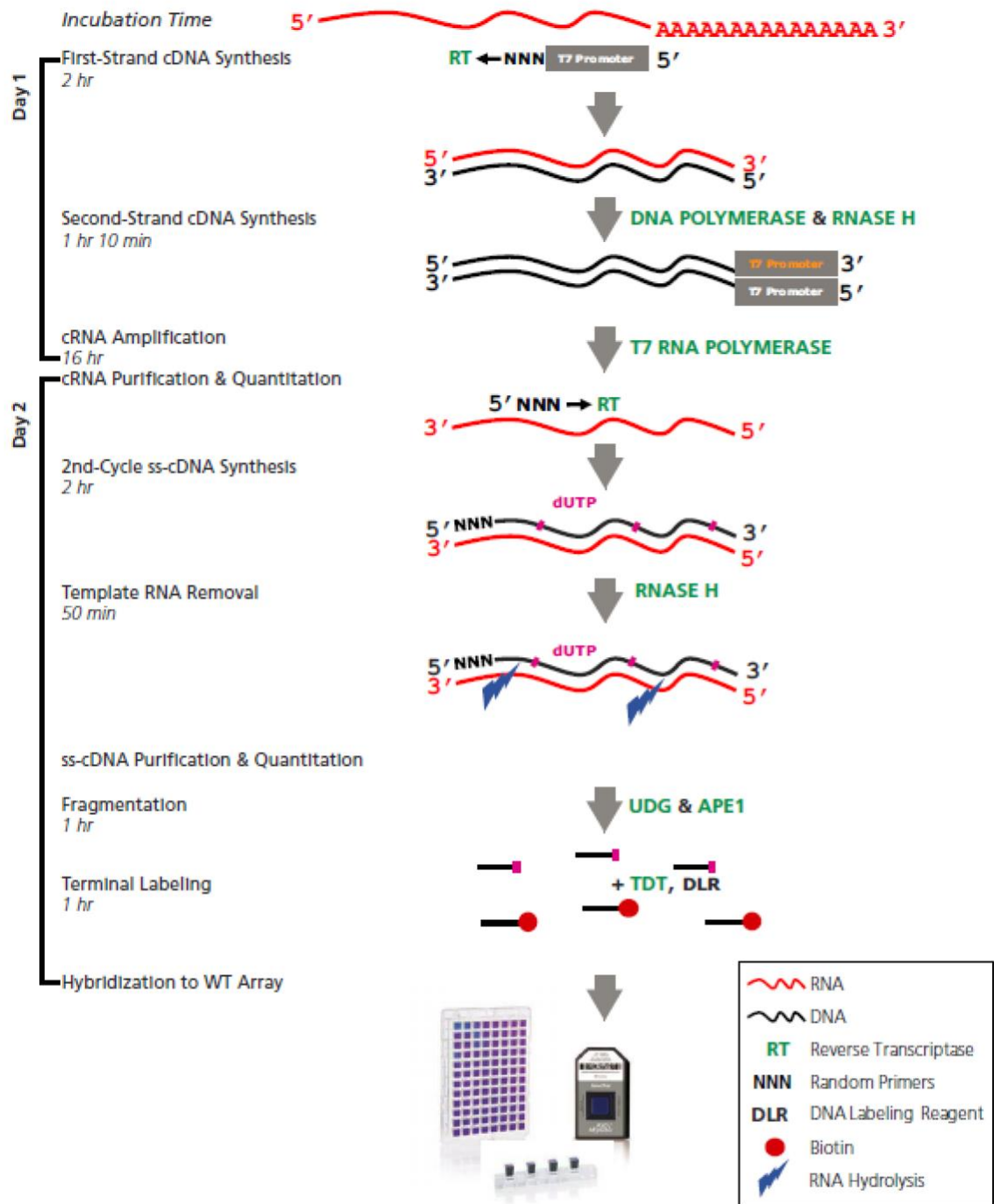
Figure 16 Amplification and labelling process, the RNA sample was converted into cDNA and then the second-strand cDNA was synthesised and used as a template for cRNA amplification. In the last amplification process, the sense-strand DNA (with dUTP) was generated, fragmented using UDG & APE1and labelled with biotin. Finally, the oligo DNA was hybridised onto microarray (Thermofisherscientific, 2017).

Prepare total RNA/poly–A RNA control mixture

Total 3 μL of total RNA samples (100 ng total input) were prepared, and then added 2 μL of the 4th dilution Poly–A spike controls, for a final volume of 5 μL each sample.

Synthesis first–strand cDNA

In the reverse transcription procedure, total RNA was primed with primers containing a T7 promoter sequence. The reaction synthesised single–stranded cDNA with T7 promoter sequence at the 5' end.

The procedure was briefly described; the first–strand master mix was prepared in a nuclease–free tube on ice (4 μL first–strand buffer and 1 μL first–strand enzyme for a reaction). The tubes were thoroughly mixed by gentle vortexing and then were briefly centrifuged. The 5 μL of the total RNA/Poly–A RNA control mixtures were transferred into the tube containing 5 μL of the first–strand master mix, the samples were thoroughly mixed by gentle vortexing. The sample tubes were incubated in a thermal cycler for 1 h at 25°C, then for 1 h at 42°C, and finally incubated for at least 2 min at 4°C. After the incubation, the tubes were immediately centrifuged to collect the first–strand cDNA at the bottom of the tube or well and then the samples were placed on ice for 2 min before proceeding immediately to the next step.

Synthesis second–strand cDNA

In this procedure, the single–stranded cDNA was converted to double–stranded cDNA, which acted as a template for *in vitro* transcription. The reaction used DNA polymerase and RNase H to simultaneously degrade the RNA and synthesis second–strand cDNA.

The second–strand master mix was prepared in a nuclease–free tube on ice, which contained 18 μL of the second–strand buffer and 2 μL of second–strand enzyme for a

reaction (total volume 20 µL). The master mix was gently vortexed and briefly centrifuged. The 20 µL was transferred to each first–strand cDNA sample (10 µL) for a final reaction volume of 30 µL, then the tubes were gently vortexed and briefly centrifuged. The sample tubes were incubated in a thermal cycler for 1 h at 16°C, then for 10 min at 65°C, then the last for at least 2 min at 4°C. After that, the samples were briefly centrifuged to collect the second–strand cDNA, before proceeding to the next step.

Synthesis cRNA by in vitro transcription

In this procedure, antisense RNA (complementary RNA or cRNA) was synthesised and amplified by *in vitro* transcription (IVT) of the second–stranded cDNA template using T7 RNA polymerase.

The IVT master mix containing 24 µL IVT Buffer and 6 µL IVT Enzyme (30–µL total volume) was prepared at room temperature. Total 30 µL of the second–strand cDNA samples were transferred to each IVT master mix (30 µL) for a final reaction volume of 60 µL. The tubes were gently vortexed and briefly centrifuged. The sample tubes were incubated in a thermal cycler for 16 h at 40°C, and then at 4°C. The samples were briefly centrifuged and then proceeded to purify cRNA.

The cRNA products were purified using the purification beads. Total of 100 µL beads were added to each (60 µL) cRNA sample. Then, it was mixed by pipetting up and down 10 times and transferred to a well of a U–bottom plate. The samples were incubated for 10 min. The sample plate was moved to a magnetic stand to capture the purification beads catching cRNA. After 10 min placing, the supernatant was carefully aspirated and discarded without disturbing the beads. The plate was still kept on the magnetic stand, a 200 µL of 80% ethanol wash solution was added to each well and incubated for 30 s. The wash solution was slowly aspirated and discarded from each well. The beads were washed twice more with 200 µL of 80% ethanol wash solution. The final wash solution was

completely removed, air–dried on the magnetic stand for 5 min until no liquid is visible. The plate was then removed from the magnetic stand, and 27 μL of the preheated (65°C) nuclease–free water was added to each sample. The sample was incubated for 1 min, then mixed by pipetting up and down 10 times. The plate was then moved back to the magnetic stand and placed for ~5 min. The supernatant which contained the eluted cRNA was transferred to a nuclease–free tube. The purified cRNA samples were placed on ice, RNA Yield was determined by UV Absorbance and quantified by 2100 Bioanalyzer Instrument.

Synthesis 2nd–cycle single–stranded cDNA

In this procedure, sense–strand cDNA is synthesised by the reverse transcription of cRNA using 2nd– cycle primers. The sense–strand cDNA contained dUTP at a fixed ratio relative to dTTP. Total 15 μg of cRNA was required for 2nd–cycle single–stranded cDNA synthesis. 15 μg cRNA in a volume of 24 μL(625 ng/μL) was prepared and placed on ice. The cRNA sample was added to 4 μL of 2nd–cycle primers, then thoroughly mixed and briefly centrifuged. The sample tubes were incubated for 5 min at 70°C, then 5 min at 25°C, and the last for 2 min at 4°C. After that, the tubes were briefly centrifuged and immediately placed on ice. The 2nd–cycle ss–cDNA master mix was prepared by pipetting 8 μL of 2nd–cycle ss–cDNA buffer and 4 μL of 2nd–cycle ss–cDNA enzyme for a reaction, then thoroughly mixed and briefly centrifuged. The sample tubes were incubated for 10 min at 25°C, then 90 min at 42°C, then 10 min at 70°C, then for at least 2 min at 4°C. Afterwards, all samples were briefly centrifuged and placed on ice and immediately proceeded to hydrolyse RNA using RNase H.

Hydrolyse RNA using RNase H

In this procedure, RNase H hydrolysed the cRNA template leaving single–stranded cDNA.

Total 4 μL of the RNase H was added to 2nd–cycle ss–cDNA sample (40 μL) for a final reaction volume of 44 μL, and then the tubes were thoroughly mixed and briefly centrifuged. The tubes incubated for 45 min at 37°C, then for 5 min at 95°C, and the last step for at least 2 min at 4°C. The samples were briefly centrifuged and placed on ice. Total 11 μL of nuclease–free water was added to each hydrolyzed 2nd–cycle ss–cDNA sample for a final reaction volume of 55 μL, thoroughly mixed and briefly centrifuged. The samples were placed on ice, then purified, or immediately frozen at –20°C for storage.

Purify 2nd–cycle single–stranded cDNA

After hydrolysis, the 2nd–cycle single–stranded cDNA was purified to remove enzymes, salts and unincorporated dNTPs. This step prepared the cDNA for fragmentation and labelling.

Total 100 μL purification beads were added of to each 2nd–cycle ss–cDNA sample (55 μL), then mixed by pipetting up and down, and transferred to a well of a u–bottom plate. 50 μL of 100% ethanol was added to the ss–cDNA/Beads sample. The sample was mixed well by pipetting up and down 10 times and then incubated at room temperature for 20 min. The plate was moved to a magnetic stand to capture the purification beads. After 10 min placing, the supernatant was carefully aspirated and discarded without disturbing the beads. The plate was still kept on the magnetic stand, total 200 μL of 80% ethanol wash solution was added to each well and incubated for 30 s. The washing solution was slowly aspirated and discarded from each well. The beads were washed 3 times more with 200

μL of 80% ethanol wash solution. The final wash solution was completely removed, air–dried on the magnetic stand for 5 min until no liquid is visible.

The plate was then removed from the magnetic stand, and 30 μL of the preheated (65°C) nuclease–free water was added to each sample and incubated for 1 min, then mixed well by pipetting up and down 10 times. The plate was then moved back to the magnetic stand and placed for ~5 min. The supernatant that contained eluted ss–cDNA was pipetted to a nuclease–free tube. The samples were put on ice, and the single–stranded cDNA was assessed for yield and size distribution, or immediately frozen at –20°C for storage.

Fragment and label single–stranded cDNA

In this procedure, the purified, sense–strand cDNA was fragmented by uracil–DNA glycosylase (UDG) and apurinic/apyrimidinic endonuclease 1 (APE 1) at the unnatural dUTP residues and broke the DNA strand. The fragmented cDNA was labelled by terminal deoxynucleotidyl transferase (TdT) using the proprietary DNA labelling reagent that was covalently linked to biotin. All 5.5 μg of single–stranded cDNA was required for fragmentation and labelling.

Total 5.5 μg of ss–cDNA in a volume of 31.2 μL (176 ng/μL) was prepared and placed on ice. The fragmentation master mix (16.8 μL total volume for a reaction) was prepared in a nuclease–free tube containing 10 μL of nuclease–free water, 4.8 μL of 10X cDNA Fragmentation Buffer, 1 μL of 10 U/μL UDG and 1 μL of 1000 U/μL APE 1. The master mix (16.8 μL) was transferred to each purified ss–cDNA sample (31.2 μL) for a final reaction volume of 48 μL. All tubes were then gently vortexed and briefly centrifuged. The sample tubes were incubated for 1 h at 37°C, then for 2 min at 93°C, and then the last incubation for at least 2 min at 4°C, briefly centrifuged and placed on ice.

Total 45 μL of the fragmented ss–cDNA sample was transferred to a new tube or well tube or well. The labelling master mix was prepared in a nuclease–free tube (15.0 μL total volume for a reaction), which combined the components following 12 μL of 5X TdT buffer, 1 μL of 5 mM DNA labelling reagent and 2 μL of 30 U/μL TdT. The tubes were gently vortexed and briefly centrifuged. 15 μL of the Labelling Master Mix was added to each fragmented ss–cDNA sample (45 μL) for a final reaction volume of 60 μL, then gently vortexed and briefly centrifuged. The sample tubes were incubated for 1 h at 37°C, then for 10 min at 70°C, then for at least 2 min at 4°C. The samples were placed on ice, then proceeded to array hybridisation, or immediately froze at –20°C for storage.

Array hybridisation

The samples were hybridised in biological triplicate to Human Clariom S arrays (a 400 format array), following the manufacturer's recommendations. Briefly, the hybridisation master mix (73 μL total volume for a reaction) was prepared by mixing components including 1.7 μL of control oligo B2 (3 nM), 5 μL of 20X hybridisation controls (bioB, bioC, bioD, cre), 50 μL of 2X hybridisation mix, 7 μL of DMSO and 9.3 μL of nuclease–free water. The solution was gently vortexed and briefly centrifuged. The hybridisation master mix was added to each 27 μL (2.3 μg) fragmented and biotin–labelled ss–cDNA sample to prepare the hybridisation cocktail for each array. The hybridisation cocktail reaction was gently vortexed and briefly centrifuged, before incubated in a thermal cycler for 5 min at 99°C (tubes) or 95°C (plates), then for 5 min at 45°C. After the incubation, the cocktail solution was briefly centrifuged, and then 80 μL of each hybridisation mix was loaded into the array. The arrays were sealed with tough spots and placed into hybridisation oven trays. Finally, the trays were loaded into the GeneChip™ hybridisation oven 645 and incubated with rotation at 60 rpm for 16 h at 45°C. The thermal cycler programmes show in Table 2.

Table 2 Thermal cycler programmes

Programme	Heated lid temp.	Alternate protocol	Step 1	Step 2	Step 3	Volume
First–strand cDNA synthesis	42°C	105°C	25°C, 60 min	42°C, 60 min	4°C, 2 min	10 μL
Second–strand cDNA synthesis	RT or disable	Lid open	16°C, 60 min	65°C, 10 min	4°C, 2 min	30 μL
In vitro transcription cRNA synthesis	40°C	40°C oven	40°C, 16 h	4°C, hold		60 μL
2nd–cycle primers– cRNA annealing	70°C	105°C	70°C, 5 min	25°C, 5 min	4°C, 2 min	28 μL
2nd–cycle ss– cDNA synthesis	70°C	105°C	25°C, 10 min	42°C, 90 min	70°C, 10 min	40 μL
RNA hydrolysis	70°C	105°C	37°C, 45min	95°C, 5 min	4°C, hold	44 μL
Fragmentation	93°C	105°C	37°C, 60 min	93°C, 2 min	4°C, hold	48 μL
Labelling	70°C	105°C	37°C, 60 min	70°C, 10 min	4°C, hold	60 μL
Hybridisation control	65°C	105°C	65°C, 5 min			
Hybridisation cocktail	99°C	105°C	95°C or 99°C, 5 min	45°C, 5 min		

Washing and staining

The arrays were removed from the oven. The tough–spots also removed and released the hybridisation cocktail mix from each array. Wash buffer A was filled into each array and allowed the arrays to equilibrate at room temperature before washing and staining. The vials of stain cocktail and array holding buffer were placed into sample holders on the GeneChip™ Fluidics Station 450 (Thermo Fisher Scientific, Palo Alto, CA, USA). The washing and staining script used was FS450_0007.

Scanning

A GeneChip 3000G scanner (Affymetrix Inc.) and the Expression Console software (Affymetrix Inc.) was used to obtain fluorescent signals and quality control data of the scanned arrays. Signal intensities from each array were analysed using Partek Genomic Suite version 6.4 (Partek, St Louis, MO, USA).

Data processing and analysis

The microarray data were deposited at the NCBI GEO database [GEO: GSE151139]. To identify those biological processes that show differentially expressed genes, The Transcriptome Analysis Console (TAC) Software (Thermo Fisher Scientific, Palo Alto, CA, USA), a bioinformatic tool used for the visualization of the expression data in the biological pathways context. The data set was analysed using this tool and a gene expression fold change > 2 or < -2. Ebayes was used for statistical analysis with a significant difference (p-value < 0.05).

2.4.4.2 Quantitative polymerase chain reaction assay

Reverse–transcription

The RNA sample was ready for reverse transcription using a master mix prepared from Quantiscript Reverse Transcriptase, Quantiscript RT Buffer, and RT Primer Mix. The entire reaction took place at 42°C and then was inactivated at 95°C.

The reverse–transcription master mix was prepared by pipetting 2 µL Quantiscript Reverse Transcriptase, 8 µL Quantiscript RT Buffer (5x) and 2 µL RT primer mix template for the total volume of 12 µL reaction. Then the 28 µL of 2 µg template RNA was added to each tube of the master mix. All tubes were mixed by pipetting and placed on ice. The tubes were incubated at 42 ºC for 15 min, then incubated at 95 ºC for 3 min. The cDNA products were quantified by NanoDrop2000 and then proceeded qPCR or stored at -20°C.

Quantitative polymerase chain reaction (qPCR)

This procedure the cDNA templates were amplified using QuantiTect SYBR Green PCR Kit (Qiagen, Valencia, CA, USA) and QuantiTect Primer Assay (Qiagen, Valencia, CA, USA). The fluorescent dye SYBR Green I in the master mix enabled the analysis of different targeted genes without having to synthesize target–specific labelled probes. High specificity and sensitivity in PCR are achieved by the use of the hot–start enzyme HotStarTaq DNA Polymerase together with a specialized PCR buffer. The buffer also contained ROX dye, which allows fluorescence normalization on certain cyclers.

QuantiTect SYBR Green PCR Master Mix, 10x QuantiTect Primer Assay, template cDNA and RNase–free were thawed and mixed individual solutions. The reaction mix was prepared by pipetting 25 µL of 2x QuantiTect SYBR Green (PCR master mix), added 5 µL 10x QuantiTect Primer Assay, added cDNA (≤500 ng cDNA template) to the

individual PCR tubes containing the reaction mix. The real–time cycler was programmed

the steps, temperature and time details in Table 4.

Table 3 Polymerase chain reaction programme

Step	Temperature (°C)	Time
PCR initial	95	15 min
Denaturation	94	15 s
Annealing	50–60*	30 s
Extension	72	30 s
Number of cycles	35–45	

*Approximately 5–8°C below Tm of primers

The PCR tubes were placed in the real–time cycler, and the cycling program was started.

mRNA ratios relative to the glyceraldehyde 3–phosphate dehydrogenase (GAPDH)

housekeeping gene were calculated for the standardization of gene expression levels. A

melting curve analysis was also performed to verify the specificity and identity of PCR

products. Finally, the products were run agarose gel electrophoresis to check the

specificity of the PCR.

Data analysis using the $2^{-\Delta\Delta Ct}$ method

For selected genes, real–time PCR was performed on the corresponding cDNA synthesized from each sample. The data were analysed using the equation described by Livak and Schmittgen (2001). Amount of target was equal to $2^{-\Delta\Delta Ct}$; The average Ct of GAPDH in each treatment was used to calculate ΔCt of the target genes and the ΔCt from OXY–untreated MCF7 cells was used as a calibrator for each gene to generate ΔΔCt. Each gene was performed in triplicate and data were presented as mean±SD. Statistical evaluation of significant differences was carried out the unpaired t–test using GraphPad Prism 8. Differences of P value less than 0.05 were considered statistically significant.

2.4.4.3 Lactate dehydrogenase release

To determine cellular toxicity of OXY, the level of lactate dehydrogenase (LDH) released from MCF7 cells was measured. After exposure to OXY for 48 h, cell–free supernatant aliquots were collected from each experimental sample, and LDH in the culture supernatants was measured using the Pierce LDH Cytotoxicity Assay Kit (ThermoScientific, Rockford, Illinois, USA). The protocol was followed by the manufacture's instructions. All samples were assayed in triplicate for LDH content by a microplate reader at the wavelength of 490 nm and 680 nm. The cytotoxicity was calculated by subtracting the background of the blank control. LDH activity of the spontaneous LDH release control (untreated) and the OXY treated groups were calculated as a percentage of the blank.

2.4.4.4 Nuclear morphological detection using Hoechst 33342 staining

The nuclear morphological changes of chromatin condensation and chromosome fragmentation induced by OXY was examined using Hoechst 33342 staining. The protocol was followed by the manufacture's instruction. Briefly, the cells were treated with different concentrations of OXY in 6–well plates for 24 and 48 h. The 10 mg/mL Hoechst stock solution was prepared and diluted with PBS (1:2000). The medium was removed from each well and then 500 µL of the dye working solution was added. The plate was incubated in the cell incubator protected from light for 10 min. Afterwards, the cells were washed with 1 mL PBS for 3 times. The cells were viewed under the fluorescence microscope (Olympus, Hamburg, Germany). The mode of cell death was then determined in term of distinct morphological changes, including membrane blebbing, nuclear and cytosolic condensation and nuclear fragmentation in the treated group compared to the untreated cells served as the control.

2.4.4.5 Determination of intracellular ROS

The intracellular ROS detection was adapted from Panich *et al.* (2012). Cells were pre-treated with different three concentrations of $Cu(OAc)_2$ for 24 h and then treated (fixed-dose) with 50 µM (for MCF7) or 100 µM (for HepG2) OXY for 2, 6, 24 and 48 h, respectively. The cells were washed twice with 100 µL PBS and then incubated with 5 µM DCFHDA for 1 h at 37ºC. DCF fluorescence intensity of ROS formation evaluated by spectrofluorometry at the excitation/emission wavelength of 485/530 nm. The data were expressed as percentage of intracellular oxidant formation (relative fluorescence units, RFUs) of the control cells.

2.4.4.6 Measurement of DNA damage by Comet Assay

The comet assay was performed under alkaline conditions. Cells were seeded in 6–well tissue–culture plates. They were treated with 25 and 50 µM OXY. After 24 and 48 h of exposure with OXY or 100 µM H_2O_2 for 4 h as the positive control, cells were collected by trypsinization, washed with PBS and resuspended in ice–cold PBS. About 10 µL of the resuspended cells was mixed with 100 µL of low melting point agarose at 37 °C and spread the suspension over the well with the pipette tip. The slides were placed at 4 °C in the dark until gelling occurred and then immersed in pre–chilled lysis buffer at 4 °C. After 60 min incubation, the buffer was aspirated and replaced with pre–chilled alkaline solution for 30 min at 4 °C. After lysis and unwinding, the slides were placed in a horizontal electrophoresis tank filled with freshly prepared alkaline electrophoresis buffer. The electrophoresis was run for 25 min at 15V and 300 mA. After electrophoresis, the slides were transferred to pre–chilled distilled water and immerse for 2 min, aspirate and repeat twice. The final water rinse was aspirated and replaced with cold 70% ethanol for 5 min. Thereafter, the slides were allowed to air dry and 100 µL/well of diluted Vista Green DNA dye was added to each slide for 15 min in the dark at room temperature for DNA staining. DNA migration was observed using the fluorescence microscope at a magnification of 10X (Leica Microsystems CMS GmbH, Germany).

2.4.4.7 Cell cycle analysis using flow cytometry

Cell cycle analysis was conducted by BD Cycletest™ Plus kit (BD biosciences, San Diego, CA, USA) using propidium iodide as a DNA stain to determine DNA content in the cells. The effect of OXY treatment on the cell cycle was determined by flow cytometry as described by the manufacturer's instruction. Briefly, MCF7 and HepG2

cells were seeded at 2.5 x 10^5 cells/well in 6–well plates. MCF7 cells were treated with OXY at the concentration of 25, 50, and 100 μM, while HepG2 cells were treated at 50, 100, and 200 μM for 6 and 24 h. Cells were trypsinised with 300 μL of 0.25% trypsin solution for 3 min in the cell incubator. A 200 μL of fetal bovine serum was added and then all of the cell suspension was transferred into a 15 mL centrifuge tube. The suspension was centrifuged at 300 rcf for 5 min. The supernatant was discarded, the cell pellet was resuspended with 1 mL buffer solution (contains sodium citrate, sucrose, and DMSO). The cells were centrifuged and resuspended one more time and then the cells were counted using hemocytometer for $5x10^5$ cells. Cells were frozen in the freezer (–80 ºC) for PI staining. The cell suspensions were thawed in a water bath, centrifuged at 400 g for 5 min at room temperature (20°C–25°C). All the supernatant was carefully decanted. A 250 μL of solution A (trypsin buffer) was added to each tube and gently mix by tapping the tube by hand, incubated for 10 min at room temperature. Afterwards, a 200 μL of Solution B (trypsin inhibitor and RNase buffer) was added to each tube and gently mix by tapping the tube by hand, incubate for 10 min at room temperature. Finally, a 200 μL solution C (PI stain solution) was added to each tube and incubated for 10 min in the dark on ice or in the refrigerator (2–8°C) until analysed by flow cytometer. A total number of 1×10^4 cells was subjected to cell cycle analysis using a flow cytometer. The detected cells were calculated into the percentage of cells population by the software.

2.4.4.8 Quantification of apoptotic cells

Annexin V is a 35–36 kDa, that was in the PE Annexin V Apoptosis Detection Kit I (BD Biosciences Inc., San Jose, CA, USA) and has a high affinity for negatively charged phospholipid phosphatidylserine, and binds to cells that are actively undergoing apoptosis was used to determined apoptotic cells after exposing to OXY; the protocol was briefly

described. MCF7 and HepG2 cells were seeded in 6–well plates and then treated with OXY at different concentrations (0, 25, 50 and 100 µM for MCF–7, while 0, 50, 100 and 200 µM for HepG2) for 3, 6, 24 and 48 h. The cells were trypsinised and washed twice with ice–cold PBS, and then cells were resuspended at a concentration of 1×10^6/mL cells in binding buffer. A 100 µL of the cell suspension was transferred into a 2 mL microcentrifuge tube and added 5 µL PE annexin V and 5 µL 7–amino–actinomycin D (a vital nucleic acid dye). The cells were gently mixed and incubated in the dark for 15 min at room temperature. Finally, a 400 µL of binding buffer was then added to each tube and the apoptotic cells were quantified using a flow cytometer within 1 h. Cells that stained positive for PE annexin V and negative for 7–amino–actinomycin D were undergoing apoptosis; cells that stain positive for both PE annexin V and 7–amino–actinomycin D were either in the end stage of apoptosis, are undergoing necrosis, or were already dead; and cells that stain negative for both PE annexin V and 7–amino–actinomycin D were alive and not undergoing measurable apoptosis.

2.4.4.9 Determination of caspase–3 expression induced by OXY

Active caspase–3 staining protocol was performed following the manufacturer's instructions (PE active caspase–3 apoptosis kit, BD biosciences, San Diego, CA, USA). The 5 x 10^5 cells of MCF7 and HepG2 treated with different concentrations of OXY were harvested and transferred into 15 mL centrifuge tubes and then the suspension was centrifuged at 300 xg for 5 min at 4 ºC. Cells were washed twice with 1 mL ice–cold PBS and then resuspended in 0.50 mL BD Cytofix/Cytoperm™ solution. The cells were incubated on ice for 20 min. After that the buffer was removed, the cells were washed twice with 0.50 mL BD Perm/Wash™ buffer at room temperature. Then, the cells were resuspended with 100 µL BD Perm/Wash™ buffer plus antibody and incubated for 30

min at room temperature. Finally, the cells were washed with 1 mL washing buffer and re–suspended in 0.50 mL washing buffer. The cells were maintained at 4 °C until analysing by flow cytometer.

2.4.4.10 Mitochondrial membrane potential ($\Delta\Psi$m) analysis by JC–1 fluorescence

Cellular mitochondrial dysfunction can be reflected by the loss of the mitochondrial membrane potential, which can be indirectly measured by the fluorescent probe JC–1 using The BDTM MitoScreen Kit (BD Biosciences, Sandiego, CA, USA). The protocol was followed manufacturer's instruction. Briefly, MCF7 and HepG2 treated with different concentrations of OXY were harvested and transferred into 15 mL centrifuge tubes and then the suspension was centrifuged at 300 x g for 5 min at 4 ºC. Then the cells were resuspended with 0.50 mL JC–1 working solution and incubated at 37ºC in a cell's incubator for 15 min. The cells pellet was washed twice with 1X assay buffer (2 mL and 1 mL, respectively). Finally, the cells were resuspended with 0.50 mL 1X assay buffer, then analysed by a flow cytometer.

2.4.4.11 Wound healing assay (scratch test)

Plates containing confluent cultures of MCF7 or HepG2 cells grown in the serum–containing medium were scratched with a sterile 200 µL pipette tip. The medium was replaced with serum–reduced medium with OXY or DMSO and returned to 37°C for designated times. Cells were captured. Distances between the gaps formed by the scratch were measured with Olympus CellSense Entry 1.16 software. The wound–closure (fold) were calculated relative to the gap size immediately after scratching.

2.4.4.12 Invasion assay

Migration assays were investigated using Corning® BioCoat™ Matrigel® invasion chamber (corning corporated, Tewksbury, MA, USA). It was coated on the lower surface with a 5 µg/mL fibronectin in FBS solution of overnight at 4°C. In a separate series of experiments to measure invasiveness, the upper surface of the inserts was coated with Matrigel and on the lower surface were coated with 5µg/mL fibronectin at 4°C for 24 h. Actively growing HCC1937 and HepG2 cells were trypsinized, washed and resuspended at 1×10^6 cells/mL in serum–free medium with either DMSO or OXY. Total 1×10^5 cells in 0.1 mL were carefully placed in the upper chamber. The upper and lower chambers contained the same media as the cell suspensions. Following incubation for 24 h, cells from the upper surface were wiped clear and cells on the lower surface were fixed with a 4% buffered formaldehyde solution. Crystal violet stained membranes were then transferred to slides, coverslipped, photographed and cells were counted manually.

2.4.4.13 Western blot analysis

Cells were seeded on the 6–well dishes and wait for the adherence. Cells were treated with OXY at the concentrations of 50 µM and 100 µM for 24 h and then washed twice with ice–cold PBS. The cells were lysed in lysis buffer (protease inhibitor cocktail). After 5 min incubation on ice, swirling the plate occasionally for uniform spreading, the solution was transferred to centrifuge tubes, sonicate the pellet for 30 seconds with 50% pulse and the lysates were centrifuged at ~14,000× g for 15 min to pellet the cell debris. The supernatants were collected, and protein concentrations were determined by the Bradford assay (Bio–Rad, Richmond CA, USA). An equal amount of protein sample (20 µg) was resolved by a volume of 2x Laemmli sample buffer, then boiled the cell lysate at

95 °C for 5 min. The protein was loaded in the well of 7.5% Mini–PROTEAN® TGX Stain–Free™ protein gels (Bio–Rad, Richmond CA, USA) and run the gel for 1 h at 180 V. The gel disassembled from the cassette and visualised via the Gel documentation system. Then, the gel was assembled to the transfer sandwich using Trans–Blot® Turbo™ mini PVDF transfer packs (Bio–Rad, Richmond CA, USA). Proteins were transferred onto PVDF membrane at 1.3 A for 7 min. Membranes were blocked with 5% skim milk/TBST for 1 h at RT and then probed with indicated primary antibody overnight at 4 °C and then blotted with appropriate horseradish peroxidase–conjugated secondary anti–rabbit antibody. Visualization was performed using an enhanced chemiluminescence kit (BioRad Inc., Hercules, CA) with Clarity™ Western ECL Substrate. Protein level was normalized to the matching densitometric value of the internal control β–actin.

2.4.5 Statistical analysis

All bioassay experiments were carried out in triplicate with a minimum of three replicates per assayed concentration. Data were expressed as means $\pm$ SEM (standard error of the mean). Statistical significance was assessed by One–way analysis of variance followed by Dunnett's test or the unpaired t–test using GraphPad Prism 8 (GraphPad Software, La Jolla CA, USA). Values of $p < 0.05$ were considered significant.

CHAPTER 3 PHYOTOCHEMICAL WORK

3.1 Introduction

A. lakoocha is a medium to large deciduous tree distributed in tropical countries of Asia. Puag–Haad, a product from aqueous extract of its heartwood, has been traditionally used as an anthelminthic medicine, and contains high amounts of OXY (Maneechai *et al.*, 2009). Previous pieces of literature including the traditional extraction reported that the method generally used was aqueous reflux extraction or boiling, which could retrieve high yield of active compounds (Mongolsuk *et al.*, 1957; Maneechai *et al.*, 2009; Preyavichyapugdee *et al.*, 2016; Borah *et al.*, 2017). Several publications used ethanol as an extracting solvent focusing on the main compound, OXY (Maneechai *et al.*, 2009; Povichit *et al.*, 2010; Singhatong *et al.*, 2010). whereas, a few studies used ethyl acetate to make it more soluble (Preyavichyapugdee *et al.*, 2016).

Geometric isomerism or configurational isomerisms (*cis–* or *trans–*) and stability of a compound in the environment also are important. In terms of stability, stilbenoids are sensitive to heat, air, light and oxidative enzymes. For example, ultraviolet and visible light could transform *trans–* to *cis–* isomerization of resveratrol (Silva *et al.*, 2013). The *trans* form is known to be the more predominant and stable natural form of resveratrol (Rius *et al.*, 2010). Therefore, the phytochemical properties of OXY illustrated in this chapter will be the background information for investigating its cytotoxicity.

3.2 Aims

To investigate the phytochemical profiles of the three *A. lakoocha* heartwood extracts, using chromatographic and spectroscopic methods. The stability of OXY was also investigated in different types of solutions including water, DMSO, methanol and acetone.

3.3 Results

3.3.1 Yield of extraction

The heartwood was ground into a powder and dried at 45–50 ℃ until constant weight. The powder was successively extracted with a reflux extraction using water and ethanol, and another fraction was extracted by a Soxhlet apparatus using ethyl acetate. The three extracts were obtained (Figure 17 and Table 4). As the three solvents used have different polarity index, the constituents of the plant were gradually extracted according to their affinity with each solvent. The highest yield percentage of extraction was that of ethanol with a 9.53 % recovery percentage while water and ethyl acetate yielded the lower extraction percentage of 7.9 % and 3.36 %, respectively.

Figure 17 *A. lakoocha* heartwood extracts a) water extract using reflux extraction; b) ethanol extract using reflux extraction; and c) ethyl acetate extract using Soxhlet apparatus.

Table 4 Extraction method and the extractive content.

	Powder weight (g)	Extract weight (g)	Yield
Water extraction	250.00	18.23	7.29
Ethanol extraction	250.00	23.83	9.53
Ethyl acetate extraction	800.00	26.88	3.36

3.3.2 Quantification of OXY and resveratrol

OXY was reported as the most abundant compound in the heartwood of *A. lakoocha* (Burns *et al.*, 2002; Maneechai *et al.*, 2009; Borah *et al.*, 2017). Therefore, the compound and the well–known stilbenoid, resveratrol were quantified in the three extracts using HPLC. The chemical profiles of the two compounds were shown in Figure 18 and Figure 19; OXY was a dominant single peak at the retention time (RT) 14.0 min in the three extracts, while resveratrol was found to be one of the minor peaks at the RT 17.4 min. The relative amount of the compounds were calculated and shown in Table 5; OXY was found to be the highest amount in ethyl acetate fraction of 642.26±0.28 µg/mL (64.23%), while in ethanol and water extracts were found to be roughly half at 378.14 µg/mL (37.81%) and 335.45 µg/mL (33.55%), respectively. Whereas, resveratrol was quantified as a minor compound, which was 0.65%, 0.45 % and 0.37% in ethyl acetate, ethanol and water extracts, respectively.
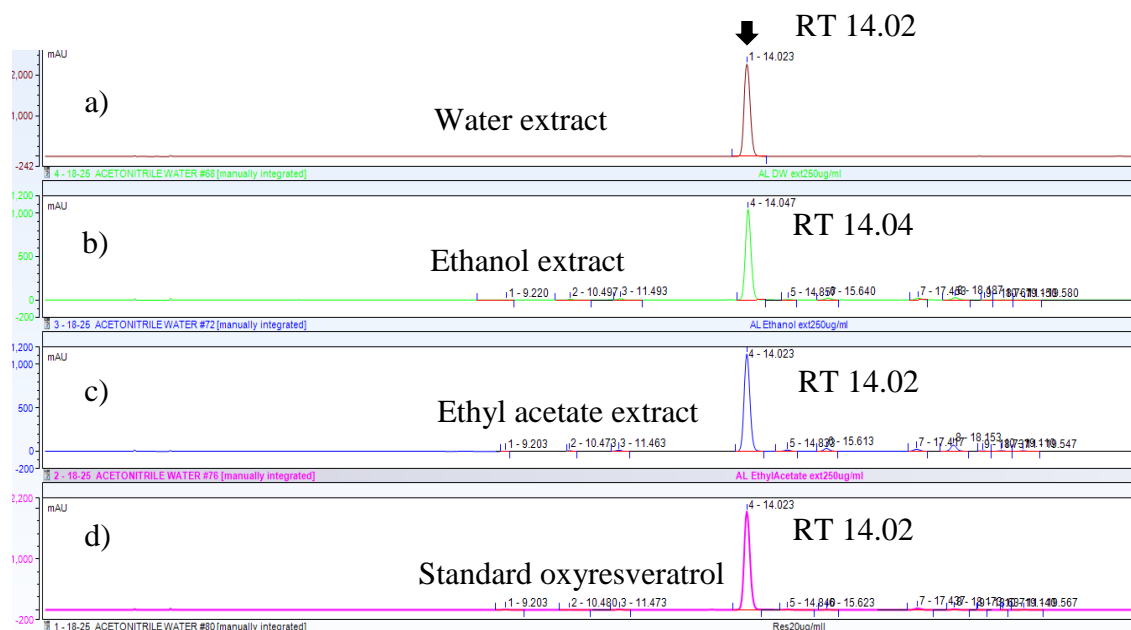
Figure 18 Chromatograms of OXY in the different three extracts, inj. vol. 20 µL, monitored at 320 nm   a) water extract 250 µg/mL; b) ethanol extract 250 µg/mL; c) ethyl acetate extract 250 µg/mL and d) Standard OXY 200 µg/mL.
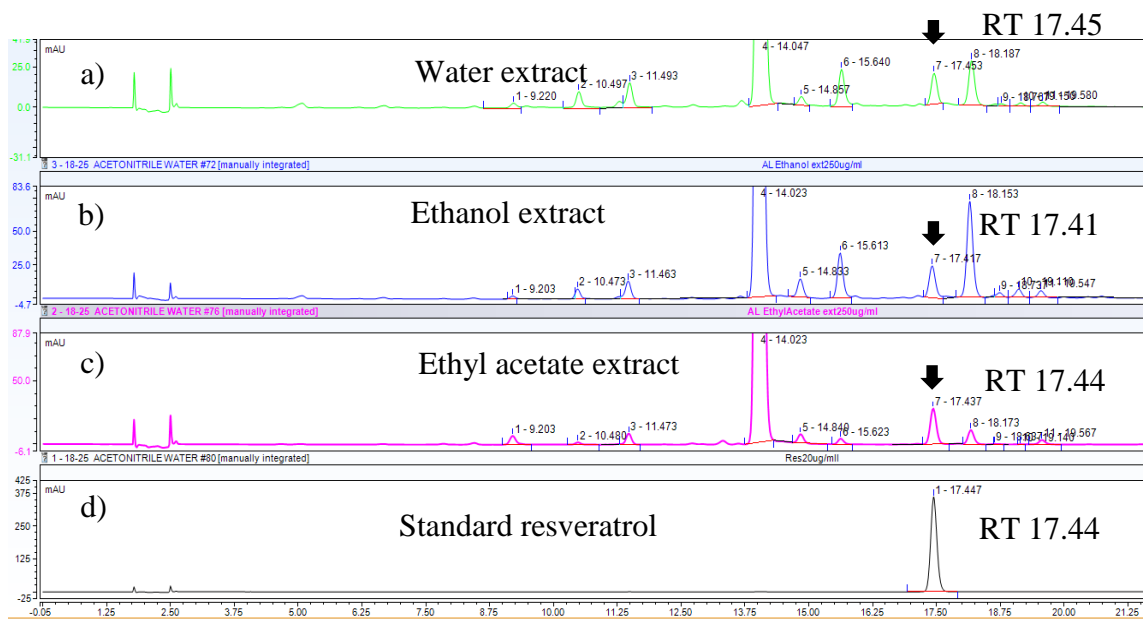
Figure 19 Chromatograms of resveratrol in the different three extracts, inj. vol. 20 µL, monitored at 320 nm a) water extract 250 µg/mL; b) ethanol extract 250 µg/mL; c) ethyl acetate extract 250 µg/mL; and d) Standard resveratrol 20 µg/mL.

Table 5 Quantity of OXY and resveratrol in water, ethanol and ethyl acetate extracts.

Values express mean ± SD (n=3).

	OXY (µg/mL±SD)	Yield (%±SD)	Resveratrol (µg/mL±SD)	Yield (%±SD)
Water extract	335.45±0.83	33.55±0.08	3.73±0.00	0.37±0.00
Ethanol extract	378.14±9.03	37.81±0.90	4.46±0.01	0.45±0.00
Ethyl acetate extract	642.26±0.28	64.23±0.03	6.54±0.14	0.65±0.01

3.3.3 Structure elucidation of *trans*–OXY

OXY collected from the peak of HPLC at the RT 14.0 min in the ethyl acetate extract was dried and obtained as a yellow powder. The authentication of the predominant peak was carried out using NMR with the ^{1}H–NMR and ^{13}C–NMR spectral patterns (Figure 20–22) of main peak were in good agreement with those of standard OXY and also with those reported in the literature (Povichit *et al.*, 2010).

The signals of ^{1}H–NMR and ^{13}C–NMR of the peak were assigned as follows: δ (ppm) 7.38 (1H, d, J=8.5 Hz, H–6), 7.31 (1H, d, J=16.4Hz, H–α), 6.86 (1H, d, J=16.4Hz, H–β), 6.50 (2H, s, H–2', H–6'), 6.40 (1H, d, J=2.4Hz, H–3), 6.38 (1H, dd, J=8.5, 2.4Hz, H–5), 6.22 (1H, s, H–4'). 158.7 (C–5' or C–3'), 158.7 (C–5' or C–3'), 158.2 (C–4), 156.0 (C–2), 140.7 (C–1'), 127.3 (C–6), 125.4 (olefinic C–β), 123.4 (olefinic C–α), 116.4 (C–1), 107.5 (C–5), 104.5 (C–6' or C–2'), 104.5 (C–6' or C–2'), 102.7 (C–3), 101.4 (C–4').
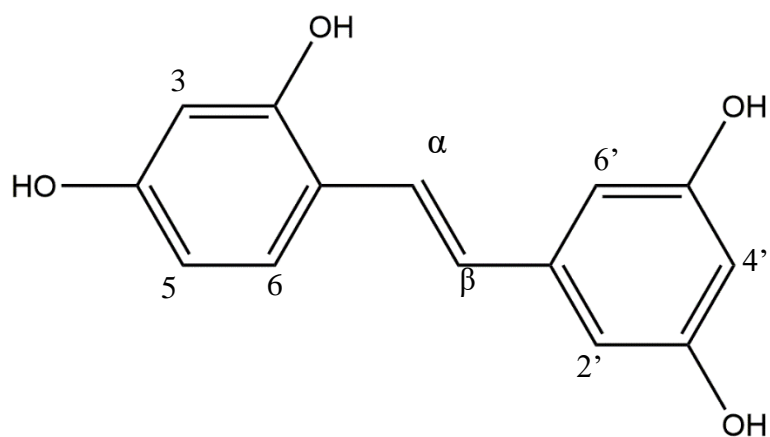
Position	δ_C	δ_H m (J in Hz)	Position	δ_C	δ_H m (J in Hz)
1	116.4	–	1'	140.7	–
2	156.0	–	2'	104.6	6.53 dd (2.1, 2.5)
3	102.7	6.44 d (2.4)	3'	158.6	–
4	158.2	–	4'	101.4	6.24 t (2.1)
5	107.5	6.39 dd (2.4, 8.4)	5'	158.6	–
6	127.3	7.41 d (8.4)	6'	104.6	6.53 dd (2.1, 2.5)
α	123.4	7.41 d (16.4)	2–OH		8.48 brs
β	125.4	6.89 d (16.4)	4–OH		8.30 brs
			3'–OH		8.09 brs
			5'–OH		8.09 brs

Figure 20 ^{13}C NMR (300 MHz, Acetone-d6) and [1]H (300 MHz, Acetone-d6) data of OXY.
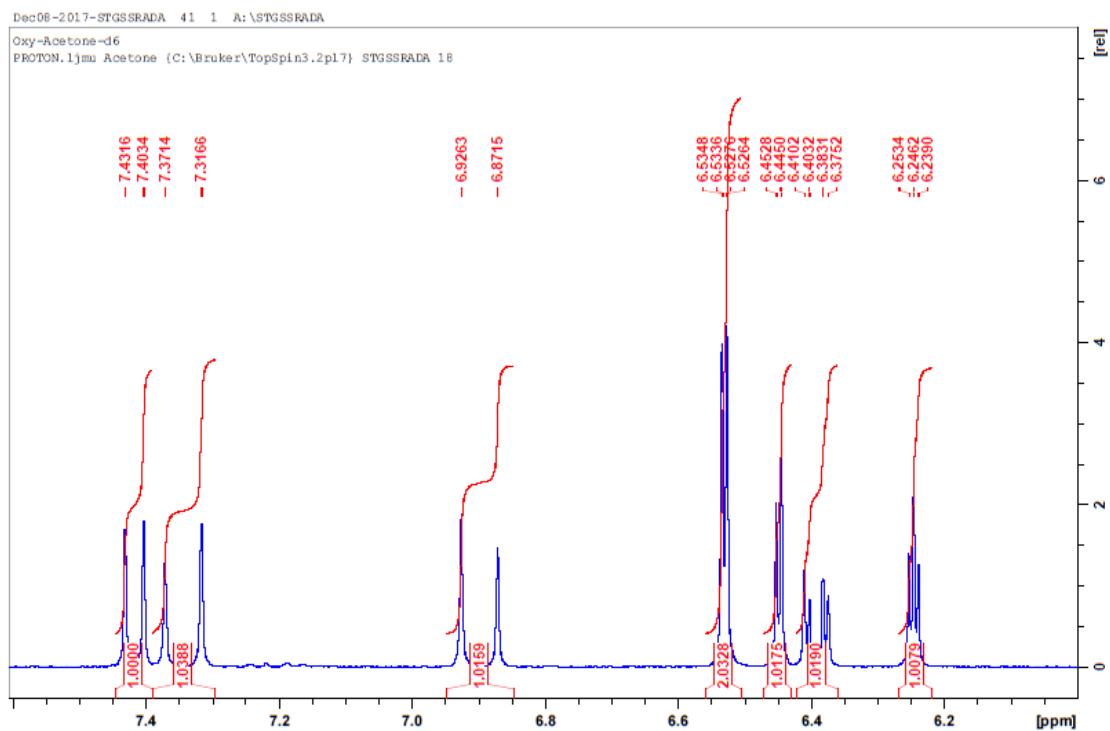
Figure 21 Integration values for the ^{1}H–NMR of OXY in acetone–d$_6$.
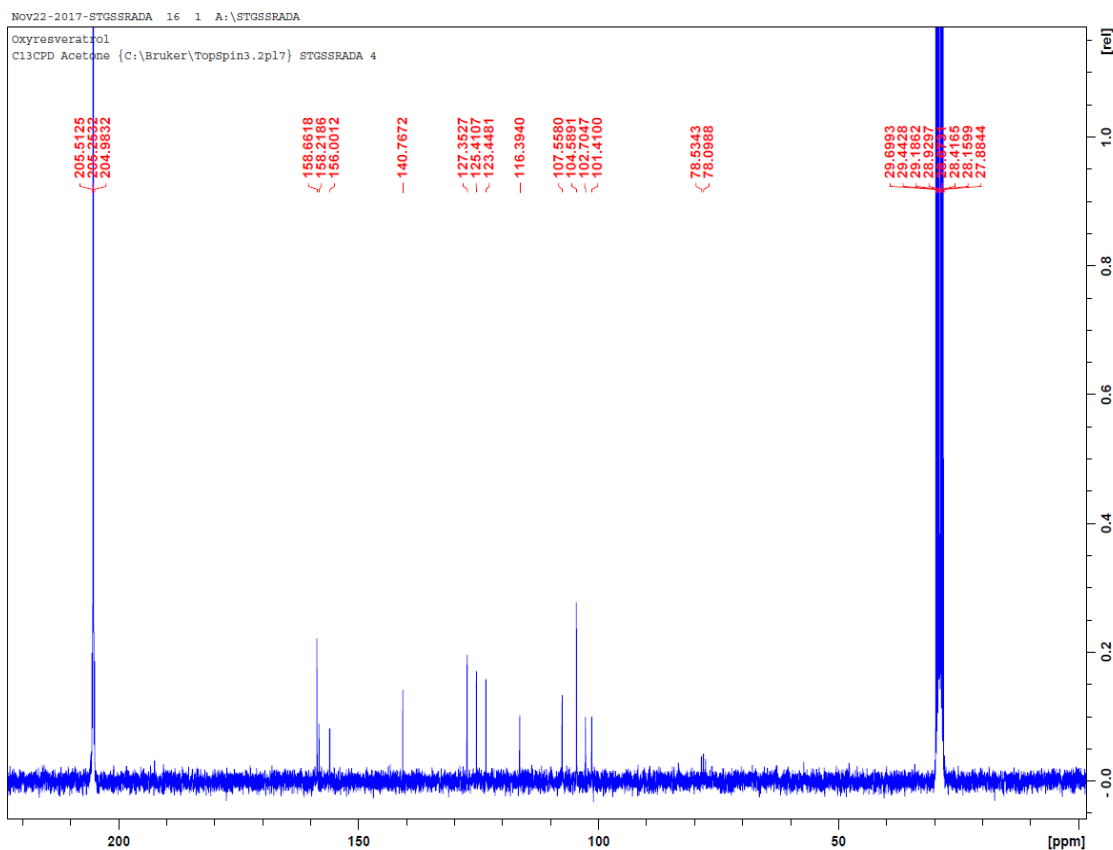
Figure 22 Integration values for the ^{13}C–NMR of OXY in acetone–d$_6$.

Mass spectra of standard OXY (Figure 23) gave the main and spectral patterns the same as the main peak detected at RT 14.0 in the three extracts of *A. lakoocha* (Figure 24–26). Its molecular formula $C_{14}H_{12}O_4$ was deduced from the ESI–MS spectrum in positive ion mode by the pseudomolecular ion peak at *m/z* 245 [M$^+$H]$^+$.

SS_MARIO OXYRESVERATROL STD 270218 841 (14.059) Cm (835:849)
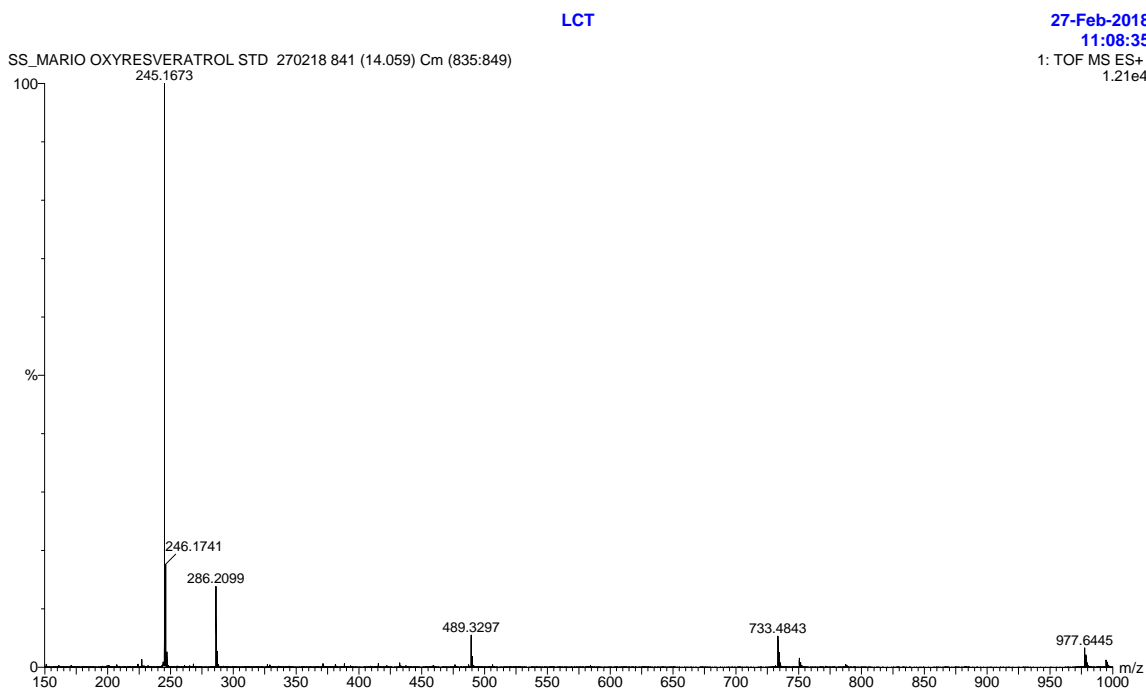
Figure 23 ESI–MS spectrum of standard OXY.

SS_MARIO WATER EXTRACT 1 CONC 270218 843 (14.093) Cm (836:850)
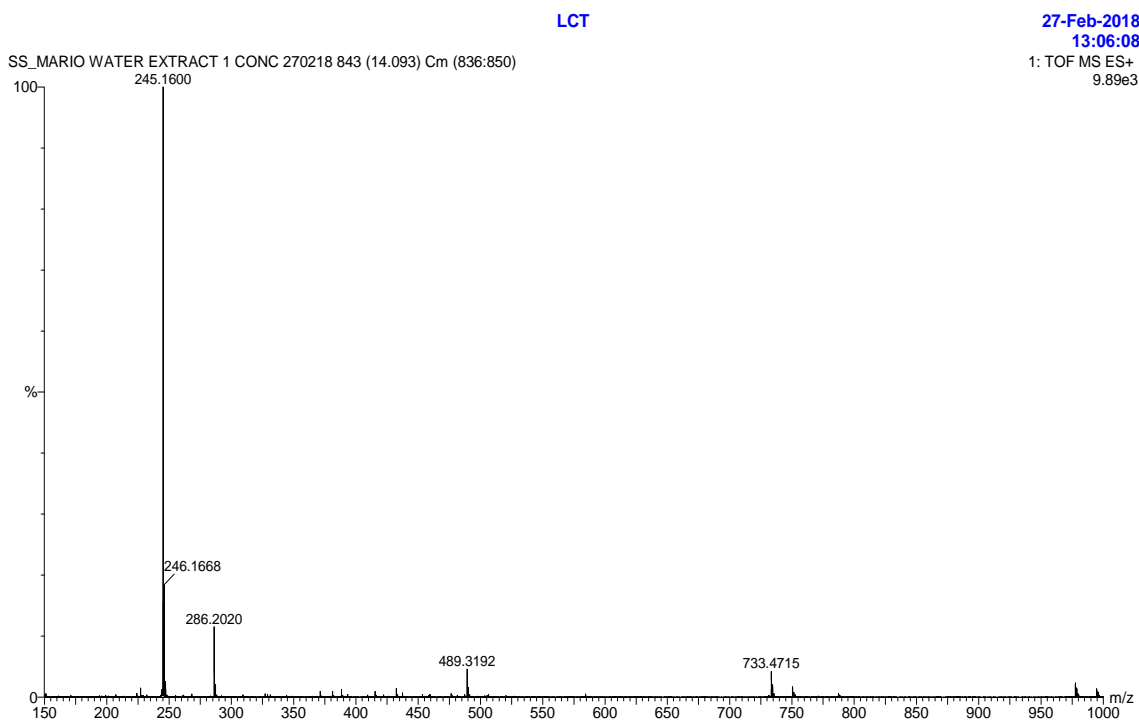
Figure 24 ESI–MS spectrum of the peak RT 14.0 in the water extract.

SS_MARIO ETHANOL EXTRACT 2 CONC 270218 843 (14.093) Cm (837:849)

1: TOF MS ES+
9.73e3
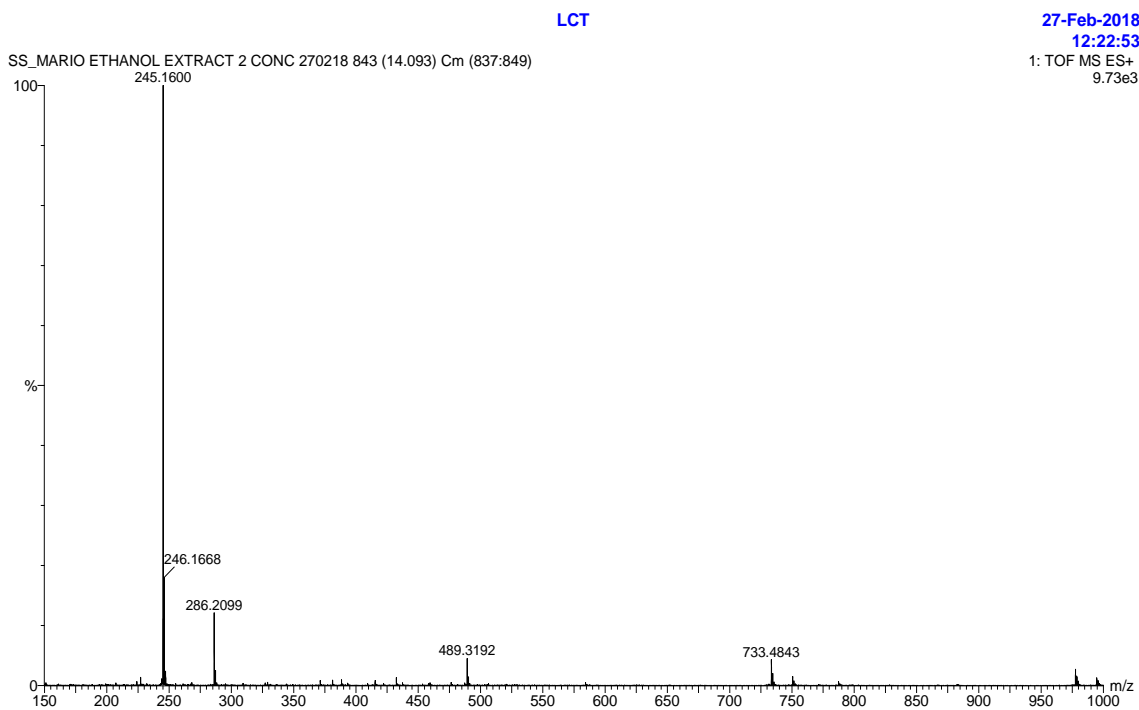
Figure 25 ESI–MS spectrum of the peak RT 14.0 in the ethanol extract.

SS_MARIO ETOAc EXTRACT 3 CONC 270218 842 (14.076) Cm (835:850)

1: TOF MS ES+
1.27e4
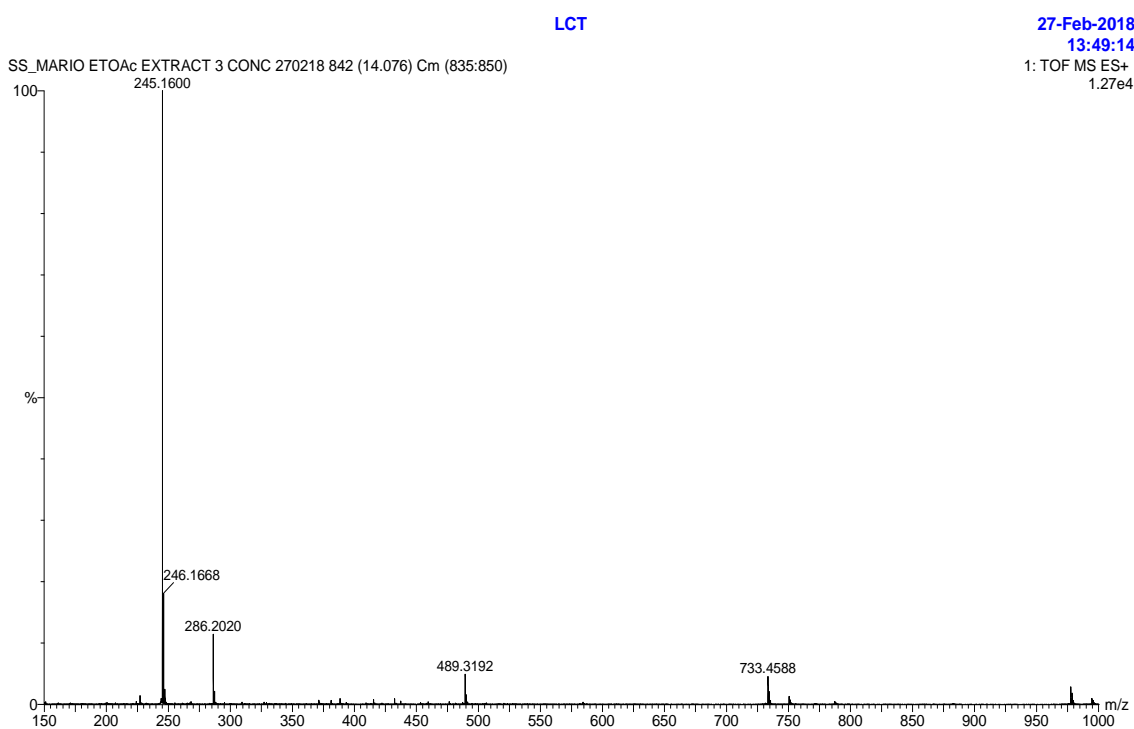
Figure 26 ESI–MS spectrum of the peak RT 14.0 in the ethyl acetate extract.

3.3.4 *Trans–*OXY stability test in different solvents

OXY dissolved in different solutions including D_2O, DMSO–d_6, CD_3OD and acetone–d_6 were investigated the configuration stability. The coupling constant of H (JHα and JHβ) was analysed at the time of 0, 0.5, 1, 2, 4, 6, 24 and 48 h. In all solutions, the coupling constants were quite stable in the normal laboratory environment for 48 h. The JHα in D_2O, DMSO–d_6, CD_3OD and Acetone–d_6 were 16.46±0.11, 16.46±0.02, 16.47±0.04 and 16.46±0.02, respectively. Whereas, The JHβ in D_2O, DMSO–d_6, CD_3OD and Acetone–d_6 were 16.50±0.00, 16.44±0.21, 16.42±0.01 and 16.41±0.01, respectively. The coupling constants are shown in Table 6.

Table 6 The coupling constant values (H_z) between H–α and H–β of OXY in different four solutions during the time 0–48 h.

h	D_2O		DMSO–d_6		CD_3OD		Acetone–d_6	
	JHα	**J**Hβ	**J**Hα	**J**Hβ	**J**Hα	**J**Hβ	**J**Hα	**J**Hβ
0	16.53	16.50	16.47	16.32	16.47	16.41	16.47	16.41
0.5	16.41	16.50	16.44	16.47	16.47	16.41	16.44	16.44
1	16.50	16.50	16.44	16.53	16.47	16.41	16.44	16.41
2	16.29	16.50	16.47	16.41	16.47	16.44	16.47	16.41
4	16.65	16.50	16.47	16.11	16.44	16.41	16.47	16.41
6	16.44	16.50	16.44	16.35	16.44	16.41	16.44	16.41
24	16.50	16.50	16.47	16.83	16.47	16.41	16.47	16.41
48	16.38	16.50	16.47	16.5	16.56	16.44	16.44	16.41

3.4 Discussion

A. lakoocha is one of the plants in the genus *Artocarpus* (Moraceae), which is an important source of edible fruit, timber and more importantly, it has been traditionally used for illness treatment in Thailand and Southeast Asia (Jagtap and Bapat, 2010). The traditional preparation of heartwood is by boiling to produce a yellowish extract, which is abundant in OXY (Mongolsuk *et al.*, 1957; Maneechai *et al.*, 2009; Saowakon *et al.*, 2009). OXY is a small polyphenolic compound belonging to stilbenes, which could be well dissolved in alcohol and some organic solvents. OXY yield extracted from the three different solvents revealed that it was the dominant stilbene in the heartwood extracts that showed a dominant peak of HPLC chromatogram in different detector's UV wavelengths of 260, 280 and 320 nm (Figure 19 a, b and c). Extraction using alcohol gave the highest yield (3.60 % w/w dried–heartwood powder), which was close to using hot water giving 2.44 % w/w dried–heartwood powder. Whereas extraction in ethyl acetate, the low polarity solvent, gave the lowest yield of 2.15 % w/w dried–heartwood powder. However, OXY extracted using ethyl acetate gave the highest purity of 64.23% OXY (HPLC), more or less two times higher than using the two solvents. Therefore, the dried extracted powder was found to show a bright yellow colour in ethyl acetate fraction compared to the two crude powders extracted with water and ethanol found to show brown–yellowish colour. Therefore, the traditional extracting method using boiled water retrieved a high amount of OXY (Mongolsuk *et al.*, 1957; Maneechai *et al.*, 2009; Preyavichyapugdee *et al.*, 2016; Borah *et al.*, 2017), which reported to show potent anthelmintic activity higher than the standard praziquantel at the concentration of 175 µg/mL (Saowakon *et al.*, 2009; Preyavichyapugdee *et al.*, 2016). There were around 10 minor peaks in the HPCL chromatogram of the three solvents when they were expanded. Each peak was a minor component compared to OXY, which was less than 1% in the extracts. One of the peaks assumed to be resveratrol (RT 17.4), which was quantified the amount of 0.37, 0.45 and

0.65 % w/w in water, ethanol and ethyl acetate, respectively. It has been reported previously that resveratrol was also found in *A. lakoocha* heartwood (Borah *et al.*, 2017).

Structure elucidation of OXY was carried out by spectroscopic analyses including 1D (^{1}H and ^{13}C NMR) and mass spectrometry. OXY collected from the dominant peak in ethyl acetate extract, which is the purest fraction. Mass spectrometry is a technique useful in the determination of the molecular weight of compounds, the possible molecular formula and fragmentation pattern (de Hoffmann *et al.*, 2007). This technique was implemented to identify the compound at the peak, which was the same retention time as the standard OXY.

OXY was evidently the most dominant compound in the three extracts of *A. lakoocha* heartwood. Extracting with ethanol gave a higher yield than what was achieved using either water or ethyl acetate. Whereas using ethyl acetate as the extracting solvent gave a higher purity than others did. The chemical profile of the extracts showed the main peak to be OXY (around 33–64%) and other peaks including resveratrol, which was lower than 1% detected. Mass and NMR spectroscopic analysis identified that the main peak presented in the three extracts was *trans*–OXY and this configuration was stable in different solutions of aqueous and some organic solvents in the normal lab environment. These provided the phytochemical information of OXY for studying its chemical and biological activities.

CHAPTER 4 PRO–OXIDANT ACTIVITIES OF OXY IN A CELL-FREE ENVIRONMENT

4.1 Introduction

OXY belongs to the group of phytochemicals known as hydroxystilbenoids, and has a molecular structure similar to the well–known phytochemical resveratrol (Riviere *et al.*, 2012). Both compounds demonstrate similar biological activities and are used in the treatment of atherosclerosis, inflammatory, pigmentation and carcinogenesis (Akinwumi *et al.*, 2018). Interestingly, however, several biological activities are unique to OXY (antivirus and anthelminthic) (Galindo *et al.*, 2011; Preyavichyapugdee *et al.*, 2016). Further, several reports suggest that OXY or the heartwood extract of *A. lakoocha* might cause DNA damage and cause oxidative stress (Singhatong *et al.*, 2010). Previous studies report that resveratrol and its derivatives are capable of double–stranded DNA cleavage specifically in the presence of copper ions and oxygen, generating ROS in the reaction. Speculation exists as to the exact mechanism responsible although it has been previously noted that Cu^+–Oxo complexes can cause DNA damage (Subramanian *et al.*, 2004). Piceatannol, a resveratrol derivative, is also able to fragment DNA in human peripheral blood (Azmi *et al.*, 2005). Copper at some certain extent is well–known to be one of the transition metals paying an important role in biological functions. However, It has been reported that significantly elevated levels of copper have been found in both serum and tissue of cancer patients (Kuo *et al.*, 2002). Moreover, elevated copper levels have been documented in breast, cervical, ovarian, lung, prostate, stomach cancers and leukemia. Serum copper concentration has also been found to correlate with tumour incidence and burden, malignant progression in Hodgkin's lymphoma, leukemic, sarcoma, brain, breast, cervical, liver and lung cancer (Gupte and Mumper, 2009). Some polyphenolic compounds are already well known to cause DNA damage and are being investigated as useful leads in the development of chemotherapeutic drugs (Yamada *et al.*, 1985).

In this study, we consequently investigated the ability of OXY from the heartwood of *A. lakoocha* to induce DNA damage and the mechanism by which the damage occurs.

4.2 Aims

To investigate the pro–oxidant properties of OXY and other stilbenes including the three extracts of *A. lakoocha* heartwood in the presence and absence of copper in a cell–free environment.

4.3 Results and discussion

4.3.1 DNA nicking assay

The gel electrophoresis pattern (Figure 27–30) showed the DNA nicking ability of OXY in the presence of 50 µM copper (II). Figure 27 shows the dose–dependent effect on DNA cleavage of OXY; in the condition of presenting only the plasmid DNA or the DNA + 50 µM OXY or the DNA + 50 µM Cu(OAc)$_2$, there was no evidence of DNA cleavage (lane 2–4). It was found that the compound damaged the double–stranded supercoil plasmid DNA dose–dependently (lane 5–10); 200 µM was by far the most active transforming all of the supercoil(S) DNA into nicked and a little linear(L) forms, while there was no nicking activity at the dose of 0.4–2.0 µM OXY (Figure 28). The DNA–nicking activity of OXY was found to be specific to the copper (II) ions, not to Fe(II) or Zn(II) shown in Figure 29. OXY in the presence of copper ion exhibited nicking DNA (lane5). Whereas, OXY or with the metal chelators themselves could not break the DNA strand (lane 3, 4, 6 and 8). Moreover, the molecule incubated with iron (II) and zinc (II) did not give a significant band of nicked–DNA (lane 7 and 9). The DNA cleavage of OXY was also

compared to the small molecular stilbenes including resveratrol and *trans–*stilbene. The DNA cleavage activity was shown in Figure 29. OXY posed the damage higher than resveratrol at the concentration of 50 µM (lane 3 and 4), while *trans–*stilbene did not show the activity (lane 5)*. A. lakoocha* extracts showed the DNA–breakage capability consistent with OXY (Figure 30). The three extracts could not break the DNA (lane 3–5), while the activity of each extract was found to pose the damage in the condition presenting copper ions and be dependent on the dose of the extracts used (lane 6–14). The three different concentrations of water extract (lane 6–8); there was complete damage to supercoil DNA at 200 µg/mL, which presented some linear fragment of the DNA (lane 6). While the nicking activity was lower at the concentrations of 25 µg/mL and 3.13 µg/mL, which transformed supercoil form to open circular form in a big band and small band, respectively (lane 7 and 8). Similarly, the effect of the three concentrations of ethanol extract posing slightly higher effect (lane 9–11), than those with the water extract. Whereas, ethyl acetate extract at the doses of 200 µg/mL and 25 µg/mL completely damaged supercoil DNA (lane 12 and 13) and partially damaged at the lowest concentration treated (lane 14).
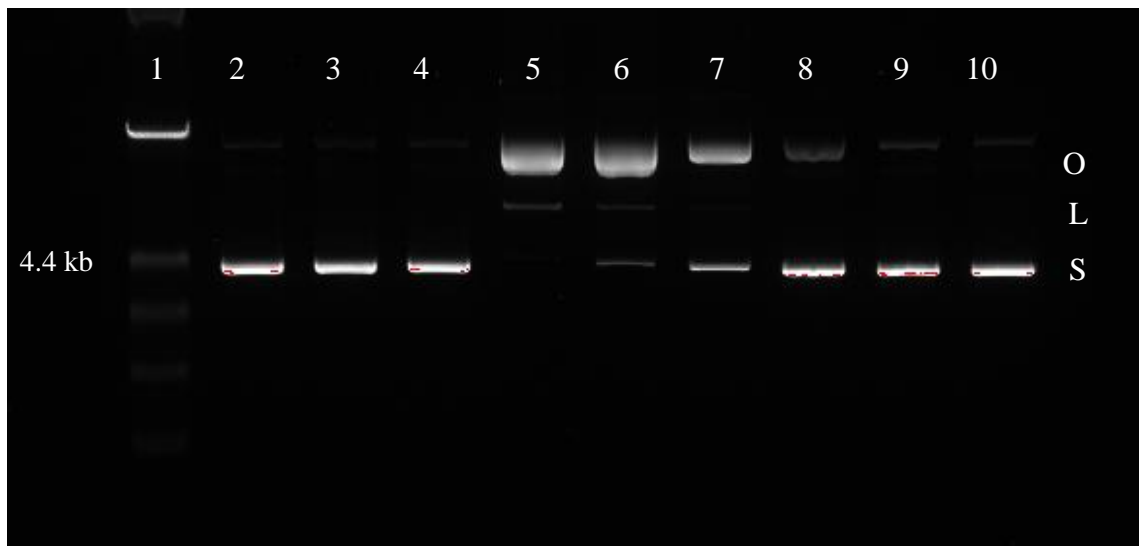
Figure 27 Gel electrophoresis pattern of supercoiled pBR322 plasmid DNA cleavage by six different concentrations of OXY in the presence of $Cu(OAc)_2$ (50 μM).

Lane 1: Ladder, Lamda DNA Hind III digest
Lane 2: pBR322
Lane 3: pBR322+50 μM OXY
Lane 4: pBR322 + 50 μM $Cu(OAc)_2$
Lane 5: pBR322 + 50 μM $Cu(OAc)_2$ + 200 μM OXY
Lane 6: pBR322 + 50 μM $Cu(OAc)_2$ + 100 μM OXY
Lane 7: pBR322 + 50 μM $Cu(OAc)_2$ + 50 μM OXY
Lane 8: pBR322 + 50 μM $Cu(OAc)_2$ + 10 μM OXY
Lane 9: pBR322 + 50 μM $Cu(OAc)_2$ + 2 μM OXY
Lane 10: pBR322 + 50 μM $Cu(OAc)_2$ + 0.4 μM OXY

O = open circular form or nicked DNA
L = linear form
S = circular form or supercoiled DNA
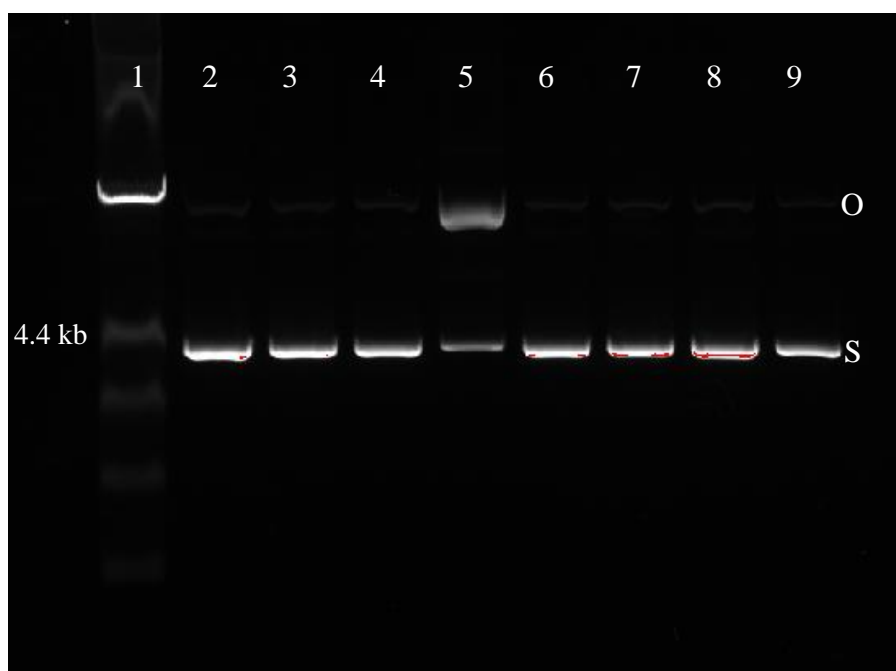
Figure 28 Gel electrophoresis pattern of supercoiled pBR322 plasmid DNA cleavage by 50 µM OXY in the presence of different chelating metals; $Cu(OAc)_2$, $FeCl_3 \cdot H_2O$ and $ZnCl_2$.

Lane 1: Ladder, Lamda DNA Hind III digest

Lane 2: pBR322

Lane 3: pBR322+50 µM OXY

Lane 4: pBR322 + 50 µM $Cu(OAc)_2$

Lane 5: pBR322 + 50 µM $Cu(OAc)_2$ + 50 µM OXY

Lane 6: pBR322 + 50 µM $FeCl_3$

Lane 7: pBR322 + 50 µM $FeCl_3$+ 50 µM OXY

Lane 8: pBR322 + 50 µM $ZnCl_2$

Lane 9: pBR322 + 50 µM $ZnCl_2$ + 50 µM OXY

O = open circular form or nicked DNA

S = circular form or supercoiled DNA
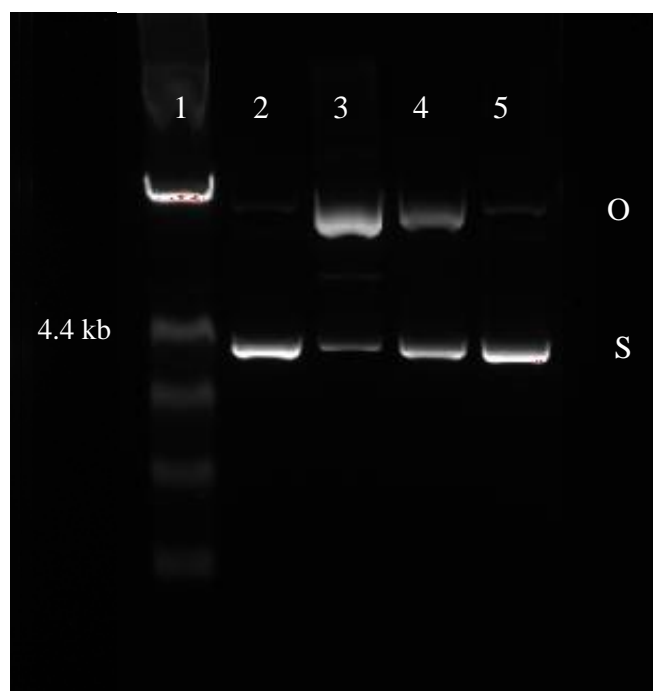
Figure 29 Gel electrophoresis pattern of supercoiled pBR322 plasmid DNA cleavage by

50 µM OXY, 50 µM resveratrol and 50 µM *trans*–stilbene in the presence of Cu(OAc)$_2$.

Lane 1: Ladder, Lamda DNA Hind III digest

Lane 2: pBR322

Lane 3: pBR322+50 µM OXY

Lane 4: pBR322+50 µM resveratrol

Lane 5: pBR322+50 µM *trans*–stilbene

O = open circular form or nicked DNA

S = circular form or supercoiled DNA
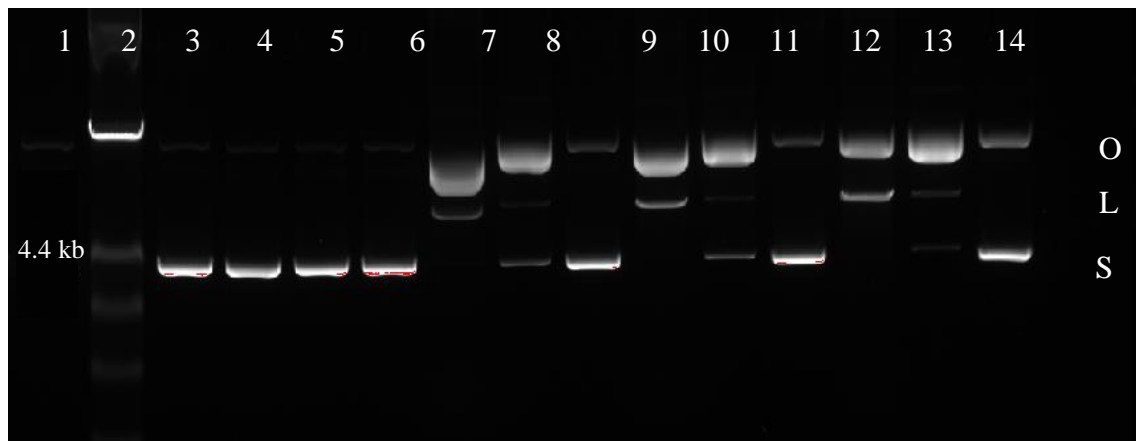
Figure 30 Gel electrophoresis pattern of supercoiled pBR322 plasmid DNA cleavage by

A. lakoocha heartwood's extracts in the presence and absence of Cu(OAc)$_2$.

Lane 1: Ladder, Lamda DNA Hind III digest

Lane 2: pBR322

Lane 3: pBR322+25 µg/mL water–extracted fraction

Lane 4: pBR322+25 µg/mL ethanol–extracted fraction

Lane 5: pBR322+25 µg/mL ethyl acetate–extracted fraction

Lane 6: pBR322 + 50 µM Cu(OAc)$_2$ + 200 µg/mL water–extracted fraction

Lane 7: pBR322 + 50 µM Cu(OAc)$_2$ + 25 µg/mL water–extracted fraction

Lane 8: pBR322 + 50 µM Cu(OAc)$_2$ + 3.13 µg/mL water–extracted fraction

Lane 9: pBR322 + 50 µM Cu(OAc)$_2$ + 200 µg/mL ethanol–extracted fraction

Lane 10: pBR322 + 50 µM Cu(OAc)$_2$ + 25 µg/mL ethanol–extracted fraction

Lane 11: pBR322 + 50 µM Cu(OAc)$_2$ + 3.13 µg/mL ethanol–extracted fraction

Lane 12: pBR322 + 50 µM Cu(OAc)$_2$ + 200 µg/mL ethyl acetate–extracted fraction

Lane 13: pBR322 + 50 µM Cu(OAc)$_2$ + 25 µg/mL ethyl acetate–extracted fraction

Lane 14: pBR322 + 50 µM Cu(OAc)$_2$ + 3.13 µg/mL ethyl acetate–extracted fraction

O = open circular form or nicked DNA

L = linear form

S = circular form or supercoiled DNA

4.3.2 Reactive oxygen species assay

The ability of OXY or *A. lakoocha* extracts to generate reactive radical species in the presence or absence of copper (II) was compared with its derivatives including resveratrol and *trans*–stilbene. Figure 31 shows the dose–dependent formation of OXY increasing the relative fluorescence signals. The formation of the relative fluorescence sharply increased from around 800 – 2,400 RFU at the low doses between 1.56 – 50 µM and linearly raised from around 2,400 – 3,300 RFU at the doses of 50 – 200 µM–OXY. These results indicated that OXY in the presence of 50 µM–copper (II) generated ROS dose–dependently. Whilst in the absence of copper ions, OXY did not cause ROS (the negative control). Comparison with its derivatives (Figure 32), OXY generated ROS formation higher than resveratrol at the same concentrations (1.56–200 µM) which resveratrol generated the fluorescence signals from around 579–2,600 RFU. While the formation did not raise in *trans*–stilbene. ROS generation by the three extracts of *A. lakoocha* was also investigated shown in Figure 33; the relative fluorescence signals generated by ethyl acetate extract was the highest compared to the others in the condition with copper. It dramatically increased at the doses tested (1.56–200.00 µg/mL). Whereas, the formation of water and ethanol extracts were similar; the relative fluorescence of the ethanol extract slightly increased from the baseline around 900 RFU at 1.56 µg/mL to reach 3,000 RFU at 200 µg/mL, but of which water extract showed a little bit lower than ethanoic extract at the highest dose. However, there was no significant formation of ROS raised by the three extracts in the absence of copper.
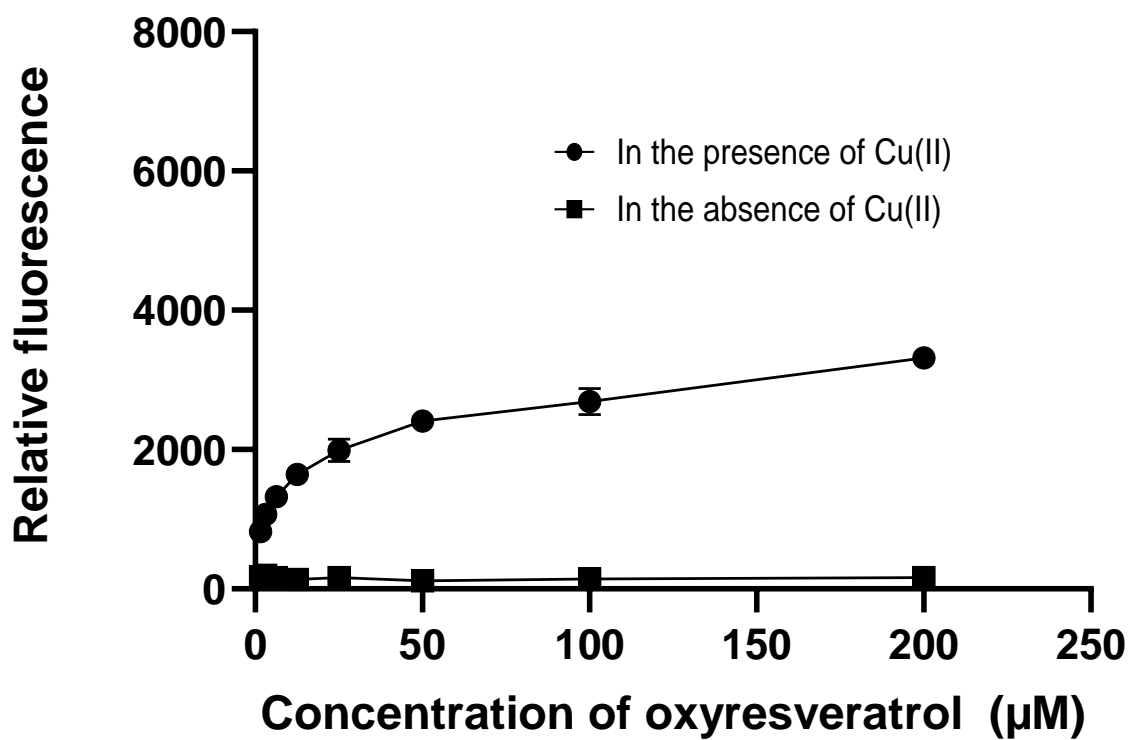
Figure 31 The relationship between the concentration of copper (µM) and the relative fluorescence in the presence of Cu(OAc)$_2$ (50µM). Values express mean ± SD (n=3).
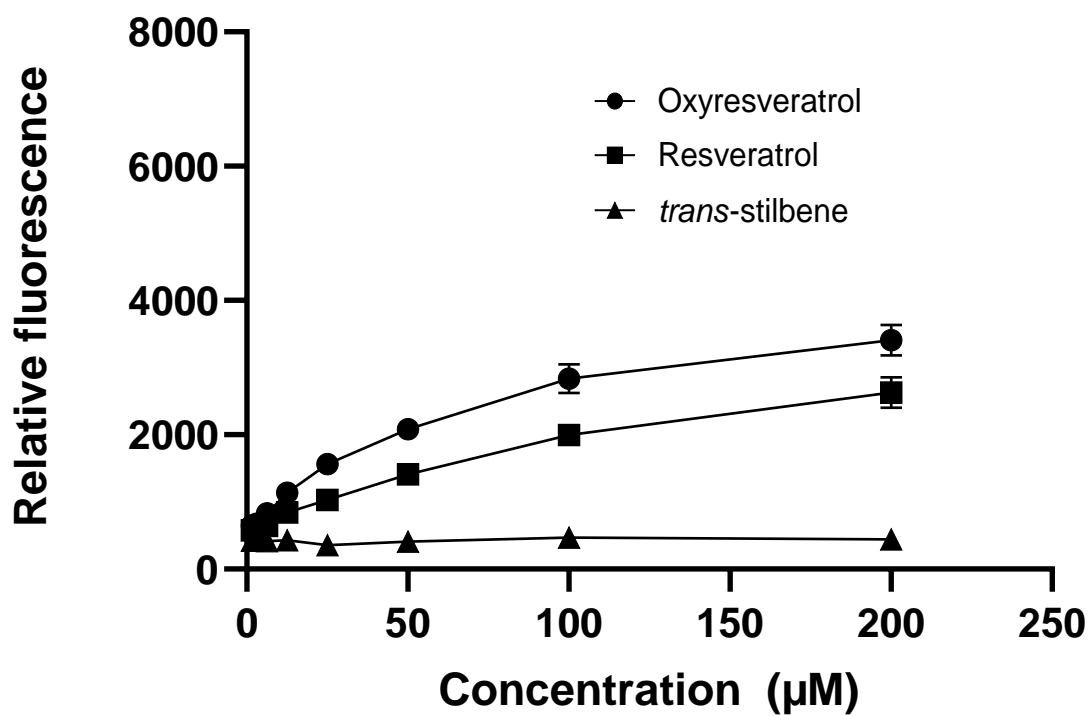
Figure 32 The relationship between the concentration of stilbenes (µM) and the relative fluorescence in the presence of $Cu(OAc)_2$ (50µM). Values express mean ± SD (n=3).
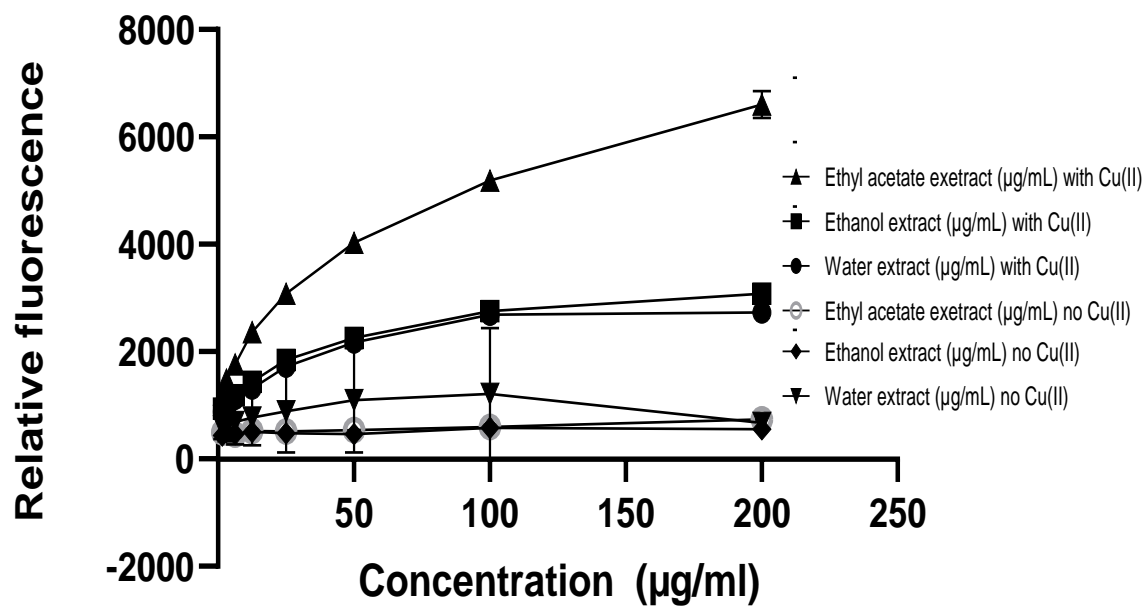
Figure 33 The relationship between the concentration of *A. lakooch*a heartwood extracts (µg/mL) and the relative fluorescence in the presence and absence of Cu(OAc)$_2$ (50µM). Values express mean ± SD (n=3).

4.3.3 Copper reducing assay

The Copper (II) reducing abilities of OXY was investigated using the Cu (I)–stabilizing reagent bathocuproine disulfonic acid. Copper (I), the product of the reactions between OXY or resveratrol with copper (II) reacted to bathocuproine disulfonic acid generating cu(I)– bathocuproinedisulfonate complex, which was detected at the wavelength 484 nm. Figure 34 showed the absorbance at 484 nm detected the reaction's product of OXY and copper (II); it was raised dose–dependently from 0.04–0.65 OD at the concentrations of 1.56–100 µM–OXY. While there was no signal increased in the condition absent of copper (II). These results indicated that OXY reduced copper (II) to copper (I). When compared to its derivatives, the reducing ability of OXY was more potent compared to resveratrol. However, the formation of copper (I) in the reactions of the two stilbenes tended to remain constant at the concentration of 50–100 µM. The *trans*–stilbene clearly showed the absorbance at the baseline in all concentrations tested (Figure 35).
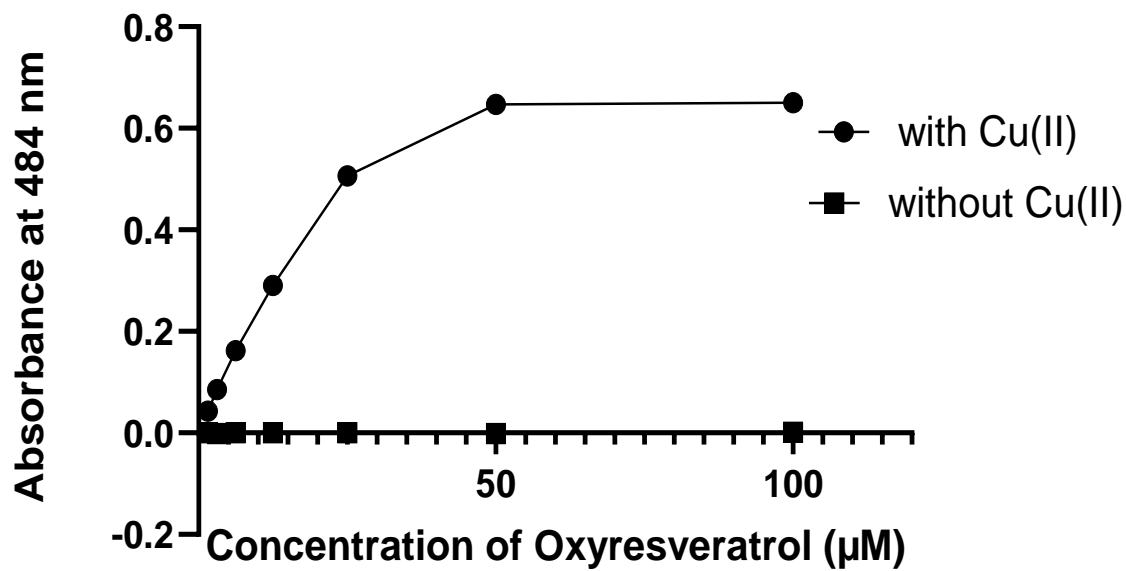
Figure 34 The relationship between the concentration of OXY (µM) and the absorbance of the Cu(I)– bathocuproinedisulfonate complex at 484 nm in the presence and absence of Cu(OAc)$_2$ (50µM). Values express mean ± SD (n=3).
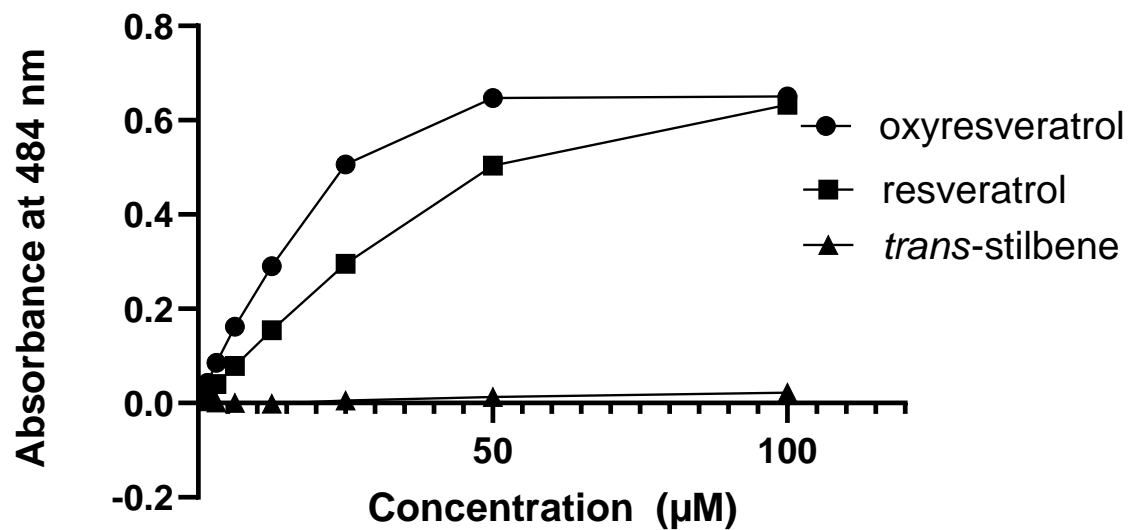
Figure 35 The relationship between the concentration (µM) of OXY, resveratrol or *trans*–stilbene and the absorbance of the Cu(I)–bathocuproinedisulfonate complex at 484 nm in the presence of $Cu(OAc)_2$ (50µM). Values express mean ± SD (n=3).

4.3.4 GSH assay

The depletion of authentic GSH was investigated in the reaction of OXY and copper (II) ions. After ROS was generated in the reaction, the authentic reduced GSH 50 nmol/mL was incubated in the reaction for 1 hour. Then the remaining GSH was measured using spectrophotometry.

The reduced GSH decreased from 100 % of control to around 93% at the concentration of OXY treated (6.25–400 µM) in the presence of copper (II). However, the GSH amount remained close to 100% of control in the reaction of OXY without copper. These results were consistent with ROS assay previously. The graph is illustrated in Figure 36. The depletion of reduced GSH was also investigated for resveratrol and *trans*–stilbene; OXY reduced GSH dose–dependently between 6.26–400 µM. The GSH depletion ability of OXY at the highest dose (400 µM) was greater than that of resveratrol (Figure 37).
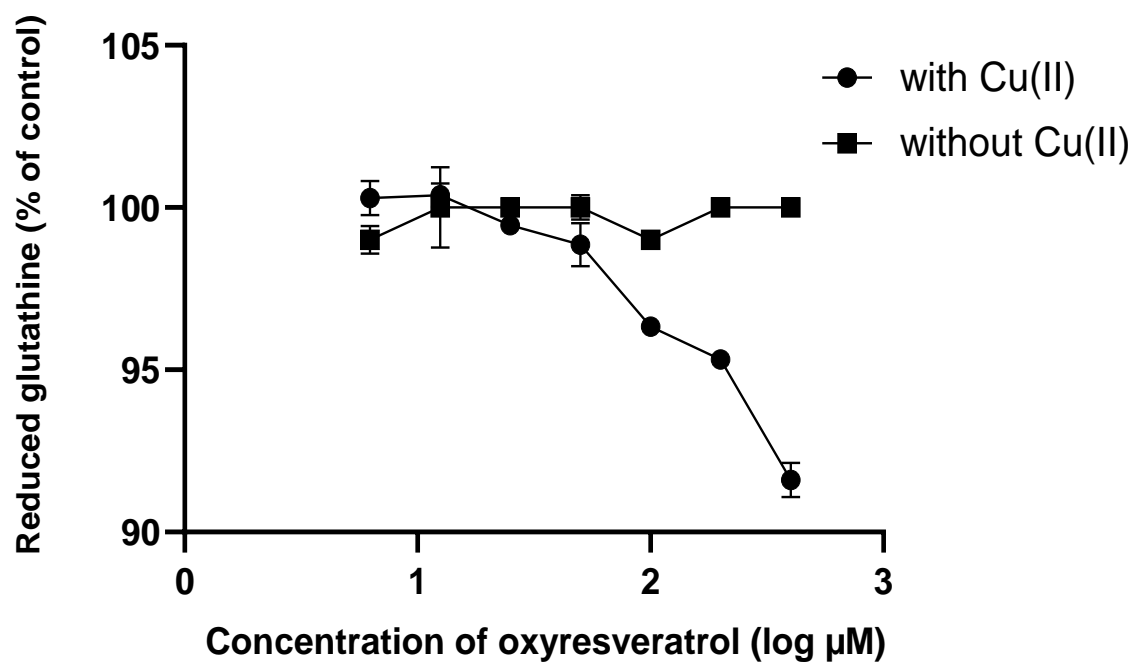
Figure 36 The relationship between the concentration (log µM) of OXY or Cu(OAc)$_2$

(50µM) and glutathione (% of control). Values express mean ± SD (n=3).
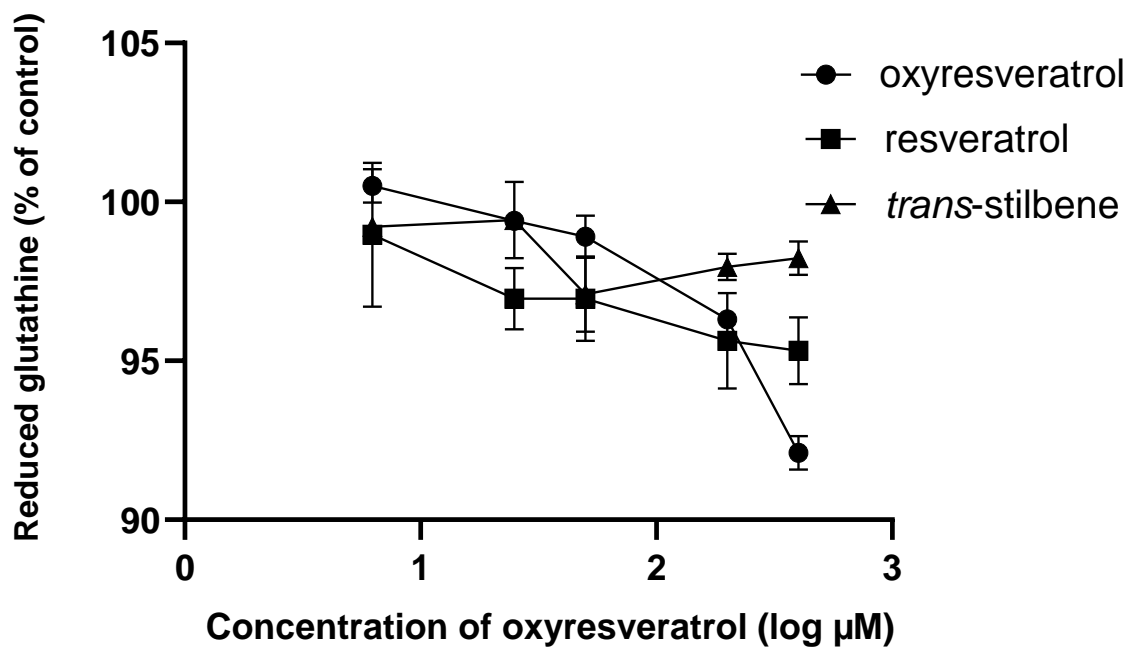
Figure 37 The relationship between the concentration (µM) of OXY, resveratrol and *trans*–stilbene and glutathione (% of control). Values express mean ± SD (n=3).

4.4 Discussion

Reports of DNA breakage mediated by hydroxystilbenoids has gained momentum in the last few years, especially resveratrol and derivatives because the compounds are capable of double–stranded DNA breakage specifically in the presence of copper ions. The condition included oxygen to promote a Cu^+–oxo intermediate and some amount of superoxide damaging the DNA. This property was expected to be the promising mechanisms of cytotoxic or anti–cancer agents (Subramanian *et al.*, 2004). The DNA break in cellular systems was confirmed in lymphocytes isolated from human peripheral blood using comet assay; the results indicated that piceatannol, which has more hydroxyl group than resveratrol, was more potent activity. Whereas, *trans*–stilbene, which does not have any hydroxyl groups, is inactive (Azmi *et al.*, 2005). Some polyphenolic compounds have been already well–known to behave as pro–oxidants in the condition of presenting only themselves or oxidized metal ions such as Fe^{3+}, Cu^{2+}, Zn^{2+} or Ni^{2+}, which trigger the Fenton–mediated ROS generation (Yamada *et al.*, 1985; Lopes *et al.*, 1999).

This current study found that OXY showed a higher ability to cleave supercoiled plasmid pBR322 DNA. The higher doses of the compound could break the supercoiled form into open circular and linear forms. The DNA nick ability was specifically induced by copper ions, one of the most abundant metal ions in the biological system (Kalinowski *et al.*, 2016), which might trigger the Fenton mediated ROS generation the same mechanism as other phenolic compounds previously reported (Moran *et al.*, 1997). More interestingly, the three extracts also showed to nick DNA at similar doses to OXY. The three dilutions of *A. lakoocha* heartwood including 200, 25 and 3.13 µg/mL of ethyl acetate extract were equivalent to OXY around 525, 65 and 8 µM, respectively. Therefore, the damaged bands of DNA were similar to those in Figure 27. Copper at some certain extent is well–known to be one of the transition metals paying an important role in biological functions. However, it

has been reported that significantly elevated levels of copper have been found in both serum and tissue of cancer patients (Kuo *et al.*, 2002).

The copper (I) detected tended to be dose–dependent on OXY. However, at the dose of 50–100 μM the formation was constant. The formation of copper (I) remained constant because it could be oxidized by O_2 or $O_2^{\bullet-}$ in the reaction and returned to copper (II) (Subramanian *et al.*, 2004; Valko *et al.*, 2004; Gupte and Mumper, 2009). The results of the three stilbenes also correlated well with their ROS generating abilities.

Glutathione (GSH) is one of the most vital antioxidants in living organisms. It is able to prevent damage to an important intracellular component from ROS, the toxicity of xenobiotic electrophiles and maintaining redox homeostasis (Forman *et al.*, 2009). Glutathione exists in reduced (GSH) and oxidized (GSSG) states. The ratio of reduced glutathione to oxidized glutathione within cells is a measure of cellular oxidative stress, therefore the conversion of GSH to oxidised GSSG is used as a model to measure ROS generated in any reaction (Babich *et al.*, 2009). The pro–oxidant activity of OXY, which caused GSH depletion was similar to the activity noted for phytochemical extracts in a previous report (Babich *et al.*, 2009). *Gingko biloba* leaf extract was found to cause pro–glutathione oxidation both in cell–free reaction and in HSC–2 cells. The property of pro–oxidant of the plant–derived compounds is illustrated and well documented to link directly to apoptosis causing cytotoxicity to cancers (Vallejo *et al*, 2017).

In this chapter should be concluded that OXY exhibited the pro–oxidant activity generating ROS in the specific presence of copper (II) ions. This could cause damage to double–stranded DNA into the open chain or linear forms. OXY was able to show higher capability than resveratrol at the same doses, while the *trans*–stilbene did not show the activity. The three *A. lakoocha* extracts also showed the damaged DNA consistent with the amount of OXY presented. OXY caused damage to DNA in a dose–dependent manner reducing copper

(II) to copper (I) and depleting GSH. In consideration of these findings, it can be implied that OXY has the potential to be developed as a promising anticancer drug candidate and to cause cytotoxicity to cancer cells.

CHAPTER 5 CYTOTOXICITY OF OXY IN THE PRESENCE COPPER (II)

5.1 Introduction

OXY has been shown to possess various potent bioactivities with the main property being an antioxidant (Lorenz *et al*., 2003), anti–inflammatory (Lee *et al*., 2015), tyrosinase inhibition (Likhitwitayawuid *et al*., 2006) anti–virus (Chuanasa *et al*., 2008) and anti–cancer (Rahman *et al*., 2017).

In consideration of its chemical structure, which is similar to the well–known antioxidant and anticancer property, resveratrol, OXY may share anti–cancer property. The previous report found that OXY posed cytotoxicity *in vitro* to some kinds of cancerous cell lines such as human hormone–dependent breast cancer (T47D), human cervical adenocarcinoma (HeLa), human non–small–cell lung carcinoma (A549) (Chatsumpun *et al.*, 2016). There have been no reports regarding the molecular targets or biological pathways affected by elevated copper levels in cancer cells.

5.2 Aims

To identify a cell line model (transformed and non–transformed) in which cytotoxicity is demonstrated in response to OXY.

5.3 Results

5.3.1 Growth curve analysis

The growth curve of different kinds of cancerous cells in the study including A549, CACO–2, HepG2, MCF7, PC–3, RAW264.7 and the two non–transformed cell lines including MRC–5 and MCF10A, was investigated (Figure 38). Growth curves of the cells

were investigated in 96–well plates to optimize the cell number used in the cytotoxicity assay. The cells were grown in growth medium depending on cell designation and then the cell number was counted for four consecutive days. The initial cell number that gave the growth curve in log phase was chosen to be optimal and used in the MTT cytotoxic assay. Growth curves of the eight cells used in the experiment were shown in Figure 39. A549, CACO–2, HepG2, MCF10A, MCF7 have an epithelial-like morphology. MRC–5 and PC–3 cells have fibroblast-like morphology. While RAW 264.7 cells are monocyte/macrophage-like cells. The initial cell number for seeding in 96–well plates were chosen from the results in Figure 39. All cell lines were initially seeded at $5x10^3$, $7.5x10^3$, $1x10^4$ and $2x10^4$ cells and left in the incubator for 4 days. The cell number was counted every day. Figure 39 showed that A–549, CACO–2, HepG2, MCF10A and RAW 264.7 increased cell number quickly; the seeding densities of $1x10^4$ and $2x10^4$ cells reached the plateau phase in 3 days. MRC–5 cells had linear growth curves for the three initial seeding densities. Whereas, MCF7 and PC–3 cells grew more slowly; Therefore, A549, CACO–2, HepG2, RAW264.7, MRC–5 and MCF10A cells were selected to be used at a seeding density of 5x103 cells/ well, while MCF7 and PC–3 cells were used at a seeding density of 1x104 cells/well for MTT assay.
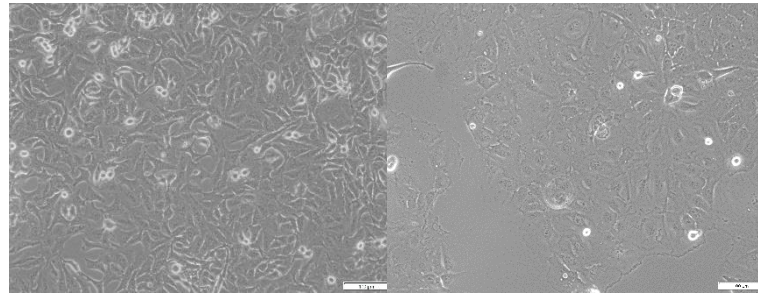
A549   CACO–2
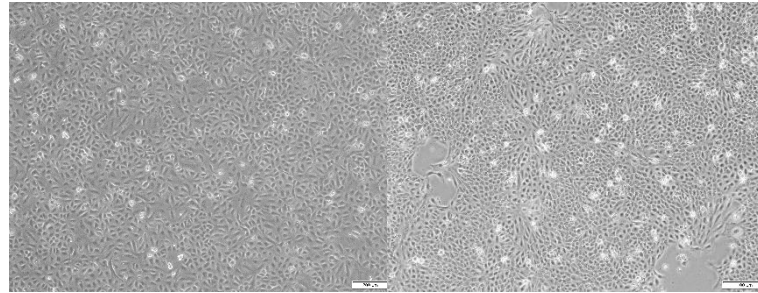
HepG2   MCF10A
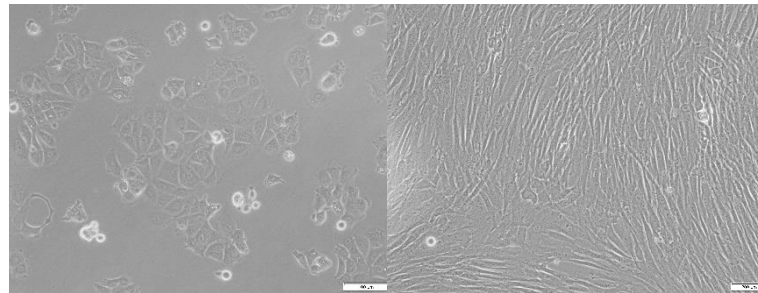
MCF7   MRC–5
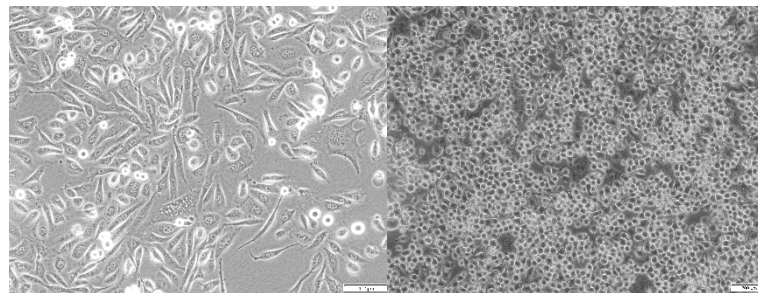
PC–3   RAW 264.7

Figure 38 Cell lines used in the cytotoxicity assay. Magnification = ×20, scale bars =

200 µm.
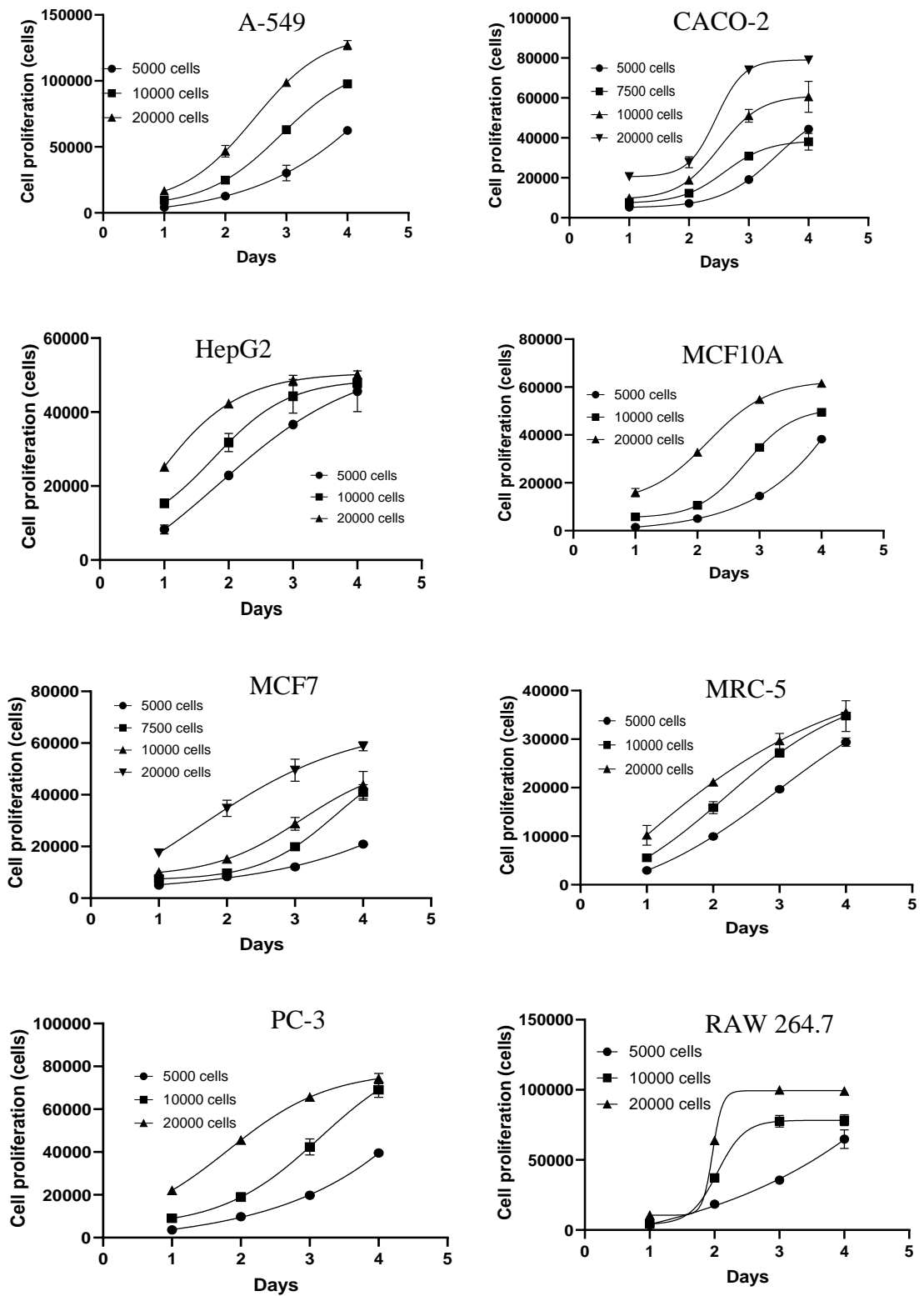
Figure 39 Growth curves of the cells used in the study with different initial cell numbers counted for four consecutive days. Values express mean ± SD (n=3).

5.3.2 Cytotoxicity of copper

Toxicity of Cu(OAc)$_2$ was also evaluated to make sure that the copper added to the reaction did not directly cause damage to the cells. The viability of the cells after incubated to different concentrations of copper (II) for 48 h shown in Figure 40.

Copper tended to cause toxicity to the cells dose–dependently between the doses of 0.13–400 μM, except in RAW 264.7 cells. A549 and MCF10A cells were significantly sensitive and vulnerable to the low doses of 1.25 up to 400–μM copper. CACO–2 cells were in moderate; 25 μM caused significant (P<0.01) toxicity and at the high dose of 400 μM reduced cell viability down to around 10%. Whereas, HepG2, MCF7, MRC–5 and PC–3 cells were tolerant to Cu(OAc)$_2$ at the dose between 0.13– 100 μM, while the higher doses reduced cell viability significantly (P<0.01) compared relatively to the control.
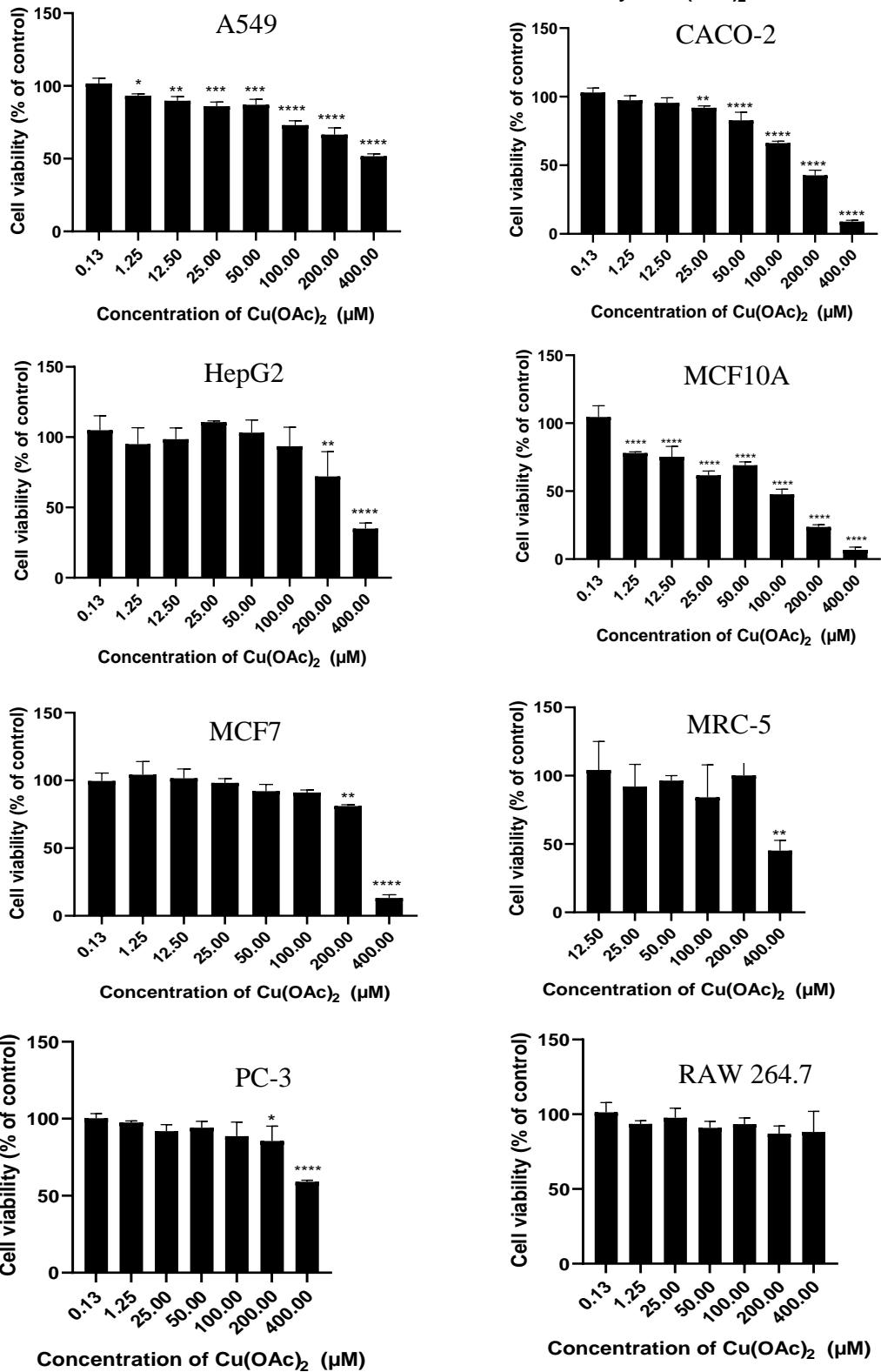
Figure 40 Toxicity of Cu(OAc)$_2$ to the cells used in the study; the cells were incubated with Cu(OAc)$_2$ with different concentrations (0.13 – 400 µM) for 48 h. Then cell viability was detect by MTT assay. Values express mean ± SD (n=3). Statistical analysis was carried out using One–way ANOVA and Dunnett's post hoc test. The significant difference was compared relatively to the control (*P < 0.1, **P < 0.01, ***P < 0.001 and ****P < 0.0001).

5.3.3 Toxicity of OXY to cancer cells in the presence or absence of copper

This assay aimed at investigating the effect of copper ions on the cytotoxicity of OXY in cancerous cells. The cells were either pre–treated with 50µM $Cu(OAc)_2$ for 24 h (OXY–Pre–Cu), or OXY in medium supplemented with 50µM $Cu(OAc)_2$ (OXY+Cu) and no $Cu(OAc)_2$ (OXY) then exposed to OXY for 48 h. The cell viability was calculated to the percentage of cell control and the non–linear regression graph of log concentration (µM) and percent viability shown in Figure 41. The inhibitory concentration (IC_{50}) of each condition was generated and summarized in Table 7. The cells that OXY caused cytotoxicity to several cell lines ranged from the highest (low IC_{50}) to the lowest (high IC_{50}) were MCF7, HepG2, PC–3, RAW 264.7 and A549 with the IC_{50} of 30.64±4.79, 104.47±0.82, 106.90±8.63, 115.95±11.28 and 148.63±4.48 µM, respectively. Whereas, the compound showed low toxicity to CACO–2, MCF10A and MRC–5 ($IC_{50} > 200$ µM). Interestingly, copper (50 µM) tended to make OXY less or no toxic to the cells. The copper–preincubated cells (OXY–Pre–Cu^{2+}) (MCF7, PC–3 and RAW 264.7) were not significantly different (P>0.1) in the IC_{50} values compared to the OXY–treated cells without copper (OXY). There was mild toxicity but not significantly different (P>0.1) from MCF10A and MRC–5. OXY in the presence of copper (OXY+Cu^{2+}) showed less toxicity to the cells than treated with only OXY, which was a significant difference (P<0.1) in MCF7 and RAW 264.7 cells. Doxorubicin was used as a standard cancer cell–toxic drug.
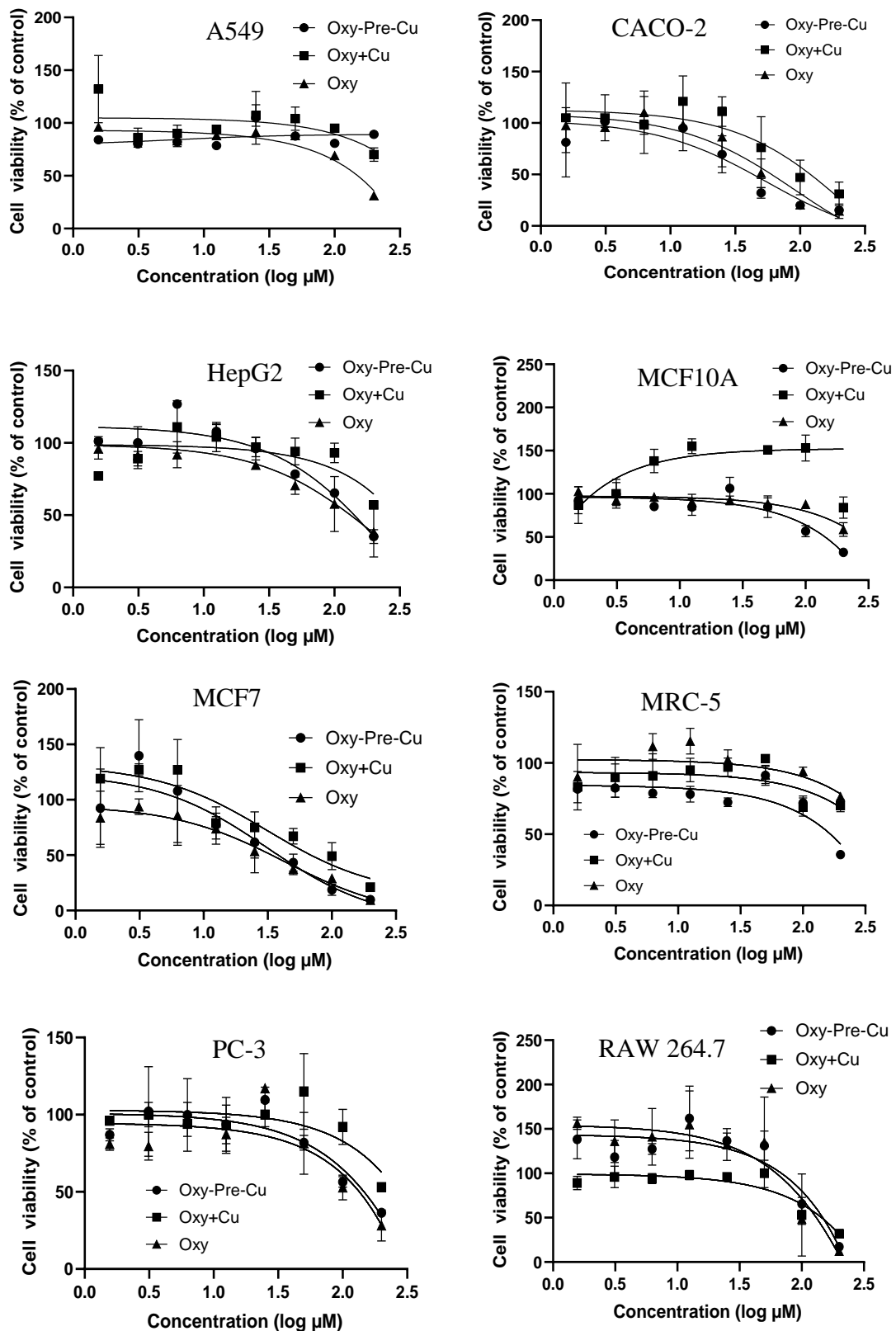
Figure 41 Cell viability (% of control) after treated with different concentrations of OXY, pre–treat with copper and treat with OXY. OXY–Pre–Cu = cells pre–treated with 50 µM Cu(OAc)$_2$ for 24 h then rinsed with medium and treated with OXY; OXY+Cu = cells treated with OXY in the medium supplemented with 50µM Cu(OAc)$_2$; and OXY= cells treated with OXY without Cu(OAc)$_2$. Values express mean ± SD (n=3).

Table 7 Inhibitory concentration (IC$_{50}$, µM) of OXY to the cells; A549, CACO–2, HepG2, MFC7, PC–3, RAW 264.7, MRC–5 and MCF10A cells in medium; cells pre–treated with 50µM Cu(OAc)$_2$ for 24 h (OXY–Pre–Cu), OXY in medium supplemented with 50 µM Cu(OAc)$_2$ (OXY+Cu) and no Cu(OAc)$_2$ (OXY). Values express mean ± SEM (n=3). Statistical analysis was carried out using One–way ANOVA and Dunnett's post hoc test or unpaired t-test. The significant difference was compared relatively to the control (OXY) (*P < 0.1 and **P < 0.01).

	OXY **(µM± SEM)**	**OXY–Pre–Cu^{2+}** **(µM± SEM)**	**OXY+Cu^{2+}** **(µM± SEM)**	**Doxorubicin** **(µM± SEM)**
A549	148.63±4.48	>200	>200	2.21±0.08
CACO–2	>200	>200	>200	13.39±4.34
HepG2	104.47±0.82	136.90±12.08*	>200	3.44±0.33
MCF7	30.64±4.79	31.31±8.25	102.17±24.37*	0.86±0.29
PC–3	106.90±8.63	109.35±9.63	>200	12.61±1.97
RAW 264.7	115.95±11.28	125.90±4.32	164.28±4.87**	0.86±0.29
MRC–5	>200	164.16±6.91	>200	1.51±0.04
MCF10A	>200	112.44±16.87	>200	NA

5.3.4 Investigation of synergizing activity between copper and OXY

MCF7 and HepG2 cells, the cell lines that demonstrated the greatest degree of OXY–induced toxicity, were chosen to study synergizing effect with copper. According to the method modified from (Andrade Volkart *et al.*, 2017), they were pre–treated with different three levels of copper including 25, 50 and 100 µM then treated with OXY. The results were illustrated in Figure 42 showing that the cells pre–incubated with the higher levels of copper were not significantly different (P>0.1) compared to those treated only with OXY in the two cell lines.
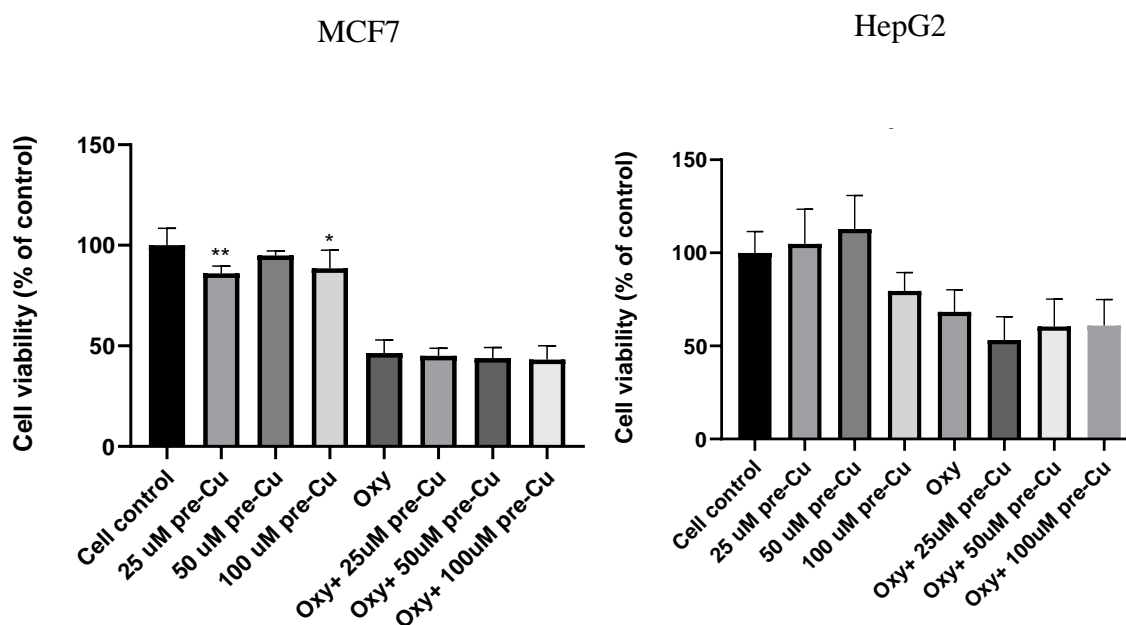
Figure 42 Cell viability (% of control) after pre–incubated with three different concentrations of copper for 24 h and then treated with 50 µM (MCF7 cells) or 100 µM (HepG2 cells) of OXY for 48 h. Values express mean ± SD (n=3). Statistical analysis was carried out using One–way ANOVA and Dunnett's post hoc test. The significant difference was compared relatively to the control (*P < 0.1 and **P < 0.01).

5.3.5 Determination of intracellular ROS production in the reactions between copper and OXY

ROS formation was investigated in the cells pre–treated with copper (II) and then treated with the fixed–dose of OXY. The intracellular ROS detected was not raised after the cells were pre–treated with copper or OXY compared relatively to cell control. Moreover, there was no correlation between the dose of copper and the time of treatment to the ROS formation. The relative fluorescence (% of control) of the conditions investigated in Figure 43.
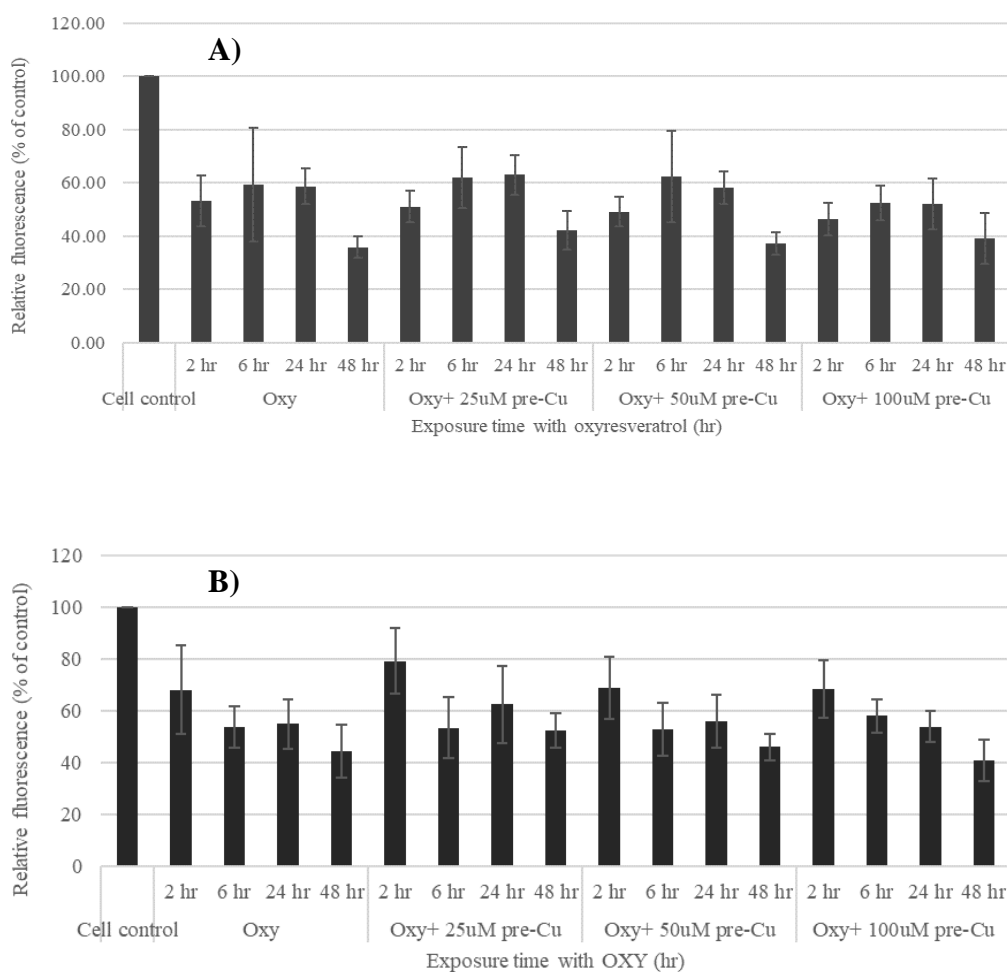
Figure 43 Relative fluorescence (% of control) of ROS formation in MCF7 cells (A) and HepG2 cells (B) after pre-treatment with three different concentrations of Cu(OAc)2 for 24 h followed by with 50 µM (for MCF7) or 100 µM (for HepG2) OXY for 2, 6, 24 and 48 h, respectively. Signal values are compared relative to the control (mean ± SD (n=3).

116

5.4 Discussion

The cancerous cells chosen to test cytotoxicity in this chapter were chosen following consideration of previous literature that reported elevation of copper level in serum and tissue of cancer patients (Gupte and Mumper, 2009)

The main cell viability–cytotoxicity assay used was MTT metabolic assay, which is suitable for high throughput screening of the cell viability that transformed MTT into formazan product. The amount of formazan is generally proportional to the number of metabolically active viable cells in log phase growth as demonstrated by the linearity of response. Therefore, each cell line needed to be evaluated the growth curve during the period of 48–72 h before implementing the assay (Riss *et al*, 2013). The results showed that the optimal cells seeded in 96–well plate were between $5x10^3$–$1x10^4$ cells/well, which gave log phase growth during the treating time.

$Cu(OAc)_2$ caused toxicity to almost of the cells at high doses. Some cell lines were vulnerable at the very low dose (1.25 µM or 25 µM) such as MCF10A and CACO–2 cells. The previous study reported that copper(II) overload caused toxicity to HepG2 (220.5 ± 23.8 µg/mL) by inducing stress genes including c–fos, HMTIIA, HSP70, GRP78, RARE, GADD153, and RARE (Tchounwou *et al.*, 2008). Copper was (200 µM) also found to induce cytotoxicity in the human colon carcinoma cell line HT–29, which correlated with the induction of cell apoptosis, increased oxidative stress, alteration of mitochondrial β oxidation, and the configuration of lipid metabolism and energy metabolism (Xiao *et al.*, 2016).

In the condition supplemented with 50 µM $Cu(OAc)_2$, demonstrated copper(II) has the tendency to make OXY less toxic to the cells than Oxy–Pre–Cu^{2+}. Copper ions oxidized OXY the same way as Fe(II) has been reported previously for piceatannol, catechin, epicatechin, hydroxytyrosol, affeic acid, chlorogenic acid, rosmarinic acid, gallic acid or

resveratrol (Shingai *et al.*, 2011). Moreover, the medium with sodium bicarbonate can oxidize or reduce the amount of phytochemicals such as resveratrol (Yang *et al.*, 2010). Therefore, the potency of OXY was attenuated. Both approaches were found to make OXY less cytotoxic. It can be assumed that copper penetrated into MCF7 cells but the amount was very low. Additionally, the intracellular copper was lower in the presence of stilbenoids (Volkart *et al*, 2017).

The synergizing effect of copper (II) to OXY toxicity was investigated by varying the pre–incubated doses of copper in the presence of 50 µM OXY in MCF7 cells or 100 µM OXY in HepG2 cells. There was no significant difference (P>0.1) between the doses applied in the two kinds of cell. Moreover, there was no significant ROS formation changed in the conditions of pre–incubated with copper. Therefore, the assumption of intracellular copper enhancing the toxicity of OXY by generating ROS has not been verified in this study.

In consideration of the abundant concentration of copper in breast cancer cells, OXY may potentially be cytotoxic to breast cancer cells *in situ*. Therefore, MCF7 cell line was chosen to be a model to study the molecular effects of OXY.

In this chapter, it can be concluded that OXY caused toxicity to MCF7, HepG2, PC–3, RAW 264.7 and A549 cells with EC_{50} of 30.64±4.79, 104.47±0.82, 106.90±8.63, 115.95±11.28 and 148.63±4.48µM, respectively without causing toxicity to the normal cells. Whereas, copper was likely to make OXY less toxic. OXY and OXY–copper (II) did not increase intracellular ROS in MCF7 and HepG2 cells.

CHAPTER 6 GENE EXPRESSION

ANALYSIS

6.1 Introduction

The microarray–based technique or GeneChip (Figure 44) is a high–throughput technology for genetic explorations including gene expression analysis. It consists of the number of technologies that have been developed as a single platform, which provides extensive information on gene networks and functions on drug efficacy and toxicity (Taylor *et al.*, 2005). Over the years, the kind of platform has been extensively implemented to evaluate the effect of OXY and derivatives, especially of resveratrol on several cancerous cell lines, such as multiple myeloma cells (Geng and Klionsky, 2008) and colorectal cancer (Lee *et al.*, 2018). However, OXY showed toxicity to MCF7 cells in this study and has several unique properties different from other stilbenoids. In consideration of this, gene expression and cellular consequences of OXY exposure need to be elucidated to provide the insight into the mechanism of actions of OXY in the cancer cells model.

To explore the mechanisms of action of a new drug or a promising compound, there are several platforms which may be used.

In the work reported here, the microarray was implemented using the human Clariom S arrays (a 400 format array) (Affymetrix Inc., Santa Clara, CA, USA) as the gene probe. The targets or the RNA samples were obtained from MCF7 cells treated with OXY at the concentrations of 0, 50, and 100 μM for 24 h. The controls and data analysis followed the manufacturer's recommendations. The genes most affected were then validated using qPCR analysis.
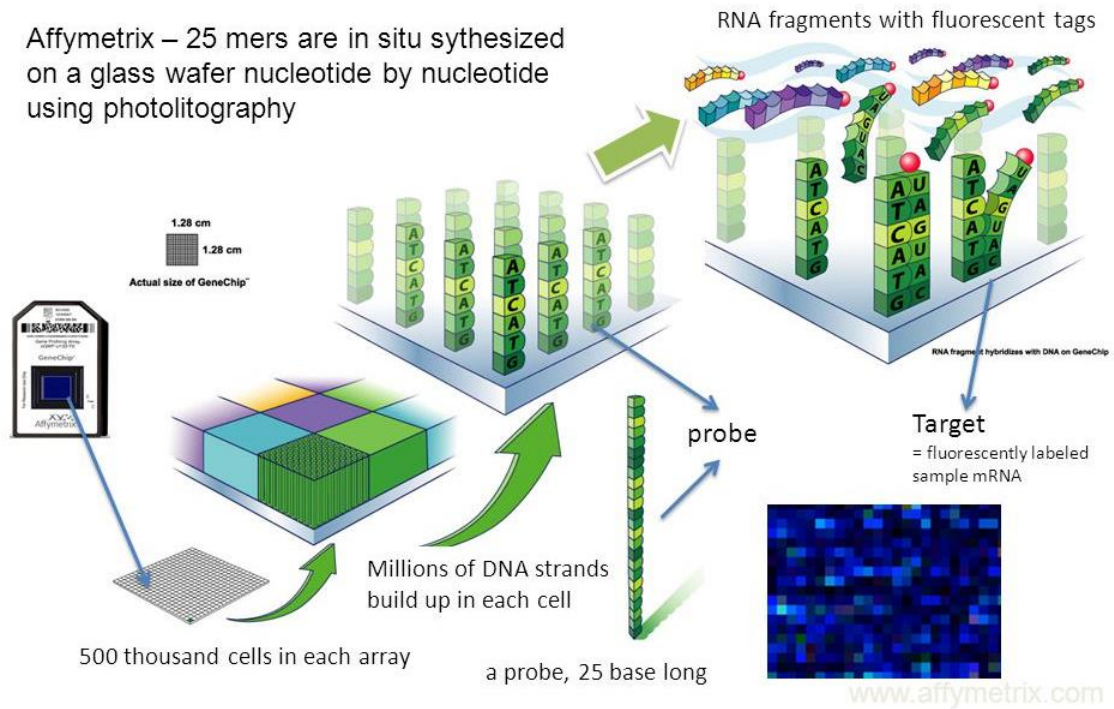
Figure 44 Affymetrix microarrays: Photolithographic synthesis of oligonucleotides on microarrays. A chip consists of hundreds of thousands of microscopically small probe cells. Each cell contains millions of copies of oligonucleotide sequences which serve as template for the hybridisation of the probes with their fluorescently labelled mRNA targets. The fluorescent signals are read by a high definition laser scanner and are combined into one raw expression value per probe set (Affymetrix, 2017).

6.2 Aims

To elucidate gene–level expression profile, and assess changes in key genes and pathways that are involved in the biological response to OXY using microarray and quantitative polymerase chain reaction analysis.

6.3 Results

6.3.1 Microarray assay

Global expression patterns of genes and pathways were obtained using microarray technology and data analysis software. The genes responsive to the treatment of OXY for 24 h was performed in three biological replicates, the samples proceeded as described in the materials and methods in chapter 2 (page 48-58). After analysis, the labelling and hybridising controls have passed the criteria. The number of different significantly (P<0.1) expressed genes under both conditions compared to the control group was observed. The gene expression summary in Figure 45 and Figure 46. The expressed genes in some significant pathways were illustrated in Figure 47.

Total 686 genes were differentially expressed in the 50 µM–treated groups; among these, 262 were upregulated and 424 were downregulated genes. While, 2,338 genes were differentially expressed in the 100 µM–treated groups; among these, 907 were upregulated and 1,431 were downregulated genes.

More than 80% of the gene population changed in the two treatments were the multi–complex genes. Therefore, the genes altered were the combinations of coding, noncoding and/or pseudogene. While the genes less than 20% were coding, noncoding and unassigned genes.

WikiPathways (wikipathways.org), a biology community maintained website that displays biological pathways, allowed to identify those in the most relevant biological mechanisms, pathways and functions of the genes altered by OXY treatments in MCF7 cells.

The affected genes from these analyses showed that the most affected processes under both conditions of OXY treatment were cell cycle control, DNA repair and autophagy, as well as apoptosis pathway (Figure 47). Majority of the genes in cell cycle control and DNA repair were downregulated, while those in apoptosis and autophagy were upregulated dose–dependently.

Expression Analysis Settings:
- Gene-Level Fold Change < -2 or > 2
- Gene-Level P-Value < 0.05
- Anova Method: ebayes
- A Probeset (Gene/Exon) is considered expressed if ≥ 50% samples have DABG values below DABG Threshold.
- DABG < 0.05

Comparison	Group 1	Group 2	Count 1	Count 2	Up	Down
50uMOxy vs 100uMOxy	50uMOxy	100uMOxy	3	3	753	339
50uMOxy vs Control	50uMOxy	Control	3	3	262	424
100uMOxy vs Control	100uMOxy	Control	3	3	907	1431
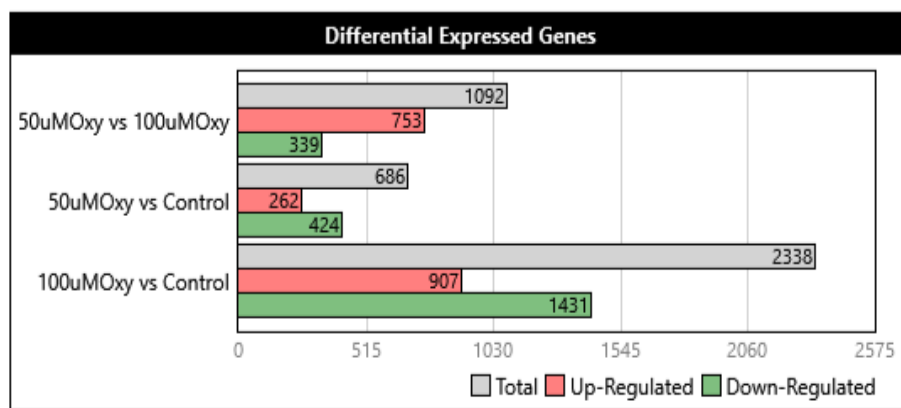
Figure 45 Gene expression summary of MCF7 cells treated with 50 µM and 100 µM compared to the untreated control ; 686 genes changed in the 50 µM–OXY treatment and 2,338 genes changed in the 100 µM–OXY treatment.
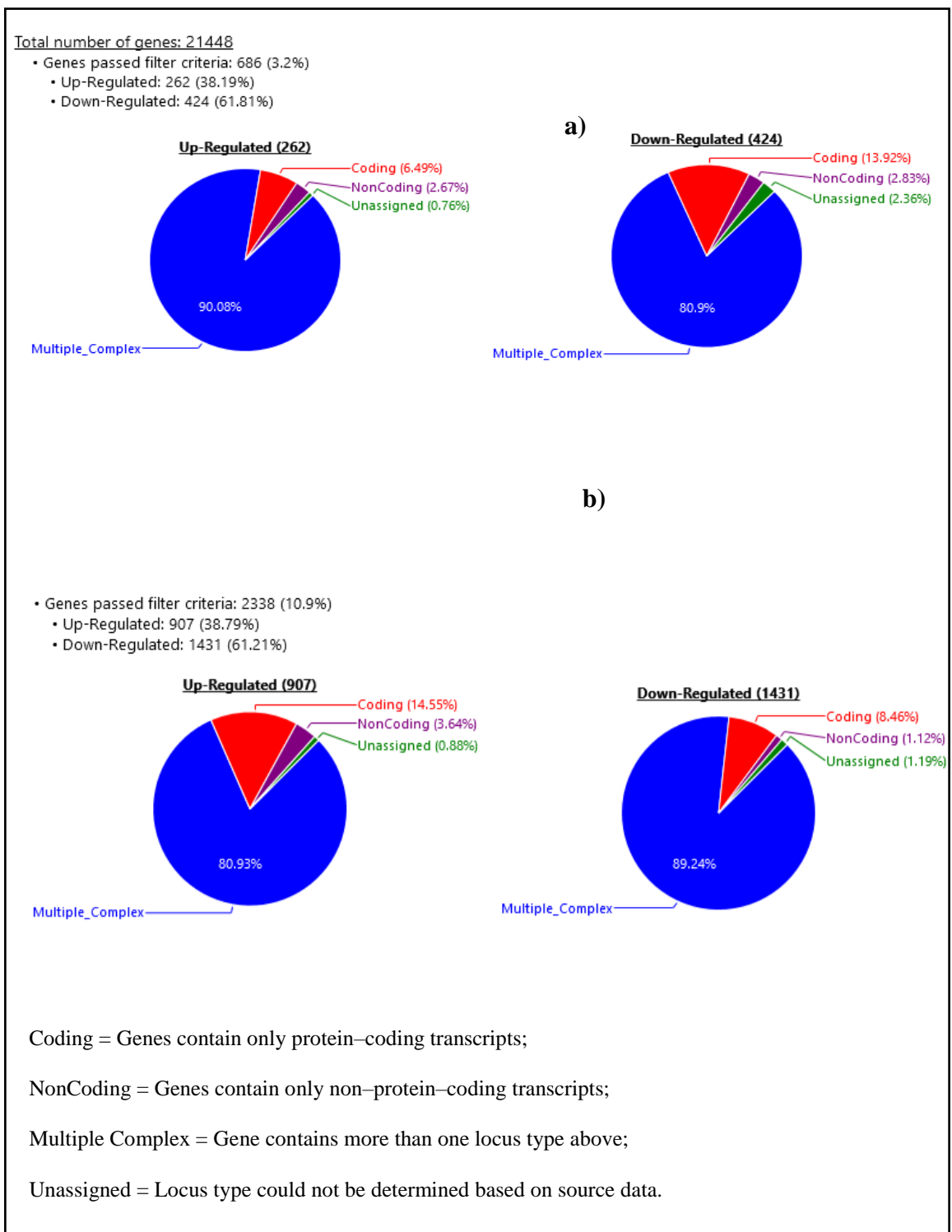
Figure 46 Differential expressed genes ; a) 686 out of 21,448 genes (3.2%) changed in the 50 µM–OXY treatment, while b) 2,338 out of 21,448 genes (10.9%) changed in the 100 µM–OXY treatment, were classified as up– and down–regulated for coding, noncoding, pseudogene, multiple complex and unassigned.
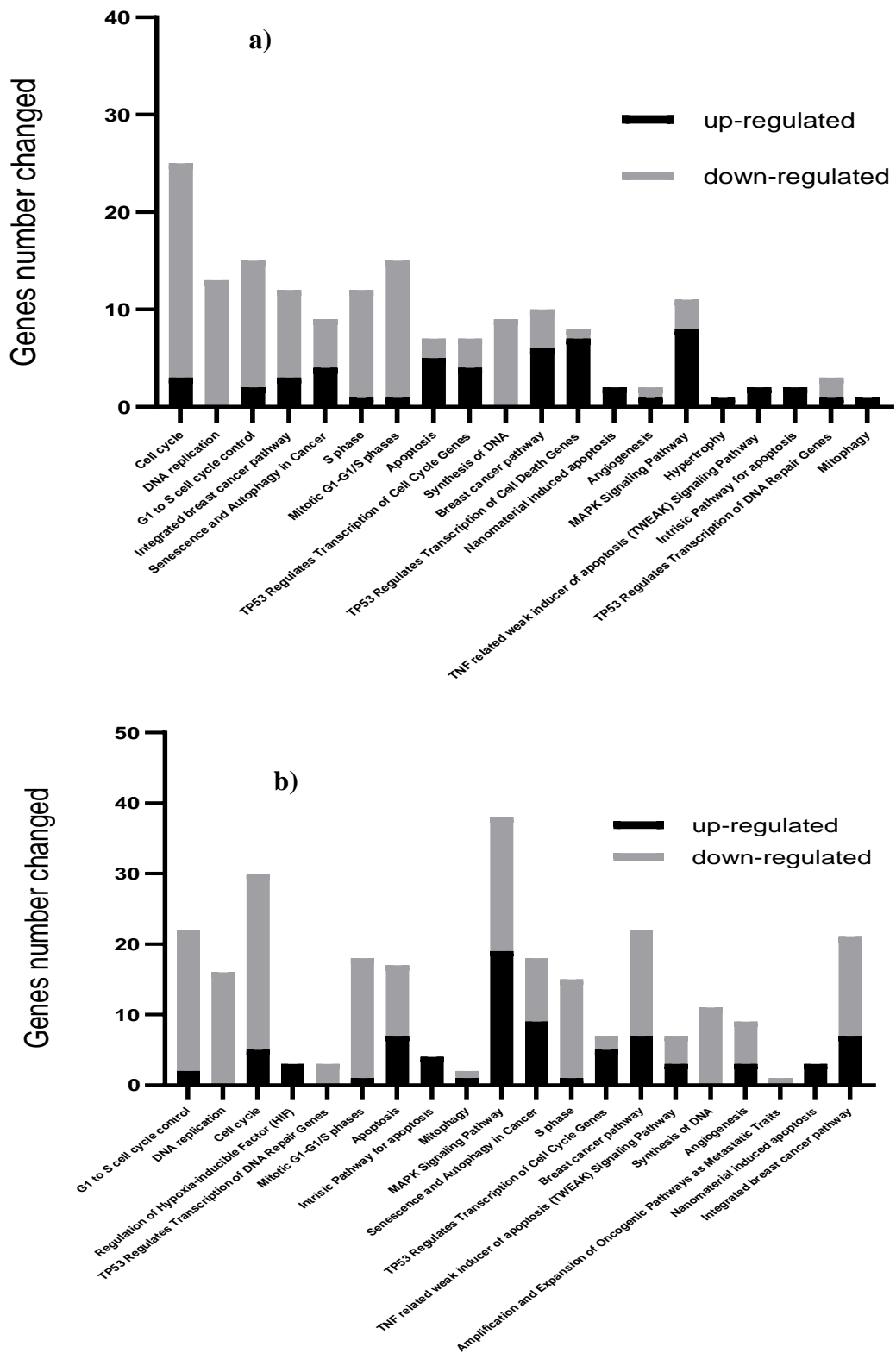
Figure 47 Gene ontology-based biological process pathways altered by OXY in MCF7 breast cancer cells. Differentially expressed genes in MCF7 cells treated with 50 μM (A) or 100 μM (B) of OXY for 24 h. To determine the biological process pathways involved, the list of significant up-regulated (P<0.1) and down-regulated genes were analysed using Fisher's Exact Test, and then analysed using WikiPathways.org.

Cell cycle control was one of the significantly-affected pathways ($P<0.05$). At the dose of 50 and 100 μM–treated MCF7 cells, DNA–damage–inducible alpha (GADD45A) and cyclin–dependent kinase inhibitor 1A (p21, Cip1) (CDKN1A) were the dramatically upregulated expression. Whereas, cyclin–dependent kinase 2 (CDK2), E2F transcription factor one (E2F1) were downregulated in G1 to S cell cycle phase (Figure 48).

At the concentration of 100 μM–treated MCF7 cells compared to the cell control, OXY appeared to upregulate the expression of genes in apoptosis both in extrinsic and intrinsic pathways including Fas cell surface death receptor (FAS), caspase 8, apoptosis–related cysteine peptidase (CASP8), tumour necrosis factor receptor superfamily, member 10b (TNFRSF10B), BCL2–associated X protein (Bax), DIABLO, BCL2 binding component 3; microRNA 3191 (BBC3) and jun proto–oncogene (Ho *et al.*) (Figure 49). The sample signals (average log 2) of the key genes in several biological pathways were elucidated in Figure 50–53. The pictures showed the signals of the genes affected by two–doses OXY treatments compared to the untreated control (0 μM OXY); CDK2 and E2F1 genes were significantly decreased ($P<0.01$) doses dependently in the G1–S cell cycle control pathway. Most of the genes in apoptosis pathway were likely to be up–regulated such as FAS, CASP8, TNFRSF10B, Bax, DIABLO, BBC3 and MAPK8. Whereas, most of the genes in DNA repair pathway tend to be down–regulated including RAD51 recombinase (RAD51), breast cancer 1, early onset (BRCA1), breast cancer 2, early onset (BRCA2), X–ray repair complementing defective repair in Chinese hamster cells 2 (XRCC2), X–ray repair complementing defective repair in Chinese hamster cells 3 (XRCC3) and poly(ADP–ribose) polymerase 1(PARP1). Some genes in senescence and autophagy in cancer pathway were upregulated significantly ($P<0.1$) such as microtubule–associated protein 1 light chain 3 beta (MAP1LC3B), sequestosome 1 (SQSTM1), GABA(A) receptor–associated protein like 2 (GABARAPL2), while AKT1 substrate 1 (proline rich) (AKT1S1) was significantly down–regulated ($P<0.01$).

127
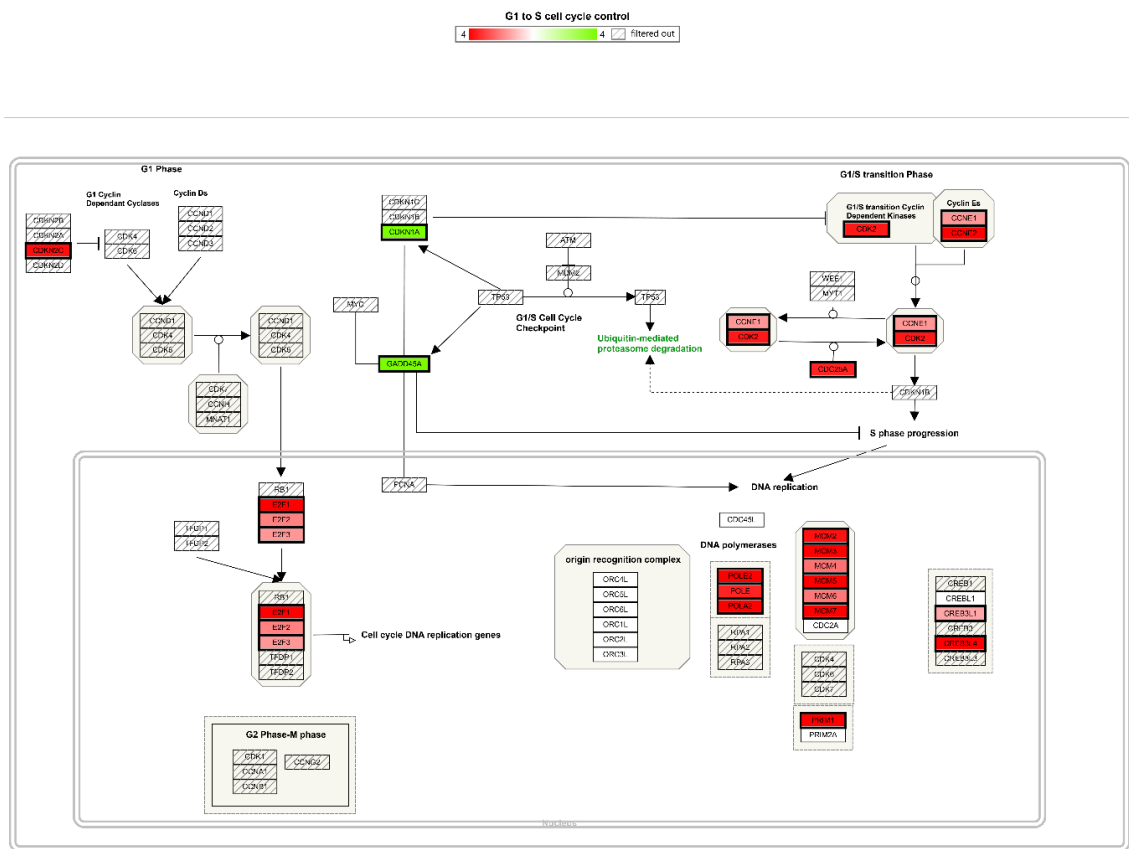
Figure 48 Cell cycle control pathway integrating expression data for MCF7 cells treated with 100 µM OXY for 24 h. Genes labelled in green are up regulated and in red are down regulated.
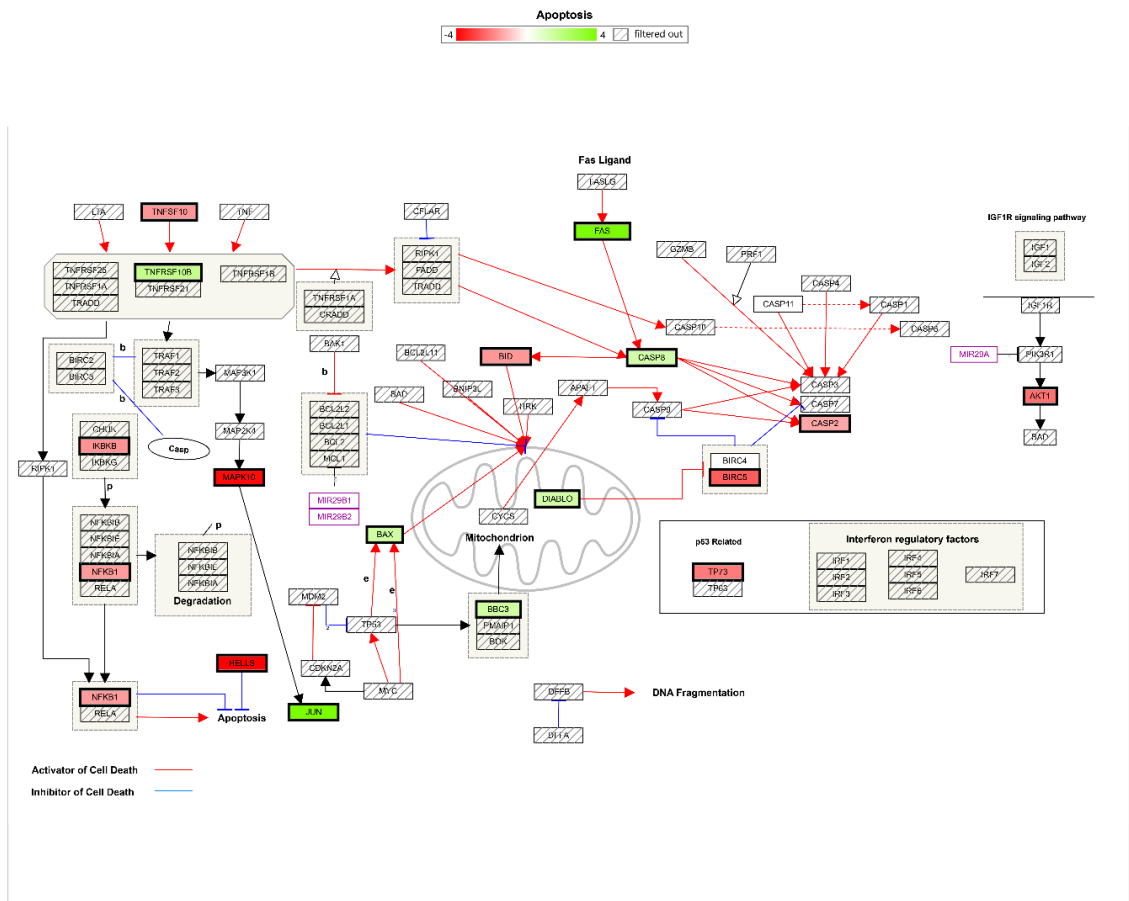
Figure 49 Apoptosis pathways integrating expression data for MCF7 cells treated with 100 µM OXY for 24 h. Genes labelled in green are up regulated and in red are down regulated.

G1 to S cell cycle control pathway
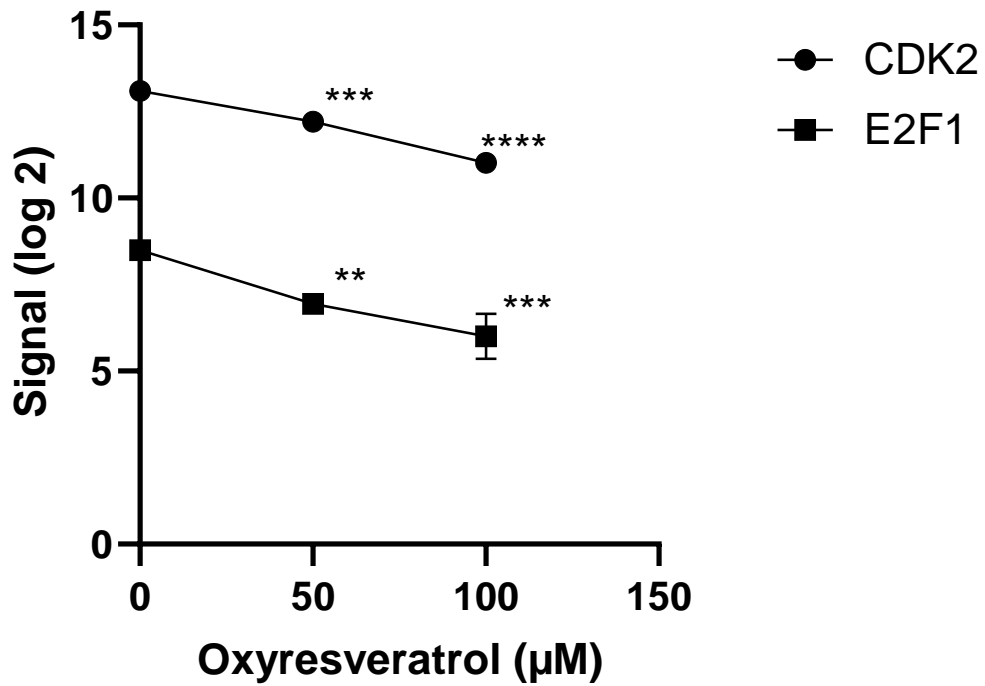
Figure 50 Expressed gene signal (log 2) in G1 to S cell cycle control pathway of MCF7 cells treated with OXY at 0 µM, 50 µM and 100 µM for 24 h. Data are the mean ± SD (n=3). Statistical analysis was carried out using One–way ANOVA and Dunnett's post hoc test. The significant difference was compared relatively to the control (**P < 0.01,***P < 0.001 and ****P < 0.0001).

Apoptosis pathway
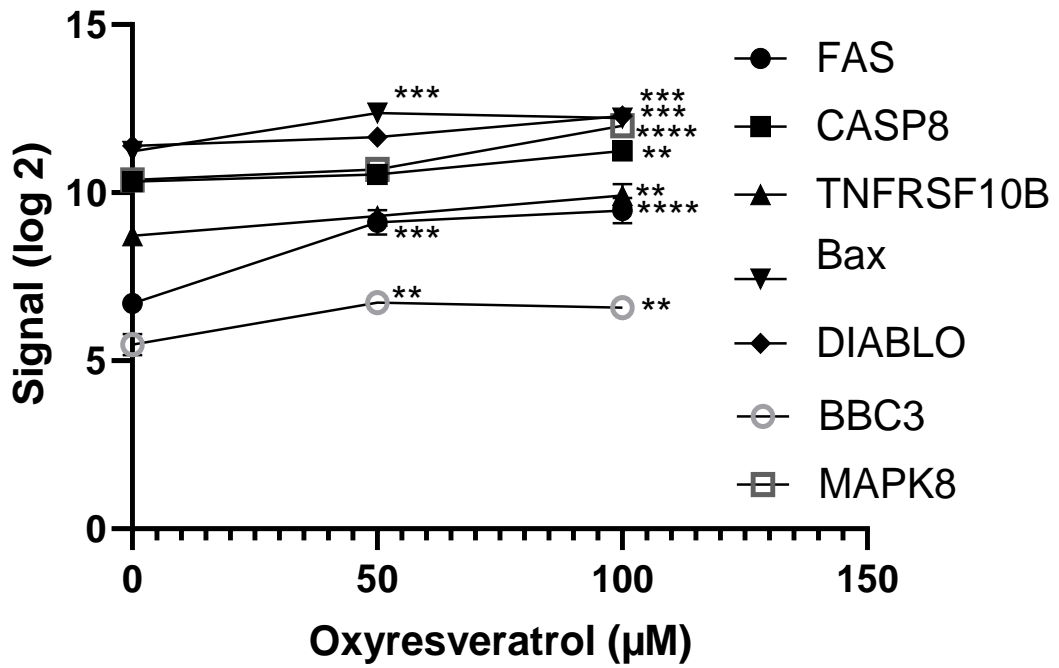
Figure 51 Expressed gene signal (log 2) in apoptosis pathway of MCF7 cells treated with OXY at 0 µM, 50 µM and 100 µM for 24 h. Data are the mean ± SD (n=3). Statistical analysis was carried out using One–way ANOVA and Dunnett's post hoc test. The significant difference was compared relatively to the control (**P < 0.01, ***P < 0.001 and ****P < 0.0001).

Senescence and autophagy in cancer pathway
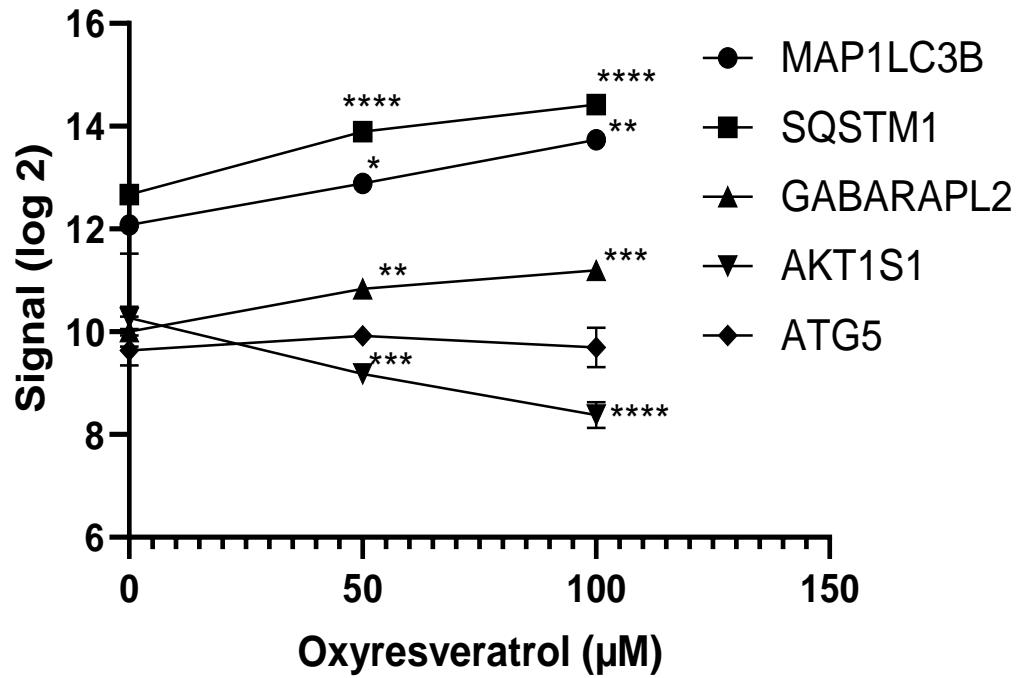
Figure 52 Expressed gene signal (log 2) in senescence and autophagy in cancer pathway of MCF7 cells treated with OXY at $0\,\mu M$, $50\,\mu M$ and $100\,\mu M$ for 24 h. Data are the mean $\pm$ SD (n=3). Statistical analysis was carried out using One–way ANOVA and Dunnett's post hoc test. The significant difference was compared relatively to the control (*$P < 0.1$, **$P < 0.01$, ***$P < 0.001$ and ****$P < 0.0001$).

DNA repair pathway
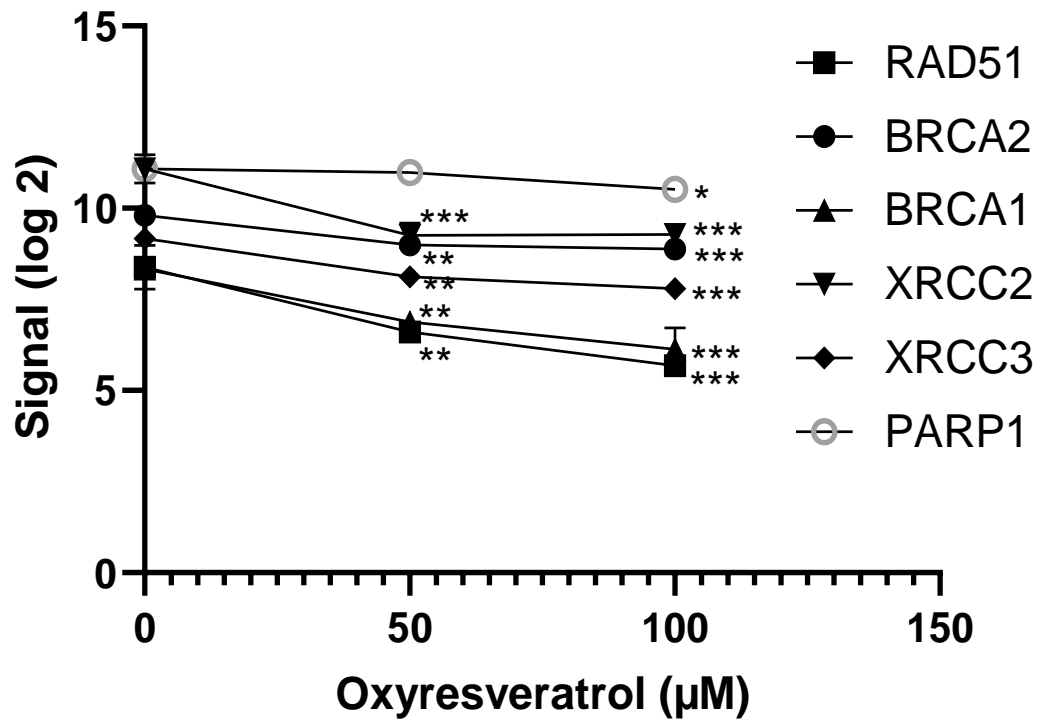
Figure 53 Expressed gene signal (log 2) in G1 to DNA repair pathway of MCF7 cells treated with OXY at 0 µM, 50 µM and 100 µM for 24 h. Data are the mean ± SD (n=3). Statistical analysis was carried out using One–way ANOVA and Dunnett's post hoc test. The significant difference was compared relatively to the control (*P < 0.1, **P < 0.01, ***P < 0.001 and ****P < 0.0001).

6.3.2 Quantitative polymerase chain reaction (qPCR)

The gold standard approach for quantitative analysis of RNA expression is quantitative polymerase chain reaction (qPCR) due to its accuracy, sensitivity, specificity, reproducibility and the potential to be a high throughput analysis. Therefore, the technique is always chosen for validating expression of the genes after microarray assay (Bustin *et al.*, 2005; Chen *et al.*, 2016). The cells were treated with OXY and extracted total RNA. All protocols followed the manufacture's instruction, especially the primers, using the validated primer sets for human.

The genes were randomly chosen and the expression was calculated as a relative quantification using the glyceraldehyde 3–phosphate dehydrogenase (GAPDH) for the standardization of gene expression levels. The Ct (cycle threshold) values from triplicates of each gene showed in Table 8.

The relative quantification of the gene expression was followed by the $2^{-\Delta\Delta Ct}$ Livak and Schmittgen method (Livak and Schmittgen, 2001). The untreated control (0 µM OXY) was used to normalise the two–OXY treatments for each target gene. The fold change of the target genes treated with 50 µM OXY and 100 µM OXY are shown in Figure 54.

Total 12 out of 19 genes (63%), the expression was increased dose–dependently including Bax, CDKN1A, GADD45A, CASP8, DIABLO, FAS, JUNB, MAPK8, TNFSF10B, GABARAPL2, MAP1LC3B and SQSTM1, while the other genes (37%) (CDK2, E2F1, PARP1, BRCA1, RAD51, AKT1, ESR1) were suppressed by the compound. The fold change of GADD45A and FAS were quite high around 7.5 times in 50 µM OXY treatment and around 15 times in 100 µM OXY treatment compared to the untreated. Whereas, the others were roughly or below 5 fold for the two treatments. Bax, CDKN1A, GADD45A, FAS, MAP1LC3B and SQSTM1 were significantly up regulated (P<0.1) compared between the two treatments. While E2F1, PARP1, BRCA1 and RAD51 were significantly down regulated (P<0.1).

Table 8 C$_t$ (cycle threshold) values of each amplified gene from MCF–7–extracted RNA treated with 50–µM OXY and 100–µM OXY compared to untreated control.

Genes	Sample	0 µM OXY	50 µM OXY	100 µM OXY
GAPDH	replicate 1	10.26	11.33	11.97
	replicate 2	10.34	11.87	10.98
	replicate 3	10.43	11.71	11.06
	average	10.34	11.64	11.34
	SD	0.09	0.28	0.55
CDK2	replicate 1	17.89	19.48	18.45
	replicate 2	18.24	19.85	18.47
	replicate 3	18.02	19.40	18.01
	average	18.05	19.58	18.31
	SD	0.18	0.24	0.26
E2F	replicate 1	20.32	21.59	21.30
	replicate 2	20.10	21.68	21.48
	replicate 3	19.49	22.03	21.57
	average	19.97	21.77	21.45
	SD	0.43	0.23	0.14
BAX	replicate 1	15.85	15.33	14.80
	replicate 2	16.15	15.55	14.91
	replicate 3	16.04	15.48	14.96
	average	16.01	15.45	14.89
	SD	0.15	0.11	0.08
CDKN1A	replicate 1	17.44	15.34	14.54
	replicate 2	17.40	15.51	14.56
	replicate 3	17.23	15.60	14.59
	average	17.36	15.48	14.56
	SD	0.11	0.13	0.03
GADD45A	replicate 1	19.13	17.54	16.36
	replicate 2	19.14	17.19	16.15
	replicate 3	18.99	17.29	16.14
	average	19.09	17.34	16.22
	SD	0.08	0.18	0.12

Table 9 *continue*

CASP8	replicate 1	20.96	22.49	19.97
	replicate 2	22.22	21.81	19.87
	replicate 3	21.23	22.53	19.75
	average	21.47	22.28	19.86
	SD	0.66	0.40	0.11
DIABLO	replicate 1	18.20	18.74	16.9
	replicate 2	17.07	18.62	17.13
	replicate 3	17.50	18.35	17.37
	average	17.59	18.57	17.13
	SD	0.57	0.20	0.24
FAS	replicate 1	22.91	21.50	19.10
	replicate 2	22.82	21.47	19.30
	replicate 3	22.90	21.22	19.38
	average	22.88	21.40	19.26
	SD	0.05	0.15	0.14
JUNB	replicate 1	24.39	25.16	29.98
	replicate 2	24.58	24.82	29.46
	replicate 3	24.41	25.00	29.65
	average	24.46	24.99	29.70
	SD	0.10	0.17	0.26
MAPK8	replicate 1	18.94	19.90	18.43
	replicate 2	18.95	19.74	18.60
	replicate 3	19.02	19.82	18.30
	average	18.97	19.82	18.44
	SD	0.03	0.36	0.29
TNFSF10	replicate 1	30.15	32.57	29.32
	replicate 2	30.30	31.78	29.98
	replicate 3	30.36	30.98	29.12
	average	30.27	31.78	29.47
	SD	0.11	0.80	0.45

Table 9 *continue*

PARP1	replicate 1	16.20	16.33	15.72
	replicate 2	15.97	16.32	15.30
	replicate 3	16.17	16.34	15.70
	average	16.11	16.33	15.57
	SD	0.13	0.01	0.24
BRCA1	replicate 1	18.76	19.53	22.67
	replicate 2	18.65	19.94	21.53
	replicate 3	18.75	19.85	21.82
	average	18.72	19.77	22.01
	SD	0.06	0.22	0.59
RAD51	replicate 1	17.64	19.04	20.40
	replicate 2	17.65	18.86	20.38
	replicate 3	17.70	19.02	20.38
	average	17.66	18.97	20.39
	SD	0.03	0.10	0.01
AKT1	replicate 1	13.84	16.72	16.88
	replicate 2	14.00	15.91	15.89
	replicate 3	14.11	16.44	15.27
	average	13.98	16.36	16.01
	SD	0.14	0.41	0.81
ESR1	replicate 1	17.07	18.99	19.3
	replicate 2	17.16	19.35	19.36
	replicate 3	16.88	18.69	19.55
	average	17.04	19.01	19.40
	SD	0.14	0.33	0.13
GABARAPL2	replicate 1	16.78	17.23	16.81
	replicate 2	16.23	17.27	16.53
	replicate 3	16.65	16.85	16.8
	average	16.55	17.12	16.71
	SD	0.29	0.23	0.16

Table 9 *continue*

MAP1LC3	replicate 1	15.97	16.11	15.41
	replicate 2	16.06	15.97	15.37
	replicate 3	16.17	15.96	15.08
	average	16.07	16.01	15.29
	SD	0.10	0.08	0.18
RAD51	replicate 1	17.64	19.04	20.40
	replicate 2	17.65	18.86	20.38
	replicate 3	17.70	19.02	20.38
	average	17.66	18.97	20.39
	SD	0.03	0.10	0.01
SQSTM1	replicate 1	16.05	16.55	15.4
	replicate 2	16.06	16.62	15.26
	replicate 3	15.9	16.66	15.36
	average	16.00	16.61	15.34
	SD	0.09	0.06	0.07
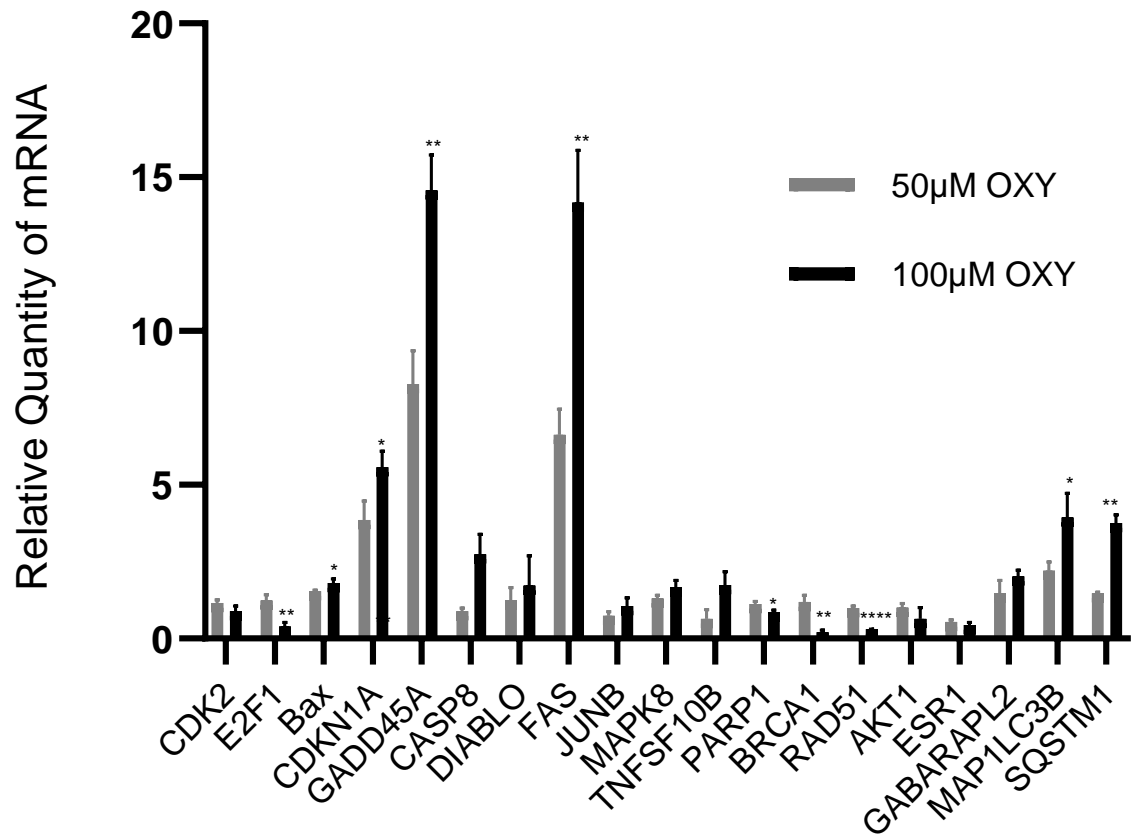
Figure 54 Relative quantity of mRNA extracted from MCF7 treated with 50 µM or 100 µM of OXY; Validation of selected genes differentially expressed from MCF7 cells treated for 24 h with 50 µM or 100 µM of OXY versus the control data set (n=3). The statistical difference between the two treatments was carried out using unpaired t-test (*P < 0.5, **P < 0.05 and ****P < 0.0001).

6.4 Discussion

The independent triplicate MCF7 cells of the control (untreated), 50 µM and 100 µM treated with OXY for 24 h (IC_{50} = 368.37 µM) were designed to analyse the gene expression, which the exposure time enough to study the main molecular changes at the early stage, especially well–known RNA and proteins inside the cells (Li and Sarkar, 2002).

The total all well–known, 21,448 human genes were investigated by the Clariom™ S assays, of which the probe sets consist of a subset of 10 probes per gene. There was enough to perform gene–level expression profiling studies and to assess changes in key genes and pathways affected by OXY (MacGregor and Squire, 2002).

The analysis was performed using the data filter of probe sets with a fold change > 2 or < –2 and with a p–value < 0.05 for the data of 50µM–OXY treatment vs the control and 100µM–OXY treatment vs the control. The statistical analysis was used eBayes correcting the variance of the ANOVA analysis with an empirical Bayes approach that used the information from all the probe sets to yield an improved estimate for the variance. The eBayes correction is especially important when the number of samples being analysed is small (Rahman *et al.*, 2017).

Total 686 genes (3.2%) passed the filter criteria in 50 µM–OXY treatment, while 2,338 genes (10.9%) passed the filter criteria in 100 µM–OXY treatment compared to the untreated control. The number of genes changed in the two groups were down–regulated roughly twice higher than those up–regulated. The gene expression was the OXY–dose dependent. The genes changed more than 90% were coding and multiple complex genes, which can translate into proteins.

The most affected and significant changed genes (P<0.1) regarding DNA synthesis such as cell cycle, cell cycle control, DNA replication, mitotic as well as DNA repair pathways

were like to be down–regulated because the compound inhibited cell proliferation and cell growth as reported in chapter 5. The inhibition of the cell cycle pathway also links directly to the DNA repair mechanism and breast cancer pathway (Helleday *et al.*, 2007). Apoptosis, programmed cell death was also induced by OXY exposure. OXY increased apoptosis genes the same as other stilbenoids, especially resveratrol (Varoni *et al.*, 2016). OXY was found here to induce the expression of several genes in the cell senescence and autophagy pathway, which has also been reported that the compound increased levels of autophagy in neuroblastoma cell lines through the mediation of PI3K or mTOR genes (Rahman *et al.*, 2017).

All gene expression validated using qPCR gave the results consistent with those from microarrays. The apoptotic process has been reported to be one of the important therapeutic hallmarks of cancer. OXY was also confirmed posing cytotoxicity through apoptosis. The expression of genes in DNA repair was the highest significant difference (P<0.0001) between the two treatments especially RAD51. This gene has been reported overexpression in several cancers (Kiyohara *et al.*, 2012). The suppression of DNA repair gene may also help increase drug sensitivity or mediate resistance. Moreover, the mediation of cell proliferation, cell growth and metastasis may play the important mechanism of action of OXY.

In this chapter should be concluded that OXY showed regulation of some genes that played an important role in the biological pathways during carcinogenesis in MCF7, human breast cancer cells. OXY decreased the expression of CDK2, E2F1 and the MCM complex, which affected the initial stage of G1–S phase of cell proliferation. OXY also enhanced apoptosis genes through extrinsic and intrinsic pathways, accompanying with autophagy and DNA repair genes. Therefore, further research is required to investigate the potential mechanisms of action.

CHAPTER 7 APOPTOSIS PATHWAY

AFFECTED BY OXY

7.1 Introduction

Apoptosis or the process of programmed cell death is generally characterized by distinct morphological characteristics and energy–dependent biochemical mechanisms. Apoptosis is considered a vital component of various processes including normal cell turnover, proper development and functioning of the immune system, hormone–dependent atrophy, embryonic development and chemical–induced cell death (Elmore, 2007). The ability to modulate the life or death of a cell is recognized for its immense therapeutic potential. Therefore, research continues to focus on the elucidation and analysis of signalling pathways that control apoptosis (Kruidering and Evan. 2000).

There are two main pathways of apoptosis (Figure 55); extrinsic and intrinsic pathways. Each route requires specific triggering signals to begin an energy–dependent cascade of molecular events. Briefly, the extrinsic pathway involves transmembrane receptor–mediated interactions. To illustrate, the interaction of FasL/FasR or TNF–α/TNFR1 then activates through procaspase–8 and caspase–8, respectively (Tummers and Green, 2017). The other, intrinsic pathway is non–receptor–mediated stimuli that produce intracellular signals within the cells or mitochondria. This cascade causes changes in the inner mitochondrial membrane resulting in losing the mitochondrial transmembrane potential, then releasing pro–apoptotic proteins such as BAX, tBID and Cytc from the intermembrane space into the cytosol (Elmore, 2007).

Both pathways activate the executioners through caspase 2, 3, 6 and 7. The execution pathway results in characteristic cytomorphological features including cell shrinkage, chromatin condensation, the formation of cytoplasmic blebs and apoptotic bodies and finally phagocytosis of the apoptotic bodies by adjacent parenchymal cells, neoplastic cells or macrophages.
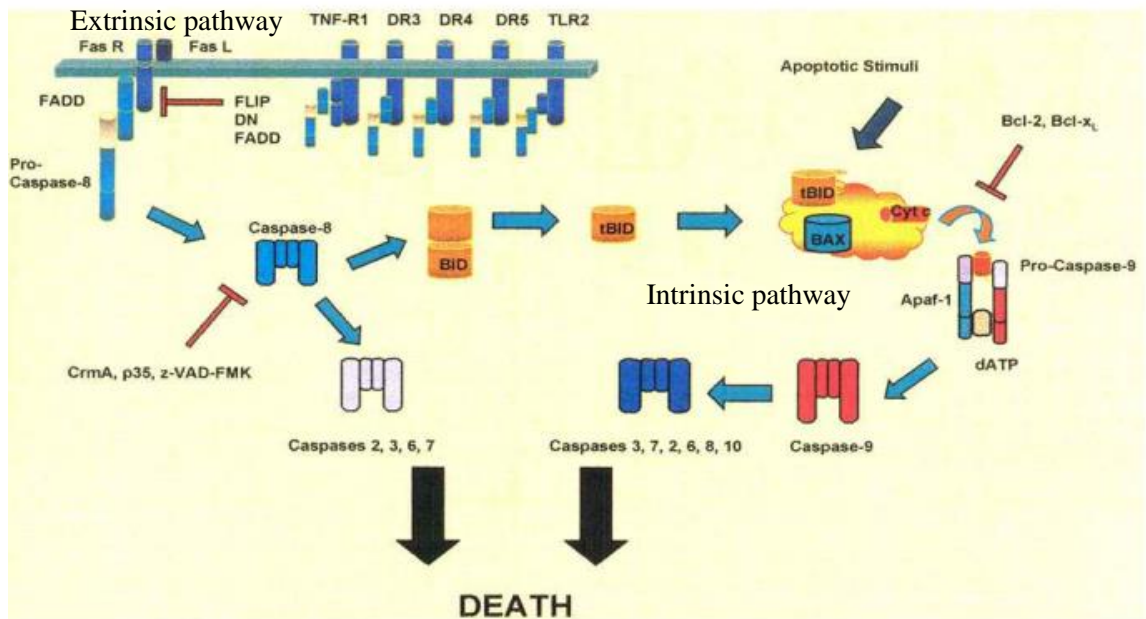
Figure 55 Apoptosis pathway adapted from Kruidering & Evan (2000)

7.2 Aims

To investigate the expression of the key genes in the apoptosis pathway in MCF7 and HepG2 cells, following treatment with OXY. This was achieved by using microarray data, qPCR, as well as flow cytometry, to analyse apoptotic cell population, caspase 3 activation and mitochondrial membrane potential ($\Delta\Psi$m). Moreover, morphological changes including plasma membrane integrity, nuclear morphology, nuclear damage and intracellular ROS generation were also investigated.

7.3 Results and discussion

7.3.1 Apoptosis gene expression

The picture (Figure 56) reveals the intensities (signal $\log_2$) of apoptotic genes in OXY–treated MCF7 cells compared to the control; all genes including apoptotic peptidase

activating factor 1 (APAF1), apolipoprotein L, 2 (APOL2), B–cell CLL/lymphoma 2 (BCL2), BCL2–antagonist/killer 1 (BAK1), BCL2–associated X protein (BAX), caspase 8, apoptosis–related cysteine peptidase (CASP8), cyclin–dependent kinase inhibitor 1A (p21, Cip1)(CDKN1A), diablo, IAP–binding mitochondrial protein (DIABLO), Fas cell surface death receptor (FAS), growth arrest and DNA–damage–inducible, alpha (GADD45A), jun B proto–oncogene (JUNB), mitogen–activated protein kinase 8 (MAPK8), tumour necrosis factor receptor superfamily, member 10b (TNFRSF10B) and TP53. APAF1, APOL2, BAK1, BAX, CASP8, CDKN1A, DIABLO, FAS, GADD45A, JUNB, MAPK8 and TNFRSF10B were significantly up–regulated ($P<0.1$) compared to the untreated control, while BCL2 was not altered by the two doses of OXY treated. Interestingly, tumour protein p53 (TP53) gene was down–regulated by the compound dose–dependently.

The selected genes were validated using RT–qPCR. Triplicates were performed for each gene and the amplification of each gene was used validated specific primer. In all cases, the RT–qPCR data confirmed those obtained from 50 and 100 μM–OXY treated array analyses (Figure 57). APARF1, APOL2, BAX, CASP8, CDKN1A, FAS, GADD45A and TNFSF10B have significantly increased ($P<0.1$) the expression dose–dependently. The two doses of OXY did not make significant changes ($P>0.1$) in BCL2 and TP53 expression.
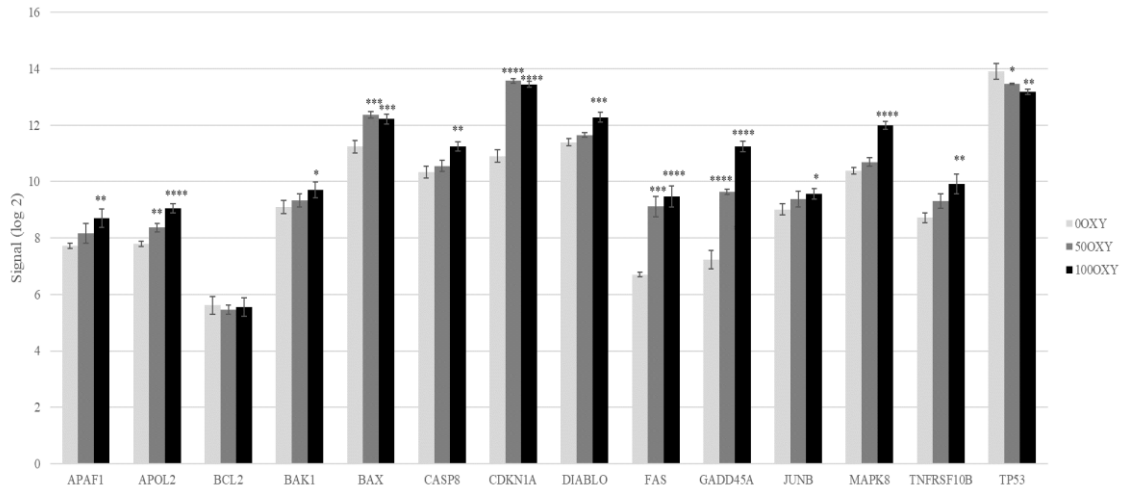
Figure 56 The expression signals of key genes in apoptotic pathways of MCF7 treated with two different doses of OXY(50 µM and 100 µM) for 24 h. Data are the mean ± SEM (n=3). Statistical analysis was carried out using One–way ANOVA and Dunnett's post hoc test. The significant difference was compared relatively to the control (*P < 0.1, **P < 0.01, ***P < 0.001 and ****P < 0.0001).
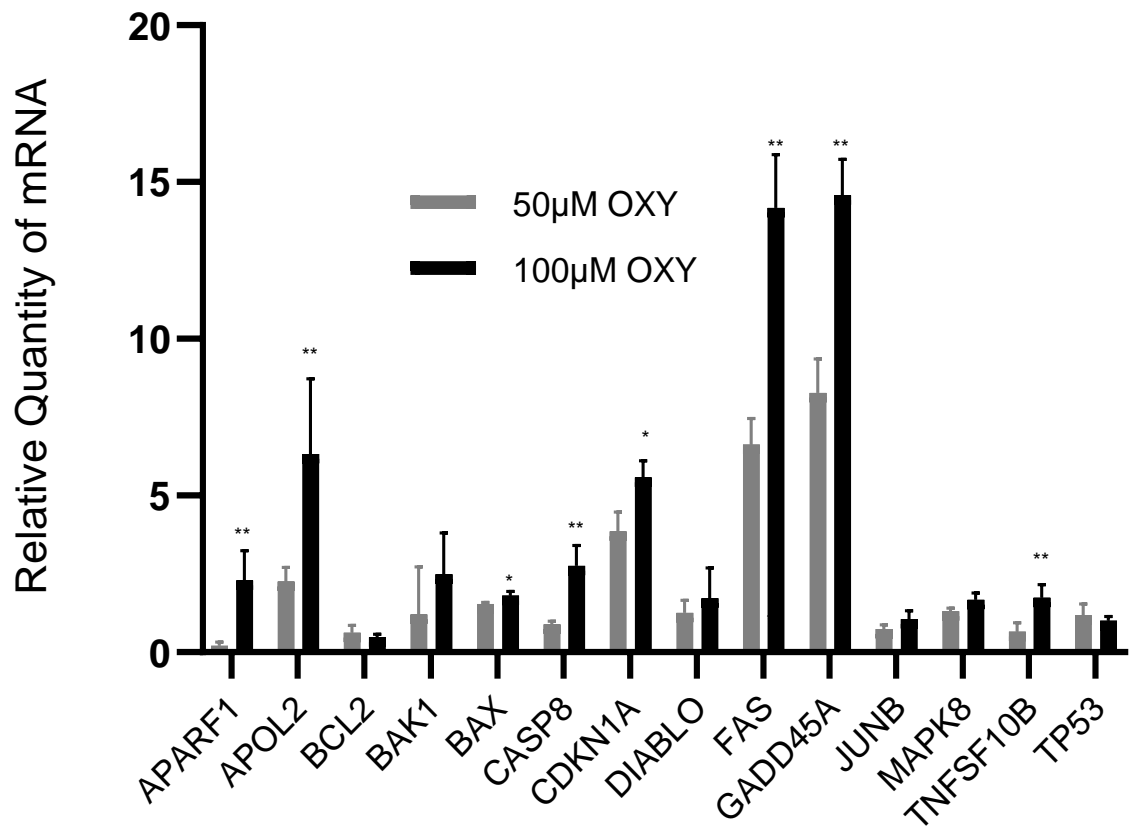
Figure 57 Relative quantity of mRNA expression acquired from qPCR of MCF7 cells treated with different two doses of OXY. Data are the mean ± SD (n=3). The statistical difference between the two treatments was carried out using unpaired t-test (*P < 0.5 and **P < 0.05).

7.3.2 Quantification of apoptotic cells

Apoptosis is a normal physiologic process, which occurs during embryonic development or in the maintenance of tissue homeostasis. In apoptotic cells, the membrane phospholipid phosphatidylserine (PS) is translocated from the inner to the outer leaflet of the plasma membrane, thereby exposing PS to the external cellular environment (Rothkamm *et al.*). Annexin V that has a high affinity for PS, conjugated to fluorochromes, phycoerythrin. Therefore, this method can be used for analysing cells that are undergoing apoptosis by flow cytometry. This platform was also provided with a vital dye, 7–Amino–Actinomycin (7–AAD) to identify early apoptotic cells (7–AAD negative, PE Annexin V positive). Viable cells with intact membranes exclude 7–AAD, whereas the membranes of dead and damaged cells are permeable to 7–AAD.

Camptothecin, the standard compound induced apoptosis around 4% of the cell population in MCF7 and HepG2 cells after treated for 4 h at the concentration of 4 µM. The cells remained alive more than 80 % and roughly 10 % were at the end of apoptosis or already dead (Table 10 and Figure 58).

Table 10 and Table 11 show OXY induced apoptosis in MCF7 cells dose–dependently at the concentrations tested of 25, 50 and 100 µM. This occurrence changed between 6–24 h treatment; the cells treated with OXY 25, 50 and 100 µM at 3 and 6 h became apoptotic but not significantly different compared to controls (P>0.1), while those treated with OXY 50 and 100 µM at 24 h treatment were significantly different (P<0.0001) from the controls. The apoptotic cells were changed from 2.85±0.60 % of the control to 3.14±0.37, 5.74±0.53 and 11.69±1.15 % of 25, 50 and 100 µM OXY, respectively. These results illustrated that most of the cells treated with 50 and 100 µM OXY within 24 h underwent apoptosis and consequently died.

Apoptosis was induced in HepG2 cells following treatment with OXY, in a dose– and time–dependent fashion, similar to that observed in MCF7 cells following OXY exposure seen in Table 12 and Table 13. There were no significant apoptotic cells during the 3–6 h treatment in HepG2 cells, while some cells turned apoptotic dose–dependently during 6– 24 h treatment; it was significantly different (P<0.01) at the doses of 100 and 200 µM– OXY, which was the apoptotic population roughly 4 and 7 %, respectively.

Table 9 Camptothecin (4 µM) induced apoptosis in MCF7 and HepG2 cells after treated for 4 h.
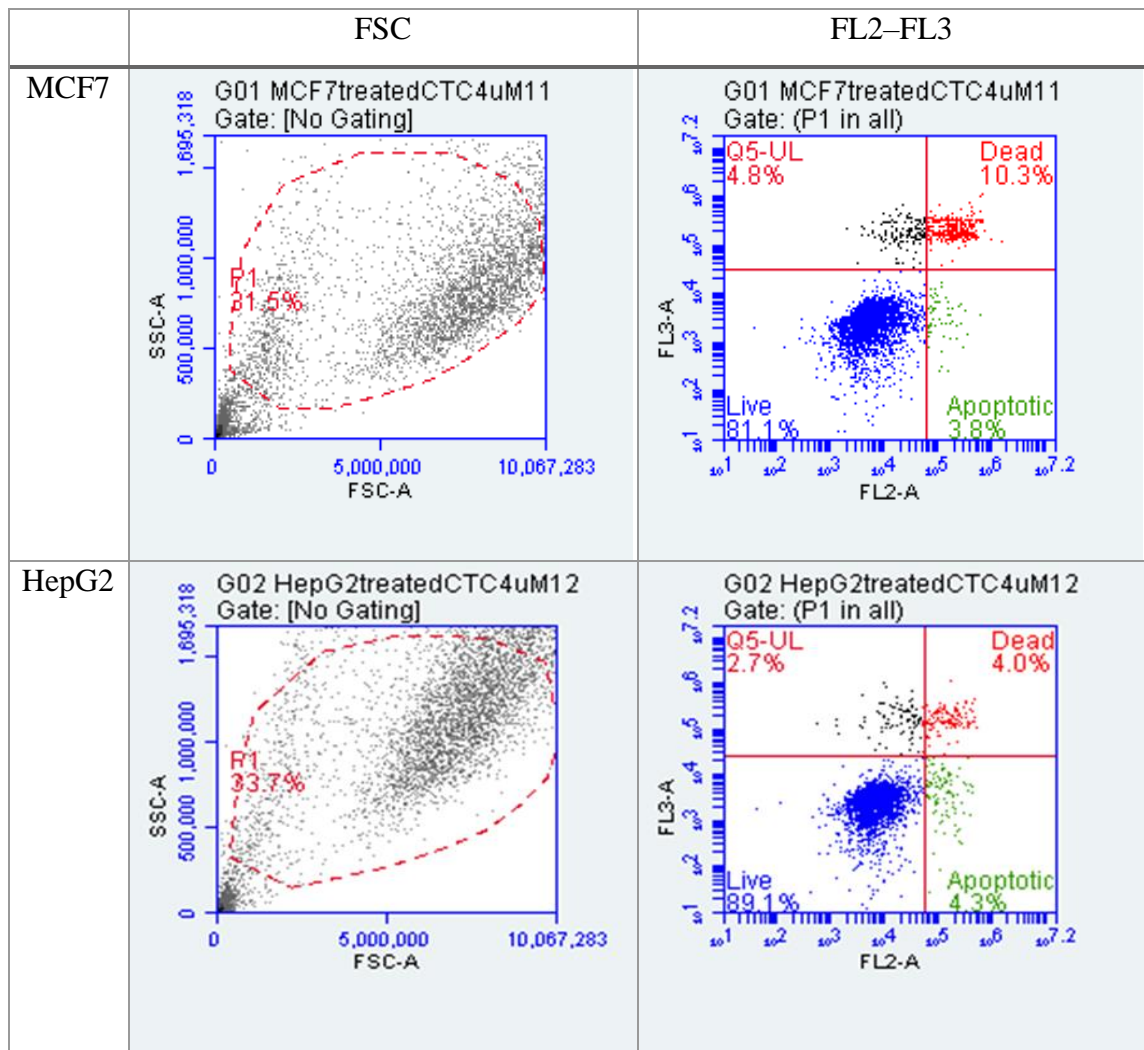
Live = cell population (%) was indicated live cells (Annexin V PE and 7–AAD negative)

Apoptotic = cell population (%) was indicated undergoing early apoptosis (Annexin V PE positive and 7–AAD negative)

Dead/late apoptosis = cell population (%) was indicated dead cells (Annexin V PE and 7–AAD positive)
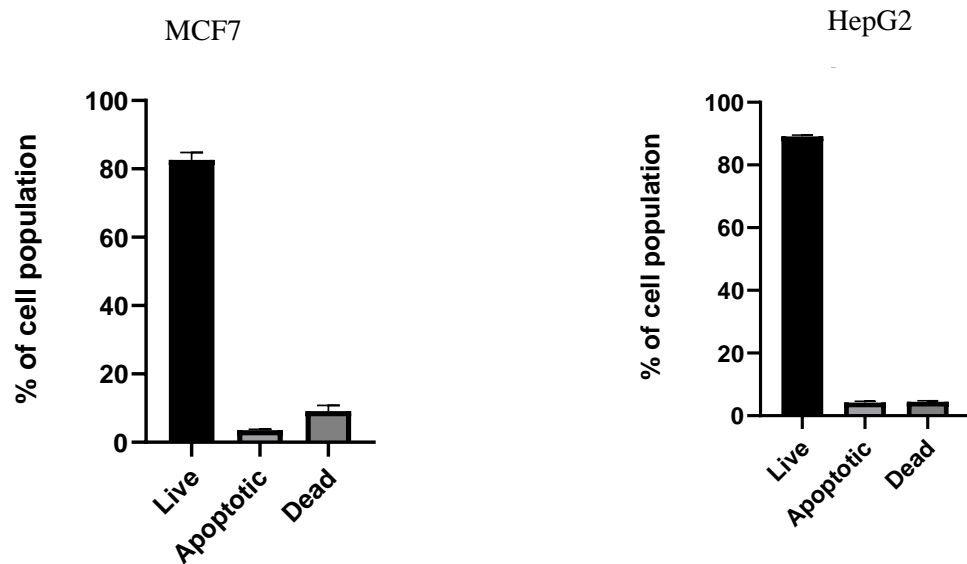
Figure 58 Apoptotic MCF7 and HepG2 cell population induced by 4 µM camptothecin after 4 h exposure. Data are the mean ± SD (n=3).

Table 10 OXY induced apoptosis in MCF7 cells dose– and time–dependently
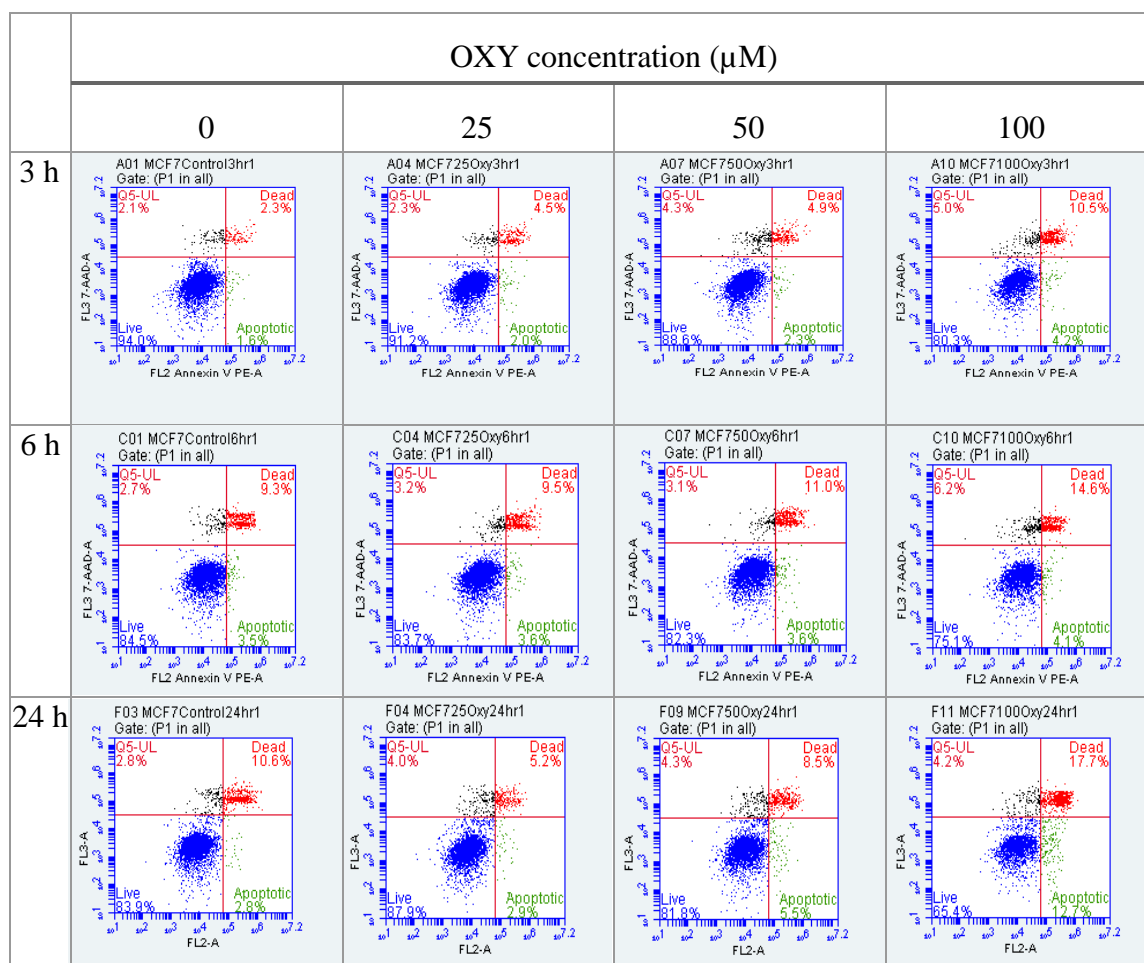
Table 11 Effect of OXY in MCF7 cells determined using flow cytometry. Bar graphs showing the percentages of MCF7 cells population (live, apoptotic and dead cells) when treated with OXY 25–100 μM for 3, 6 and 24 h and then subjected to flow cytometric analysis. Data are the mean ± SD (n=3).
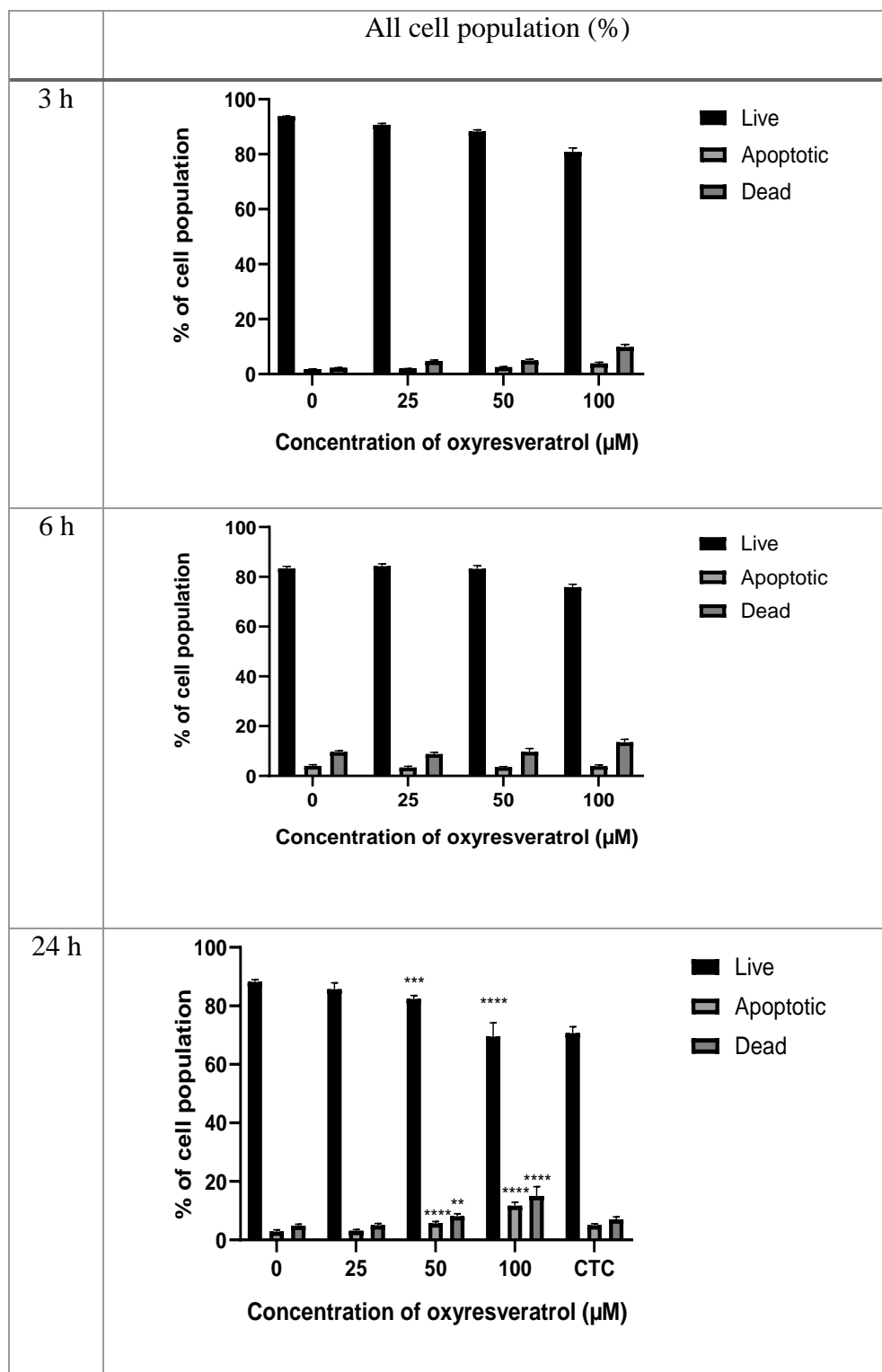
*CTC = 4 μM Camptothecin

Table 12 OXY induced apoptosis in HepG2 cells dose– and time–dependently.
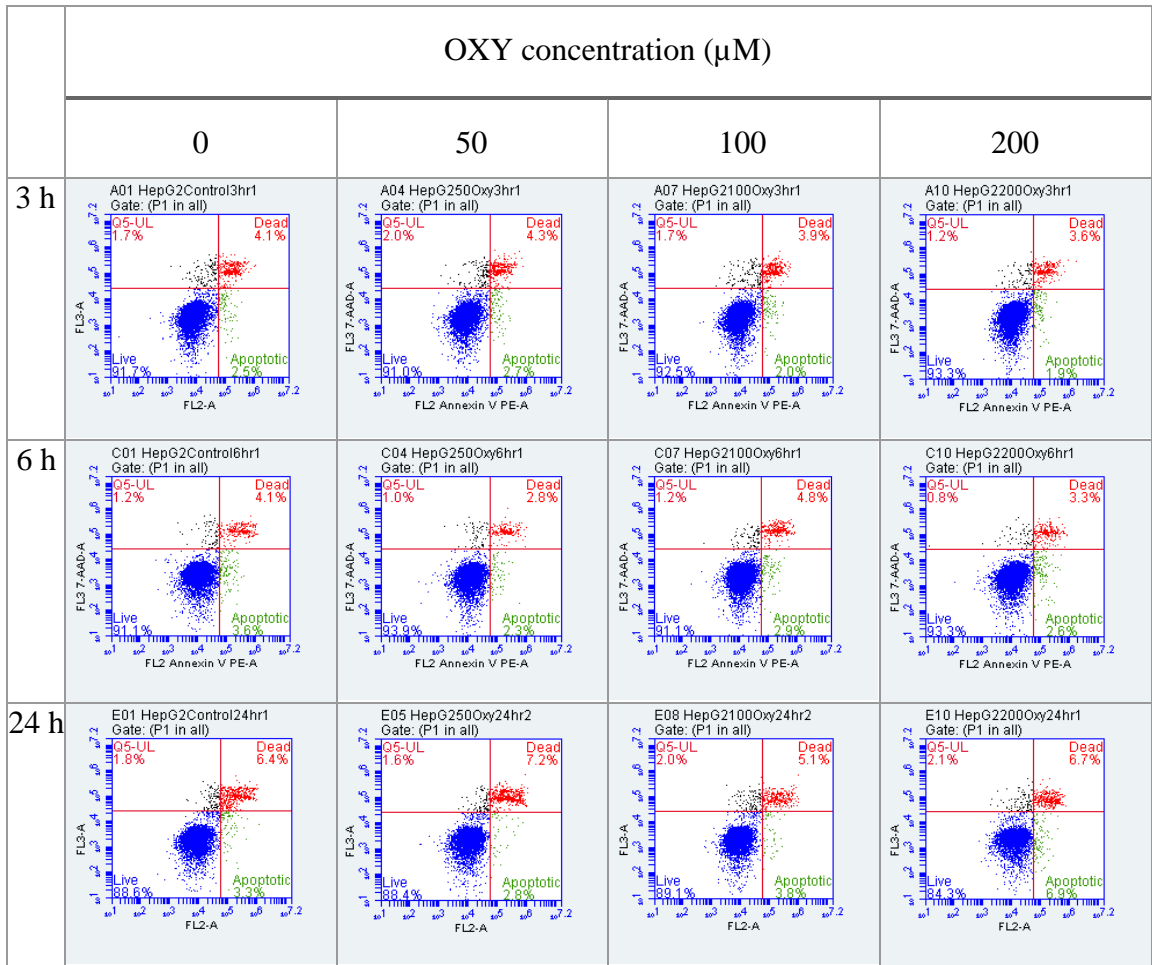
Table 13 Effect of OXY in HepG2 cells determined using flow cytometry. Bar graphs showing the percentages of HepG2 cells population (live, apoptotic and dead cells) when treated with OXY 25–100 μM for 3, 6 and 24 h and then subjected to flow cytometric analysis. Data are the mean ± SD (n=3).

	All cell population (%)
3 h	
6 h	
24 h	
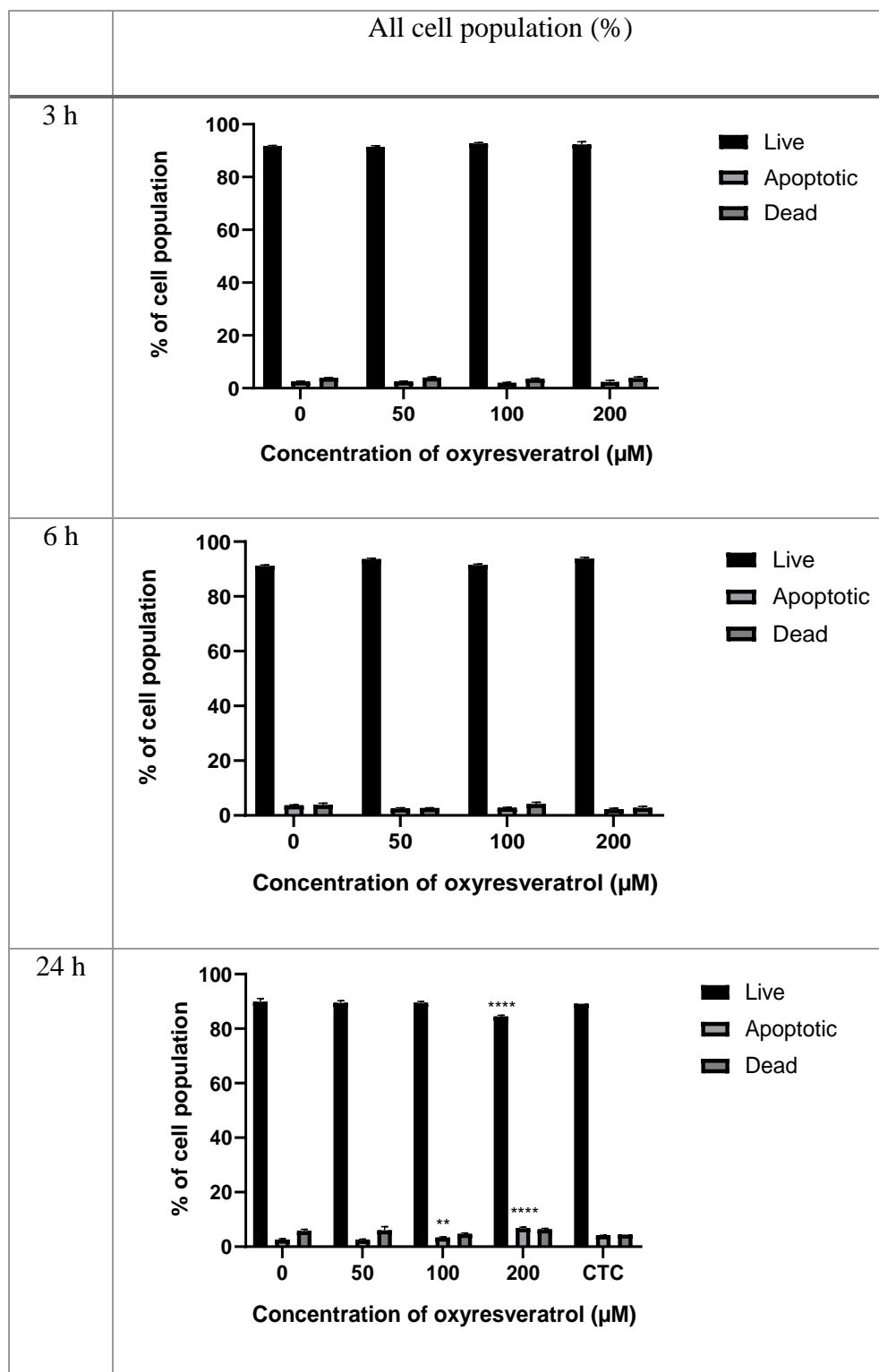
*CTC = 4 μM Camptothecin

7.3.3 Determination of Caspase–3

Camptothecin could induce the expression of caspase–3 in around 1% of MCF7 and HepG2 cells at 4 µM for 4 h in (Table 15 and Figure 59).

 MCF7 cells treated with different concentrations of OXY at the doses of (25, 50 and 100 µM for 24 h) showed a dramatically changed amount of caspase–3 compared to the control; more than 98% population was caspase–3 positive, while the cell population of the caspase–3 negative decreased. All treatments were significantly different ($P<0.0001$) compared with the control (Table 16 and Figure 60).

Likewise, HepG2 cells were also investigated the expression of caspase–3 at 24h–OXY treatment. The results showed that the caspase–3 expression was dose–dependent; the expression remained roughly 86 % at 50 µM–OXY treatment and then they were increased to around 99% and close to 100% at the doses of 100 and 200 µM, respectively, while the population of caspase–3 negative were in the opposite direction. The expression of caspase–3 positive in HepG2 cells was also significantly different ($P<0.01$) compared with the control (Table 16 and Figure 61).

Table 14 Camptothecin induced expression of active caspase–3 expression in MCF7
and HepG2 cells.

	FSC	FL2–A
MCF7	B01 ControlMCF74hr1 Gate: [No Gating] P1 81.9%	B01 MCF7treatedCTC11 Gate: (P1 in all) Caspase 3– 98.6% Caspase 3+ 1.4% FL2 Active Caspase-3 PE-A
HepG2	A07 HepG2treatedCTC4uM11 Gate: [No Gating] P1 84.2%	B04 HepG2treatedCTC4uM21 Gate: (P1 in all) Caspase 3– 98.9% Caspase 3+ 1.1% FL2-A
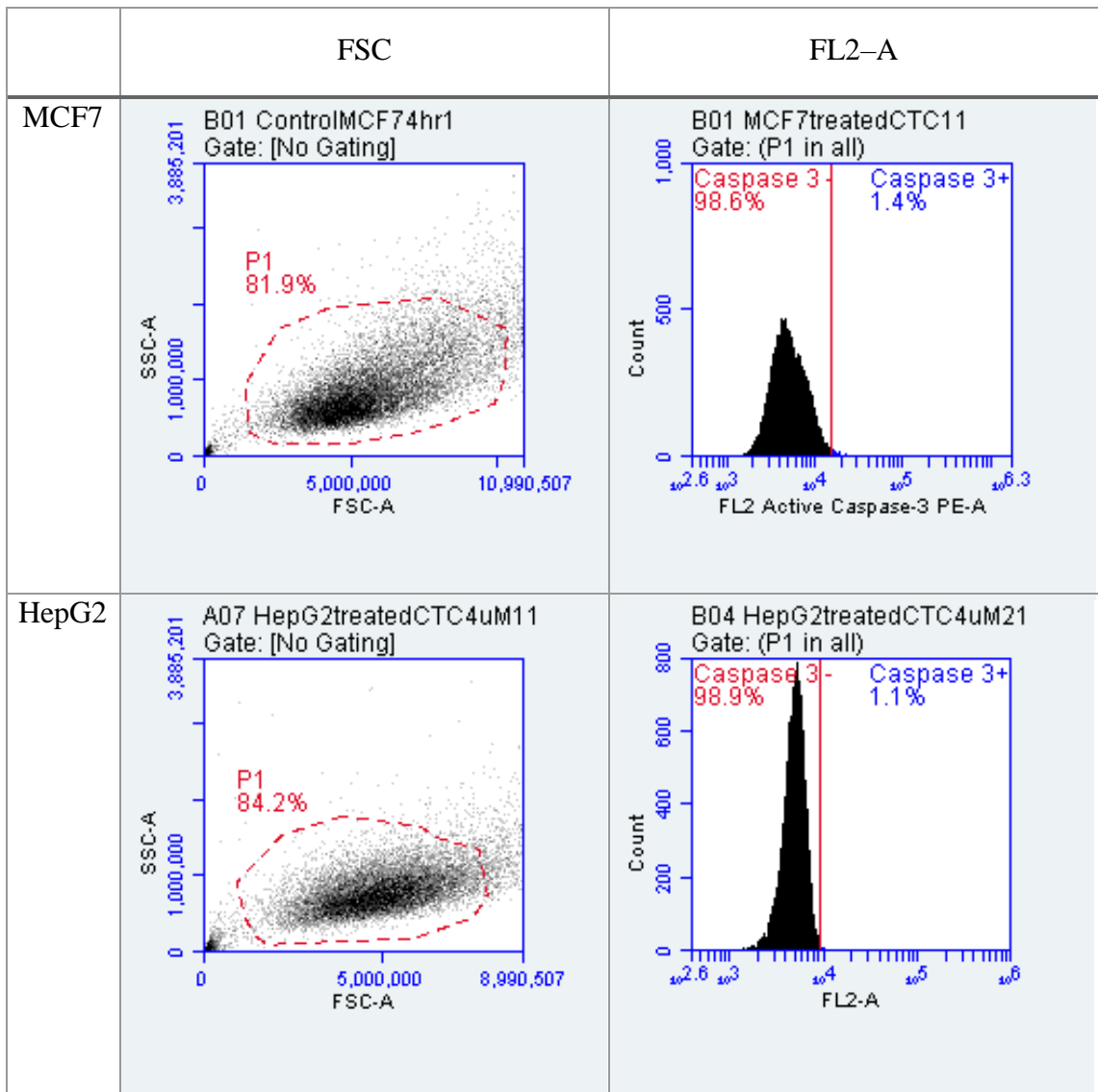
Caspase 3– = cell population (%) did not express caspase–3

Caspase 3+ = cell population (%) expressed caspase–3
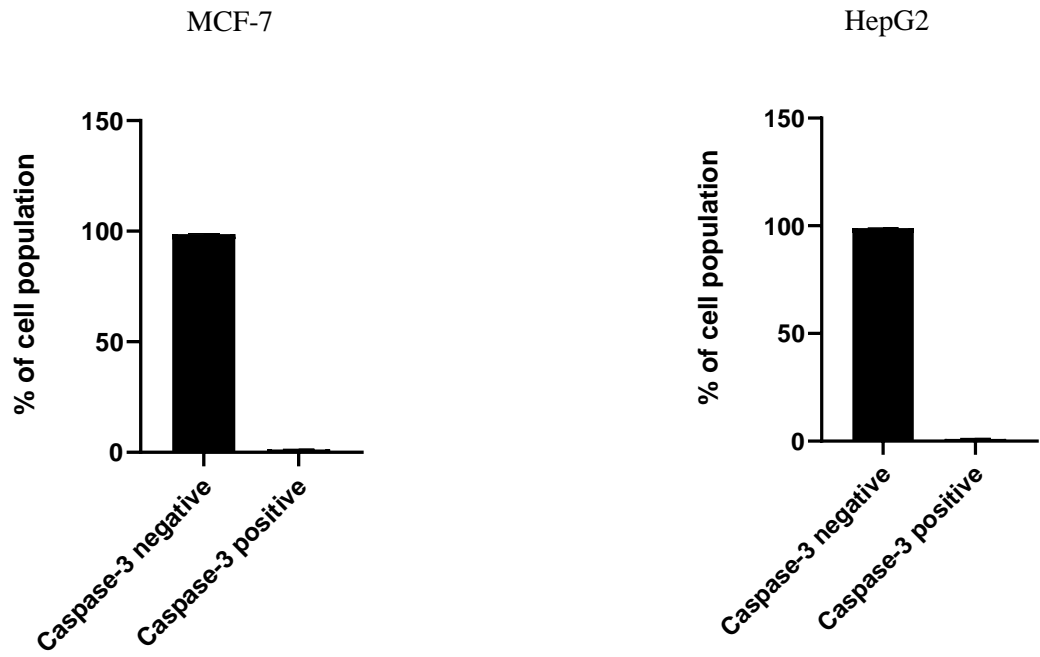
Figure 59 Caspase–3 expression of MCF7 and HepG2 cells following exposure to 4 µM camptothecin (CTC) for 4 h. The cells were stained with PE rabbit anti– caspase–3 and analysed by flow cytometry. Data are the mean ± SD (n=3).

Table 15 OXY induced active caspase–3 expression in MCF7 cells.

Concentration (µM)	FSC	FL2–A
0		
25		
50		
100		

Figure 60 Caspase–3 expression in MCF7 cells following exposure to various concentrations of OXY for 24 h and camptothecin (CTC) for 4 h. The cells were stained with anti– active caspase–3 and analysed by flow cytometry. Data are the mean ± SD (n=3). Statistical analysis was carried out using One-way ANOVA analysis of variance followed by Dunnett's test. The significant difference was compared relatively to control (****P < 0.0001).

Table 16 OXY induced active caspase–3 expression in HepG2 cells.

Concentration (μM)	FSC	FL2–A
0		
50		
100		
200		

Figure 61 Caspase–3 expression in HepG2 cells following exposure to various concentrations of OXY for 24 h and camptothecin (CTC) for 4 h. The cells were stained with anti– active caspase–3 and analysed by flow cytometry. Data are the mean $\pm$ SD (n=3). Statistical analysis was carried out using One-way ANOVA analysis of variance followed by Dunnett's test. The significant difference was compared relatively to control (**P < 0.01 and ****P < 0.0001).

7.3.4 Mitochondrial membrane potential ($\Delta\Psi$m)

Camptothecin was used as a positive control in this assay to cause the loss of mitochondria membrane potential (MMP) in MCF7 and HepG2 cells as analysed using flow cytometry. The cells were exposed to 4 µM camptothecin for 4 h; MCF7 and HepG2 cells showed loss of membrane potential of 7.56±0.41 and 2.39 ±0.16 % cell population (Table 18 and Figure 62).

MCF7 cells lost mitochondria membrane potential dose–dependently (Table 19 and Figure 63) following exposure to several concentrations of OXY, which caused MCF7 cells to undergo apoptosis (24 h–treatment). They also were found to cause loss membrane potential to a significant degree (P<0.001) compared to the untreated control (4.15%±0.08, 4.77%±2.56 and 11.47%±2.75 for 25, 50 and 100 µM–OXY, respectively). Whereas, the normal potential cells also decreased significantly (P<0.001) with the higher doses treated.

HepG2 cells also lost mitochondria potential following treatment with OXY at 100 and 200 µM (Table 20 and Figure 64). The membrane potential loss in HepG2 cells was 0.85%±0.21, 1.58%±0.02 and 2.96%±0.49 at 50, 100 and 200 µM–OXY.

Table 17 Mitochondrial membrane potential of MCF7 cells following exposure to various concentrations of the standard drug, camptothecin at 4 µM for 4 h. The cells were stained with JC–1 and analysed by flow cytometry.

	FSC	JC–1A
MCF7	F01 MCFCamptothecin6h / Gate: [No Gating] / P1 63.2%	F01 MCFCamptothecin6h / Gate: (P1 in all) / P4 91.4% / P5 7.9%
HepG2	F01 HepG2Camptothecin6hr / Gate: [No Gating] / P1 82.9%	F01 HepG2Camptothecin6hr / Gate: (P1 in all) / P4 97.2% / P5 2.4%
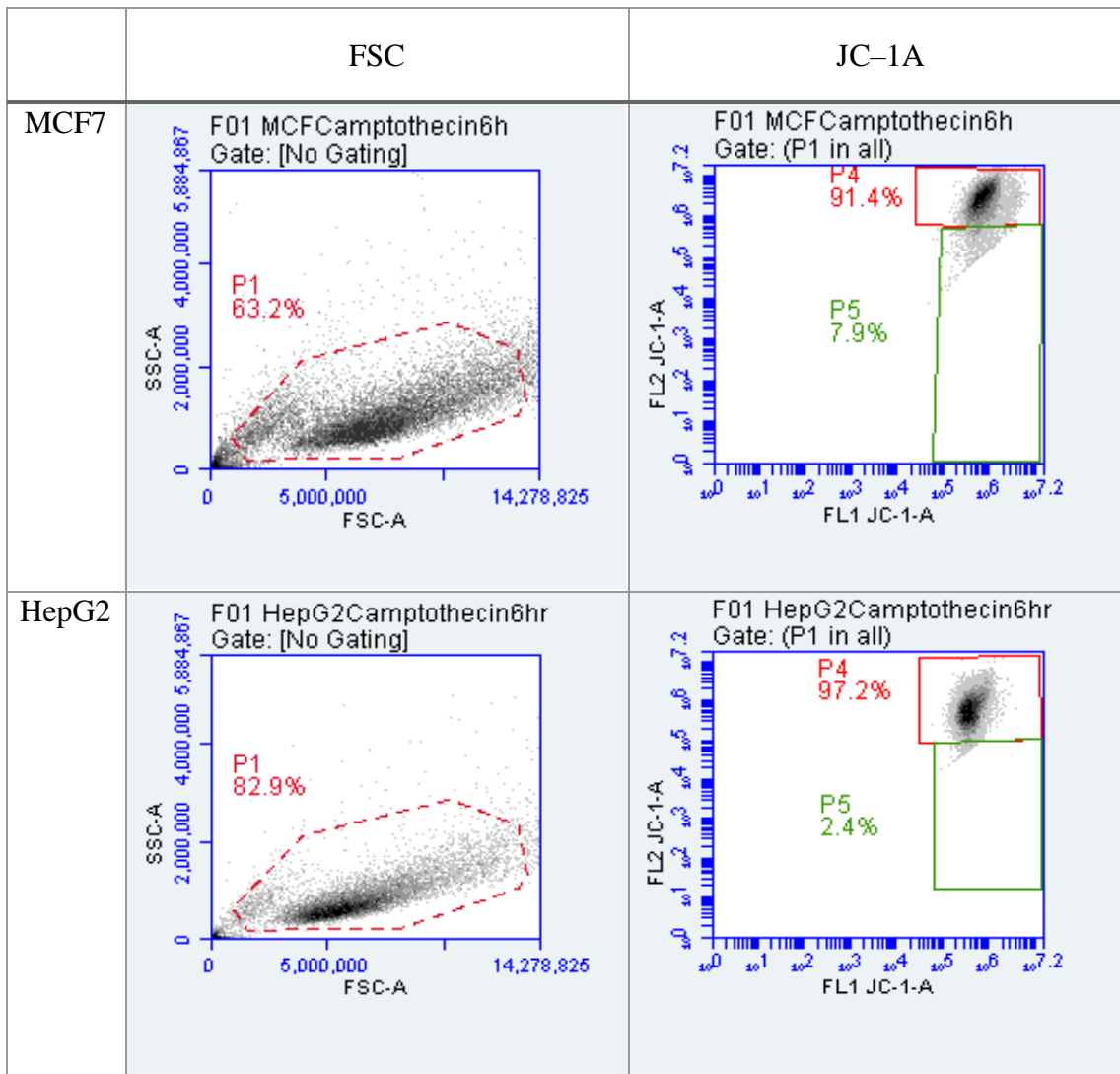
P1 = Single cells

P4 = normal mitochondrial potential

P5 = lost mitochondrial potential
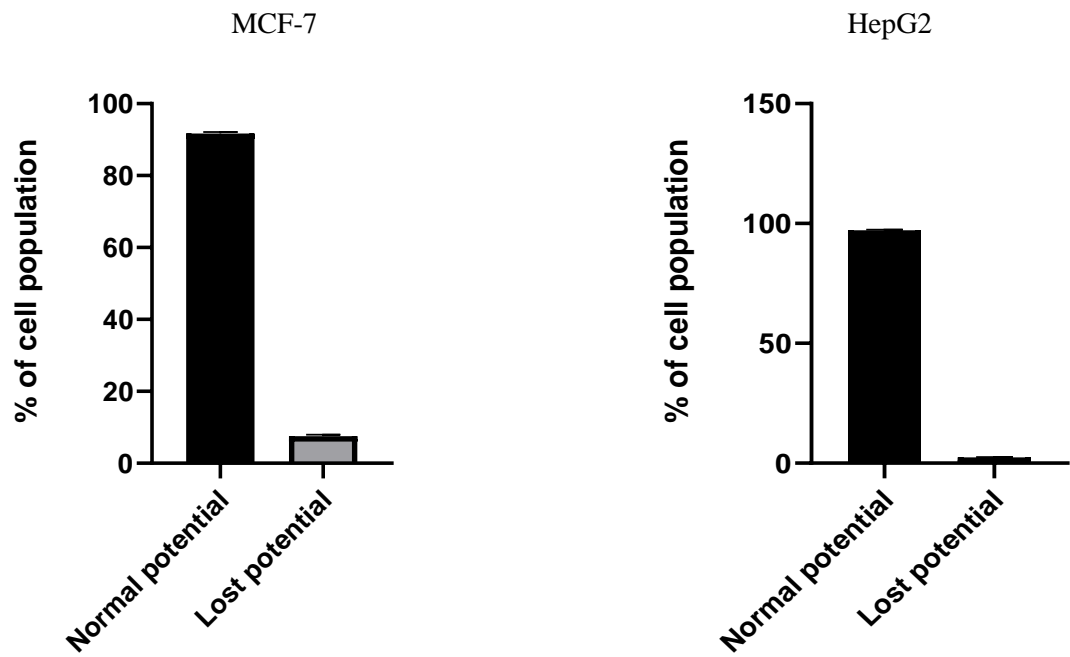
Figure 62 Mitochondrial membrane potential of MCF7 and HepG2 cells following exposure to 4 µM camptothecin (CTC) for 4 h. The cells were stained with JC–1 and analysed by flow cytometry. Data are the mean ± SD (n=3).

Table 18 Mitochondrial membrane potential of MCF7 cells following exposure to various concentrations of OXY. The cells were stained with JC–1 and analysed by flow cytometry.

Concentration (µM)	FSC	JC–1A
0		
25		
50		
100		

Figure 63 Mitochondrial membrane potential of MCF7 cells following exposure to various concentrations of OXY for 24 h and camptothecin (CTC) for 4 h. The cells were stained with JC–1 and analysed by flow cytometry. Data are the mean $\pm$ SD (n=3). Statistical analysis was carried out using One-way ANOVA analysis of variance followed by Dunnett's test. The significant difference was compared relatively to the control (***$P < 0.001$ and ****$P < 0.0001$).

Table 19 Mitochondrial membrane potential of HepG2 cells following exposure to various concentrations of OXY. The cells were stained with JC–1 and analysed by flow cytometry.

Concentration (µM)	FSC	JC–1A
0		
50		
100		
200		

Figure 64 Mitochondrial membrane potential of HepG2 cells following exposure to various concentrations of OXY for 24 h and camptothecin (CTC) for 4 h. The cells were stained with JC–1 and analysed by flow cytometry. Data are the mean ± SD (n=3). Statistical analysis was carried out using One-way ANOVA analysis of variance followed by Dunnett's test. The significant difference was compared relatively to the control (***P < 0.001; and ****P < 0.0001).

7.3.5 Lactate dehydrogenase (LDH) cytotoxicity assay

The results of LDH cytotoxic assay of OXY to MCF7 and HepG2 cells are shown in Figure 65. MCF7 cells released LDH dose–dependently after treatment with OXY for 48 h with 11±4, 20±6, 28±5 and 41±9 % of the control at the concentration of 0, 25, 50 and 100 µM–OXY. Whereas, HepG2 gave the LDH detected with 12±2, 13±2, 17±2 and 81±27 % of the control at the concentration of 0, 50, 100 and 200 µM–OXY.

7.3.6 Nuclear morphology detection using Hoechst 33342 staining

MCF7 and HepG2 have been investigated the nuclear and chromatin changes after treated with OXY and the pictures of chromatin changed shown in Table 20. MCF7 cells were observed the chromatin condensation at all doses treated; the higher doses of 50 µM and 100 µM gave clearly condensed chromatin. Likewise, HepG2 showed condensed chromatins at the high doses of 100 µM and 200 µM–OXY treatment.

7.3.7 Measurement of DNA damage by Comet assay

MCF7 cells treated with OXY were investigated the DNA damage shown in Table 21. The cells treated with 25 and 50 µM of OXY for 24 and 48 h were found not to have damage the DNA compared to the cell treated with 100 µM H_2O_2. OXY at the effective doses did not cause damage to DNA in MCF7 cells.
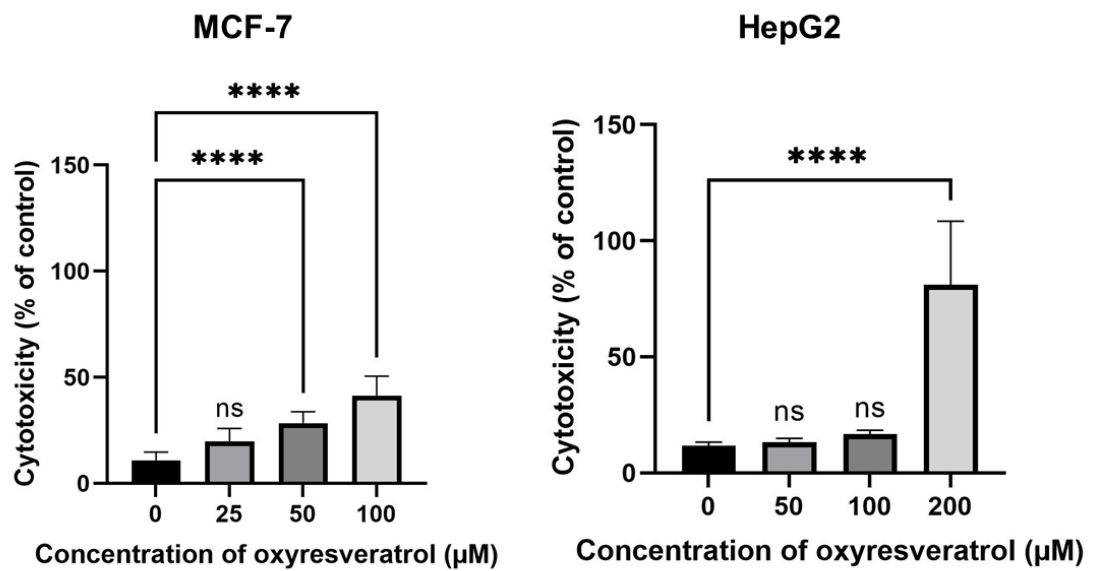
Figure 65 Lactate dehydrogenase cytotoxicity assay for MCF7 and HepG2 cells after OXY exposure. Data are the mean ± SEM (n=3). Statistical analysis was carried out using One-way ANOVA analysis of variance followed by Dunnett's test. The significant difference was compared relatively to the control (*P < 0.1 and ****P < 0.0001).

Table 20 MCF7 and HepG2 nuclei staining by Hoechst 33342 for apoptosis detection treated with different concentrations of OXY for 24 h (control cells are untreated). Condensed nuclei at the area with white arrows. Magnification = ×20; scale bars = 200 µm.
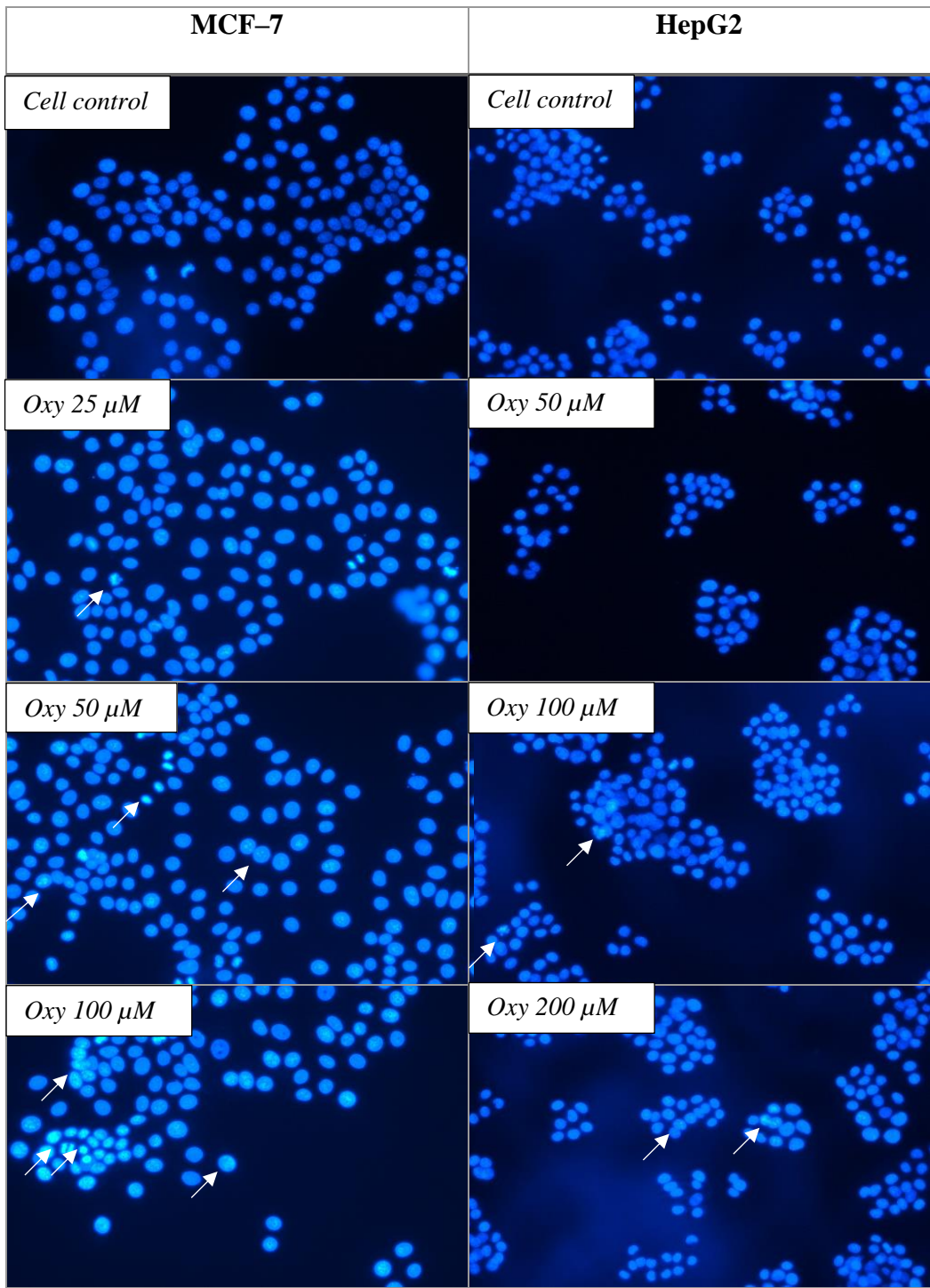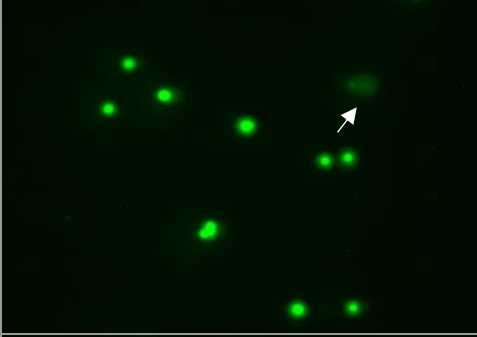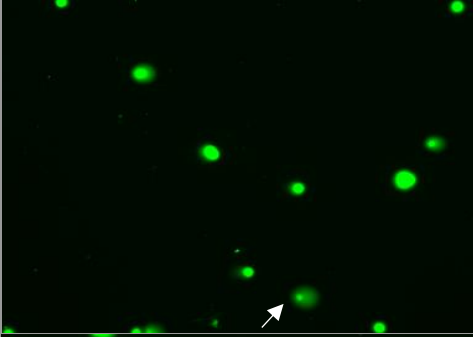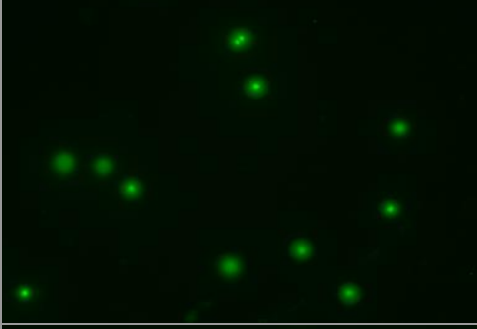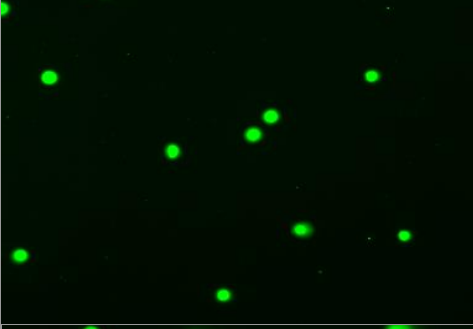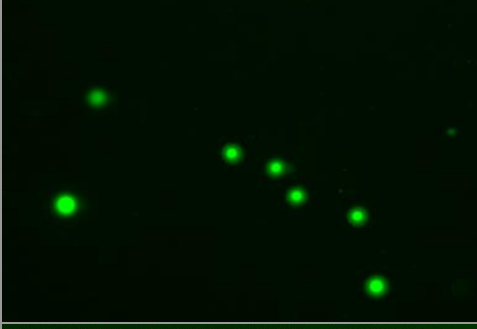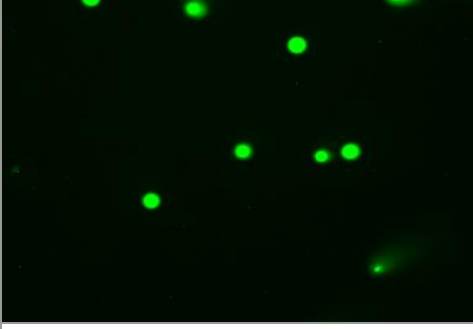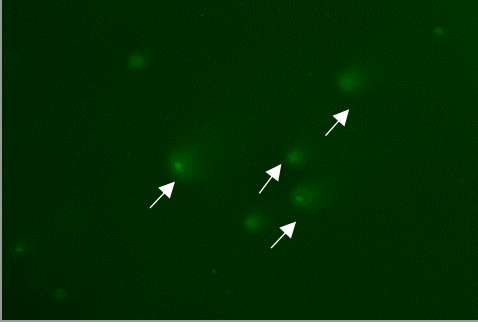
Table 21 Photomicrographs of stained DNA of MCF7 cells for alkaline comet assay.

Damaged DNA at the areas with white arrows. Magnification, ×20; scale bars, 200 µm.

	24 h of OXY treatment	48 h of OXY treatment
Control		
Oxy50µM		
Oxy100 µM		
H_2O_2 100 µM for 4 h treatment		

7.4 Discussion

Apoptosis has been triggered in MCF7 and HepG2 cells following treatment with OXY. The mechanisms of action via this pathway could be elucidated through two main routes: the extrinsic or death receptor pathway and the intrinsic or mitochondrial pathway. However, the two pathways have been proved that it is interconnected and the molecules in one could influence the other (Igney and Krammer, 2002). FAS and TNFRSF10B, the two well–characterised death receptors, were up–regulated (Ashkenazi and Dixit, 1998). FAS was activated and induced the recruitment of Fas–associated death domain (FADD), which then activated caspase–8 (CASP8). Apoptosis ligand 2/tumour necrosis factor–related apoptosis–inducing ligand (Apo2L/TRAIL) is one of the pro–apoptotic ligands at the cell membrane, which can activate apoptosis through FADD and caspase 8. The activation of apoptosis via the Apo2L/TRAIL pathway has reported to be significant potential for cancer therapy and act independently from p53 (Ashkenazi *et al.*, 1999). The cascade of apoptotic molecules was then activated through caspase 3 or mitochondrial routes; the genes up–regulated including BAX, BAK1, DIABLO and APAF1. The activation via caspase–8 is known to propagate the apoptotic signal either by directly cleaving and activating downstream caspases or by cleaving the BH3 Bcl2–interacting protein, which leads to the release of cytochrome c from mitochondria, triggering activation of caspase–9 in a complex with dATP and APAF1 and induce cells death (Kruidering and Evan, 2000).

The induction of apoptosis by OXY in MCF7 cells was interesting because TP53 was not activated as indicated by the gene expression and comet assay results. Even though TP53 functionally responds to cell cycle arrest, cell senescence, DNA repair, metabolic adaptation and cell death (Aubrey *et al.*, 2018), The modulation of OXY dependently from TP53 has also been reported in neuroblastoma cell lines (Rahman *et al*., 2017) or prostate cancer cell lines treated with camptothecin. The report also found that p53–mediated apoptosis only occurred in severe DNA damage, not with low DNA damage

(Ho *et al.*, 2019). The results also found not to generate severe DNA damage and ROS generation (Chapter 5) at the doses apoptosis occurred. The genes responsible for ROS including adaptor–related protein complex 1 sigma (AP1), activating transcription factor 1 (ATF1) and nuclear factor of kappa light polypeptide gene enhancer in B–cells 1(NFKB1) (Turpaev, 2002) were not activated (data was not shown). OXY did not significantly cause loss of the cell membrane integrity after treated for 48 h, it may indicate the compound did not directly change the physical properties of the cells. The release of LDH detected in the two kinds of cells may be the effect of apoptosis in late stage.

Caspase–3, a key protease in the executed phase of apoptosis, was also determined in MCF7 and HepG2 cells. Although MCF7 cells have been reported not to express caspase–3 protein (Janicke, 2009), the antibody can be positive to key enzymes involved in cellular repair and maintenance such as poly(ADP–ribose) polymerase (PARP), the 70–kD unit of theU1–ribonucleoprotein (U1–70kD), the catalytic subunit of DNA–dependent protein kinase (DNA–PK) and sterol–regulatory element binding proteins (SREBP) (Alam *et al.*, 1997). These proteins are also involved in apoptosis events (Cohausz and Althaus, 2009). The loss of mitochondria membrane potential (MMP) in the two cell lines occurred dose–dependently after OXY exposure 24 h. Therefore, OXY mainly modulated apoptosis pathway via intrinsic pathway dependent from TP53.

In this chapter should be concluded that OXY induced apoptosis in MCF7 and HepG2 cells. The cascade events were activated through extrinsic and extrinsic pathways. Death receptors, TNFRSF10B, FAS and Apo2L were increased in expression. CASP 8 caused activation via intrinsic genes and proteins including BAX, BAK, DIABLO and APAF1 resulting in the loss of mitochondria membrane potential. The executioners, mainly caspase 3 and its paralogues were activated resulting in loss integrity of the cell membrane, chromatin condensation and eventually cell death. However, OXY did not cause TP53 activation, ROS generation and severe cellular DNA breakage. The findings reported in this chapter consequently demonstrate that OXY can induce apoptosis.

CHAPTER 8 EFFECT OF OXY ON PROLIFERATION, METASTASIS AND DNA REPAIR PATHWAYS

8.1 Introduction

Transforming growth factor–β (TGFβ) signalling, which is in TGFβ superfamily consists of more than 30 different members play crucial roles in tumour initiation, development and metastasis. Therefore, the inhibition of epidermal growth factor is one of the targets of cancer therapeutics (Smith *et al.*, 2012; Neuzillet *et al.*, 2015). Some stilbenes such as resveratrol, have been reported inhibiting epidermal growth factor (EGF) and related receptor (EGF–R), a transmembrane tyrosine kinase activated by ligands, and the transforming growth factor–beta (TGF–β) (Zhao *et al.*, 2018). Some other genes in MEK/ERK signalling cascades such as CXCR4 and its ligands also take part in controlling proliferation and metastasis of cancer cells and may be mediated by stilbenoids (Bhattacharya *et al.*, 2011; Chen *et al.*, 2013; Wang *et al.*, 2017). Therefore, such genes may be thought of as indicator genes that should be monitored if a compound, such as OXY is considered to shows anti–proliferation, anti–migration or anti–invasion in cancer cells.

Cyclin–dependent kinases (CDKs) play a crucial role in cell proliferation and control of the cell cycle and are moderated by interactions with cyclins or CDKs inhibitors. For example, CDK2 and CDK4/6 in association with their respective catalytic partners including cyclin D and E types are responsible for retinoblastoma proteins (Rbs) and then bind to sequester members of the E2F family of transcription factors directly regulating S phase of the cell cycle (Lim and Kaldis, 2013). CDK2 could also be inhibited by p21 (CDKN1A) which represents a major target of p53 activity. Recently, CDK2 inhibitor has been reported as a possible therapeutic target for new cancer therapeutics to limit tumour growth and help reduce the side effects of current chemotherapy drugs (Wood *et al.*, 2019). P53 also strictly controls GADD45A, one of the apoptotic inducers, playing a negative role in cell proliferation and cell growth (Jin *et al.*, 2002).

The interconnected link between the cell cycle and DNA repair is a cell cycle stage in which the double–strand breaks (DSB) may be generated. Most homologous recombination events occur during sister chromatid synthesised in S–G2 phase of the cell cycle (Rothkamm *et al.*, 2003). The regulation of CDKs in the cell cycle is directly related to homologous recombination and restricted the process in G1–S phase in eukaryotic cells (Aylon *et al.*, 2004). Therefore, inhibition of CDKs activities may affect the cell cycle process and homologous recombination repair accordingly. Cisplatin (Cis) is a platinum-based chemotherapy drug widely used to treat several types of solid cancer including breast cancer. However, this drug can cause a toxic side effect and resistance to cancer (Dasari and Bernard Tchounwou, 2014). The inhibition of the gene overexpression in DNA repair pathway has been reported to be one of the new strategies to overcome the resistance or re-sensitise them to chemotherapeutic compounds (Kelley *et al.*, 2014; Leon-Galicia *et al.*, 2018). OXY was also investigated for its ability to increase the sensitivity of selected cancer cells to selected chemotherapeutic drugs.

8.2 Aims

To investigate the effect of OXY exposure on the key genes and proteins in cell proliferation, metastasis and DNA repair pathways in MCF7 and HepG2 cells. The investigation was carried out using microarray data, qPCR, as well as flow cytometry to analyse the cell cycle, cell migration and invasion.

8.3 Results

8.3.1 Effect of OXY on cell proliferation and cell growth

8.3.1.1 Genes expression

OXY inhibited genes involving in transforming growth factor–β (TGFβ) signalling including TGFβ1, TGFRB2 and LTBP1 through down–streamed deregulation of Smad1, Smad3, Smad4, Smad6, Smad7 and Smad9 (Figure 66–68). Moreover, OXY also down–regulated genes in SMAD–independent pathways including NFkB, TNF, MAPK of TGFβ signalling family and genes in PI3K/AKT signal transduction pathways (Figure 66), which involved in cell proliferation process. OXY significantly (P<0.05) inhibited the expression of genes in DNA synthesis and cell cycle pathways (Figure 67), directly related to cell proliferation and growth. The key genes in this process including CDK2, CDK4 and E2F. Several genes in G1 phase such as CDK4/CCND complexes were also significantly inhibited. While, G1/S transition phase was the most down–regulated of CDK2 and Cyclin Es complex. The process was also disphosphorylated by the expression of CDKN1A and GADD45A resulting in blocking the DNA polymerase and DNA replication. While, the gene in G2 phase–M phase such as CDK1 was not significantly affected by the OXY–treatment. The expression signals of key genes in MCF7 cells treated with 0 µM, 50 µM and 100 µM for 24 h were elucidated in Figure 68; CDK2, CDK4, E2F1, FoxM1, TP53 and TGFB1 were significantly down–regulated, while CDKN1A and GADD45A were significantly up–regulated.

The relative quantity of mRNA expression of the relevant genes to cell proliferation and growth was validated by qPCR using specific primer sets. The gene expression was consistent with the data acquired from microarray shown in Figure 69; CDK4 and E2F1 were significantly down–regulated, while CDKN1A and GADD45A were significantly up–regulated dose–dependently.
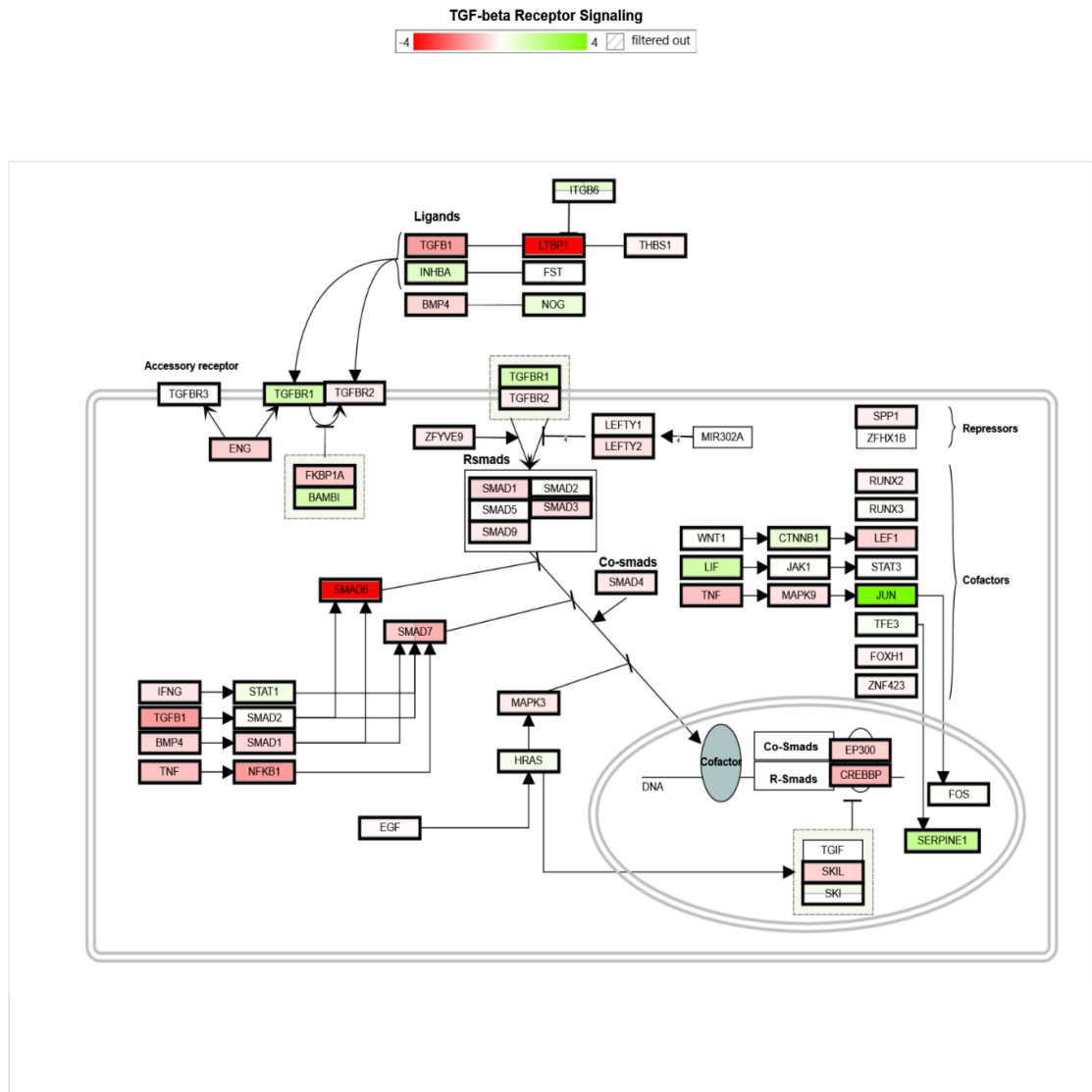
Figure 66 Gene expression in TFG–beta receptor pathway altered by 100 µM–OXY treatment in MCF7 breast cancer cells and then the genes were imported to the database of WikiPathways.org. Genes labelled in green were up regulated and in red were down regulated.

Figure 67 Gene expression in G1 to S phase of cell cycle control pathway altered by 100 µM–OXY treatment in MCF7 breast cancer cells and then the genes were imported to the database of WikiPathways.org. Genes labelled in green were up regulated and in red were down regulated.
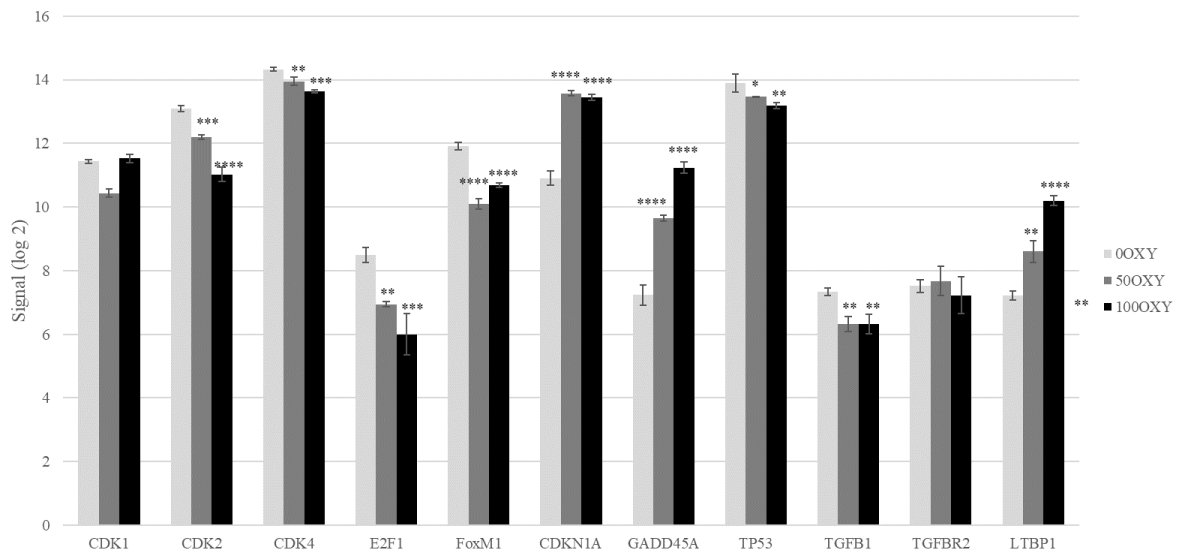
Figure 68 The expression signals of key genes in cell cycle control pathway of MCF7 treated with two different doses of OXY(50 µM and 100 µM) for 24 h. Data are the mean ± SEM (n=3). Statistical analysis was carried out using One-way ANOVA analysis of variance followed by Dunnett's test. The significant difference was compared relatively to the control (*P < 0.1, **P < 0.01, ***P < 0.001 and ****P < 0.0001).
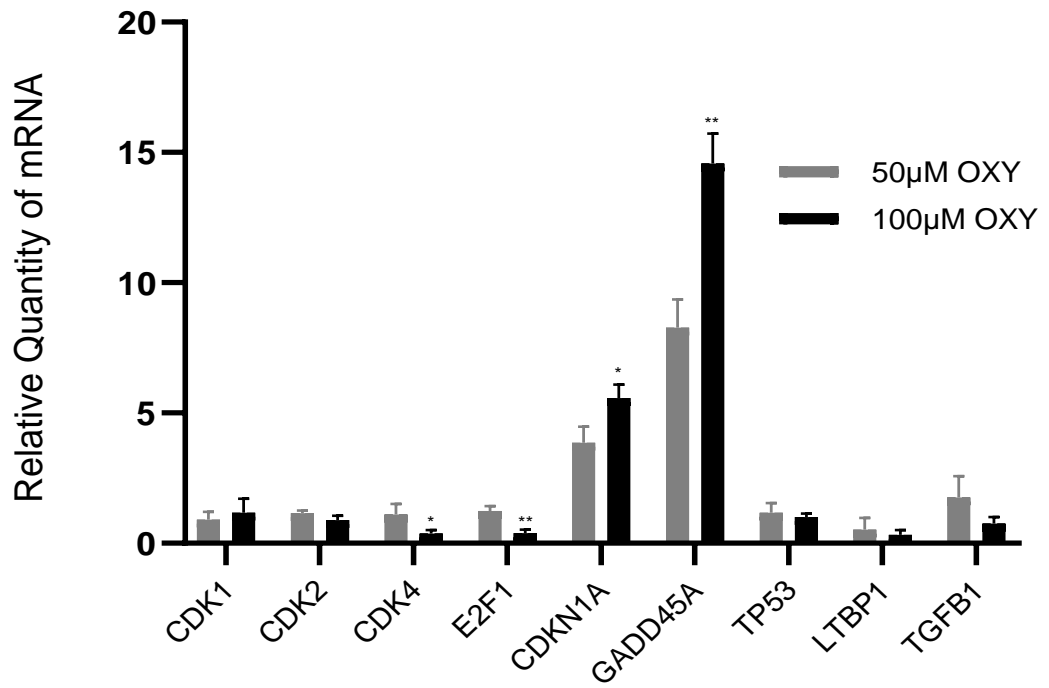
Figure 69 Relative quantity of mRNA expression acquired from qPCR of MCF7 cells treated with different two doses of OXY. Data are the mean ± SD (n=3). Statistical analysis was carried out using unpaired t-test. The statistical difference between the two treatments was carried out using unpaired t-test (*P < 0.5 and **P < 0.05).

8.3.1.2 Cell cycle analysis

To investigate the effect of OXY on cell growth and division, the cell cycle analysis was implemented using flow cytometry technique. Generally, after receiving signals for proliferation, diploid cells exit the resting state Gap 0 (G0) phase and enter the Gap 1 (G1) phase. At this stage, the diploid cells maintain their ploidy by retaining two complete sets of chromosomes (2N). As the cells enter the synthesis (S) phase, DNA replication starts, and in this phase, cells contain varying amounts of DNA. The DNA replication continues until the DNA content reaches a tetraploid state (4N) with twice the DNA content of the diploid state. Tetraploid cells in the G2 phase start preparing for division and enter the mitosis (M) phase when the cells divide into two identical diploids (2N) daughter cells. Therefore, when based on DNA content, cell cycle is commonly described by the G0/G1, S, and G2/M phases.

The results show (Table 23–26) that although OXY did not affect DNA content in MCF7 and HepG2 cells following three hours of exposure. the compound decreased DNA content dose-dependently in G0/G1 phase of the cell cycle at 24 h. Compared with the untreated control (0 µM), 25, 50 and 100 µM OXY decreased the percentage of the cell population from 85.43±0.34 to 75.39±0.75, 72.34±0.82 and 62.27±0.68%, respectively. S phase also significantly decreased from 19.37±0.09 to 19.35±0.48, 16.47±0.63 and 14.66±0.57%, respectively. Whereas G2/M phase was likely to be induced from 3.52±0.11 to 4.50±0.46, 3.68±0.17 and 7.40±0.38%, respectively during the time incubated.

Likewise, there were no changes in the DNA content of HepG2 cells within 6 h exposure. However, the cell population in G0/G1 and S phases was decreased dose–dependently. These results indicated that OXY arrested G0/G1 and S phases of the cell cycle.

Table 22 Effect of OXY on cell cycle distribution in MCF7 cells determined using flow cytometry. The histograms showing the numbers of cells in different phases after MCF7 cells were treated with OXY 25–100 μM for 3–24 h and then subject to flow cytometric analysis.
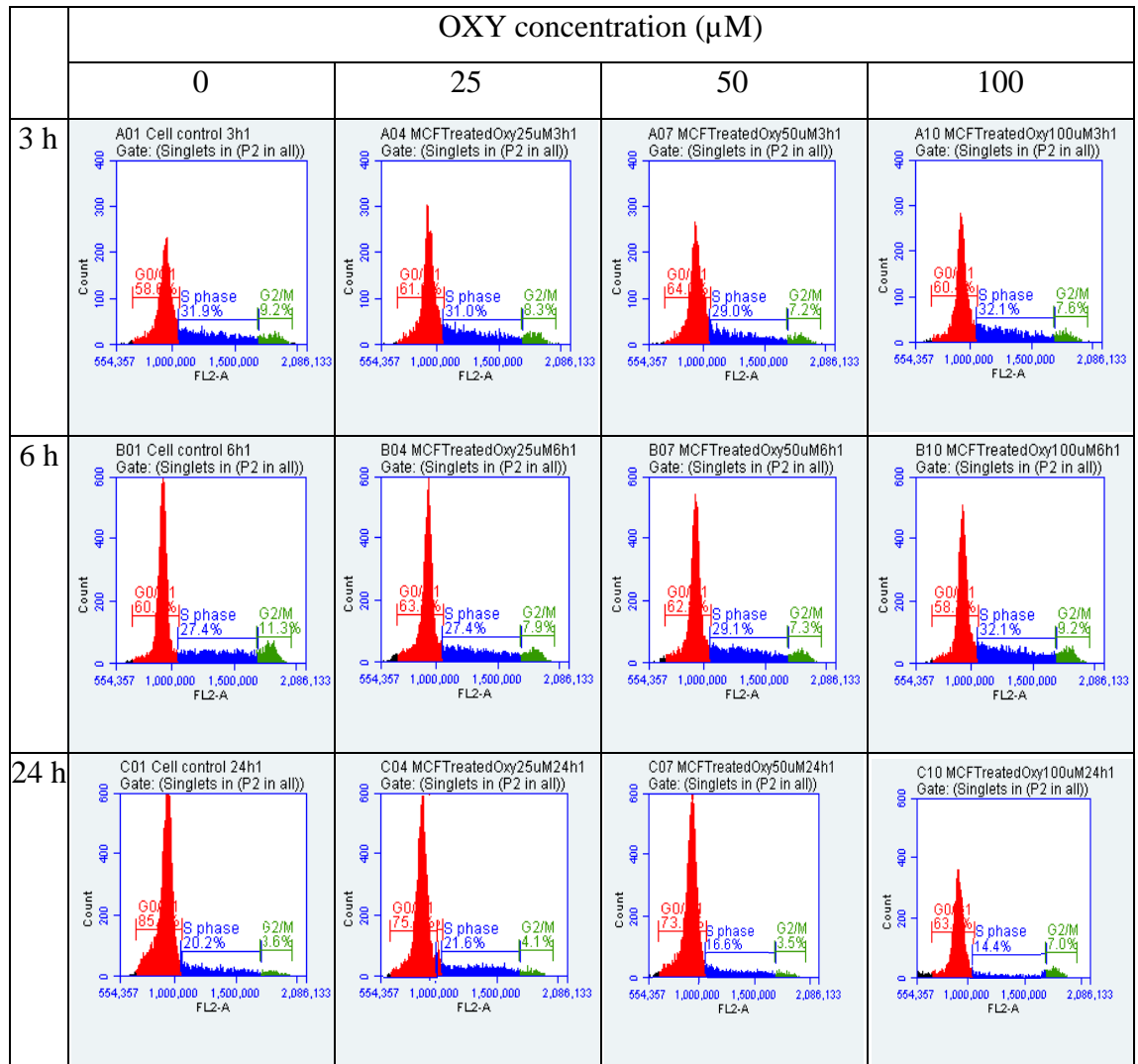
Table 23 Effect of OXY on cell cycle distribution in MCF7 cells determined using flow cytometry. Bar graphs showing the percentages of MCF7 cells in G0/G1, S phases and G2/M when treated with OXY 25–100 µM for 3–24 h and then subjected to flow cytometric analysis. Data are the mean ± SD (n=3).

Table 24 Effect of OXY on cell cycle distribution in HepG2 cells determined using flow cytometry. The histograms showing the numbers of cells in different phases after HepG2 cells were treated with OXY 50–200 μM for 3–24 h and then subjected to flow cytometric analysis.

	OXY concentration (μM)			
	0	50	100	200
3 h	A01 Cell control3h1 G0/G1 60.3% S phase 24.5% G2/M 10.5%	A04 HepG2treatedOxy50uM3h1 G0/G1 65.8% S phase 22.2% G2/M 10.0%	A07 HepG2treatedOxy100uM3h1 G0/G1 66.4% S phase 21.6% G2/M 9.4%	A10 HepG2treatedOxy200uM3h1 G0/G1 63.3% S phase 23.3% G2/M 11.4%
6 h	B01 Cell control6h1 G0/G1 63.8% S phase 21.6% G2/M 13.0%	B04 HepG2treatedOxy50uM6h1 G0/G1 67.5% S phase 20.7% G2/M 6.8%	B07 HepG2treatedOxy100uM6h1 G0/G1 70.2% S phase 20.3% G2/M 6.5%	B10 HepG2treatedOxy200uM6h1 G0/G1 68.7% S phase 21.5% G2/M 8.0%
24 h	C01 Cell control24h1 G0/G1 68.6% S phase 33.3% G2/M 6.8%	C04 HepG2treatedOxy50uM24h1 G0/G1 70.6% S phase 32.5% G2/M 6.7%	C07 HepG2treatedOxy100uM24h1 G0/G1 69.2% S phase 24.4% G2/M 4.2%	C04 HepG2treatedOxy50uM24h1 G0/G1 59.5% S phase 32.5% G2/M 6.7%

Table 25 Effect of OXY on cell cycle distribution in HepG2 cells determined using flow cytometry. Bar graphs showing the percentages of HepG2 cells in G0/G1, S phases and G2/M when treated with OXY 50–200 μM for 3–24 h and then subject to flow cytometric analysis. Data are the mean ± SD (n=3).

	G0/G1	S phase	G2/M
3 h			
6 h			
24 h			
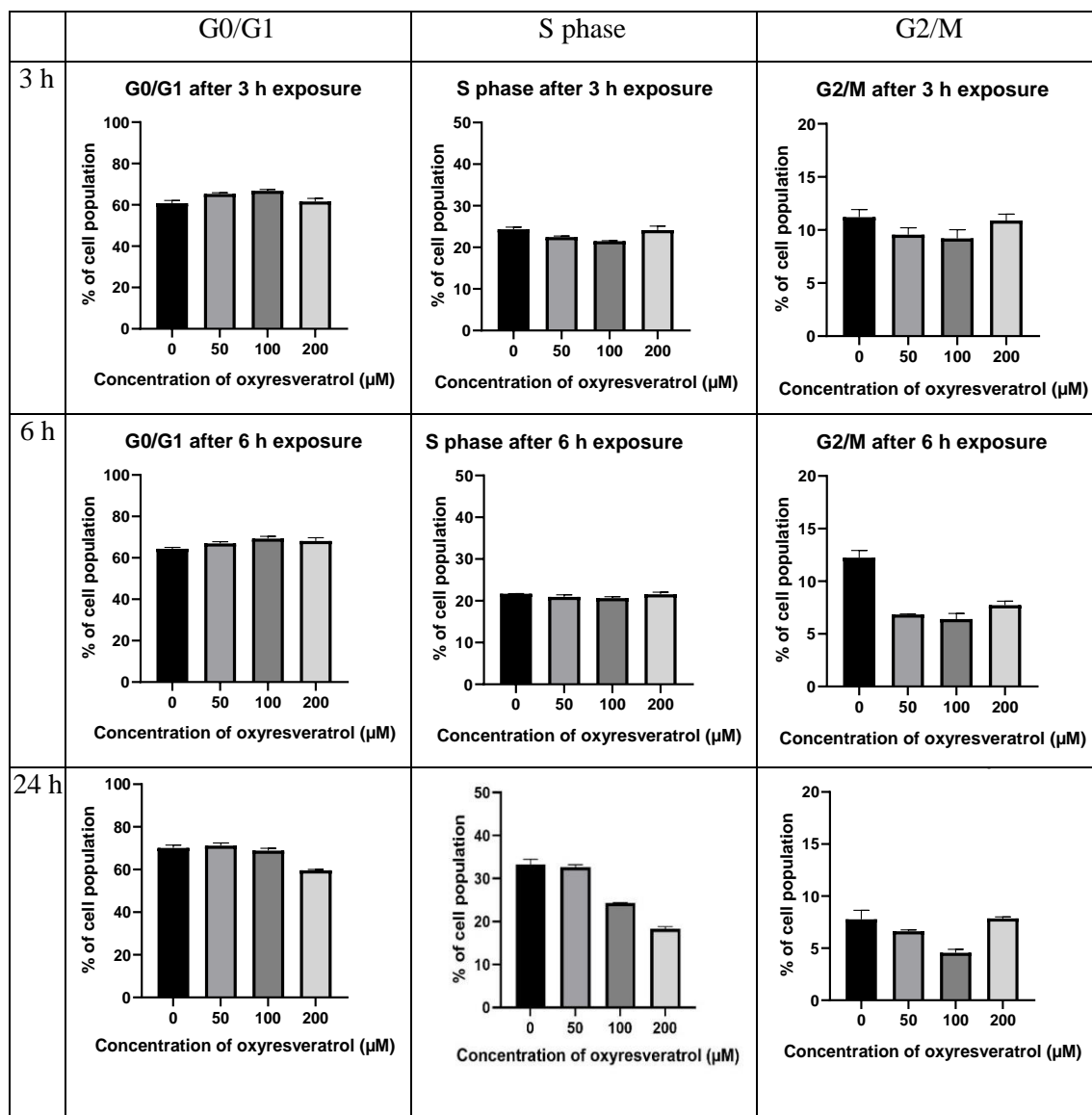
8.3.2 Effect of OXY on cell migration, invasion and metastasis

8.3.2.1 Gene expression results

OXY was found to down–regulate genes involved in chemotaxis and metastasis (Figure 70) including chemokine (C–X–C motif) receptor 4 (CXCR4), chemokine (C–C motif) receptor 7 (CCR7) and chemokine (C–X–C motif) ligand 12 (CXCL12). Moreover, the compound also down–regulated the important genes in the PI3K/Akt signal transduction pathway (Figure 70) including phosphoinositide–3–kinase, PI3KR1, phosphoinositide–3–kinase, regulatory subunit 2 (beta); interferon, gamma–inducible protein 30 (PI3KR2), phosphoinositide–3–kinase, regulatory subunit 3 (gamma) (PI3KR3), AKT1, AKT2 and other down–stream genes, which inhibited cell growth, migration and survival. The average signal (log2) of the key genes in cell migration, invasion and metastasis pathways of MCF7 treated with 0 µM, 50 µM and 100 µM for 24 h retrieved from microarray shown in Figure 71. Gene CXCR4, CCR, XCL12, PI3KR2, PI3KR3, AKT1 and AKT2 were down–regulated significantly compared to the controls.

The relative quantity of mRNA expression of the several genes in cell migration, invasion and metastasis pathways was also validated by qPCR using specific primer sets. The gene expression was consistent with the data acquired from microarray shown in Figure 72; all gene selected including CXCR4, CXCL12 and PIK3R were significantly down–regulated dose–dependently, while AKT1 was not significantly different.

189
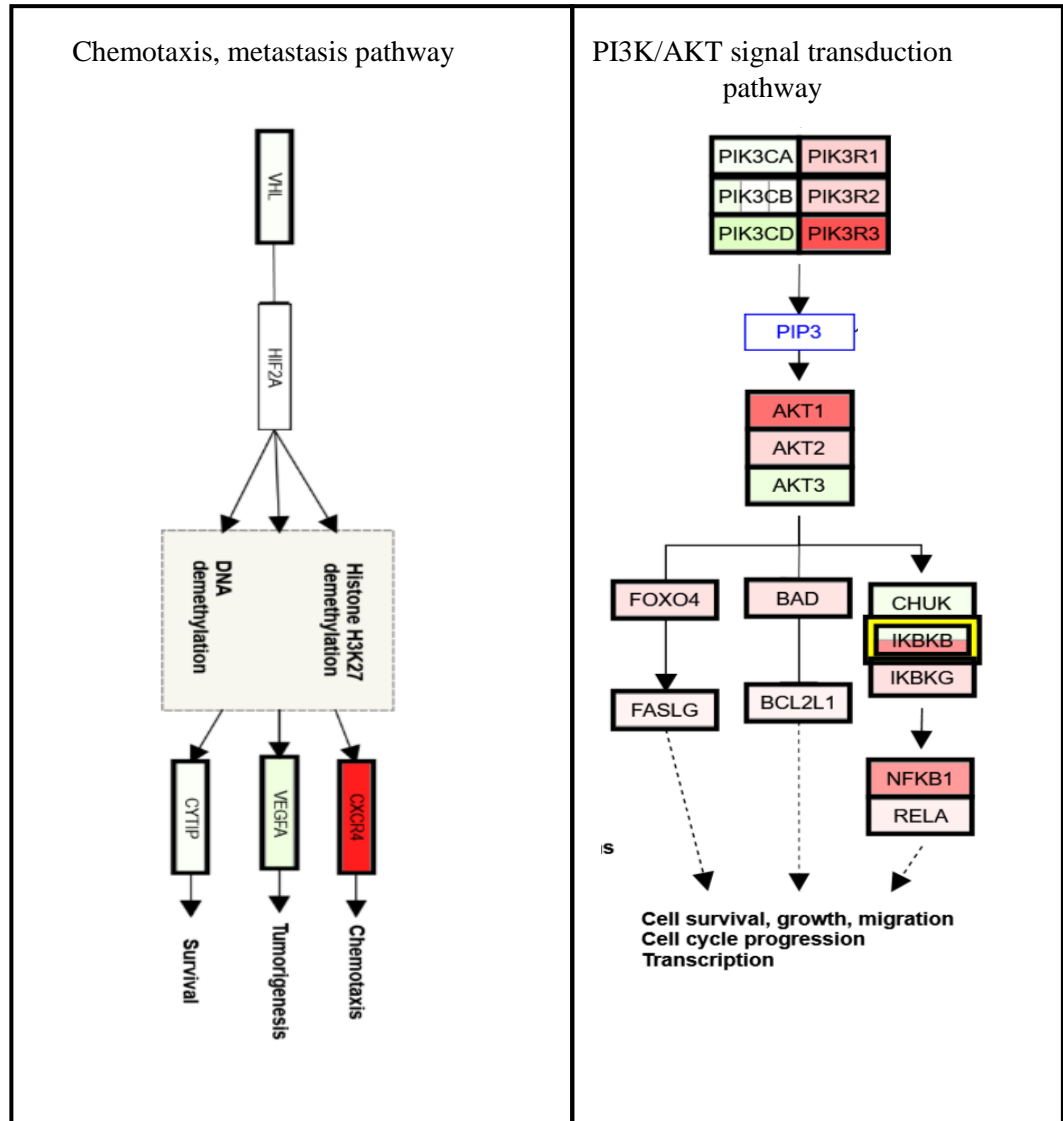
Figure 70 Chemotaxis, metastasis and PI3K/AKT signal transduction pathways integrating expression data of MCF7 cells treated with 100 µM OXY for 24 h. Genes labelled in green were up regulated and in red were down regulated.
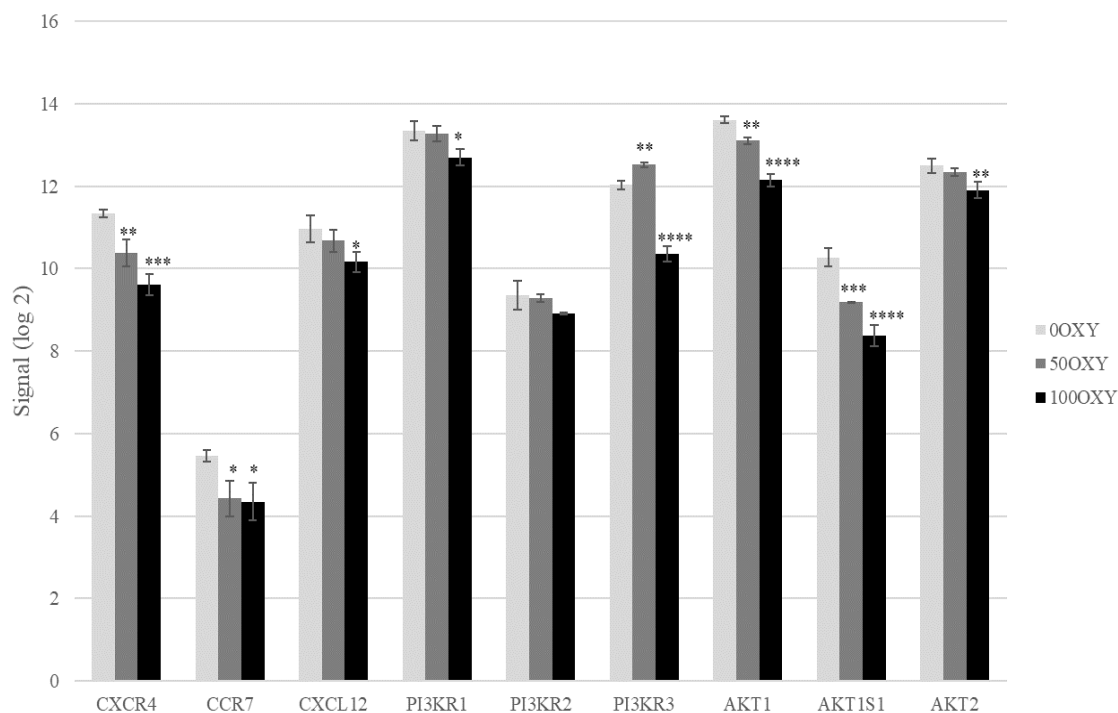
Figure 71 The expression signals of key genes in cell migration, invasion and metastasis pathways of MCF7 treated with two different doses of OXY(50 µM and 100 µM) for 24 h. Data are the mean ± SEM (n=3). Statistical analysis was carried out using One-way ANOVA analysis of variance followed by Dunnett's test. The significant difference was compared relatively to the control (*P < 0.1, **P < 0.01, ***P < 0.001 and ****P < 0.0001).
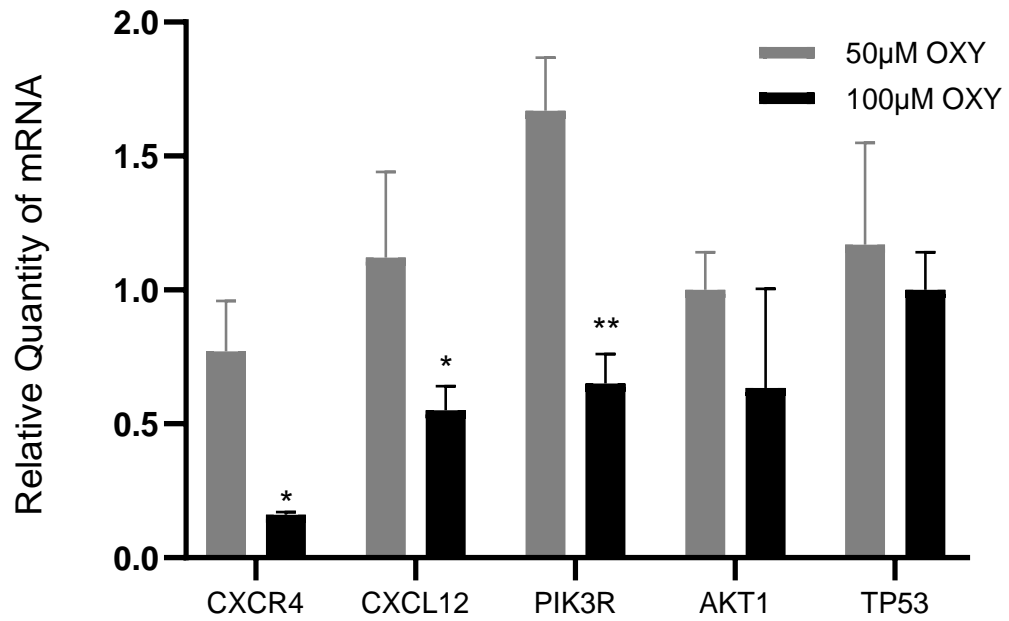
Figure 72 Real–time qPCR from MCF7 cells treated with OXY. Validation of selected genes differentially expressed from MCF7 cells treated for 24 h with 50 µM or 100 µM of OXY versus the control data set. Data are the mean ± SD (n=3). Statistical difference between the two treatments was carried out using unpaired t-test (*P < 0.5 and **P < 0.05).

8.3.2.2 Wound–healing assay

The wound–healing assay was developed and implemented to study directional cell migration *in vitro*. This method mimics cell migration during wound healing *in vivo* (Rodriguez *et al.*, 2005). OXY inhibited the cell migration dose–dependently. Figure 73 elucidated the gaps and wound–closure folds of MCF7 cells treated with different three doses of OXY; 25 µM, 50 µM and 100 µM compared to untreated control (0 µM). The untreated cells migrated to each other and nearly closed the gap at 48 h. The cell treated with 25 µM–OXY the gap also closed time–dependently in 24 h. However, the gaps remained the same at the doses of 50–µM and 100–µM treatments. The wound–closure folds compared to the gaps at the beginning of each treatment. The untreated cells did not close the gaps completely moving around half of the wounds. The 25–µM OXY made the fold a bit closer than the control at 24–h and 48–h treatments. While 50–µM and 100–µM OXY inhibited the wound closure to around 0.1 and 0.2 fold at 24–h and 48–h treatments, respectively.

Likewise, wound–healing results in HepG2 were also dose–dependently effect shown in Figure 74. The monolayer cells closed the gap time–dependently in 48 h and some cells closed the gaps completely at 48–h treatment of untreated control and 50–OXY. Whereas, the gaps tended to be constant at 24–h and 48–h of 100 µM–OXY and 200 µM–OXY treatment. Figure 74 shows line graphs of the wound–closure fold of HepG2 treated with different three doses of OXY(50 µM, 100 µM and 200 µM) compared to the untreated control. The untreated control cells closed the gaps linearly given around 0.4 fold and 0.7 fold at 24 h and 48 h treatment. Similarly, the closing fold of 50–µM treatment was in linear given the values around 0.25 fold and 0.5 fold at 24 h and 48 h treatment, respectively. Whereas 100 µM OXY made the gaps close at around 0.1 fold and 0.2 fold at 24 h and 48 h treatment, respectively. Moreover, the wound–closure tend to be completely inhibited at the dose of 200 µM OXY.
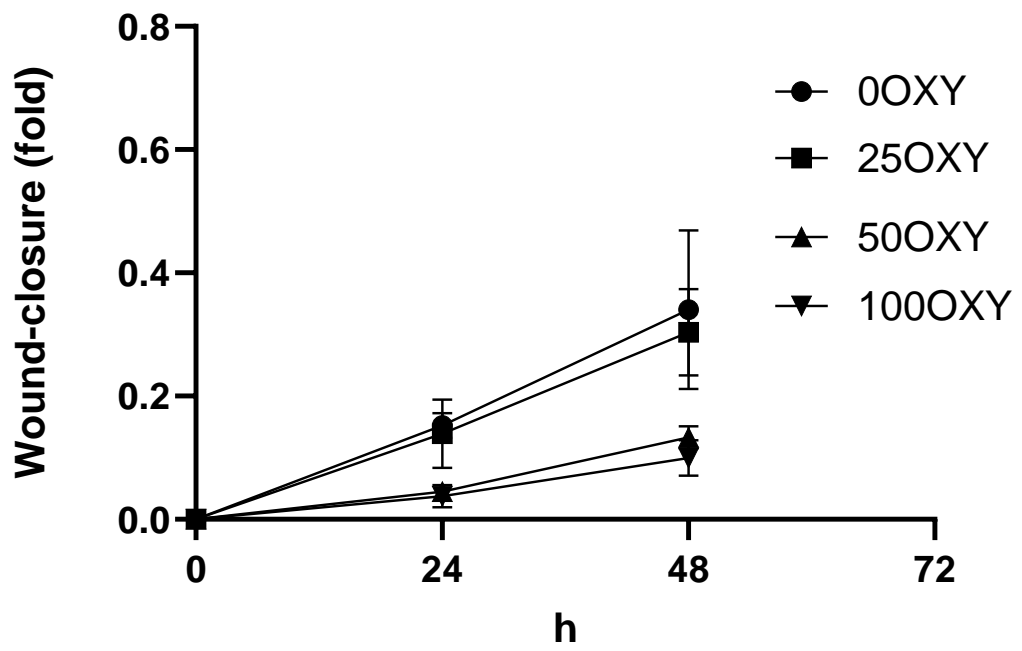
Figure 73 OXY inhibits MCF7 cell migration; average number of cells migrating to the scratch lines and treated with 50 µM 100 µM and 200 µM OXY compared to the untreated group. The gaps were measured at 0, 24 and 48 h after exposed to the compound. Data are the mean ± SEM (n=3).
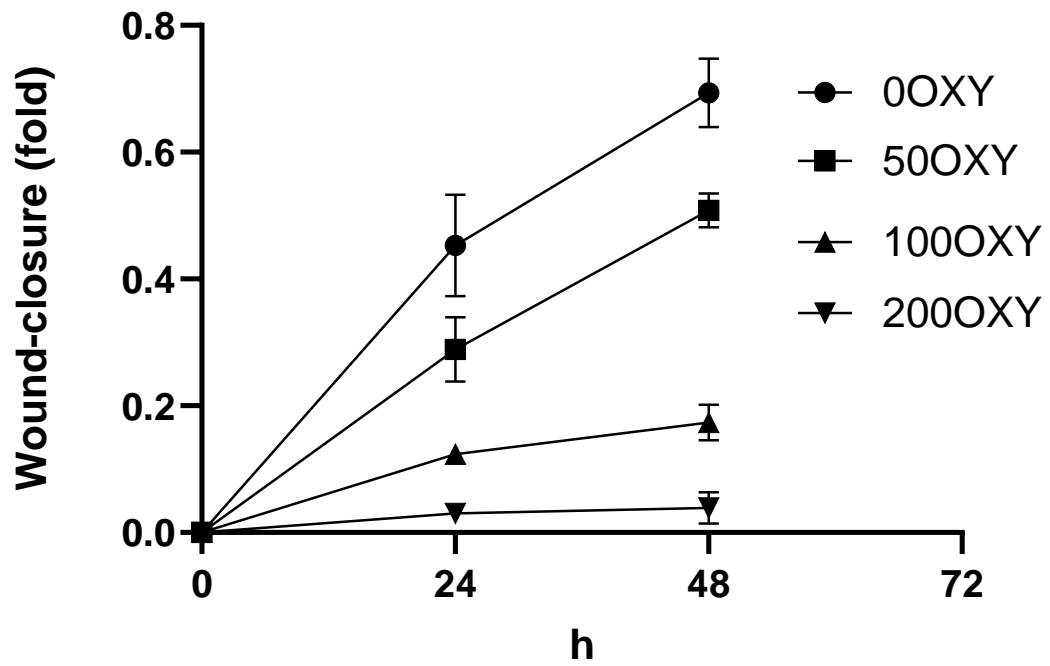
Figure 74 OXY inhibited HepG2 cell migration; average number of cells migrating to the scratch lines and treated with 50 µM 100 µM and 200 µM OXY the gaps were measured at 0, 24 and 48 h after exposed to the compound. Data are the mean ± SEM (n=3).

8.3.2.3 Invasion assay

Transwell invasion assay was conducted in HCC1937 (invasive breast cancer cells) and HepG2 cells. Cells were plated into the matrigel–coated upper chamber of a 24–well format transwell plate and then challenged with OXY. Total 5µg/mL fibronectin was used as a chemoattractant. After 24 h of incubation, cells that invaded through the membrane were stained with crystal violet. The representative fields of three independent experiments are shown in Table 26. The relative invasion was evaluated by counting the number of stained cells shown in Figure 75. HCC1937 and HepG2 cells invaded through matrigel at some certain numbers. The two kinds of the cell were inhibited the invasion dose–dependently. The relative invasion of HCC1937 cells was reduced to roughly 25% and 10% in 50–µM and 100–µM OXY treatments, respectively. Likewise, OXY also inhibited the HepG2 invasion to around 50% and 10% in 50–µM and 100–µM treatment, respectively.

Table 26 OXY inhibits HCC1937 and HepG2 cell invasion; cells migrating through matrigel in the medium treated with 50 µM 100 µM µM OXY compared to the untreated group for 24 h. Each of the figures is representative of three separate experiments. Magnification = ×20; scale bars = 200 µm.

	0OXY	50OXY	100OXY
HCC1937			
HepG2			
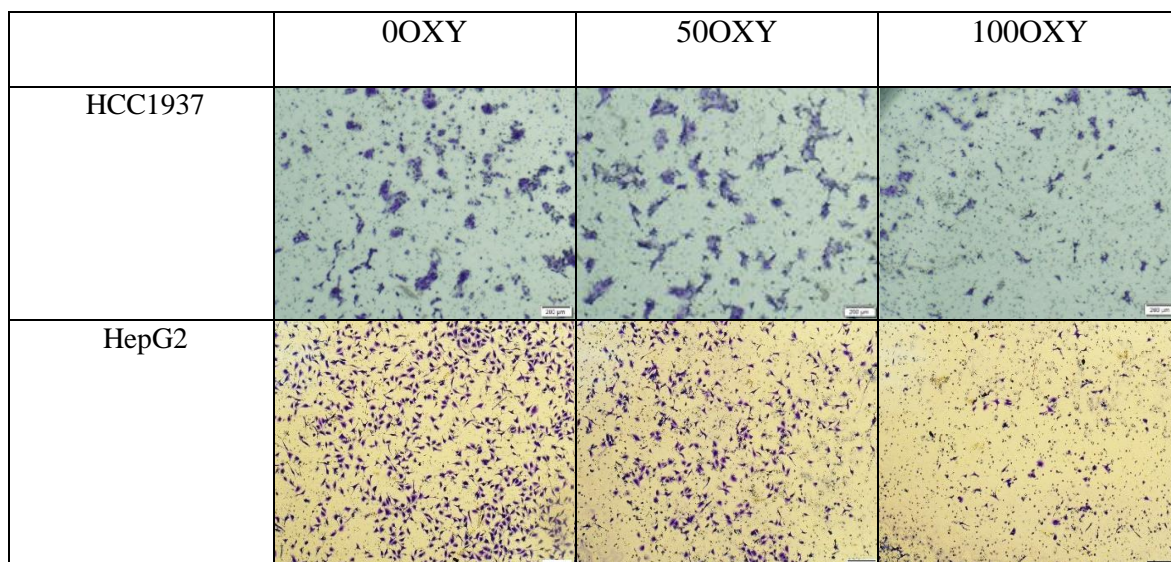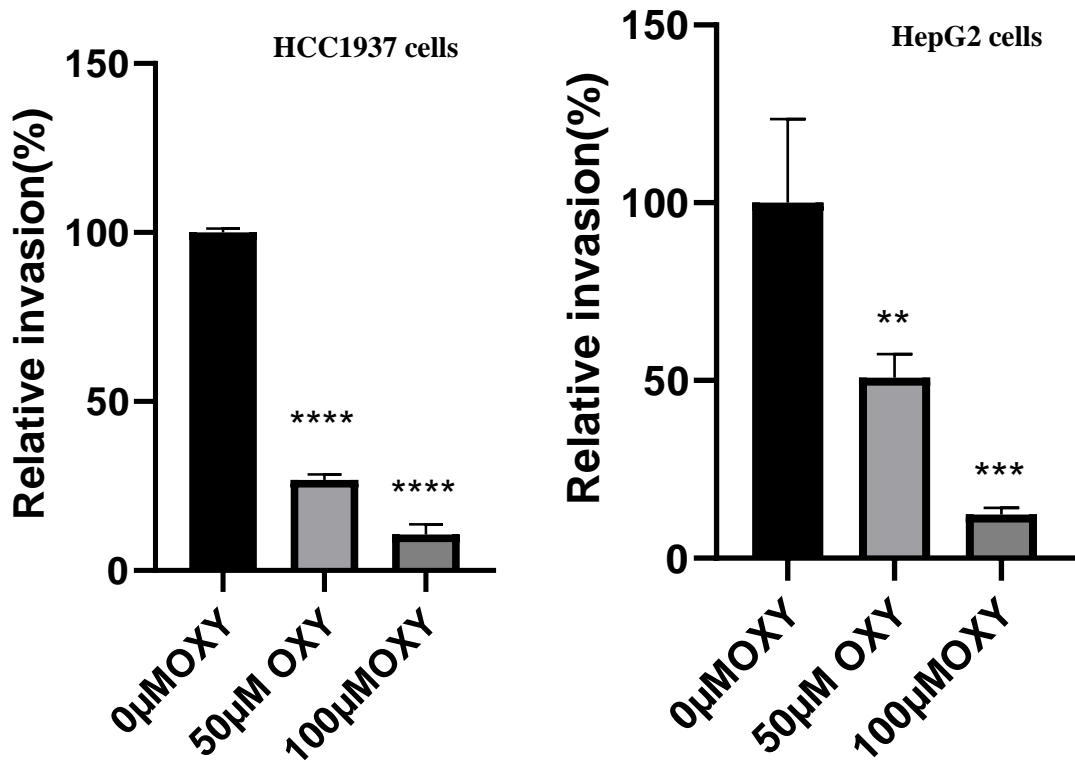
Figure 75 Relative invasion through Transwell of HCC1937 breast cancer and HepG2 cells treated with 50 µM and 100 µM OXY. The data were expressed as the mean ± SEM (n=3). Statistical analysis was carried out using One-way ANOVA analysis of variance followed by Dunnett's test. The significant difference was compared relatively to the control (**P < 0.01, ***P < 0.001 and ****P < 0.0001).

8.3.3 Effect of OXY on DNA repair pathway

8.3.3.1 Gene expression

OXY–mediated DNA repair gene expression in MCF7 cells dose–dependently, especially genes associated with homologous recombination (Figure 76) including RAD51 recombinase (RAD51), MRE11 homolog A, double–strand break repair nuclease (MRE11A), Nibrin (NBN), breast cancer 1, early onset (BRCA1), breast cancer 2, early onset (BRCA2), RAD54 homolog B (*S. cerevisiae*); fibrinogen silencer binding protein (RAD54B), RAD50 homolog, double strand break repair protein (RAD50), RAD52 homolog, DNA repair protein (RAD52) and poly(ADP–ribose) polymerase 1(PARP1).

RAD51, MRE11A, NBN, BRCA1, BRCA2, RAD54B and PARP1 found to be down–regulated, while RAD50 and RAD52 were not affected by the compound (Figure 77).

The qPCR was implemented to confirm that expression of the selected genes using validated specific primer sets to the genes. Most of the relative quantity mRNA were consistent with the results of the microarray. OXY decreased the expression of RAD51, NBN, BRCA1, BRCA2 and PARP1 dose–dependently. Interestingly, RAD51 was the most significantly down–regulated (p < 0.0001). Whereas, MRE11A and RAD50 gene were not significantly different (Figure 78).

Total cell lysates were blotted and identified as described in the materials and methods section with RAD51, PARP1 and BRCA1–specific antibodies and the appropriate secondary antibody with anti–β–actin as a loading control. The western blot analysis demonstrated that OXY also inhibited the enzymatic expression of RAD51 and PARP1 dose–dependently. While BRCA1was slightly decreased shown in Figure 79.
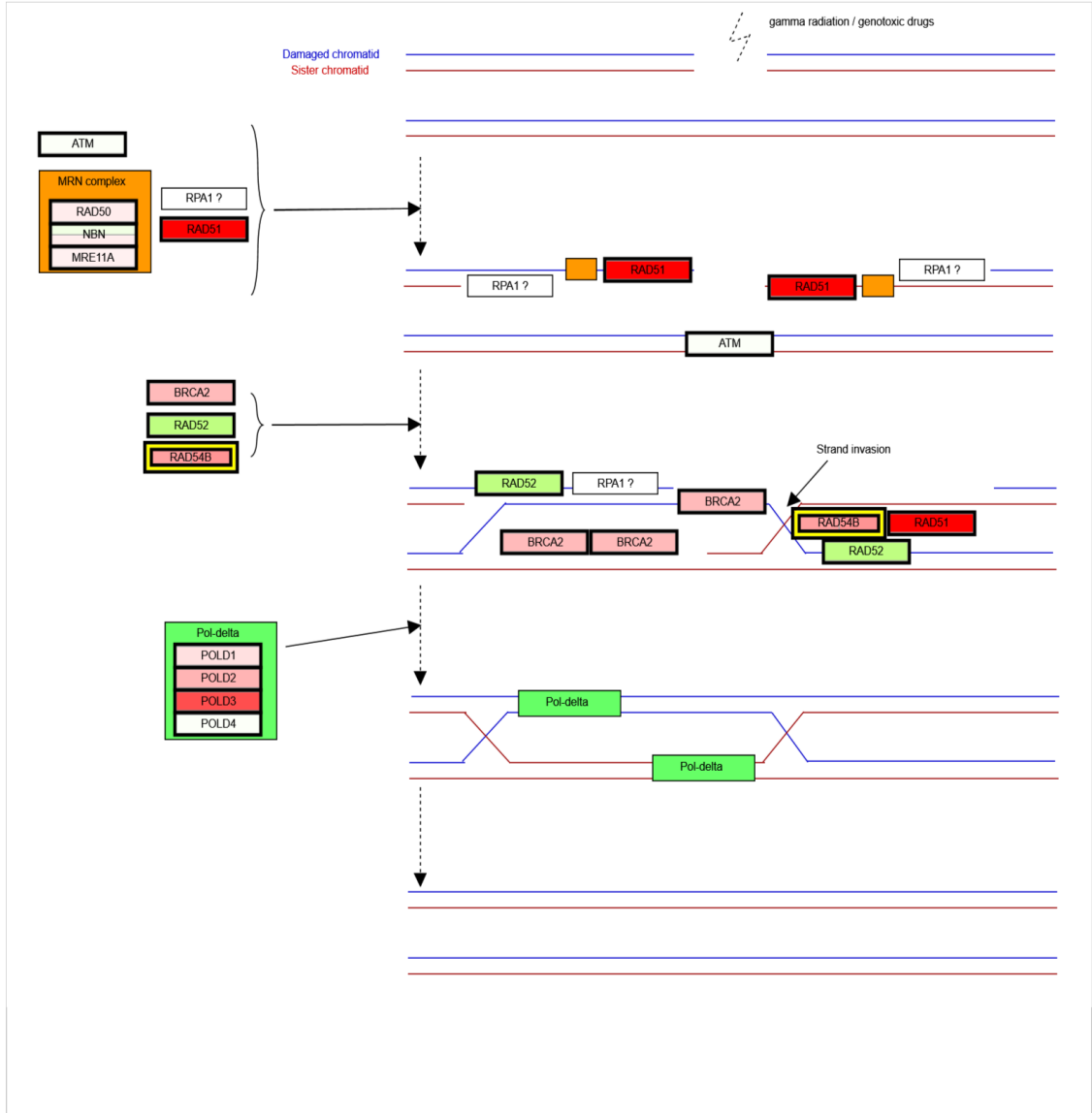
Figure 76 Homologous recombination pathways integrating expression data of MCF7 cells treated with 100 µM OXY for 24 h. Genes labelled in green were up regulated and in red were down regulated.
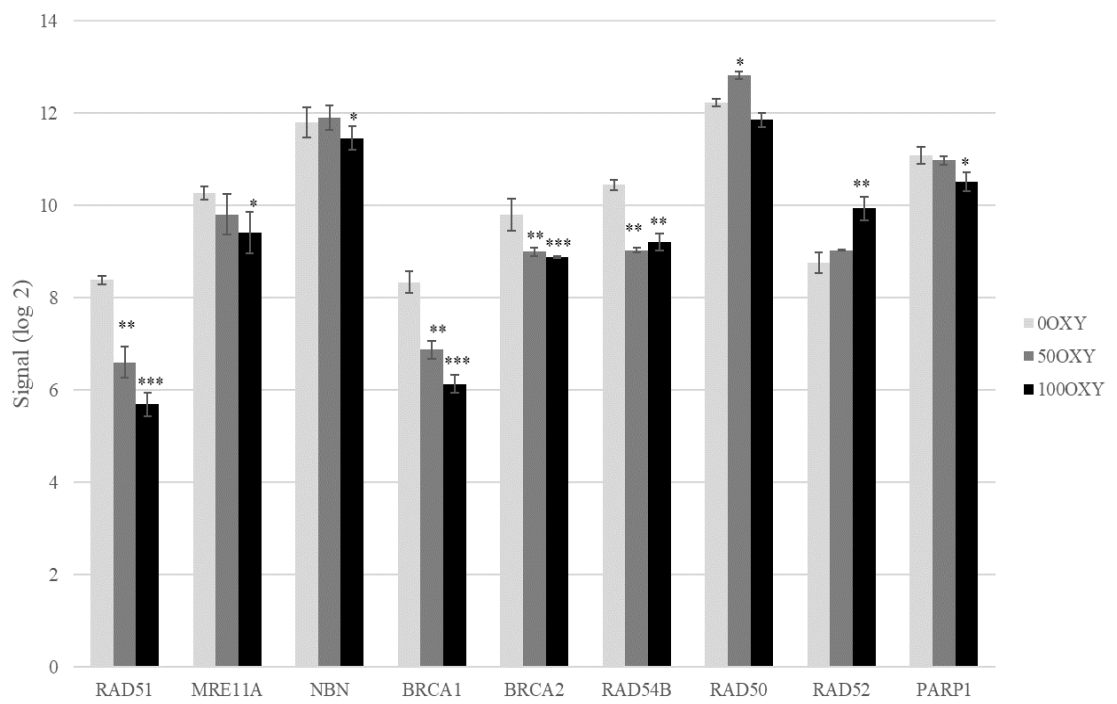
Figure 77 The expression signals of key genes in DNA repair pathway of MCF7 treated with two different doses of OXY(50 µM and 100 µM) for 24 h. Data are the mean ± SEM (n=3). Statistical analysis was carried out using One–way ANOVA and Dunnett's post hoc test (*P < 0.1, **P < 0.01 and ***P < 0.001).
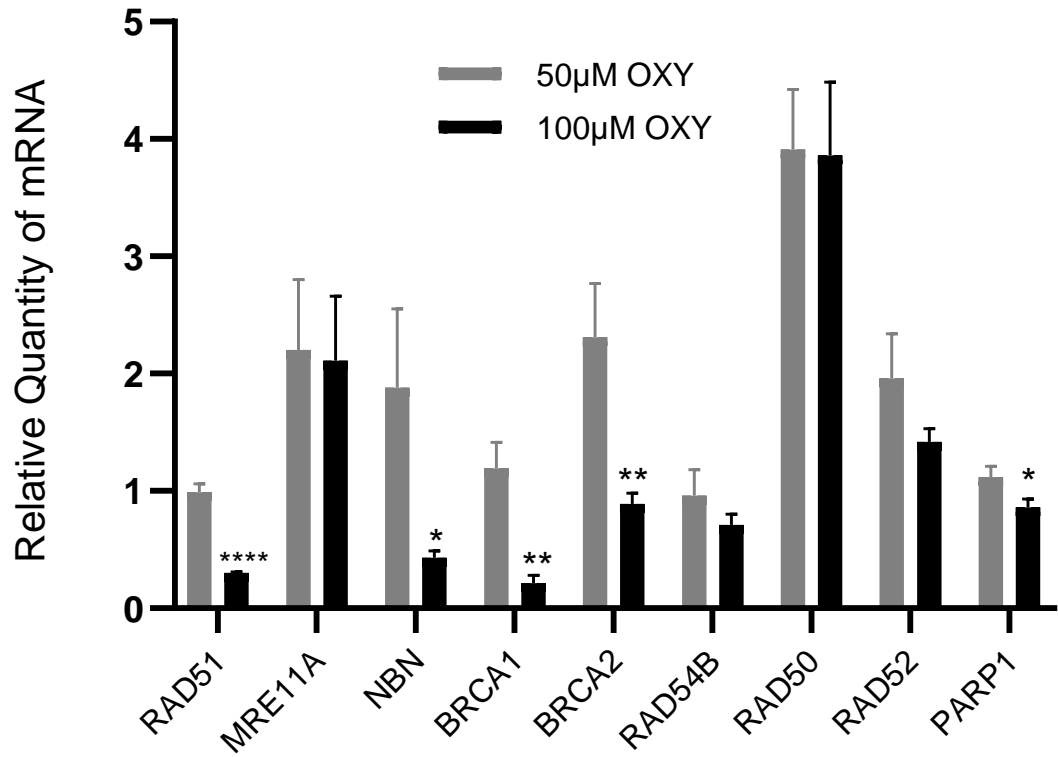
Figure 78 Real–time qPCR from MCF7 cells treated with OXY. Validation of selected genes differentially expressed from MCF7 cells treated for 24 h with 50 µM or 100 µM of OXY versus the control data set. Data are the mean ± SD (n=3). Statistical difference between the two treatments was carried out using unpaired t-test (*P < 0.5, **P < 0.05 and ****P < 0.0001).
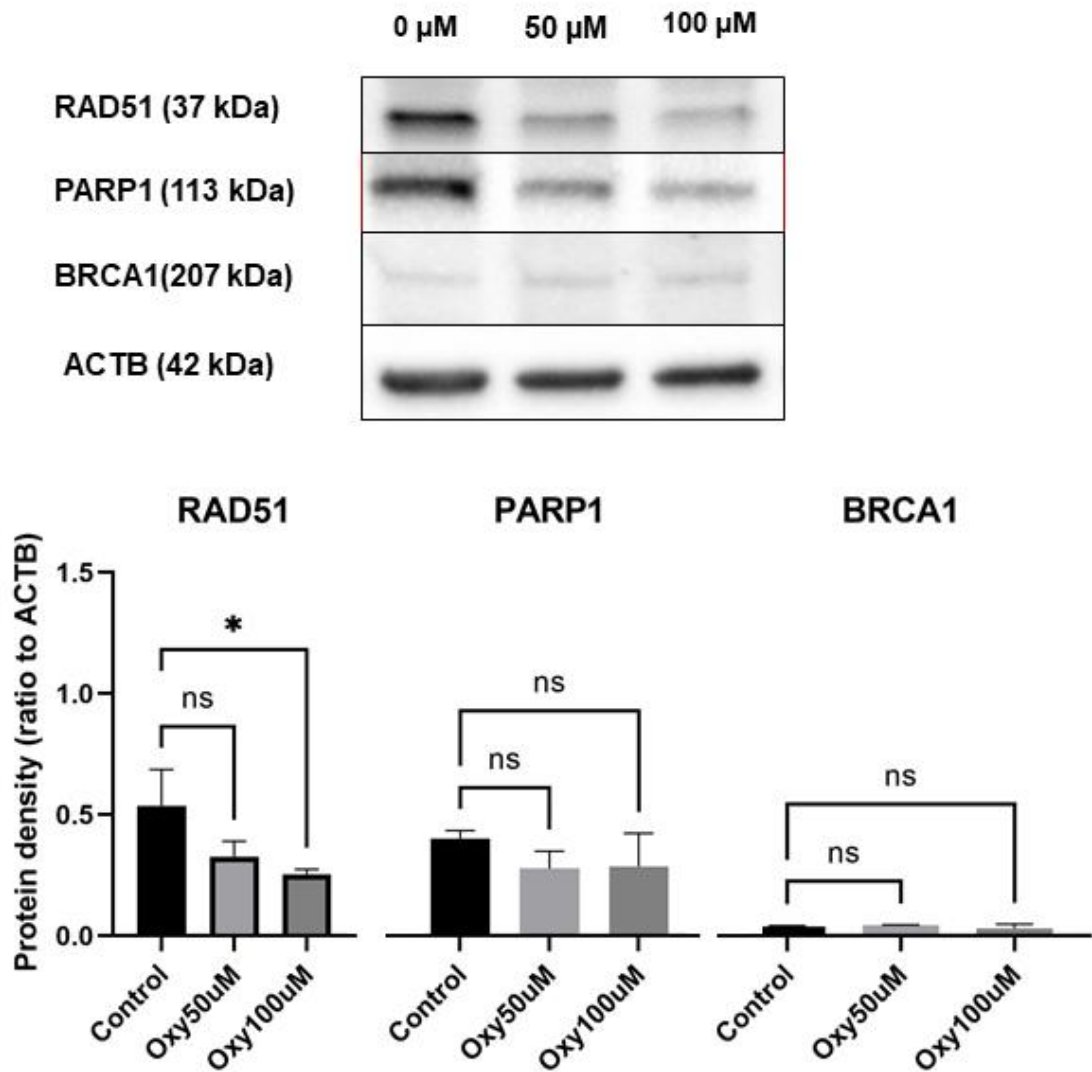
Figure 79 Western blot analysis of DNA repair proteins in the MCF7 breast cancer cells treated for 24 h with 50 and 100 uM of OXY compared with the untreated control. Data are the mean ± SD (n=3). Statistical analysis was carried out using One-Way analysis of variance followed by Dunnett's test (*P < 0.5).

8.3.3.2 OXY enhanced the sensitivity of breast cancer cell lines to cisplatin

Cisplatin and OXY caused cytotoxicity to MCF7 cells (IC_{50} of 18.32 µM and 385.1 µM following 24–h exposure)(Figure 80). Cisplatin was prepared and diluted with the medium at the concentration between 5–200 µM and then exposed to the cells for 24 h. While OXY was diluted with the medium between 5–500 µM for eight concentrations. The MTT assay and the calculation of the IC_{50} values were indicated in Chapter 2.

OXY enhanced the sensitivity of MCF7 to cisplatin. The anti–proliferative effect of cisplatin combined with 50–µM and 100–µM OXY was also investigated using MTT assay. The IC_{50} of cisplatin decreased significantly ($P < 0.05$) given 18.32 µM, 15.78 µM and 5.22 µM in 0–µM, 50–µM and 100–µM OXY, respectively (Figure 81). OXY reduced the viability of the cells treated with cisplatin at the doses between 5–20 µM.
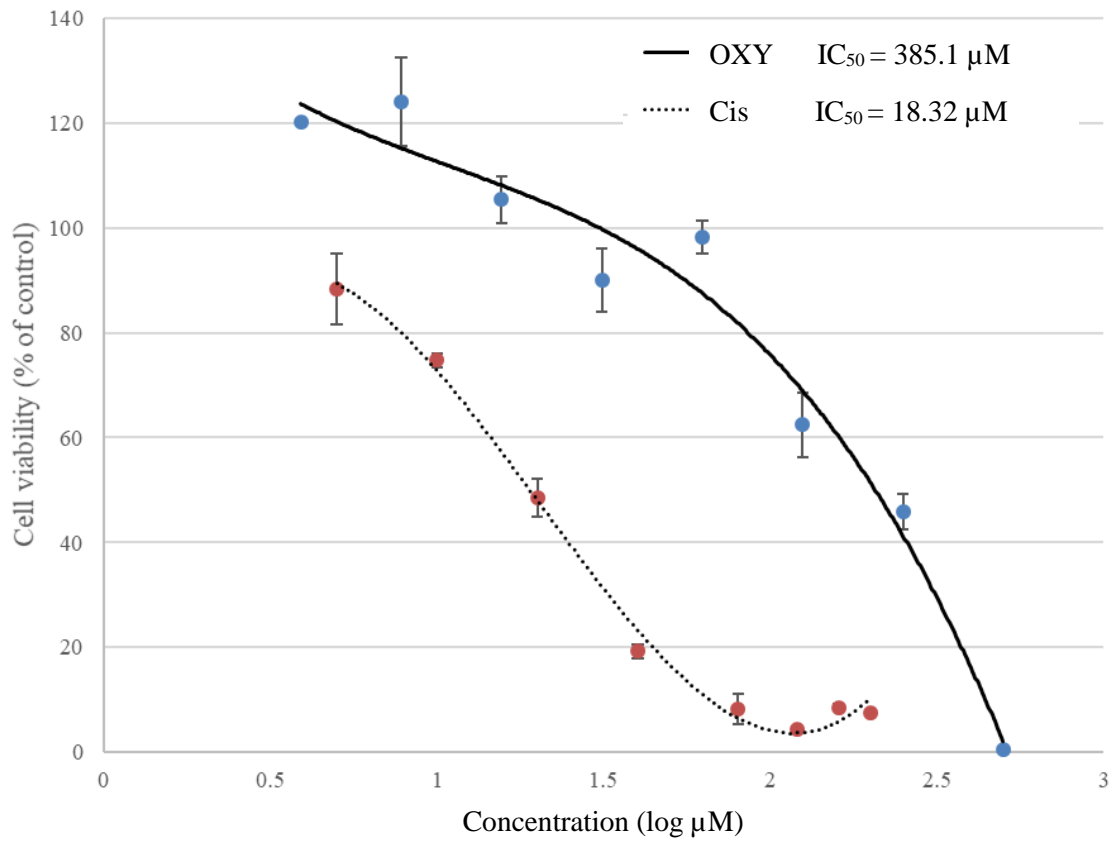
Figure 80 OXY and cisplatin toxicity to MCF7 cells treated for 24 h with different concentrations of OXY and cisplatin. The results are mean ± SD (n=3). The IC_{50} values was calculated using GraphPad Prism 5 programme.
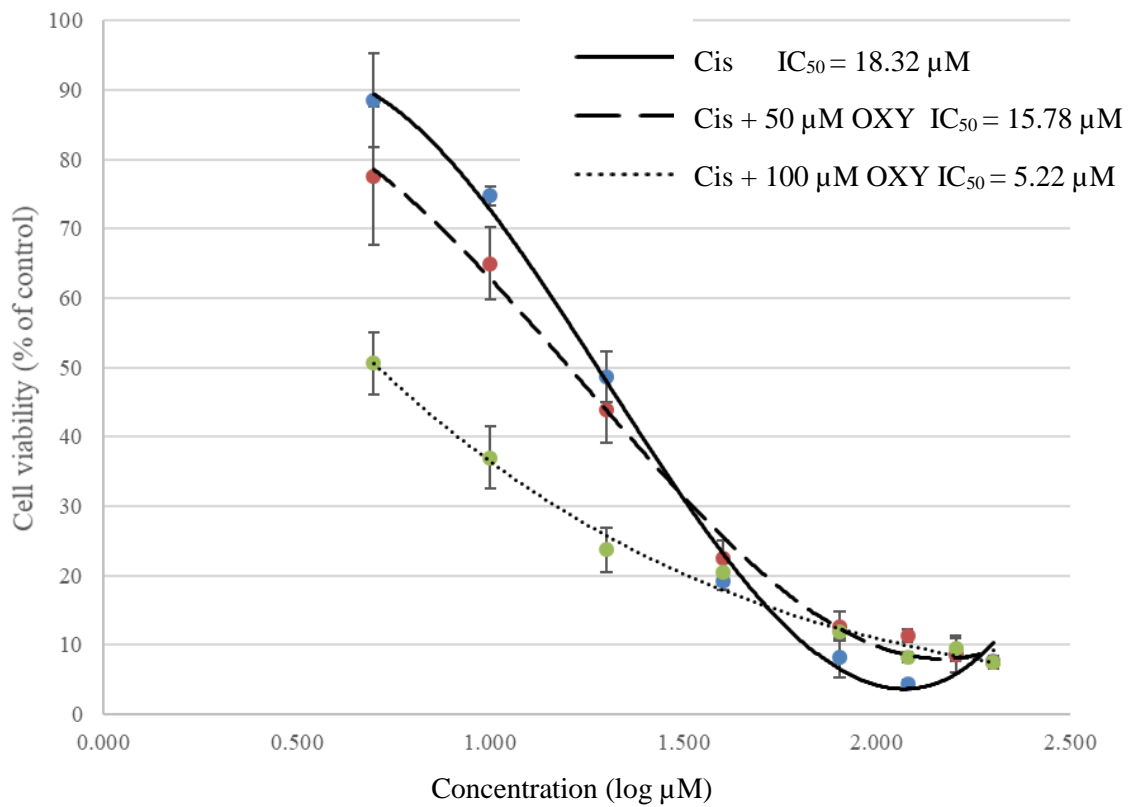
Figure 81 OXY enhanced the toxicity of cisplatin in MCF7 cells treated for 24 h with different cisplatin concentrations alone or together with 50 or 100 μM OXY. The results are mean ± SD (n=3). The IC_{50} values was calculated using GraphPad Prism 5 programme.

8.4 Discussion

The TGFβ signalling pathway regulates not only cancer progression, but also cell growth, differentiation, apoptosis, motility and invasion, extracellular matrix production, angiogenesis and immune response (Smith *et al.*, 2012). However, the TGFβ signalling deregulation is in all steps of carcinogenesis. OXY down–regulated the expression of genes in TGFβ signalling pathways including TGFβ1, TGFRB2 and LTBP1 including mild inhibition of SMADs expression. The key genes in this pathway included TGFβ1, TGFβ2, TGFβR1 and TGFβR2, which are targets of anti-cancer drugs in development (Smith *et al.*, 2012; Katz *et al.*, 2013). However, OXY showed inhibition of TGFβ1 and TGFβR2, not TGFβ2 and TGFβR1 in canonical (SMAD–dependent) pathway. Therefore, the genes in the non–canonical pathway (SMAD–independent) such as PI3K/AKT, NF–κB, TNF–α were also taken in consideration as the results shown in Figure 70.

The inhibition of gene expression in the PI3K/AKT may be the key pathway through G1 to S phase of cell cycle control pathway and affected the downstream process of cell growth, proliferation, cell cycle, migration, metastasis and survival.

OXY significantly inhibited CDK2/CCNE1 (cyclin E1) complex. The overexpression of CDKN1A (a potent cyclin–dependent kinase inhibitor) and GADD45A, suppressed the phosphorylation of several proteins including E2F1 decreasing the synthesis of histone proteins and DNA replication involved in this phase (Jin *et al.*, 2002; Caruso *et al.*, 2018; Wood *et al.*, 2019).

Chemokines and their respective receptors that regulate chemotaxis were recently observed to play an important role in the metastasis of various cancers. Specifically, breast cancer cells express high levels of the CXCR4 and CCR7 receptors (Youngs *et al.*, 1997). CXCR4 and its ligand CXCL12 have also been shown to be involved in metastasis of prostate and ovarian cancers (Fernandis *et al.*, 2004). OXY also has been reported to

be the potent inhibitor of leukocyte migration through the inactivation of MEK/ERK signalling cascade (Chen *et al*., 2013).

Rad51 and its paralogues (RAD51B, RAD51C, RAD51D, XRCC2 and XRCC3) including genes in homologous recombination pathway (Figure 76), are central players in the regulation of DNA repair and centrosome number, involved in the maintenance of genome stability and double–strand DNA repair (Helleday *et al*., 2007). It has been reported that the up-regulation of DNA repair mechanism, especially RAD51 and homologous recombination, is also associated with the resistance of chemotherapeutics and radiation. Protein expression of RAD51 in 17 cancer cells increased 2–7-fold compared to the control primary cells. Treatment of some chemotherapeutics decreased the expression of the protein (Chaney and Sancar, 1996; Raderschall *et al.*, 2002; Yang *et al.*, 2012; Leon-Galicia *et al.*, 2018). The significantly down–regulated expression of RAD51 by OXY may have a key role to play in cancer inhibition. This selective property of OXY may be key to increasing the efficacy of chemotherapeutics.

CHAPTER 9 CONCLUSION AND

FUTURE PROSPECTS

OXY was the dominant compound in water, ethanol and ethyl acetate extracts of *A. lakoocha* heartwood. Extracting with ethanol gave a higher yield than what was achieved using either water or ethyl acetate presenting 3.60 %, 2.44 % and 2.15 %, respectively. Whereas using ethyl acetate as the extracting solvent gave higher purity (64.23%±0.03%) than others (37.81%±0.90% using ethanol and 33.55%±0.08% using water). The chemical profile of the extracts showed the main peak to be OXY and other peaks including resveratrol, which was lower than 1% detected. Authentication of the predominant peak was carried out using NMR with the ^{13}C–NMR and ^{1}H–NMR; the chemical shifts and structure elucidated were in good agreement with the standard. Mass spectra of the main peak detected at RT 14.0 supposed to be OXY showed the spectra patterns were the same as the standard. Its molecular formula $C_{14}H_{12}O_4$ was deduced from the ESI-MS spectrum in positive ion mode by the hydriated molecular ion peak at *m/z* 245 $[M + H]^+$. OXY was stable in different solutions including aqueous and DMSO–d_6, CD_3OD and Acetone–d_6 in the normal lab environment up to 48 h. These provided the phytochemical information of OXY for studying its chemical and biological activities.

In cell–free model, OXY exhibited the pro–oxidant activity generating ROS in the specific presence of copper (II) ions, not Fe(II) or Zn(II). This could cause damage to double–stranded DNA into the open chain or linear forms. OXY was able to show higher capability than resveratrol at the same doses, while *trans*–stilbene did not show the activity. The three *A. lakoocha* extracts also showed the ability to damage DNA consistent with the amount of OXY presented. OXY generated ROS in dose–dependent manner, reduced copper (II) to copper (I) and depleted GSH. In consideration of these findings, OXY has the potential to be developed as a promising anticancer drug candidate and to cause cytotoxicity to cancer cells.

OXY caused toxicity in cancer cells including MCF7, HepG2, PC–3, RAW 264.7 and A549 with the EC$_{50}$ of 30.64±4.79, 104.47±0.82, 106.90±8.63, 115.95±11.28 and 148.63±4.48µM, respectively without causing toxicity to the normal cells (MCF10A and MRC–5 cells). Copper made OXY less toxic. Moreover, OXY and OXY–copper (II) did not increase intracellular ROS in MCF7 and HepG2 cells. OXY also did not cause damage to cellular DNA as investigated using the comet assay.

The gene expression profiling and biological pathways involved in the OXY–mediated cytotoxicity in human breast cancer cells (MCF7) were elucidated. The Clariom Affymetrix microarray was implemented to investigate the expression of more than 20,000 human well-annotated genes in the cells treated with two different OXY doses (50 µM and 100 µM) for 24 h. Total of 686 genes was found to have altered mRNA expression levels of two–fold or more in the 50 µM OXY–treated group (262 upregulated and 424 downregulated genes). While the total of 2,338 genes was found to be differentially expressed in the 100 µM–treated group (907 upregulated and 1,431 downregulated genes). Interestingly, OXY was found to moderate genes mainly involved in apoptosis by activating key genes involved in both extrinsic and intrinsic apoptotic pathways (FAS, TNFR1 and APOL2/TRAIL) and mitochondrial apoptotic genes (BAX, BAK, DIABLO and APAF1), respectively through the caspase cascade. Cyclin–dependent kinases (CDKs) are the main enzymes that play a crucial role in cell proliferation including CDK2, CDK4 and cyclin proteins, which were also suppressed by OXY resulting in blocking DNA synthesis in G1 and S phase and the cell cycle was subsequently arrested. OXY also inhibited the expression of CXCR4 and its ligand (CXCL12) causing anti–cell spreading or metastasis. Most importantly, OXY inhibited the genes in cancer DNA repair pathway; the most affected were RAD51 and genes in homologous recombination, which can break the mechanism of self–repair resulting in enhancing cisplatin sensitivity or overcoming drug resistance. The main genes and biological pathways affected showed in Figure 82.
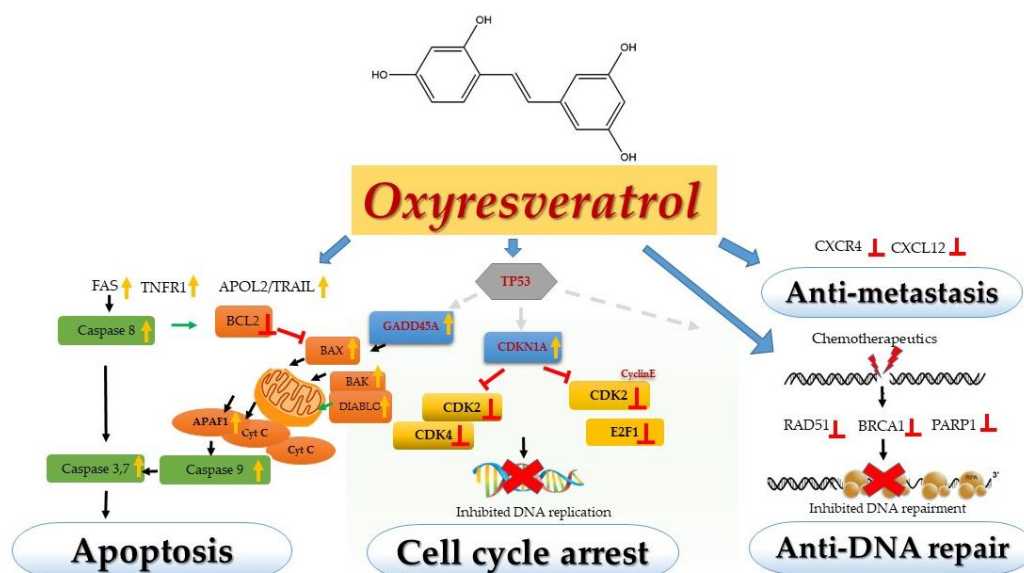
Figure 82 OXY moderated gene expression of apoptosis, cell cycle control, metastasis and DNA repair.

This study showed that OXY posed cytotoxicity to several kinds of cancerous cells with some molecular pathways illustrated. These support the use of OXY as an alternative and complementary medicine for the treatment and prevention of cancer.

Future studies may involve modification of the chemical structure of OXY and corresponding investigations into cytotoxicity in various cancerous cells to investigate if the efficacy of OXY in inducing cancer cell death can be improved. Concurrent with that would be continued investigations into the mechanism of action. The ability of OXY to induce similar effects to those observed in this thesis, *in vivo*, in both animals and then ultimately in human would be the ultimate goal of the research that was initiated in this project.

REFERENCES

Adhami, V.M., Afaq, F. and Ahmad, N. (2001) Involvement of the Retinoblastoma (pRb)-E2F/DP Pathway during Antiproliferative Effects of Resveratrol in Human Epidermoid Carcinoma (A431) Cells. *Biochem. Biophys. Res. Commun.*, 288 (3), 579-585.

Affymetrix. (2017) Affymetrix microarray. [online] Available at: http://images.slideplayer.com/ 15/4665315/slides/slide_17.jpg [Accessed 22 December 2020].

Ahmad, N., Adhami, V.M., Afaq, F., Feyes, D.K. and Mukhtar, H. (2001) Resveratrol causes WAF-1/p21-mediated G1-phase arrest of cell cycle and induction of apoptosis in human epidermoid carcinoma A431 cells. *Clin. Cancer Res.*, 7 (5), 1466-1473.

Akinwumi, B.C., Bordun, K.-A.M. and Anderson, H.D. (2018) Biological activities of stilbenoids. *Int. J. Mol. Sci.*, 19 (3), 792/791-792/725.

Alam, A., Braun, M.Y., Hartgers, F., Lesage, S., Cohen, L., Hugo, P., Denis, F. and Sekaly, R.-P. (1997) Specific activation of the cysteine protease CPP32 during the negative selection of T cells in the thymus. *J. Exp. Med.*, 186 (9), 1503-1512.

Alarcon de la lastra, C. and Villegas, I. (2007) Resveratrol as an antioxidant and pro-oxidant agent: mechanisms and clinical implications. *Biochem. Soc. Trans.*, 35 (5), 1156-1160.

Andrabi, S.A., Spina, M.G., Lorenz, P., Ebmeyer, U., Wolf, G. and Horn, T.F.W. (2004) Oxyresveratrol (trans-2,3',4,5'-tetrahydroxystilbene) is neuroprotective and inhibits the apoptotic cell death in transient cerebral ischemia. *Brain Res.*, 1017 (1,2), 98-107.

Andrade Volkart, P., Benedetti Gassen, R., Muhlen Nogueira, B., Nery Porto, B., Eduardo Vargas, J. and Arigony Souto, A. (2017) Antitumor activity of resveratrol is independent of Cu(II) complex formation in MCF-7 cell line. *Bioorg. Med. Chem. Lett.*, 27 (15), 3238-3242.

Ashkenazi, A. and Dixit, V.M. (1998) Death receptors: Signaling and modulation. *Science (Washington, D. C.)*, 281 (5381), 1305-1308.

Ashkenazi, A., Pai, R.C., Fong, S., Leung, S., Lawrence, D.A., Marsters, S.A., Blackie, C., Chang, L., McMurtrey, A.E., Hebert, A., DeForge, L., Koumenis, I.L., Lewis, D., Harris, L., Bussiere, J., Koeppen, H., Shahrokh, Z. and Schwall, R.H. (1999) Safety and antitumor activity of recombinant soluble Apo2 ligand. *J. Clin. Invest.*, 104 (2), 155-162.

Aubrey, B.J., Kelly, G.L., Janic, A., Herold, M.J. and Strasser, A. (2018) How does p53 induce apoptosis and how does this relate to p53-mediated tumour suppression? *Cell Death Differ.*, 25 (1), 104-113.

Aylon, Y., Liefshitz, B. and Kupiec, M. (2004) The CDK regulates repair of double-strand breaks by homologous recombination during the cell cycle. *EMBO J.*, 23 (24), 4868-4875.

Azmi, A.S., Bhat, S.H. and Hadi, S.M. (2005) Resveratrol-Cu(II) induced DNA breakage in human peripheral lymphocytes: Implications for anticancer properties. *FEBS Lett.*, 579 (14), 3131-3135.

Babich, H., Ackerman, N.J., Burekhovich, F., Zuckerbraun, H.L. and Schuck, A.G. (2009) Gingko biloba leaf extract induces oxidative stress in carcinoma HSC-2 cells. *Toxicol. in Vitro*, 23 (6), 992-999.

Basu, S., Cheriyamundath, S. and Ben-Ze'ev, A. (2018) Cell-cell adhesion: linking Wnt/β-catenin signaling with partial EMT and stemness traits in tumorigenesis [version 1; referees: 4 approved]. *F1000Research*, 7, 1488/1481-1488/1489.

Berman, A.Y., Motechin, R.A., Wiesenfeld, M.Y., Holz, M.K. and Holz, M.K. (2017) The therapeutic potential of resveratrol: a review of clinical trials. *NPJ Precis Oncol*, 1.

Bernabeu, E., Cagel, M., Lagomarsino, E., Moretton, M. and Chiappetta, D.A. (2017) Paclitaxel: What has been done and the challenges remain ahead. *Int. J. Pharm. (Amsterdam, Neth.)*, 526 (1-2), 474-495.

Bhattacharya, S., Darjatmoko, S.R. and Polans, A.S. (2011) Resveratrol modulates the malignant properties of cutaneous melanoma through changes in the activation and attenuation of the antiapoptotic protooncogenic protein Akt/PKB. *Melanoma Res.*, 21 (3), 180-187.

Blasco, M.A. (2005) Telomeres and human disease: Ageing, cancer and beyond. *Nat. Rev. Genet.*, 6 (8), 611-622.

Borah, H.J., Singhal, R. and Hazarika, S. (2017) Artocarpus lakoocha roxb.: An untapped bioresource of resveratrol from North East India, its extractive separation and antioxidant activity. *Ind. Crops Prod.*, 95, 75-82.

Burns, J., Yokota, T., Ashihara, H., Lean, M.E.J. and Crozier, A. (2002) Plant Foods and Herbal Sources of Resveratrol. *J. Agric. Food Chem.*, 50 (11), 3337-3340.

Bustin, S.A., Benes, V., Nolan, T. and Pfaffl, M.W. (2005) Quantitative real-time RT-PCR - a perspective. *J. Mol. Endocrinol.*, 34 (3), 597-601.

Cadet, J. and Wagner, J.R. (2013) DNA base damage by reactive oxygen species, oxidizing agents, and UV radiation. *Cold Spring Harbor Perspect. Biol.*, 5 (2), A012559/012551-A012559/012518.

Carmeliet, P. and Jain, R.K. (2000) Angiogenesis in cancer and other diseases. *Nature (London)*, 407 (6801), 249-257.

Carpentieri, U., Myers, J., Thorpe, L., Daeschner, C.W., III and Haggard, M.E. (1986) Copper, zinc, and iron in normal and leukemic lymphocytes from children. *Cancer Res.*, 46 (2), 981-984.

Carr, A. and Frei, B. (1999) Does vitamin C act as a pro-oxidant under physiological conditions? *FASEB J.*, 13 (9), 1007-1024.

Caruso, J.A., Duong, M.T., Carey, J.P.W., Hunt, K.K. and Keyomarsi, K. (2018) Low-molecular-weight cyclin E in human cancer: cellular consequences and opportunities for targeted therapies. *Cancer Res.*, 78 (19), 5481-5491.

Chaney, S.G. and Sancar, A. (1996) DNA repair: enzymatic mechanisms and relevance to drug response. *J Natl Cancer Inst*, 88 (19), 1346-1360.

Chatsumpun, N., Chuanasa, T., Sritularak, B., Lipipun, V., Jongbunprasert, V., Ruchirawat, S., Ploypradith, P. and Likhitwitayawuid, K. (2016) Oxyresveratrol: Structural modification and evaluation of biological activities. *Molecules*, 21 (4), 489/481-489/419.

Chen, J., Li, K., Pang, Q., Yang, C., Zhang, H., Wu, F., Cao, H., Liu, H., Wan, Y., Xia, W., Wang, J., Dai, Z. and Li, Y. (2016) Identification of suitable reference gene and biomarkers of serum miRNAs for osteoporosis. *Sci. Rep.*, 6, 36347.

Chen, Q.W., Zhu, X.Y., Li, Y.Y. and Meng, Z.Q. (2014) Epigenetic regulation and cancer (review). *Oncol. Rep.*, 31 (2), 523-532.

Chen, Y.-C., Tien, Y.-J., Chen, C.-H., Beltran, F.N., Amor, E.C., Wang, R.-J., Wu, D.-J., Mettling, C., Lin, Y.-L. and Yang, W.-C. (2013) Morus alba and active compound oxyresveratrol exert anti-inflammatory activity via inhibition of leukocyte migration involving MEK/ERK signaling. *BMC Complement Altern Med*, 13, 45.

Choi, H.Y., Lee, J.-H., Jegal, K.H., Cho, I.J., Kim, Y.W. and Kim, S.C. (2016) Oxyresveratrol abrogates oxidative stress by activating ERK-Nrf2 pathway in the liver. *Chem.-Biol. Interact.*, 245, 110-121.

Chuanasa, T., Phromjai, J., Lipipun, V., Likhitwitayawuid, K., Suzuki, M., Pramyothin, P., Hattori, M. and Shiraki, K. (2008) Anti-herpes simplex virus (HSV-1) activity of oxyresveratrol derived from Thai medicinal plant: Mechanism of action and therapeutic efficacy on cutaneous HSV-1 infection in mice. *Antiviral Res.*, 80 (1), 62-70.

Chung, K.-O., Kim, B.-Y., Lee, M.-H., Kim, Y.-R., Chung, H.-Y., Park, J.-H. and Moon, J.-O. (2003) In-vitro and in-vivo anti-inflammatory effect of oxyresveratrol from Morus alba L. *J. Pharm. Pharmacol.*, 55 (12), 1695-1700.

Cohausz, O. and Althaus, F.R. (2009) Role of PARP-1 and PARP-2 in the expression of apoptosis-regulating genes in HeLa cells. *Cell Biol. Toxicol.*, 25 (4), 379-391.

Cohn, C.A., Simon, S.R. and Schoonen, M.A.A. (2008) Comparison of fluorescence-based techniques for the quantification of particle-induced hydroxyl radicals. *Part. Fibre Toxicol.*, 5, No pp. given.

Cragg, G.M. and Pezzuto, J.M. (2016) Natural Products as a Vital Source for the Discovery of Cancer Chemotherapeutic and Chemopreventive Agents. *Med Princ Pract*, 25 Suppl 2, 41-59.

Czop, M., Bogucka-Kocka, A., Kubrak, T., Knap-Czop, K., Makuch-Kocka, A., Galkowski, D., Wawer, J., Kocki, T. and Kocki, J. (2019) Imaging flow cytometric analysis of stilbene-dependent apoptosis in drug resistant human leukemic cell lines. *Molecules*, 24 (10), 1896.

Dasari, S. and Bernard Tchounwou, P. (2014) Cisplatin in cancer therapy: Molecular mechanisms of action. *Eur. J. Pharmacol.*, 740, 364-378.

Datto, M.B., Hu, P.P.-C., Kowalik, T.F., Yingling, J. and Wang, X.-F. (1997) The viral oncoprotein E1A blocks transforming growth factor β-mediated induction of p21/WAF1/Cip1 and p15/INK4B. *Mol. Cell. Biol.*, 17 (4), 2030-2037.

de Hoffmann, E., Stroobant, V. and Editors (2007) *Mass Spectrometry: Principles and Applications, Third Edition*. John Wiley & Sons, Ltd.

Demoulin, B., Hermant, M., Castrogiovanni, C., Staudt, C. and Dumont, P. (2015) Resveratrol induces DNA damage in colon cancer cells by poisoning topoisomerase II and activates the ATM kinase to trigger p53-dependent apoptosis. *Toxicol. In Vitro*, 29 (5), 1156-1165.

Desai, A.G., Qazi, G.N., Ganju, R.K., El-Tamer, M., Singh, J., Saxena, A.K., Bedi, Y.S., Taneja, S.C. and Bhat, H.K. (2008) Medicinal plants and cancer chemoprevention. *Curr. Drug Metab.*, 9 (7), 581-591.

Duffy, A., Le, J., Sausville, E. and Emadi, A. (2015) Autophagy modulation: a target for cancer treatment development. *Cancer Chemother. Pharmacol.*, 75 (3), 439-447.

Duronio, R.J. and Xiong, Y. (2013) Signaling pathways that control cell proliferation. *Cold Spring Harbor Perspect. Biol.*, 5 (3), a008904/008901-a008904/008912.

Elmore, S. (2007) Apoptosis: A Review of Programmed Cell Death. *Toxicol. Pathol.*, 35 (4), 495-516.

Farra, R., Dapas, B., Grassi, M., Benedetti, F. and Grassi, G. (2019) E2F1 as a molecular drug target in ovarian cancer. *Expert Opin. Ther. Targets*, 23 (3), 161-164.

Fernandis, A.Z., Prasad, A., Band, H., Kloesel, R. and Ganju, R.K. (2004) Regulation of CXCR4-mediated chemotaxis and chemoinvasion of breast cancer cells. *Oncogene*, 23 (1), 157-167.

Forman, H.J., Zhang, H. and Rinna, A. (2009) Glutathione: Overview of its protective roles, measurement, and biosynthesis. *Mol. Aspects Med.*, 30 (1-2), 1-12.

Fulda, S. and Debatin, K.-M. (2005) Resveratrol-mediated sensitisation to TRAIL-induced apoptosis depends on death receptor and mitochondrial signalling. *Eur. J. Cancer*, 41 (5), 786-798.

Galindo, I., Hernaez, B., Berna, J., Fenoll, J., Cenis, J.L., Escribano, J.M. and Alonso, C. (2011) Comparative inhibitory activity of the stilbenes resveratrol and oxyresveratrol on African swine fever virus replication. *Antiviral Res.*, 91 (1), 57-63.

Geng, J. and Klionsky, D.J. (2008) The Atg8 and Atg12 ubiquitin-like conjugation systems in macroautophagy. Protein Modifications: Beyond the Usual Suspects' Review Series. *EMBO Rep.*, 9 (9), 859-864.

Greenwell, M. and Rahman, P.K.S.M. (2015) Medicinal plants: their use in anticancer treatment. *Int. J. Pharm. Sci. Res.*, 6 (10), 4103-4112.

Guan, X. (2015) Cancer metastases: challenges and opportunities. *Acta Pharm Sin B*, 5 (5), 402-418.

Gupte, A. and Mumper, R.J. (2009) Elevated copper and oxidative stress in cancer cells as a target for cancer treatment. *Cancer Treat. Rev.*, 35 (1), 32-46.

Hanahan, D. and Weinberg, R.A. (2000) The hallmarks of cancer. *Cell (Cambridge, Mass.)*, 100 (1), 57-70.

Hanahan, D. and Weinberg, R.A. (2011) Hallmarks of cancer: the next generation. *Cell (Cambridge, MA, U. S.)*, 144 (5), 646-674.

Hannay, J.A.F., Liu, J., Zhu, Q.-S., Bolshakov, S.V., Li, L., Pisters, P.W.T., Lazar, A.J.F., Yu, D., Pollock, R.E. and Lev, D. (2007) Rad51 overexpression contributes to chemoresistance in human soft tissue sarcoma cells: a role for p53/activator protein 2 transcriptional regulation. *Mol. Cancer Ther.*, 6 (5), 1650-1660.

Helleday, T., Lo, J., van Gent, D.C. and Engelward, B.P. (2007) DNA double-strand break repair: From mechanistic understanding to cancer treatment. *DNA Repair*, 6 (7), 923-935.

Ho, C.-J., Lin, R.-W., Zhu, W.-H., Wen, T.-K., Hu, C.-J., Lee, Y.-L., Hung, T.-I. and Wang, C. (2019) Transcription-independent and -dependent p53-mediated apoptosis in response to genotoxic and non-genotoxic stress. *Cell Death Discovery*, 5 (1), 1-9.

Hogg, S.J., Chitcholtan, K., Hassan, W., Sykes, P.H. and Garrill, A. (2015) Resveratrol, acetyl-resveratrol, and polydatin exhibit antigrowth activity against 3D cell aggregates of the SKOV-3 and OVCAR-8 ovarian cancer cell lines. *Obstet. Gynecol. Int.*, 279591/279591-279591/279514.

Hu, S., Chen, F. and Wang, M. (2015) Photoprotective Effects of Oxyresveratrol and Kuwanon O on DNA Damage Induced by UVA in Human Epidermal Keratinocytes. *Chem. Res. Toxicol.*, 28 (3), 541-548.

Huang, C.-Y., Ju, D.-T., Chang, C.-F., Muralidhar, R.P. and Velmurugan, B.K. (2017) A review on the effects of current chemotherapy drugs and natural agents in treating non-small cell lung cancer. *Biomedicine (Taipei)*, 7 (4), 23.

Iglehart, J.D. and Silver, D.P. (2009) Synthetic lethality - a new direction in cancer-drug development. *N. Engl. J. Med.*, 361 (2), 189-191.

Igney, F.H. and Krammer, P.H. (2002) Death and anti-death: tumour resistance to apoptosis. *Nat Rev Cancer*, 2 (4), 277-288.

Jacquemin, G., Shirley, S. and Micheau, O. (2010) Combining naturally occurring polyphenols with TNF-related apoptosis-inducing ligand: a promising approach to kill resistant cancer cells? *Cell. Mol. Life Sci.*, 67 (18), 3115-3130.

Jagtap, U.B. and Bapat, V.A. (2010) Artocarpus: A review of its traditional uses, phytochemistry and pharmacology. *J. Ethnopharmacol.*, 129 (2), 142-166.

Janicke, R.U. (2009) MCF-7 breast carcinoma cells do not express caspase-3. *Breast Cancer Res Treat*, 117 (1), 219-221.

Jin, S., Tong, T., Fan, W., Fan, F., Antinore, M.J., Zhu, X., Mazzacurati, L., Li, X., Petrik, K.L., Rajasekaran, B., Wu, M. and Zhan, Q. (2002) GADD45-induced cell cycle G2-M arrest associates with altered subcellular distribution of cyclin B1 and is independent of p38 kinase activity. *Oncogene*, 21 (57), 8696-8704.

Kalinowski, D.S., Stefani, C., Toyokuni, S., Ganz, T., Anderson, G.J., Subramaniam, N.V., Trinder, D., Olynyk, J.K., Chua, A., Jansson, P.J., Sahni, S., Lane, D.J.R., Merlot, A.M., Kovacevic, Z., Huang, M.L.H., Lee, C.S. and Richardson, D.R. (2016) Redox cycling metals: Pedaling their roles in metabolism and their use in the development of novel therapeutics. *Biochim. Biophys. Acta, Mol. Cell Res.*, 1863 (4), 727-748.

Katz, L.H., Li, Y., Chen, J.-S., Munoz, N.M., Majumdar, A., Chen, J. and Mishra, L. (2013) Targeting TGF-β signaling in cancer. *Expert Opin. Ther. Targets*, 17 (7), 743-760.

Kelley, M.R., Logsdon, D. and Fishel, M.L. (2014) Targeting DNA repair pathways for cancer treatment: what's new? *Future Oncol.*, 10 (7), 1215-1237.

Kim, S.M. and Kim, S.Z. (2018) Biological activities of resveratrol against cancer. *J. Phys. Chem. Biophys.*, 8 (2), 1000267/1000261-1000267/1000216.

Kim, S.W., Jung, H.K. and Kim, M.Y. (2008) Induction of p27(kip1) by 2,4,3',5'-tetramethoxystilbene is regulated by protein phosphatase 2A-dependent Akt dephosphorylation in PC-3 prostate cancer cells. *Arch Pharm Res*, 31 (9), 1187-1194.

Kiyohara, E., Tamai, K., Katayama, I. and Kaneda, Y. (2012) The combination of chemotherapy with HVJ-E containing Rad51 siRNA elicited diverse anti-tumor effects and synergistically suppressed melanoma. *Gene Ther.*, 19 (7), 734-741.

Kruidering, M. and Evan, G.I. (2000) Caspase-8 in apoptosis: the beginning of "the end"? *IUBMB Life*, 50 (2), 85-90.

Kubota, T., Uemura, Y., Kobayashi, M. and Taguchi, H. (2003) Combined effects of resveratrol and paclitaxel on lung cancer cells. *Anticancer Res*, 23 (5A), 4039-4046.

Kuo, H.W., Chen, S.F., Wu, C.C., Chen, D.R. and Lee, J.H. (2002) Serum and tissue trace elements in patients with breast cancer in Taiwan. *Biol. Trace Elem. Res.*, 89 (1), 1-11.

Lee, H.S., Kim, D.H., Hong, J.E., Lee, J.Y. and Kim, E.J. (2015) Oxyresveratrol suppresses lipopolysaccharide-induced inflammatory responses in murine macrophages. *Hum. Exp. Toxicol.*, 34 (8), 808-818.

Lee, S.-R., Kim, W.-T., Kim, W.-J., Leem, S.-H., Jin, H., Kim, S.Z. and Kim, S.M. (2018) Tristetraprolin activation by resveratrol inhibits the proliferation and metastasis of colorectal cancer cells. *Int J Oncol*, 53 (3), 1269-1278.

Leon-Galicia, I., Diaz-Chavez, J., Albino-Sanchez, M.E., Garcia-Villa, E., Bermudez-Cruz, R., Garcia-Mena, J., Herrera, L.A., Garcia-Carranca, A. and Gariglio, P. (2018) Resveratrol decreases Rad51 expression and sensitizes cisplatin-resistant MCF-7 breast cancer cells. *Oncol. Rep.*, 39 (6), 3025-3033.

Li, Y. and Sarkar, F.H. (2002) Gene expression profiles of genistein-treated PC3 prostate cancer cells. *J. Nutr.*, 132 (12), 3623-3631.

Likhitwitayawuid, K., Sornsute, A., Sritularak, B. and Ploypradith, P. (2006) Chemical transformations of oxyresveratrol (trans-2,4,3',5'-tetrahydroxystilbene) into a potent

tyrosinase inhibitor and a strong cytotoxic agent. *Bioorg. Med. Chem. Lett.*, 16 (21), 5650-5653.

Lim, S. and Kaldis, P. (2013) Cdks, cyclins and CKIs: roles beyond cell cycle regulation. *Development (Cambridge, U. K.)*, 140 (15), 3079-3093.

Linder, M.C., Moor, J.R. and Wright, K. (1981) Ceruloplasmin assays in diagnosis and treatment of human lung, breast, and gastrointestinal cancers. *J Natl Cancer Inst*, 67 (2), 263-275.

Liu, Y., Ren, W., Bai, Y., Wan, L., Sun, X., Liu, Y., Xiong, W., Zhang, Y.-Y. and Zhou, L. (2018) Oxyresveratrol prevents murine H22 hepatocellular carcinoma growth and lymph node metastasis via inhibiting tumor angiogenesis and lymphangiogenesis. *J. Nat. Med.*, 72 (2), 481-492.

Livak, K.J. and Schmittgen, T.D. (2001) Analysis of relative gene expression data using real-time quantitative PCR and the 2-ΔΔCT method. Methods (San Diego, CA, U. S.), 25 (4), 402-408.

Livraghi, L. and Garber, J.E. (2015) PARP inhibitors in the management of breast cancer: current data and future prospects. *BMC Med.*, 13, 1-16.

Lopes, G.K.B., Schulman, H.M. and Hermes-Lima, M. (1999) Polyphenol tannic acid inhibits hydroxyl radical formation from Fenton reaction by complexing ferrous ions. *Biochim. Biophys. Acta, Gen. Subj.*, 1472 (1-2), 142-152.

Lorenz, P., Roychowdhury, S., Engelmann, M., Wolf, G. and Horn, T.F.W. (2003) Oxyresveratrol and resveratrol are potent antioxidants and free radical scavengers: effect on nitrosative and oxidative stress derived from microglial cells. *Nitric Oxide*, 9 (2), 64-76.

MacGregor, P.F. and Squire, J.A. (2002) Application of microarrays to the analysis of gene expression in cancer. *Clin. Chem. (Washington, DC, U. S.)*, 48 (8), 1170-1177.

Majumder, S., Chatterjee, S., Pal, S., Biswas, J., Efferth, T. and Choudhuri, S.K. (2009) The role of copper in drug-resistant murine and human tumors. *BioMetals*, 22 (2), 377-384.

Maneechai, S., Likhitwitayawuid, K., Sritularak, B., Palanuvej, C., Ruangrungsi, N. and Sirisa-Ard, P. (2009) Quantitative analysis of oxyresveratrol content in Artocarpus lakoocha and 'Puag-Haad'. *Med Princ Pract*, 18 (3), 223-227.

Mantovani, A., Garlanda, C. and Allavena, P. (2010) Molecular pathways and targets in cancer-related inflammation. *Ann. Med. (London, U. K.)*, 42 (3-4), 161-170.

Matson, J.P. and Cook, J.G. (2017) Cell cycle proliferation decisions: the impact of single cell analyses. *FEBS J.*, 284 (3), 362-375.

Merlo, L.M.F., Pepper, J.W., Reid, B.J. and Maley, C.C. (2006) Cancer as an evolutionary and ecological process. *Nat. Rev. Cancer*, 6 (12), 924-935.

Mongolsuk, S., Robertson, A. and Towers, R. (1957) 2,3',4,5'-Tetrahydroxystilbene from Artocarpus lakoocha. *J. Chem. Soc.*, 2231-2233.

Moran, J.F., Klucas, R.V., Grayer, R.J., Abian, J. and Becana, M. (1997) Complexes of iron with phenolic compounds from soybean nodules and other legume tissues: prooxidant and antioxidant properties. *Free Radical Biol. Med.*, 22 (5), 861-870.

Neuzillet, C., Tijeras-Raballand, A., Cohen, R., Cros, J., Faivre, S., Raymond, E. and de Gramont, A. (2015) Targeting the TGFβ pathway for cancer therapy. *Pharmacol. Ther.*, 147, 22-31.

Panich, U., Onkoksoong, T., Limsaengurai, S., Akarasereenont, P. and Wongkajornsilp, A. (2012) UVA-induced melanogenesis and modulation of glutathione redox system in different melanoma cell lines: The protective effect of gallic acid. *J. Photochem. Photobiol., B*, 108, 16-22.

Pfeffer, C.M. and Singh, A.T.K. (2018) Apoptosis: a target for anticancer therapy. *Int. J. Mol. Sci.*, 19 (2), 448/441-448/410.

Plaut, K. (1993) Role of epidermal growth factor and transforming growth factors in mammary development and lactation. *J. Dairy Sci.*, 76 (6), 1526-1538.

Povichit, N., Phrutivorapongkul, A., Suttajit, M. and Leelapornpisid, P. (2010) Antiglycation and antioxidant activities of oxyresveratrol extracted from the heartwood of Artocarpus lakoocha Roxb. *Maejo Int. J. Sci. Technol.*, 4 (3), 454-461.

Preyavichyapugdee, N., Sangfuang, M., Chaiyapum, S., Sriburin, S., Pootaeng-on, Y., Chusongsang, P., Jiraungkoorskul, W., Preyavichyapugdee, M. and Sobhon, P. (2016) SCHISTOSOMICIDAL ACTIVITY OF THE CRUDE EXTRACT OF ARTOCARPUS LAKOOCHA. *Southeast Asian J Trop Med Public Health*, 47 (1), 1-15.

Principe, D.R., Diaz, A.M., Torres, C., Mangan, R.J., DeCant, B., McKinney, R., Tsao, M.S., Lowy, A., Munshi, H.G., Jung, B. and Grippo, P.J. (2017) TGFβ engages MEK/ERK to differentially regulate benign and malignant pancreas cell function. *Oncogene*, 36 (30), 4336-4348.

Raderschall, E., Stout, K., Freier, S., Suckow, V., Schweiger, S. and Haaf, T. (2002) Elevated levels of Rad51 recombination protein in tumor cells. *Cancer Res*, 62 (1), 219-225.

Rahman, M.A., Bishayee, K., Sadra, A. and Huh, S.-O. (2017) Oxyresveratrol activates parallel apoptotic and autophagic cell death pathways in neuroblastoma cells. *Biochim. Biophys. Acta, Gen. Subj.*, 1861 (2), 23-36.

Rius, C., Abu-Taha, M., Hermenegildo, C., Piqueras, L., Cerda-Nicolas, J.-M., Issekutz, A.C., Estan, L., Cortijo, J., Morcillo, E.J., Orallo, F. and Sanz, M.-J. (2010) Trans- but not Cis-Resveratrol Impairs Angiotensin-II-Mediated Vascular Inflammation through Inhibition of NF-κB Activation and Peroxisome Proliferator-Activated Receptor-γ Upregulation. *J. Immunol.*, 185 (6), 3718-3727.

Riviere, C., Pawlus, A.D. and Merillon, J.-M. (2012) Natural stilbenoids: distribution in the plant kingdom and chemotaxonomic interest in Vitaceae. *Nat. Prod. Rep.*, 29 (11), 1317-1333.

Rodriguez, L.G., Wu, X. and Guan, J.-L. (2005) Wound-healing assay. *Methods Mol Biol*, 294, 23-29.

Rothkamm, K., Krueger, I., Thompson, L.H. and Loebrich, M. (2003) Pathways of DNA double-strand break repair during the mammalian cell cycle. *Mol. Cell. Biol.*, 23 (16), 5706-5715.

Saowakon, N., Tansatit, T., Wanichanon, C., Chanakul, W., Reutrakul, V. and Sobhon, P. (2009) Fasciola gigantica: anthelmintic effect of the aqueous extract of Artocarpus lakoocha. *Exp Parasitol*, 122 (4), 289-298.

Schnekenburger, M., Dicato, M. and Diederich, M. (2014) Plant-derived epigenetic modulators for cancer treatment and prevention. *Biotechnol. Adv.*, 32 (6), 1123-1132.

Seca, A.M.L. and Pinto, D.C.G.A. (2018) Plant secondary metabolites as anticancer agents: successes in clinical trials and therapeutic application. *Int. J. Mol. Sci.*, 19 (1), 263/261-263/222.

Shankar, S., Singh, G. and Srivastava, R.K. (2007) Chemoprevention by resveratrol: molecular mechanisms and therapeutic potential. *Front. Biosci.*, 12, 4839-4854.

Shay, J.W. and Wright, W.E. (2000) Hayflick, his limit, and cellular ageing. *Nat. Rev. Mol. Cell Biol.*, 1 (1), 72-76.

Shibuya, M. (2011) Vascular endothelial growth factor (VEGF) and its receptor (VEGFR) signaling in angiogenesis: a crucial target for anti- and pro-angiogenic therapies. *Genes Cancer*, 2 (12), 1097-1105, 1099 pp.

Shingai, Y., Fujimoto, A., Nakamura, M. and Masuda, T. (2011) Structure and Function of the Oxidation Products of Polyphenols and Identification of Potent Lipoxygenase

Inhibitors from Fe-Catalyzed Oxidation of Resveratrol. *J. Agric. Food Chem.*, 59 (15), 8180-8186.

Silva, C.G., Monteiro, J., Marques, R.R.N., Silva, A.M.T., Martinez, C., Canle L, M. and Faria, J.L. (2013) Photochemical and photocatalytic degradation of trans-resveratrol. *Photochem. Photobiol. Sci.*, 12 (4), 638-644.

Singhatong, S., Leelarungrayub, D. and Chaiyasut, C. (2010) Antioxidant and toxicity activities of Artocarpus lakoocha Roxb. heartwood extract. *J. Med. Plants Res.*, 4 (10), 947-953.

Slupianek, A., Schmutte, C., Tombline, G., Nieborowska-Skorska, M., Hoser, G., Nowicki, M.O., Pierce, A.J., Fishel, R. and Skorski, T. (2001) BCR/ABL regulates mammalian RecA homologs, resulting in drug resistance. *Mol. Cell*, 8 (4), 795-806.

Smith, A.L., Robin, T.P. and Ford, H.L. (2012) Molecular Pathways: Targeting the TGF-β Pathway for Cancer Therapy. *Clin. Cancer Res.*, 18 (17), 4514-4521.

Stratton, M.R., Campbell, P.J. and Futreal, P.A. (2009) The cancer genome. *Nature (London, U. K.)*, 458 (7239), 719-724.

Subramanian, M., Shadakshari, U. and Chattopadhyay, S. (2004) A mechanistic study on the nuclease activities of some hydroxystilbenes. *Bioorg. Med. Chem.*, 12 (5), 1231-1237.

Suvarna, V., Singh, V. and Murahari, M. (2019) Current overview on the clinical update of Bcl-2 anti-apoptotic inhibitors for cancer therapy. *Eur. J. Pharmacol.*, 862, 172655.

Tan, H.-Y., Tse, I.M.Y., Li, E.T.S. and Wang, M. (2015) Inhibitory effects of oxyresveratrol and cyanomaclurin on adipogenesis of 3T3-L1 cells. *J. Funct. Foods*, 15, 207-216.

Taylor, I., Pauloski, N.R. and Bigwood, D. (2005) *Gene expression profiles and microarrays for use in diagnosis and drug screening for lung cancer*. Bayer Pharmaceuticals Corp., USA . 60 pp.

Tchounwou, P.B., Newsome, C., Williams, J. and Glass, K. (2008) Copper-Induced Cytotoxicity and Transcriptional Activation of Stress Genes in Human Liver Carcinoma (HepG(2)) Cells. *Met Ions Biol Med*, 10, 285-290.

Teanpaisan, R., Ruangkiatkul, P., Thammasitboon, K., Puripattanavong, J. and Faroongsarng, D. (2013) Effectiveness of Artocarpus lakoocha extract, poloxamer 407, on Enterococcus faecalis in vitro. *J Investig Clin Dent*, 4 (4), 219-224.

Tengamnuay, P., Pengrungruangwong, K., Pheansri, I. and Likhitwitayawuid, K. (2006) Artocarpus lakoocha heartwood extract as a novel cosmetic ingredient: evaluation of the

in vitro anti-tyrosinase and in vivo skin whitening activities. *Int J Cosmet Sci*, 28 (4), 269-276.

Thermofisherscientific. (2017) GeneChip™ WT PLUS Reagent Kit
USER GUIDE. [online] Available at: https://assets.thermofisher.com/TFS-Assets/LSG/manuals/MAN0018137_703174_WTPlus_Reagentkit_Assay_UG.pdf [Accessed 22 December 2020].

Tsimberidou, A.M., Fountzilas, E., Nikanjam, M. and Kurzrock, R. (2020) Review of precision cancer medicine: Evolution of the treatment paradigm. *Cancer Treat. Rev.*, 86, 102019.

Tummers, B. and Green, D.R. (2017) Caspase-8: regulating life and death. *Immunol. Rev.*, 277 (1), 76-89.

Turpaev, K.T. (2002) Reactive oxygen species and regulation of gene expression. *Biochemistry (Moscow, Russ. Fed.)*, 67 (3), 281-292.

Valko, M., Izakovic, M., Mazur, M., Rhodes, C.J. and Telser, J. (2004) Role of oxygen radicals in DNA damage and cancer incidence. *Mol. Cell. Biochem.*, 266 (1&2), 37-56.

Varoni, E.M., Lo Faro, A.F., Sharifi-Rad, J. and Iriti, M. (2016) Anticancer molecular mechanisms of resveratrol. *Front. Nutr.*, 8/1-8/15.

Wang, Y.-J., Lin, J.-F., Cheng, L.-H., Chang, W.-T., Kao, Y.-H., Chang, M.-M., Wang, B., Jr. and Cheng, H.-C. (2017) Pterostilbene prevents AKT-ERK axis-mediated polymerization of surface fibronectin on suspended lung cancer cells independently of apoptosis and suppresses metastasis. *J. Hematol. Oncol.*, 10, 72/71-72/14.

Weaver, B.A. (2014) How taxol/paclitaxel kills cancer cells. *Mol. Biol. Cell*, 25 (18), 2677-2681, 2675 pp.

Weber, J.T., Lamont, M., Chibrikova, L., Fekkes, D., Vlug, A.S., Lorenz, P., Kreutzmann, P. and Slemmer, J.E. (2012) Potential neuroprotective effects of oxyresveratrol against traumatic injury. *Eur. J. Pharmacol.*, 680 (1-3), 55-62.

Who.int. (2020) Cancer. [online] Available at: <https://www.who.int/news-room/fact-sheets/detail/cancer> [Accessed 22 December 2020].

Wood, D.J., Korolchuk, S., Tatum, N.J., Wang, L.-Z., Endicott, J.A., Noble, M.E.M. and Martin, M.P. (2019) Differences in the Conformational Energy Landscape of CDK1 and CDK2 Suggest a Mechanism for Achieving Selective CDK Inhibition. *Cell Chem. Biol.*, 26 (1), 121-130.e125.

Xiao, Y., Zhai, Q., Wang, G., Liu, X., Zhao, J., Tian, F., Zhang, H. and Chen, W. (2016) Metabolomics analysis reveals heavy metal copper-induced cytotoxicity in HT-29 human colon cancer cells. *RSC Adv.*, 6 (82), 78445-78456.

Yamada, K., Shirahata, S., Murakami, H., Nishiyama, K., Shinohara, K. and Omura, H. (1985) DNA breakage by phenyl compounds. *Agric. Biol. Chem.*, 49 (5), 1423-1428.

Yang, N.-C., Lee, C.-H. and Song, T.-Y. (2010) Evaluation of resveratrol oxidation in vitro and the crucial role of bicarbonate ions. *Biosci., Biotechnol., Biochem.*, 74 (1), 63-68.

Yang, Z., Waldman, A.S. and Wyatt, M.D. (2012) Expression and regulation of RAD51 mediate cellular responses to chemotherapeutics. *Biochem. Pharmacol.*, 83 (6), 741-746.

Yingling, J.M., Blanchard, K.L. and Sawyer, J.S. (2004) Development of TGF-β signalling inhibitors for cancer therapy. *Nat. Rev. Drug Discovery*, 3 (12), 1011-1022.

Youngs, S.J., Ali, S.A., Taub, D.D. and Rees, R.C. (1997) Chemokines induce migrational responses in human breast carcinoma cell lines. *Int. J. Cancer*, 71 (2), 257-266.

Zhao, Y., Ma, J., Fan, Y., Wang, Z., Tian, R., Ji, W., Zhang, F. and Niu, R. (2018) TGF-β transactivates EGFR and facilitates breast cancer migration and invasion through canonical Smad3 and ERK/Sp1 signaling pathways. *Mol. Oncol.*, 12 (3), 305-321.

Zugazagoitia, J., Ponce, S., Guedes, C., Ferrer, I., Molina-Pinelo, S. and Paz-Ares, L. (2016) Current Challenges in Cancer Treatment. *Clin Ther*, 38 (7), 1551-1566.

APPENDIX I
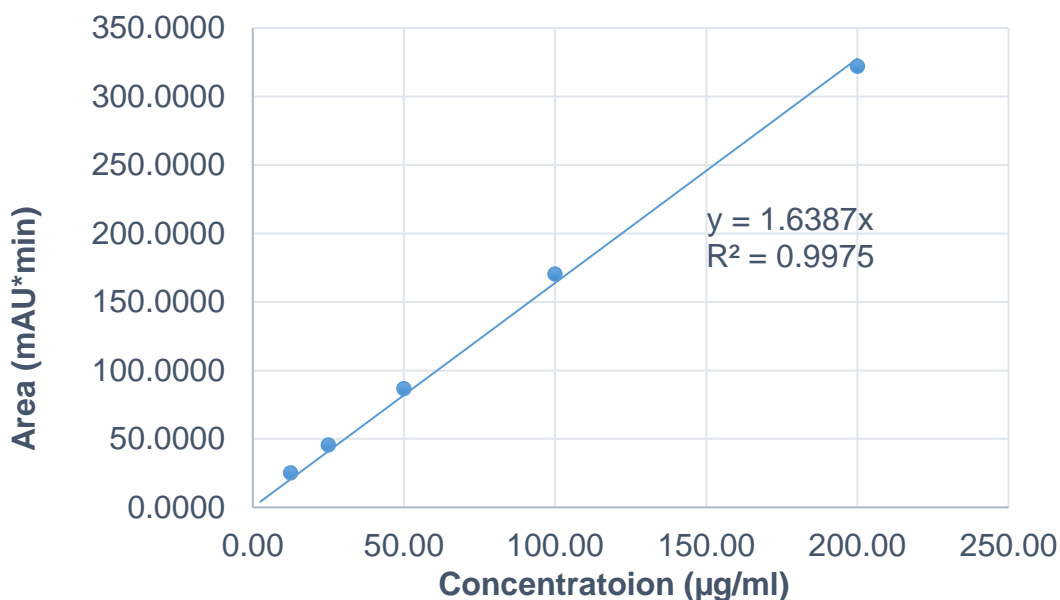
Figure Standard curve of 0.00 – 250 µM OXY measured using a Phenomenex liquid chromatography system, separation was achieved on a Luna@ C18 column (4.6 mm × 15 cm, 5 µm), mobile phase were water (0.5% acetic acid) and acetonitrile, absorbance measured at 320 nm
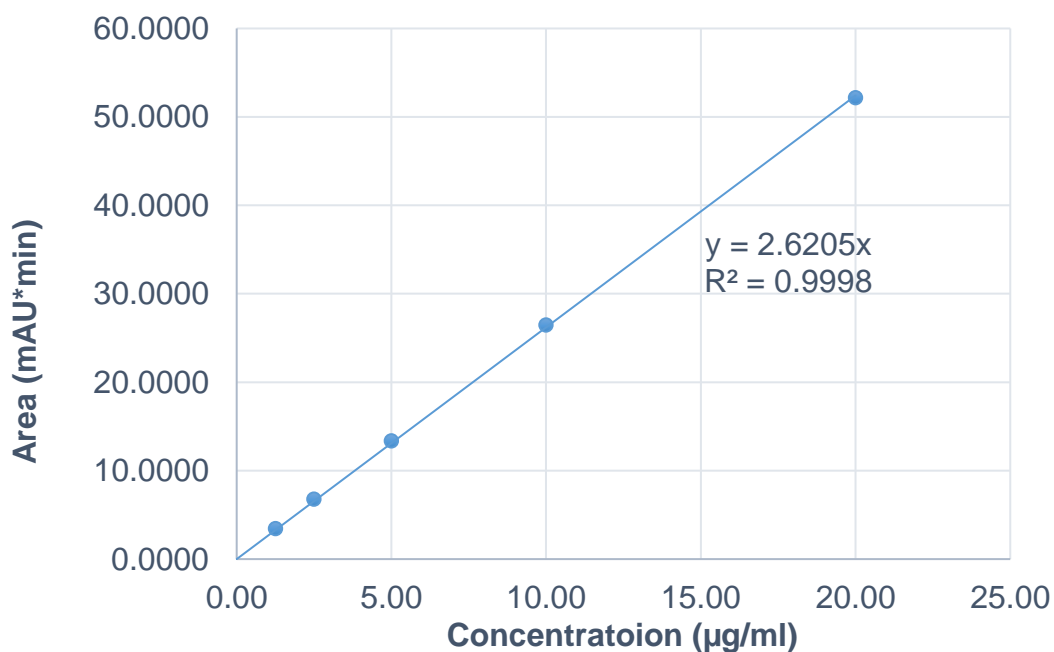
Figure Standard curve of 0.00 – 25.00 µM resveratrol measured using a Phenomenex liquid chromatography system, separation was achieved on a Luna@ C18 column (4.6 mm × 15 cm, 5 µm), mobile phase were water (0.5% acetic acid) and acetonitrile, absorbance measured at 320 nm
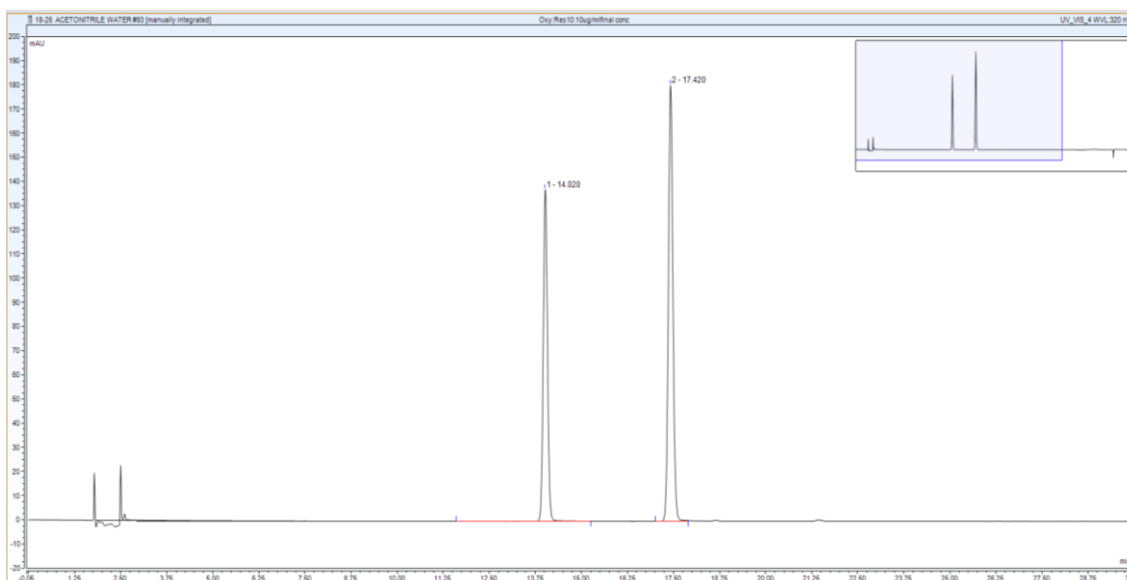
Figure HPLC chromatogram of the standards and the extracts; OXY and Resveratrol at the concentration of 10.00 µg/mL analysed using a Phenomenex liquid chromatography system, separation was achieved on a Luna@ C18 column (150 × 4.6 mm, 5 µm), mobile phase were water (0.5% acetic acid) and acetonitrile, absorbance measured at 320 nm

Table ROS formation generated by OXY in the condition with and without Cu(II)

OXY	In the presence of Cu(II)		In the absence of Cu(II)	
(µM)	Average	SD	Average	SD
1.56	824.67	54.24	177.67	44.43
3.13	1071.67	116.38	195.67	30.01
6.25	1322.67	77.22	160.33	10.26
12.50	1642.33	90.16	139.00	25.51
25.00	1990.33	160.22	161.67	36.12
50.00	2412.00	72.69	114.00	26.00
100.00	2692.00	190.25	145.00	31.95
200.00	3317.67	135.40	164.33	39.00

Table ROS formation generated by OXY, resveratrol and *tran–*stilbene in the condition with Cu(II)

Concentration (µM)	OXY		Resveratrol		*Trans*–stilbene	
	Average	SD	Average	SD	Average	SD
1.56	650.00	32.19	579.67	44.99	422.67	33.84
3.13	674.00	57.66	611.00	41.04	435.33	69.87
6.25	831.00	46.03	645.67	7.23	418.33	38.42
12.50	1135.67	60.93	845.00	87.07	430.00	81.96
25.00	1562.00	65.39	1028.00	56.56	355.67	38.00
50.00	2085.33	103.59	1410.00	43.55	413.33	90.00
100.00	2835.33	216.32	1996.33	85.00	472.33	40.20
200.00	3411.67	229.40	2632.00	226.93	446.33	17.93

Table ROS formation generated by *A. lakoocha* heartwood extracts; ethyl acetate, ethanol and water extracts in the condition with and without Cu(II)

Concentration (µg/mL)	water–extracted fraction		ethanol–extracted fraction		ethylacetate–extracted fraction	
	Average	SD	Average	SD	Average	SD
1.56	877.00	8.72	939.33	71.50	1205.67	88.04
3.13	955.67	76.17	1066.00	62.36	1477.00	34.66
6.25	1120.33	52.56	1187.00	71.27	1765.33	27.50
12.50	1313.33	42.44	1436.00	67.56	2362.33	86.43
25.00	1722.67	42.39	1846.67	30.07	3078.00	95.36
50.00	2167.00	64.55	2251.67	71.00	4027.33	191.91
100.00	2691.00	65.96	2755.67	26.27	5185.67	118.95
200.00	2727.00	101.82	3076.00	91.83	6600.33	252.23

Table The concentration of OXY and the absorbance of the Cu(I)–Bathocuproinedisulfonate complex at 484 nm in the presence and absence of Cu(OAc)$_2$.

Concentration (µM)	The absorbance of the Cu(I)–Bathocuproinedisulfonate complex at 484 nm			Average	SD
	Replicate 1	Replicate 2	Replicate 3		
1.56	0.0402	0.0432	0.0442	0.0425	0.0021
3.13	0.0822	0.0872	0.0842	0.0845	0.0025
6.25	0.1602	0.1622	0.1642	0.1622	0.0020
12.50	0.2882	0.2902	0.2922	0.2902	0.0020
25.00	0.5012	0.5132	0.5032	0.5058	0.0064
50.00	0.6492	0.6492	0.6432	0.6472	0.0035
100.00	0.6482	0.6492	0.6532	0.6502	0.0026

Table The concentration of OXY, Resveratrol or *Trans*–stilbene and the absorbance of the Cu(I)–Bathocuproinedisulfonate complex at 484 nm in the presence of Cu(OAc)$_2$.

Concentration (µM)	OXY		Resveratrol		*Trans*–stilbene	
	Average	SD	Average	SD	Average	SD
1.56	0.043	0.002	0.019	0.001	0.004	0.007
3.13	0.085	0.003	0.040	0.001	0.001	0.001
6.25	0.162	0.002	0.079	0.001	0.000	0.001
12.50	0.290	0.002	0.155	0.002	0.001	0.001
25.00	0.506	0.006	0.295	0.004	0.005	0.002
50.00	0.647	0.003	0.504	0.002	0.013	0.004
100.00	0.650	0.003	0.633	0.004	0.022	0.007

Table The absorbance at 412 nm of GSH standard solutions

GSH concentration (nmoles/mL)	Absorbance at 412 nm			Average	SD
7.51	0.061	0.064	0.062	0.062	0.002
10.01	0.082	0.084	0.083	0.083	0.001
13.35	0.109	0.110	0.109	0.109	0.001
17.80	0.142	0.141	0.141	0.141	0.001
23.73	0.188	0.193	0.190	0.190	0.003
31.64	0.257	0.254	0.255	0.255	0.002
42.19	0.338	0.345	0.341	0.341	0.004
56.25	0.449	0.456	0.452	0.452	0.004
75.00	0.602	0.593	0.597	0.597	0.005
100.00	0.790	0.804	0.797	0.797	0.007
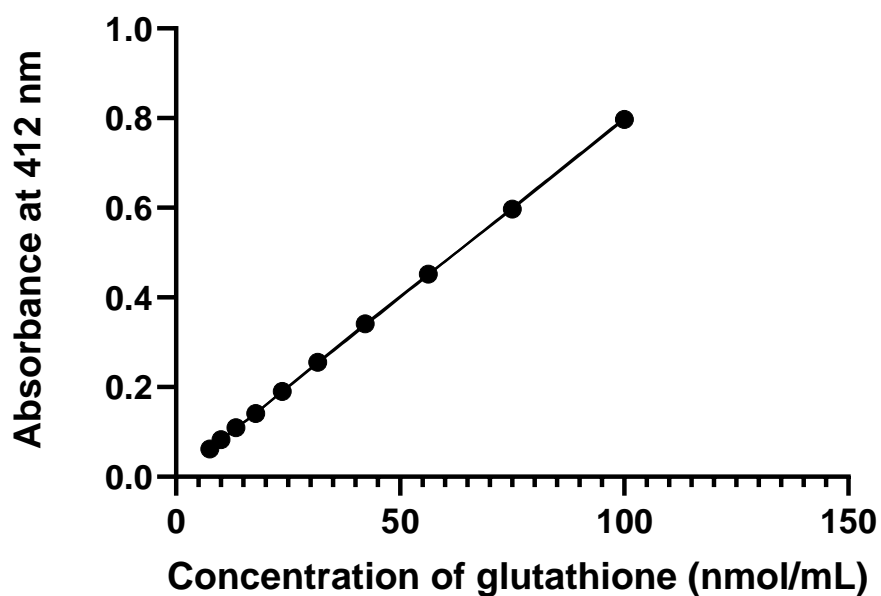
Figure The relationship between the standard GSH concentration (nmoles/mL) and the absorbance at 412 nm

Table The average and standard deviation of % glutathione incubated with OXY in the presence and absence of Cu (II).

Concentration of OXY (μM)	In the presence of Cu(II)		In the absence of Cu(II)	
	Average	SD	Average	SD
6.25	100.29	0.53	99	0.43
12.5	100.38	0.36	100	1.24
25	99.45	0.29	100	0.14
50	98.86	0.67	100	0.38
100	96.33	0.00	99	0.17
200	95.32	0.25	100	0.17
400	91.61	0.53	100	0.14

Table Cell number of A549 cells, which were different initial cells; 5×10^3, 1×10^4 and 2×10^4 cells/ well during 4 days cultured in 96–well plate

Initial Cells (cells/well)	5×10^3		1×10^4		2×10^4	
	Average	SD	Average	SD	Average	SD
Day 1	4218.75	309.36	9406.25	309.36	16500.50	795.50
Day 2	12687.50	265.17	24750.00	1767.77	46625.00	4419.42
Day 3	30166.67	5892.56	63000.00	707.11	98625.00	1590.99
Day 4	62375.00	1237.44	97750.00	1060.66	127000.00	3535.53

Table Pictures of A549 cell confluence, which were different initial cells; $5x10^3$, $1x10^4$ and $2x10^4$ cells/ well during 4 days cultured in 96–well plate.

Initial ells (cells/well)	$5x10^3$	$1x10^4$	$2x10^4$
Day 1			95-100% confluency
Day 2		95-100% confluency	
Day 3	95-100% confluency		
Day 4			
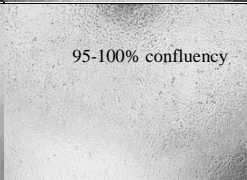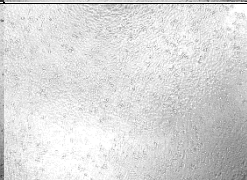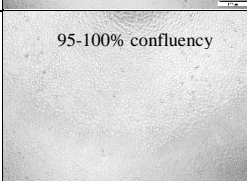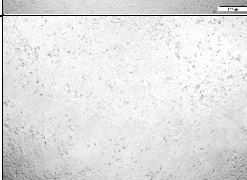
Table Cell numbers of CACO–2 cells, which were different initial cells; $5x10^3$, 7.5 x103, $1x10^4$ and $2x10^4$ cells/ well during 4 days cultured in 96–well plate

Initial Cells (cells/ well)	$5x10^3$		$7.5x10^3$		$1x10^4$		$2x10^4$	
	Average	SD	Average	SD	Average	SD	Average	SD
Day 1	5250.0	353.6	7625.0	176.8	9875.0	530.3	20625.0	1591.0
Day 2	7187.5	88.4	12312.5	972.3	18812.5	265.2	27812.5	2740.0
Day 3	19125.0	1060.7	30875.0	530.3	51000.0	3182.0	74000.0	1414.2
Day 4	44375.0	883.9	38000.0	4242.6	60500.0	7778.2	79000.0	1414.2

Table Pictures of CACO–2 cell confluence, which were different initial cells; $5x10^3$, $7.5x10^3$, $1x10^4$ and $2x10^4$ cells/ well during 4 days cultured in 96–well plate

Initial Cells (cells/well)	$5x10^3$	$7.5x10^3$	$1x10^4$	$2x10^4$
Day 1				
Day 2		90-100% confluency		
Day 3	95-100% confluency		Dead cells	
Day 4		Dead cells	Dead cells	
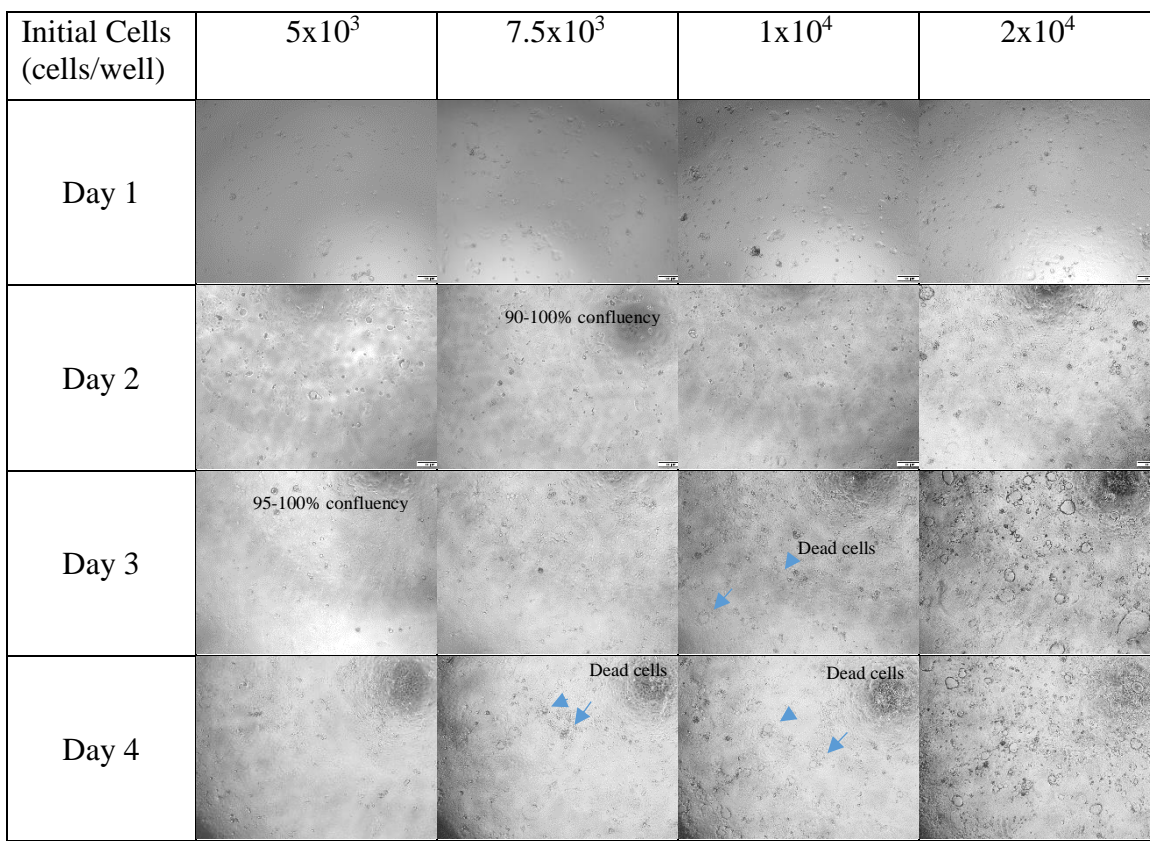
Table Cell number of HepG2 cells, which were different initial cells; $5x10^3$, $1x10^4$ and $2x10^4$ cells/ well during 4 days cultured in 96–well plate

Initial Cells (cells/well)	$5x10^3$		$1x10^4$		$2x10^4$	
	Average	SD	Average	SD	Average	SD
Day 1	8250.0	1237.4	15333.3	1178.5	25187.5	1149.0
Day 2	22875.0	530.3	31750.0	2474.9	42250.0	353.6
Day 3	36625.0	530.3	44250.0	4596.2	48500.0	1414.2
Day 4	45625.0	5480.1	47875.0	1237.4	50125.0	883.9

Table Pictures of HepG2 cells, which were different initial cells; $5x10^3$, $1x10^4$ and $2x10^4$ cells/ well during 4 days cultured in 96–well plate

Initial Cells (cells/well)	$5x10^3$	$1x10^4$	$2x10^4$
Day 1			95-100% confluency
Day 2		95-100% confluency	
Day 3	95-100% confluency		
Day 4			
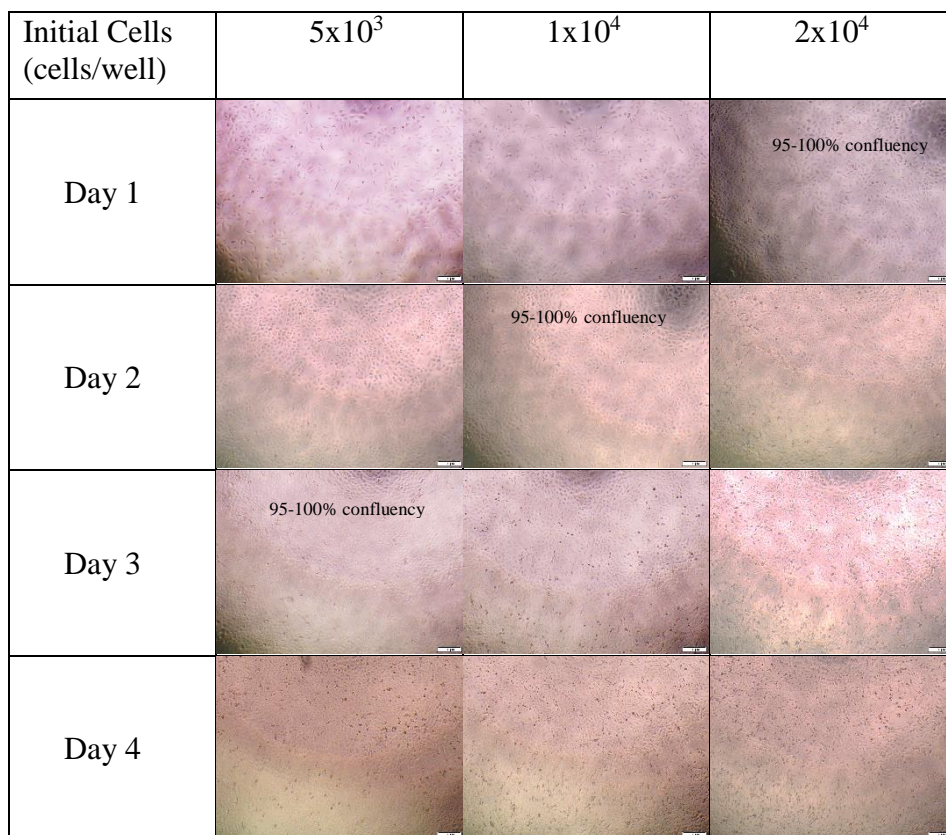
Table Cell number of MCF10A cells, which were different initial cells; $5x10^3$, $1x10^4$ and $2x10^4$ cells/ well during 4 days cultured in 96–well plate

Initial Cells (cells/well)	$5x10^3$		$1x10^4$		$2x10^4$	
	Average	SD	Average	SD	Average	SD
Day 1	1500.0	88.4	5750.0	1060.7	15875.0	1767.8
Day 2	5031.3	221.0	10562.5	265.2	32687.5	1502.6
Day 3	14531.3	221.0	34750.0	707.1	54750.0	353.6
Day 4	38250.0	707.1	49500.0	1414.2	61500.0	707.1

Table Pictures of MCF10A cell confluence, which were different initial cells; $5x10^3$, $1x10^4$ and $2x10^4$ cells/ well during 4 days cultured in 96–well plate
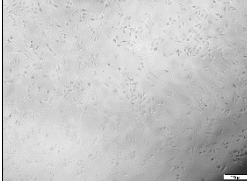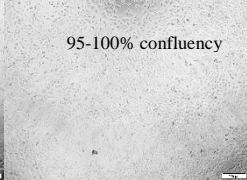
Initial Cells (cells/well)	$5x10^3$	$1x10^4$	$2x10^4$
Day 1			95-100% confluency
Day 2			
Day 3		95-100% confluency	
Day 4	95-100% confluency		

Table Cell number of MCF7 cells, which were different initial cells; $5x10^3$, 7.5 x103, $1x10^4$ and $2x10^4$ cells/ well during 4 days cultured in 96–well plate

Initial Cells (cells/well)	$5x10^3$		$7.5x10^3$		$1x10^4$		$2x10^4$	
	Average	SD	Average	SD	Average	SD	Average	SD
Day 1	5000.0	353.6	7500.0	353.6	10000.0	707.1	17500.0	353.6
Day 2	8312.5	441.9	9750.0	353.6	15125.0	1591.0	34750.0	3182.0
Day 3	12125.0	176.8	19875.0	883.9	28750.0	2474.9	49500.0	4242.6
Day 4	20875.0	1591.0	40875.0	3005.2	43750.0	5303.3	58750.0	1767.8

Table Pictures of MCF7 cell confluence, which were different initial cells; $5x10^3$, $7.5x10^3$, $1x10^4$ and $2x10^4$ cells/ well during 4 days cultured in 96–well plate

Initial Cells (cells/well)	$5x10^3$	$7.5x10^3$	$1x10^4$	$2x10^4$
Day 1				
Day 2				
Day 3				95-100% confluency
Day 4		95-100% confluency	95-100% confluency	95-100% confluency
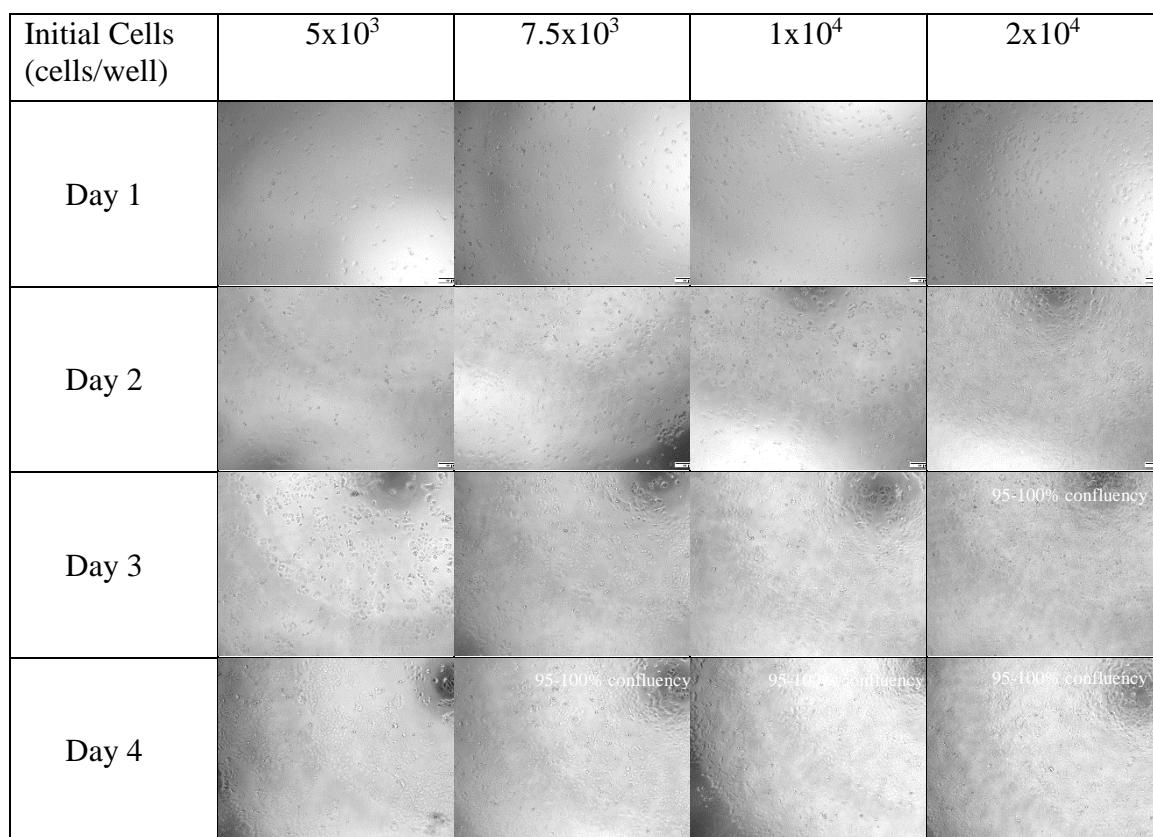
Table Cell number of MRC–5 cells, which were different initial cells; $7.5x10^3$, $1x10^4$ and $2x10^4$ cells/ well during 4 days cultured in 96–well plate

Initial Cells (cells/well)	$7.5x10^3$		$1x10^4$		$2x10^4$	
	Average	SD	Average	SD	Average	SD
Day 1	2937.50	265.17	5562.50	265.17	10187.50	2032.93
Day 2	9937.50	795.50	15875.00	1237.44	21125.00	707.11
Day 3	19687.50	441.94	27125.00	707.11	29625.00	1590.99
Day 4	29375.00	883.88	34750.00	3181.98	35500.00	707.11

Table Pictures of MRC–5 cell confluence, which were different initial cells; 7.5×10^3, 1×10^4 and 2×10^4 cells/ well during 4 days cultured in 96–well plate

Initial Cells (cells/well)	7.5×10^3	1×10^4	2×10^4
Day 1			
Day 2		95-100% confluency	
Day 3	95-100% confluency		
Day 4			
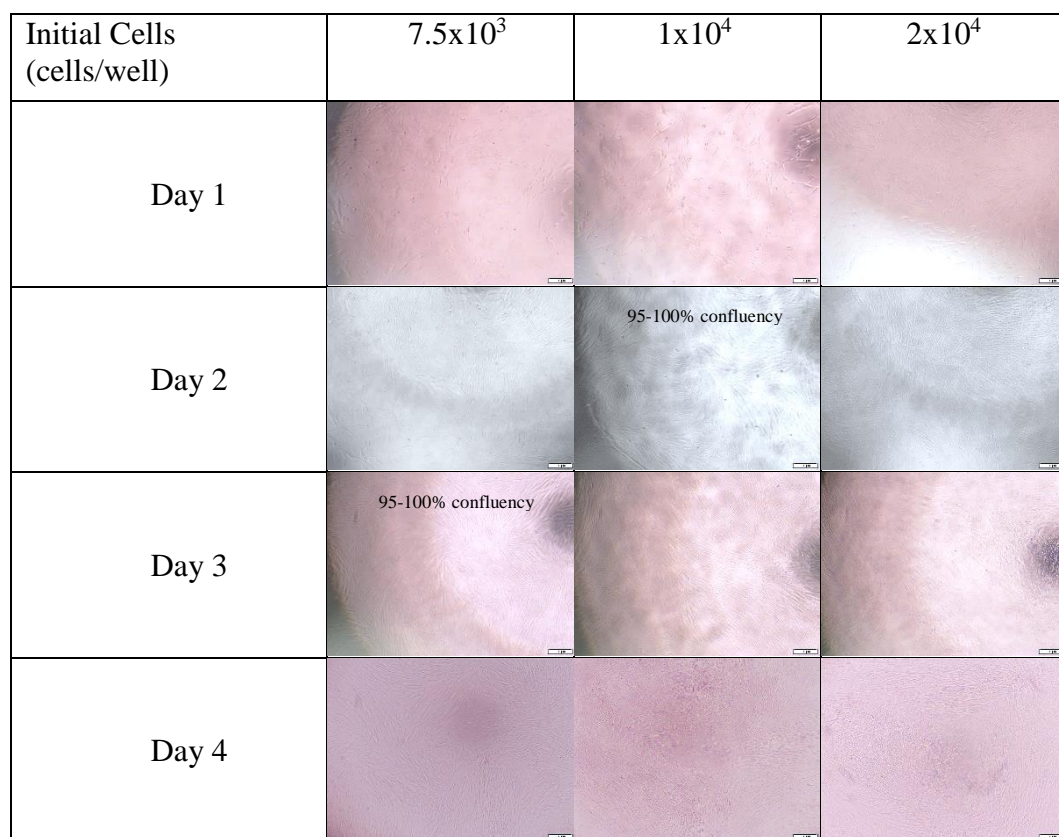
Table Cell number of PC–3 cells, which were different initial cells; 5×10^3, 1×10^4 and 2×10^4 cells/ well during 4 days cultured in 96–well plate

Initial Cells (cells/well)	5×10^3		1×10^4		2×10^4	
	Average	SD	Average	SD	Average	SD
Day 1	3656.25	928.08	9000.00	618.72	22062.50	176.78
Day 2	9812.50	265.17	18937.50	2032.93	45500.00	1060.66
Day 3	19812.50	618.72	42375.00	3712.31	65625.00	1237.44
Day 4	39500.00	1414.21	69000.00	3535.53	74250.00	2474.87

Table Pictures of PC–3 cell confluence, which were different initial cells; 5×10^3, 1×10^4 and 2×10^4 cells/ well during 4 days cultured in 96–well plate

Initial Cells (cells/well)	5×10^3	1×10^4	2×10^4
Day 1			95-100% confluency
Day 2		95-100% confluency	Cell dead
Day 3	95-100% confluency	Cell dead	Cell dead
Day 4		Cell dead	Cell dead

Table Cell number of RAW264.7 cells, which were different initial cells; 5×10^3, 1×10^4 and 2×10^4 cells/ well during 4 days cultured in 96–well plate

Initial Cells (cells/well)	5×10^3		1×10^4		2×10^4	
	Average	SD	Average	SD	Average	SD
Day 1	3562.50	265.17	4312.50	265.17	10562.50	1502.60
Day 2	18437.50	1149.05	37125.00	2298.10	63750.00	1767.77
Day 3	35500.00	2474.87	77500.00	4242.64	99750.00	1060.66
Day 4	64750.00	6717.51	78250.00	3889.09	99000.00	2121.32

Table Pictures of RAW264.7 cell confluence, which were different initial cells; 5×10^3, 1×10^4 and 2×10^4 cells/ well during 4 days cultured in 96–well plate
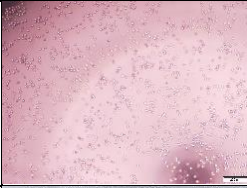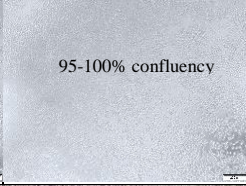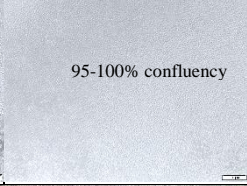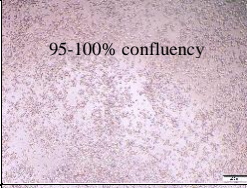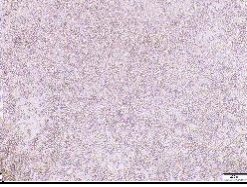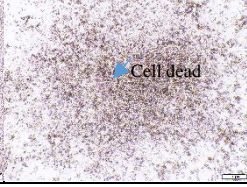
Initial Cells (cells/well)	7.5×10^3	1×10^4	2×10^4
Day 1			
Day 2		95-100% confluency	95-100% confluency
Day 3	95-100% confluency		
Day 4			Cell dead

Table Cell viability of A–459 cells in different concentrations of Cu(OAc)$_2$.

Concentration (µm)	Cell viability (% of control)			Mean	SD
0.13	105.58	101.11	98.33	101.67	3.66
1.25	92.78	92.47	94.78	93.34	1.26
12.50	93.08	87.84	88.46	89.79	2.87
25.00	88.61	82.90	86.60	86.04	2.90
50.00	84.75	84.91	91.39	87.02	3.79
100.00	70.25	72.72	76.27	73.08	3.02
200.00	63.47	64.55	71.80	66.60	4.53
400.00	51.59	50.20	53.44	51.74	1.63

Table Cell viability of CACO–2 cells in different concentrations of Cu(OAc)$_2$.

Concentration (μm)	Cell viability (% of control)			Mean	SD
0.13	106.85	101.28	100.90	103.01	3.33
1.25	93.79	99.74	98.78	97.44	3.20
12.50	92.83	99.74	94.18	95.58	3.66
25.00	90.72	93.41	91.68	91.94	1.36
50.00	76.13	84.96	87.26	82.78	5.88
100.00	67.68	64.99	65.95	66.21	1.36
200.00	45.60	38.50	44.06	42.72	3.74
400.00	7.78	9.31	9.70	8.93	1.02

Table Cell viability of HepG2 cells in different concentrations of Cu(OAc)$_2$.

Concentration (μm)	Cell viability (% of control)			mean	SD
0.13	103.59	95.34	115.83	104.92	10.31
1.25	83.11	95.88	106.25	95.08	11.59
12.50	100.50	89.76	105.45	98.57	8.02
25.00	111.57	109.71	110.64	110.64	0.93
50.00	93.75	103.86	111.84	103.15	9.07
100.00	83.91	87.90	108.91	93.57	13.43
200.00	57.57	67.15	91.62	72.11	17.56
400.00	30.70	35.76	38.42	34.96	3.92

Table Cell viability of MCF10A cells in different concentrations of $Cu(OAc)_2$.

Concentration (µm)	Cell viability (% of control)			Mean	SD
0.13	110.71	95.14	107.81	104.56	8.28
1.25	77.04	78.85	78.31	78.07	0.93
12.50	72.70	69.44	83.92	75.35	7.60
25.00	64.92	58.76	61.30	61.66	3.09
50.00	71.61	68.90	66.73	69.08	2.45
100.00	48.08	51.16	43.74	47.66	3.73
200.00	23.47	22.20	25.46	23.71	1.64
400.00	7.00	8.63	4.65	6.76	2.00

Table Cell viability of MCF7 cells in different concentrations of $Cu(OAc)_2$.

Concentration (µm)	Cell viability (% of control)			Mean	SD
0.13	95.14	106.15	97.52	99.60	5.80
1.25	109.18	110.47	92.98	104.21	9.75
12.50	104.86	106.15	93.63	101.55	6.89
25.00	95.36	101.62	97.52	98.16	3.18
50.00	90.39	97.73	88.23	92.12	4.98
100.00	89.96	93.20	89.96	91.04	1.87
200.00	80.00	82.18	80.89	81.02	1.10
400.00	11.57	15.89	12.00	13.15	2.38

Table Cell viability of MRC–5 cells in different concentrations of $Cu(OAc)_2$.

Concentration (µm)	Cell viability (% of control)			Mean	SD
12.50	127.06	86.30	99.21	104.19	20.83
25.00	100.57	73.40	102.38	92.11	16.23
50.00	92.87	96.72	99.89	96.49	3.51
100.00	56.87	95.58	100.11	84.19	23.77
200.00	84.72	102.60	113.25	100.19	14.42
400.00	48.94	50.08	36.72	45.25	7.41

Table Cell viability of PC–3 cells in different concentrations of $Cu(OAc)_2$.

Concentration (µm)	Cell viability (% of control)			Mean	SD
0.13	103.64	97.90	99.43	100.32	2.97
1.25	96.36	97.90	98.28	97.51	1.01
25.00	96.36	87.95	91.39	91.90	4.23
50.00	94.83	89.86	97.90	94.20	4.06
100.00	98.66	80.68	86.80	88.71	9.14
200.00	92.16	90.00	74.55	85.57	9.60
400.00	58.10	59.25	60.01	59.12	0.96

Table Cell viability of RAW264.7 cells in different concentrations of Cu(OAc)$_2$.

Concentration (μm)	Cell viability (% of control)			Mean	SD
0.13	104.32	105.78	93.89	101.33	6.48
1.25	91.56	93.41	95.84	93.60	2.15
25.00	104.81	95.65	92.63	97.69	6.34
50.00	94.77	91.94	86.20	90.97	4.37
100.00	88.63	95.16	96.43	93.41	4.18
200.00	81.23	90.78	89.22	87.07	5.12
400.00	74.60	101.98	88.05	88.21	13.69

Table Viability of A549 cells treated with different concentrations of Doxorubicin. Values express mean ± SD (n=3).

Concentration (μM)	Cell viability (% of control)				
	Rep 1	Rep 2	Rep 3	Average	SD
0.08	100.11	100.25	100.12	100.16	0.08
0.16	100.00	100.36	123.98	108.11	0.16
0.31	66.24	64.26	58.19	62.89	0.31
0.63	38.99	38.28	34.47	37.25	0.63
1.25	19.65	14.85	16.82	17.11	1.25
2.50	12.02	10.47	13.01	11.84	2.50
5.00	33.20	27.98	37.86	33.01	5.00
10.00	30.80	26.00	27.98	28.26	10.00

Table Viability of A549 cells treated with different concentrations of OXY; cells pre–treated with 50μM Cu(OAc)$_2$ for 24 h (OXY–Pre–Cu), OXY in medium supplemented with 50μM Cu(OAc)$_2$ (OXY+Cu) and no Cu(OAc)$_2$ (OXY). Values express mean $\pm$ SD (n=3).

Concentration (μM)	Cell viability (% of control)					
	OXY–Pre–Cu		OXY +Cu		OXY	
	Average	SD	Average	SD	Average	SD
1.56	84.03	2.82	132.87	31.99	96.76	3.38
3.13	80.00	1.73	86.79	9.01	85.55	1.44
6.25	82.04	4.53	90.53	7.94	83.10	3.11
12.50	78.65	1.44	94.05	3.87	88.41	0.11
25.00	104.86	25.09	107.98	10.26	91.58	1.90
50.00	87.55	0.51	104.46	11.06	88.74	3.82
100.00	80.77	2.37	95.05	0.07	69.30	3.61
200.00	89.33	0.18	70.99	6.45	31.37	1.66

Table Viability of CACO–2 cells treated with different concentrations of Doxorubicin. Values express mean ± SD (n=3).

Concentration	Cell viability (% of control)				
(µM)	Rep 1	Rep 2	Rep 3	Average	SD
0.08	96.49	114.00	117.07	109.19	11.10
0.16	93.42	106.32	103.86	101.20	6.85
0.31	96.19	103.56	105.09	101.61	4.76
0.63	96.80	100.79	90.35	95.98	5.27
1.25	67.01	84.51	82.36	77.96	9.55
2.50	34.45	51.96	66.70	51.04	16.14
5.00	30.15	42.13	35.68	35.99	6.00
10.00	20.02	21.55	25.54	22.37	2.85

Table Viability of CACO–2 cells treated with different concentrations of OXY in the medium; cells pre–treated with 50µM Cu(OAc)$_2$ for 24 h (OXY–Pre–Cu), OXY in medium supplemented with 50µM Cu(OAc)$_2$ (OXY+Cu) and no Cu(OAc)$_2$ (OXY). Values express mean ± SD (n=3).

Concentration (µM)	Cell viability (% of control)					
	OXY–Pre–Cu		OXY+Cu		OXY	
	Average	SD	Average	SD	Average	SD
1.56	97.85	7.08	97.91	3.68	95.82	7.50
3.13	92.64	3.75	87.90	7.12	91.15	9.40
6.25	97.09	2.67	100.11	5.01	91.86	9.24
12.50	93.20	3.56	98.24	4.66	108.10	5.82
25.00	90.58	3.28	101.87	3.25	84.50	2.54
50.00	89.26	4.71	100.88	3.72	70.40	6.94
100.00	75.67	5.32	91.97	1.51	57.65	19.63
200.00	64.42	2.55	68.21	5.61	38.09	17.72

Table Viability of HepG2 cells treated with different concentrations of Doxorubicin. Values express mean ± SD (n=3).

Concentration (µM)	Cell viability (% of control)				
	Rep 1	Rep 2	Rep 3	Average	SD
0.08	92.89	75.55	84.58	84.34	8.67
0.16	81.01	74.84	77.21	77.69	3.12
0.31	90.75	77.93	91.47	86.72	7.62
0.63	80.30	71.99	79.35	77.21	4.55
1.25	10.93	12.12	12.35	11.80	0.76
2.50	23.04	20.91	24.00	22.65	1.58
5.00	28.98	24.71	34.92	29.54	5.13
10.00	27.80	26.13	29.46	27.80	1.66

Table Viability of HepG2 cells treated with different concentrations of OXY; cells pre–treated with 50µM Cu(OAc)$_2$ for 24 h (OXY–Pre–Cu), OXY in medium supplemented with 50µM Cu(OAc)$_2$ (OXY+Cu) and no Cu(OAc)$_2$ (OXY). Values express mean ± SD (n=3).

Concentration (µM)	Cell viability (% of control)					
	OXY–Pre–Cu		OXY +Cu		OXY	
	Average	SD	Average	SD	Average	SD
1.56	101.23	3.12	77.17	1.77	95.82	7.50
3.13	100.10	11.11	89.05	5.11	91.15	9.40
6.25	126.87	0.46	111.88	18.17	91.86	9.24
12.50	107.99	4.80	104.40	10.14	108.10	5.82
25.00	96.01	7.90	97.95	6.68	84.50	2.54
50.00	78.40	1.52	94.16	9.37	70.40	6.94
100.00	65.29	2.51	93.14	6.76	57.65	19.63
200.00	35.19	4.80	57.41	2.26	38.09	17.72

Table Viability of MCF10A cells treated with different concentrations of OXY; cells pre–treated with 50µM Cu(OAc)$_2$ for 24 h (OXY–Pre–Cu), OXY in medium supplemented with 50µM Cu(OAc)$_2$ (OXY+Cu) and no Cu(OAc)$_2$ (OXY). Values express mean ± SD (n=3).

Concentration (µM)	Cell viability (% of control)					
	OXY–Pre–Cu		OXY+Cu		OXY	
	Average	SD	Average	SD	Average	SD
1.56	92.69	15.62	87.43	21.19	102.76	1.25
3.13	99.60	13.46	100.20	16.78	92.55	5.61
6.25	85.26	0.21	138.93	13.55	96.20	4.34
12.50	84.72	9.53	155.70	8.63	90.45	9.34
25.00	106.29	12.82	214.85	8.31	92.46	5.04
50.00	85.19	12.68	151.22	4.30	88.54	7.25
100.00	56.78	6.38	153.50	14.93	87.72	3.43
200.00	32.29	3.18	84.17	12.37	58.65	8.12

Table Viability of MCF7 cells treated with different concentrations of OXY; cells pre–treated with 50µM Cu(OAc)$_2$ for 24 h (OXY–Pre–Cu), OXY in medium supplemented with 50µM Cu(OAc)$_2$ (OXY+Cu) and no Cu(OAc)$_2$ (OXY). Values express mean ± SD (n=3).

Concentration (µM)	Cell viability (% of control)					
	OXY–Pre–Cu		OXY+Cu		OXY	
	Average	SD	Average	SD	Average	SD
1.56	92.41	35.33	119.45	28.06	83.79	24.14
3.13	139.80	32.56	127.79	5.34	93.70	7.15
6.25	107.94	46.54	127.08	2.79	85.95	27.86
12.50	77.49	7.45	79.65	14.66	73.88	14.19
25.00	61.52	27.52	75.60	2.50	53.42	6.99
50.00	43.26	7.64	67.74	7.14	37.48	5.02
100.00	18.69	5.02	49.51	12.29	28.86	3.60
200.00	9.74	2.41	21.86	1.97	9.48	1.71

Table Viability of MRC–5 cells treated with different concentrations of OXY; cells pre–treated with 50μM Cu(OAc)$_2$ for 24 h (OXY–Pre–Cu), OXY in medium supplemented with 50μM Cu(OAc)$_2$ (OXY+Cu) and no Cu(OAc)$_2$ (OXY). Values express mean ± SD (n=3).

Concentration (μM)	Cell viability (% of control)					
	OXY–Pre–Cu		OXY+Cu		OXY	
	Average	SD	Average	SD	Average	SD
1.56	81.71	2.56	83.41	11.06	90.09	23.88
3.13	82.43	6.45	90.03	9.30	89.91	14.81
6.25	78.85	2.35	91.33	15.38	111.52	9.70
12.50	78.03	5.48	95.29	8.34	115.26	9.14
25.00	72.47	3.03	97.68	6.39	102.14	7.63
50.00	91.28	7.01	103.14	2.59	91.52	6.07
100.00	72.08	4.81	69.12	6.39	94.11	3.01
200.00	35.67	0.76	70.78	4.30	76.26	2.28

Table Viability of PC–3 cells treated with different concentrations of OXY; cells pre–treated with 50μM Cu(OAc)$_2$ for 24 h (OXY–Pre–Cu), OXY in medium supplemented with 50μM Cu(OAc)$_2$ (OXY+Cu) and no Cu(OAc)$_2$ (OXY). Values express mean ± SD (n=3).

Concentration (μM)	Cell viability (% of control)					
	OXY–Pre–Cu		OXY+Cu		OXY	
	Average	SD	Average	SD	Average	SD
1.56	86.94	3.90	96.49	2.97	80.88	4.39
3.13	102.01	29.10	100.17	7.90	79.60	9.81
6.25	99.80	23.54	94.90	2.57	96.99	11.78
12.50	93.67	12.57	93.31	18.14	87.30	11.13
25.00	109.60	8.35	100.60	7.90	117.12	2.28
50.00	81.79	4.73	115.48	24.55	81.47	20.15
100.00	56.43	3.32	92.33	11.46	52.87	8.75
200.00	36.45	1.60	53.48	1.66	28.24	10.70

Table Viability of RAW264.7 cells treated with different concentrations of OXY; cells pre–treated with 50µM Cu(OAc)$_2$ for 24 h (OXY–Pre–Cu), OXY in medium supplemented with 50µM Cu(OAc)$_2$ (OXY+Cu) and no Cu(OAc)$_2$ (OXY). Values express mean ± SD (n=3).

Concentration (µM)	Cell viability (% of control)					
	OXY–Pre–Cu		OXY +Cu		OXY	
	Average	SD	Average	SD	Average	SD
1.56	138.31	21.95	89.66	7.52	156.32	7.36
3.13	118.23	18.76	96.01	12.09	136.14	24.61
6.25	127.49	6.20	94.09	5.78	141.07	32.20
12.50	161.71	36.42	98.88	5.25	154.99	38.86
25.00	136.50	8.80	96.30	3.02	132.32	18.05
50.00	131.09	16.57	100.99	3.61	134.87	51.76
100.00	65.57	7.43	53.01	46.20	48.49	6.15
200.00	17.20	4.14	32.07	1.13	12.43	2.75

Table Amount of total RNA extracted from MCF7 cells analysed by Nanodrop 2000

Sample ID	Sample name	260:280 ratio	260:230 ratio	Concent ration (ng/uL)	Volume (µL)	Total quantity (µg)
18159_1	MCFCon_1	2.1	2.15	162.7	30	4.88
18159_2	MCFCon_2	2.13	2.03	332	30	9.96
18159_3	MCFCon_3	2.1	2.08	388.7	30	11.66
18159_4	MCFOxy50_1	2.15	2.21	187.4	30	5.62
18159_5	MCFOxy50_2	2.13	2.2	761.1	30	22.83
18159_6	MCFOxy50_3	2.13	1.24	730.9	30	21.93
18159_7	MCFOxy100_1	2.14	2.09	585.3	30	17.56
18159_8	MCFOxy100_2	2.15	2.19	632.4	30	18.97
18159_9	MCFOxy100_3	2.16	2.22	764	30	22.92
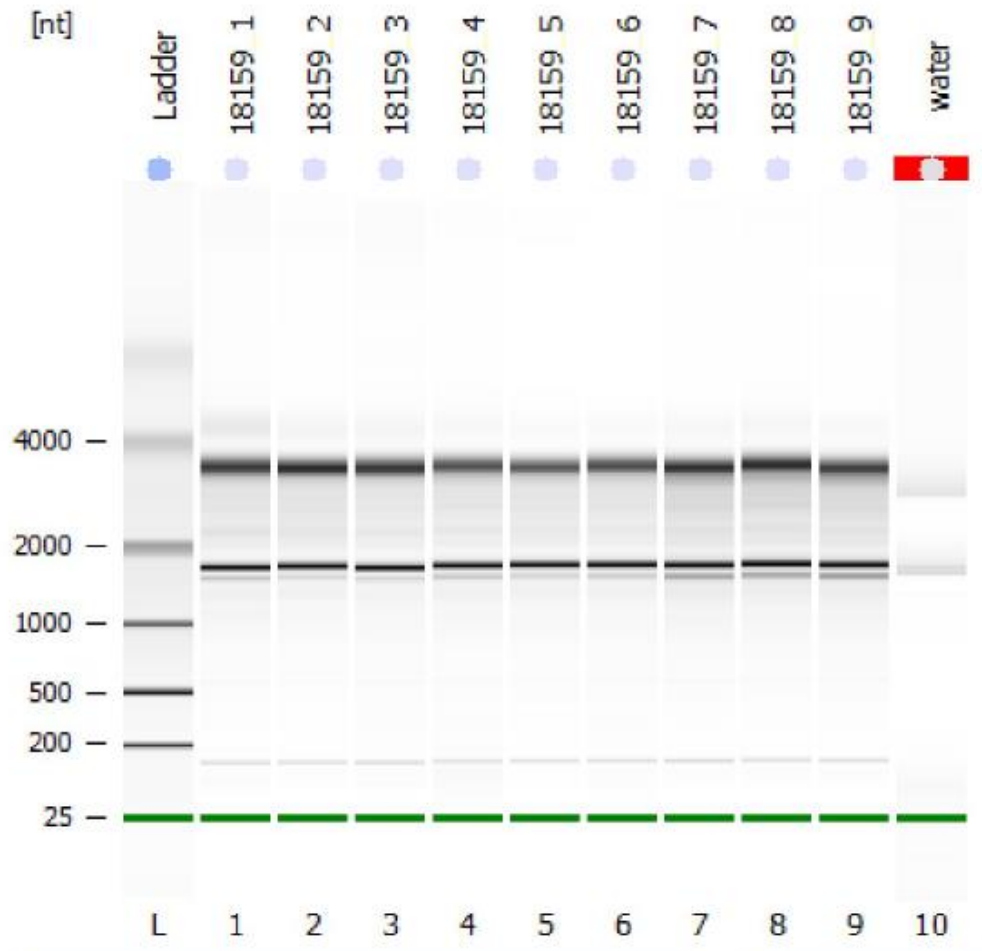
Figure An Agilent Bioanalyzer 2100 gel showing a separation of extracted total RNA obtained from MCF7 cells treated with OXY 50–100 µM. L = ladder (nucleotide length); lanes 1 – 3 = MCF7 cells control; lanes 4 – 6 = MCF7 cells treated with 50 µM OXY; lanes 7 – 9 = MCF7 cells treated with 100 µM OXY; and lane 10 = water.

Figure Microfluidic electrophoretic separation and RNA integrity numbers

(RIN) analysis using Agilent Bioanalyzer 2100. (A) electrograms of total RNA samples

and (B) RIN analysis results of electrophoresis.

Table Amount of cRNA analysed by Nanodrop 2000

Sample ID	Concentration (ng/µL)	Amount for 15 µg	Vol. of water to 24 µL	Vol. of 2nd cycle primer
18159_1	2640.9	5.68	18.32	4
18159_2	2527.1	5.94	18.06	4
18159_3	2301.4	6.52	17.48	4
18159_4	2454.8	6.11	17.89	4
18159_5	2744	5.47	18.53	4
18159_6	2175.9	6.89	17.11	4
18159_7	2655.8	5.65	18.35	4
18159_8	2937.7	5.11	18.89	4
18159_9	2839.3	5.28	18.72	4
Control	1221.9	12.28	11.72	4
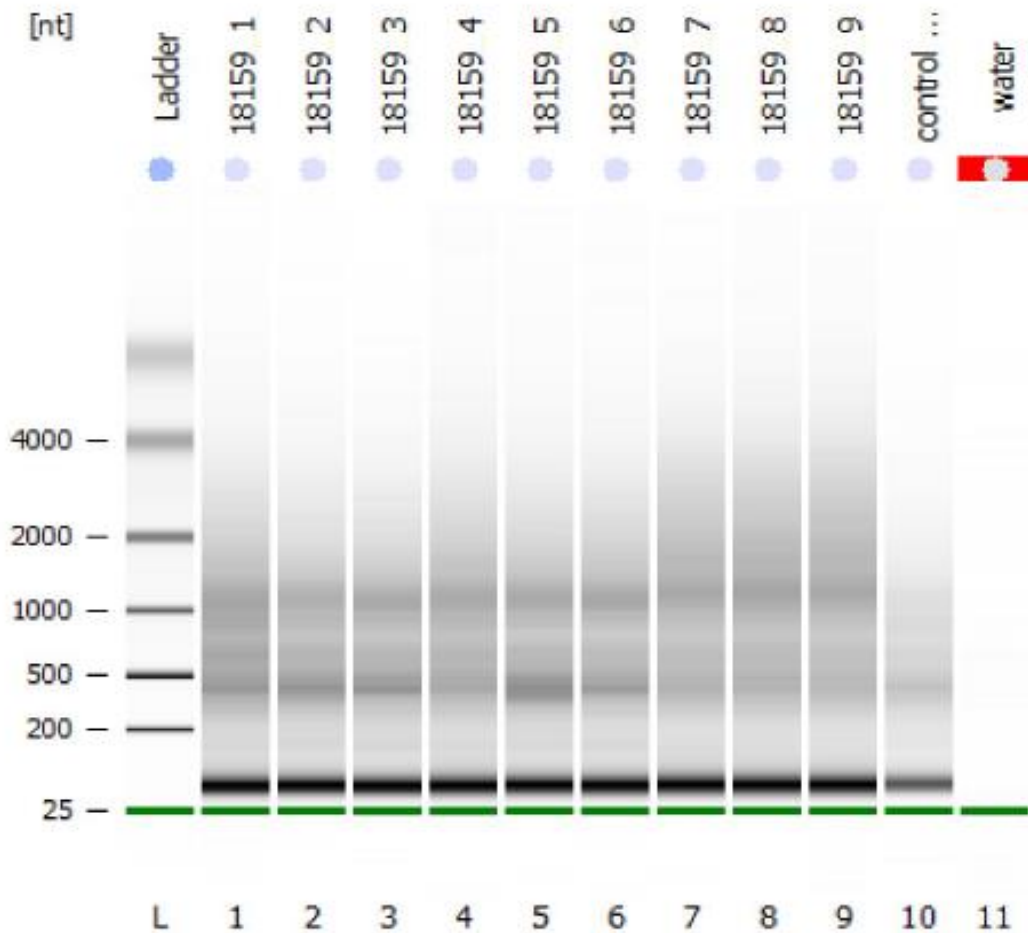
Figure An Agilent Bioanalyzer 2100 gel electrophoresis showing a separation of cRNA synthesized by *in vitro* transcription. L = ladder (nucleotide length); lanes 1 – 3 = cRNA synthesized from MCF7 cells controls; lanes 4 – 6 = cRNA synthesized from MCF7 cells treated with 50 µM OXY; lanes 7 – 9 = cRNA synthesized from MCF7 cells treated with 100 µM OXY; and lane 10 = water

Table Amount of ss–cDNA analysed by Nanodrop 2000

Sample ID	ss–cDNA conc.n (ng/µL)	Amount for 5.5 µg	Vol. of water to 31.2 µL
18159_1	668.5	8.23	22.97
18159_2	665	8.27	22.93
18159_3	643.2	8.55	22.65
18159_4	654.7	8.40	22.80
18159_5	639.4	8.60	22.60
18159_6	636.8	8.64	22.56
18159_7	644.1	8.54	22.66
18159_8	681.3	8.07	23.13
18159_9	650.1	8.46	22.74
Control	507.8	10.83	20.37
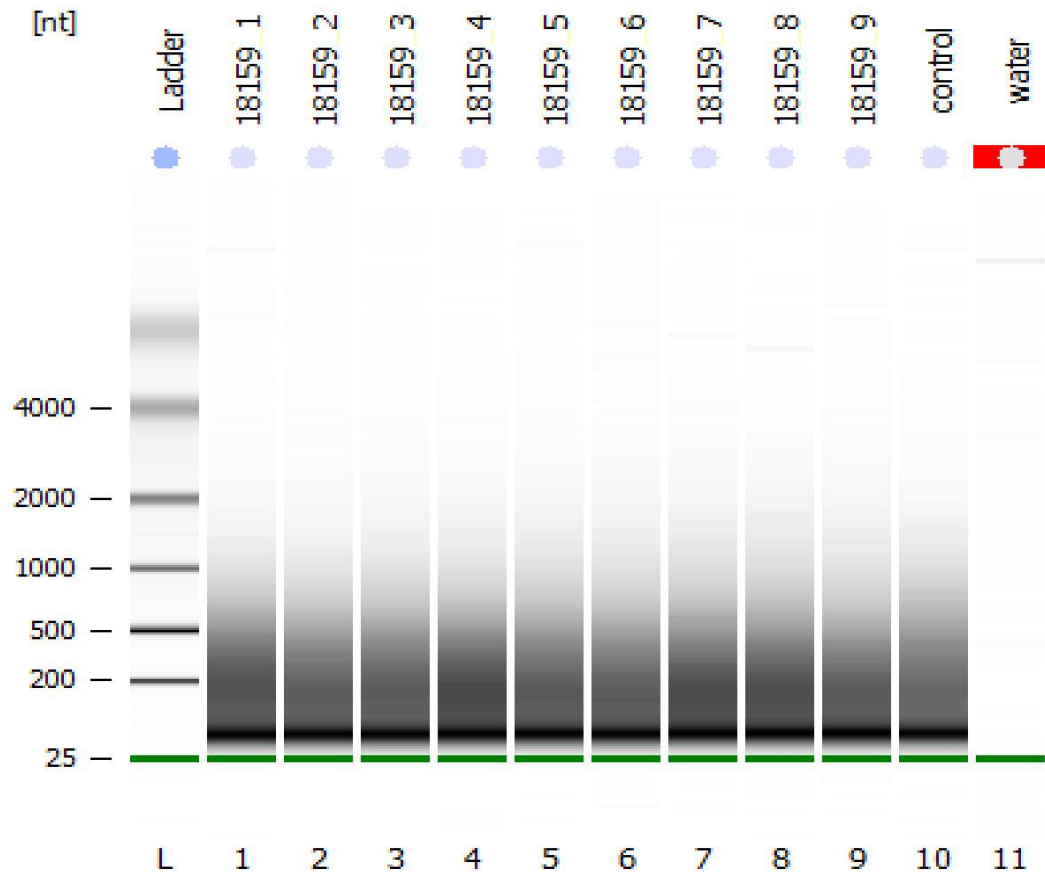
Figure Agilent Bioanalyzer 2100 gel electrophoresis showing a separation of

ss–cDNA synthesized by the reverse transcription of cRNA using 2nd– Cycle Primers. L

= ladder (nucleotide length); lanes 1 – 3 = ss–cDNA synthesized from cRNA of MCF7

cells controls; lanes 4 – 6 = ss–cDNA synthesized from cRNA of MCF7 cells treated with

50 µM OXY; lanes 7 – 9 = ss–cDNA synthesized from cRNA of MCF7 cells treated with

100 µM OXY; and lane 10 = water.

Table Amount of template RNA for RT PCR analysed by Nanodrop 2000

Sample ID	Concentration (ng/µL)	Amount for 2 µg	Vol. of water to 28 µL
MCFCon_1	176.10	11.4	16.6
MCFCon_2	344.40	5.8	22.2
MCFCon_3	412.70	4.8	23.2
MCFOxy50_1	201.27	9.9	18.1
MCFOxy50_2	800.07	2.5	25.5
MCFOxy50_3	753.50	2.7	25.3
MCFOxy100_1	566.83	3.5	24.5
MCFOxy100_2	619.20	3.2	24.8
MCFOxy100_3	813.43	2.5	25.5

Table Amount of cDNA for qPCR analysed by Nanodrop 2000

Sample ID	Concentration (ng/µL)	Amount for 1 ug	Diluted10x (uL)	Vol. of water to 20µL
MCFCon_1	1269.35	0.7878	8	12
MCFCon_2	1147.9	0.8712	9	11
MCFCon_3	1288.45	0.7761	8	12
MCFOxy50_1	1204.3	0.8304	8	12
MCFOxy50_2	1061.8	0.9418	9	11
MCFOxy50_3	1115	0.8969	9	11
MCFOxy100_1	1106.3	0.9039	9	11
MCFOxy100_2	1252.2	0.7986	8	12
MCFOxy100_3	1140.7	0.8767	9	11
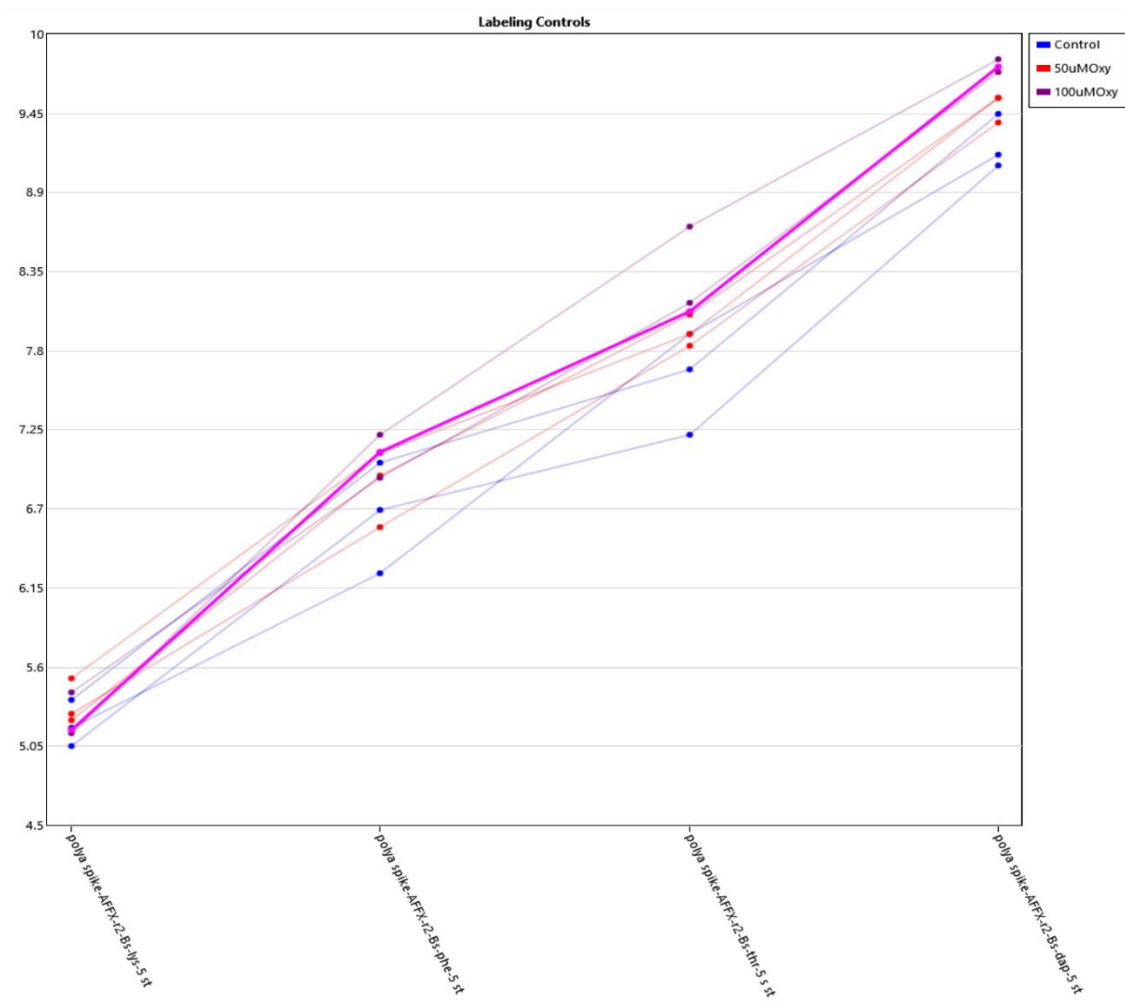
Picture Four exogenous, premixed control spikes including Lys:AFFX-r2-Bs-lys (1:100,000), Phe: AFFX-r2-Bs-phe (1:50,000), Thr: AFFX-r2-Bs-thr(1:25,000) and Dap: AFFX-r2-Bs-dap (1:6,667) were used as the internal controls for labelling process of the microarray platform.
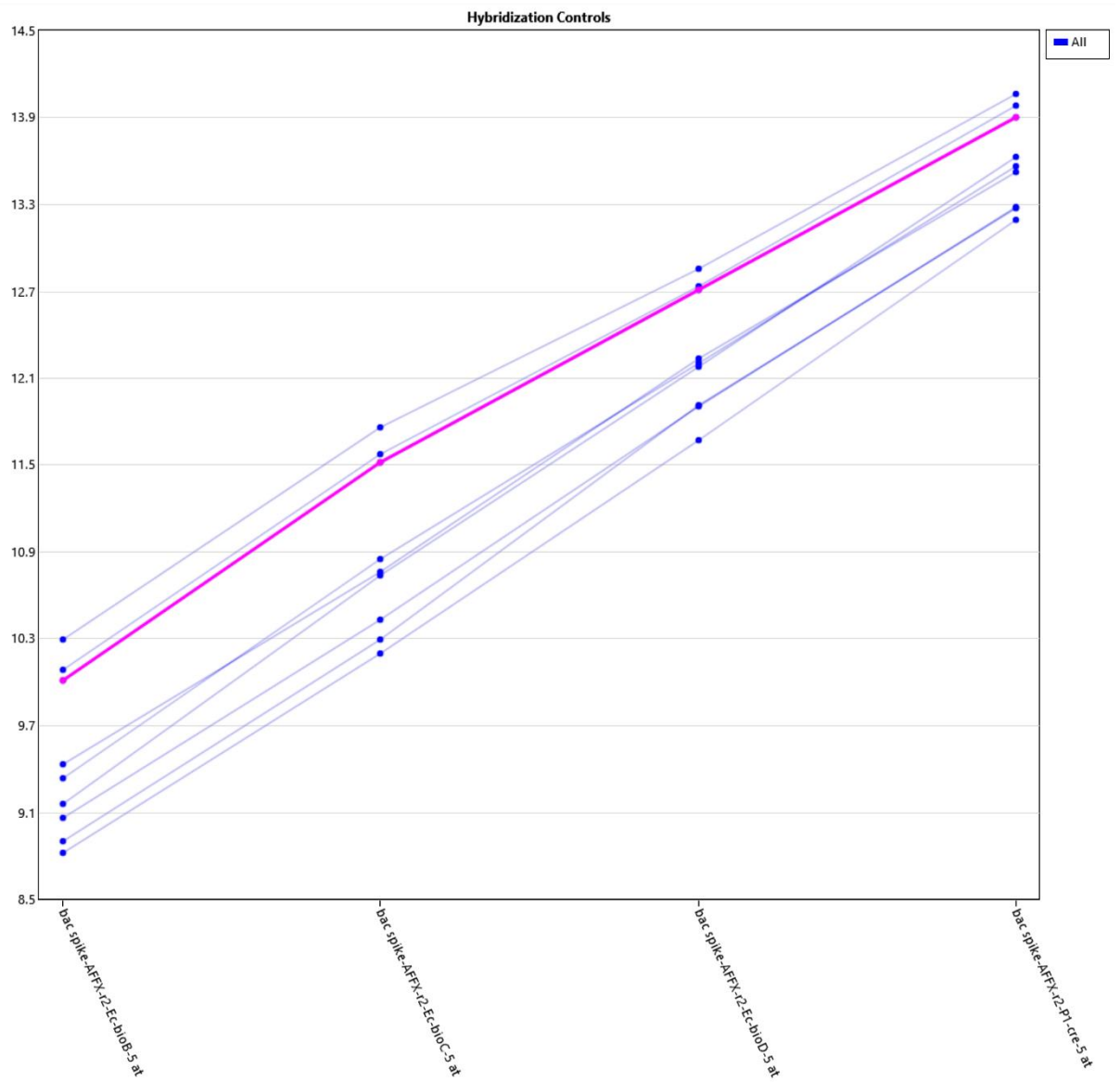
Picture Four hybridisation controls including AFFX-r2-Ec-BioB, AFFX-r2-Ec-BioC, AFFX-r2-Ec-BioD and AFFX-r2-P1-Cre were added in the hybridisation buffer have increasing signal values, reflecting their increasing relative concentrations.
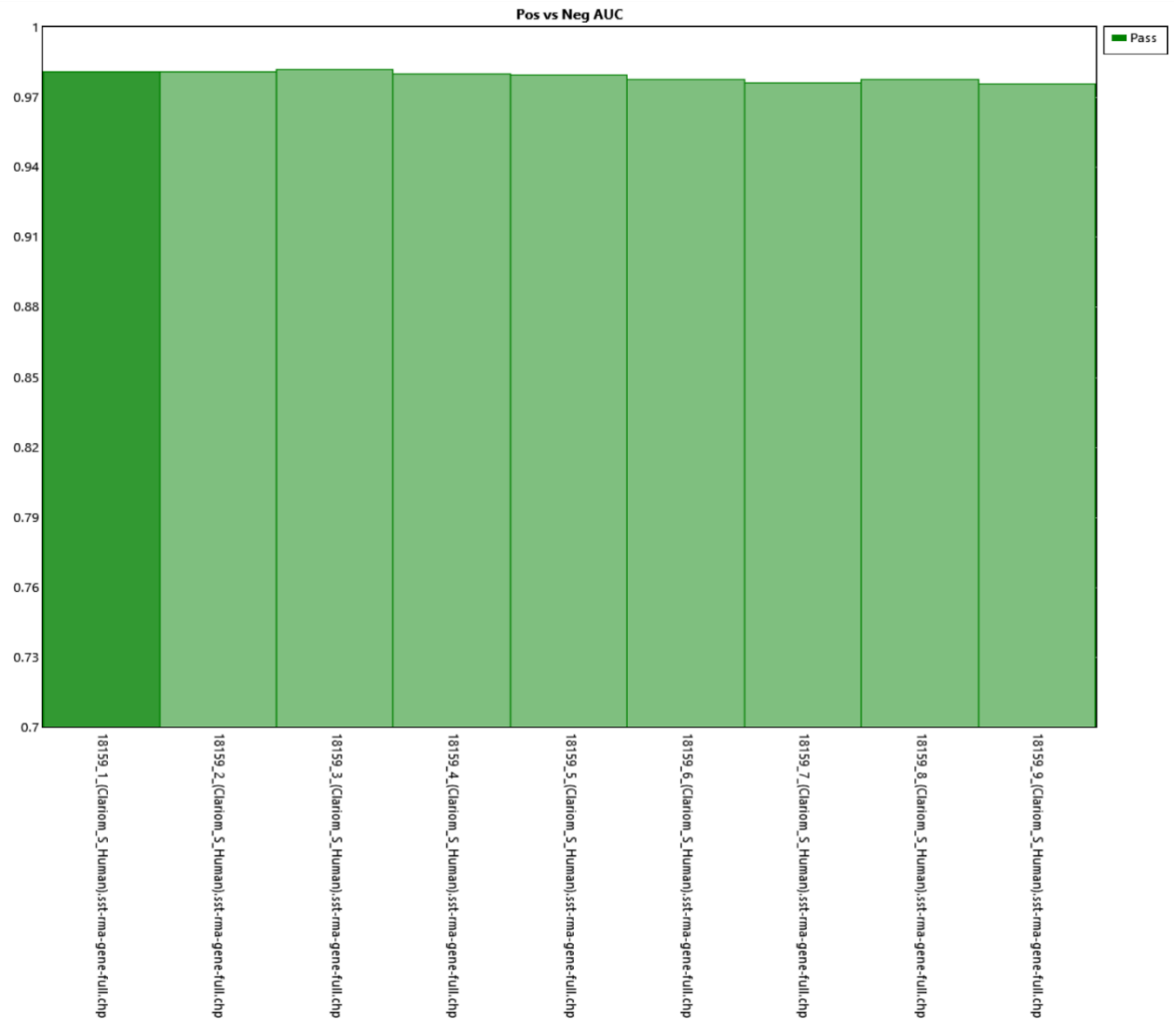
Picture The area under the curve (AUC) was generated by evaluating how well the probe set summary separates the positive controls from the negative controls; An AUC of 1 reflects perfect separation whereas as an AUC value under 0.5 would reflect no separation.

Table QC summary of all samples generated by Transcriptome Analysis Console (TAC) Software; all samples passed the criteria of labelling, hybridising and the positive vs negative probe sets.

| Apply View ▼ | Filters ▼ | Show/Hide Columns | Export ▼ | Add Column | Reanalyze Samples ▼ | Create Line Graph |

| File Name count: 9	Labeling Controls Threshold	Hybridization Controls Threshold	Pos vs Neg AUC Threshold	Condition
18159_1_(Clariom_S_Human).sst-rma-gene-full.chp	Pass	Pass	Pass	Control
18159_2_(Clariom_S_Human).sst-rma-gene-full.chp	Pass	Pass	Pass	Control
18159_3_(Clariom_S_Human).sst-rma-gene-full.chp	Pass	Pass	Pass	Control
18159_4_(Clariom_S_Human).sst-rma-gene-full.chp	Pass	Pass	Pass	50uMOxy
18159_5_(Clariom_S_Human).sst-rma-gene-full.chp	Pass	Pass	Pass	50uMOxy
18159_6_(Clariom_S_Human).sst-rma-gene-full.chp	Pass	Pass	Pass	50uMOxy
18159_7_(Clariom_S_Human).sst-rma-gene-full.chp	Pass	Pass	Pass	100uMOxy
18159_8_(Clariom_S_Human).sst-rma-gene-full.chp	Pass	Pass	Pass	100uMOxy
18159_9_(Clariom_S_Human).sst-rma-gene-full.chp	Pass	Pass	Pass	100uMOxy
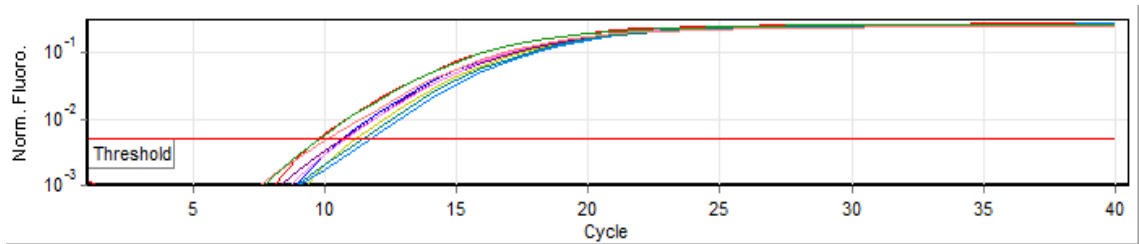
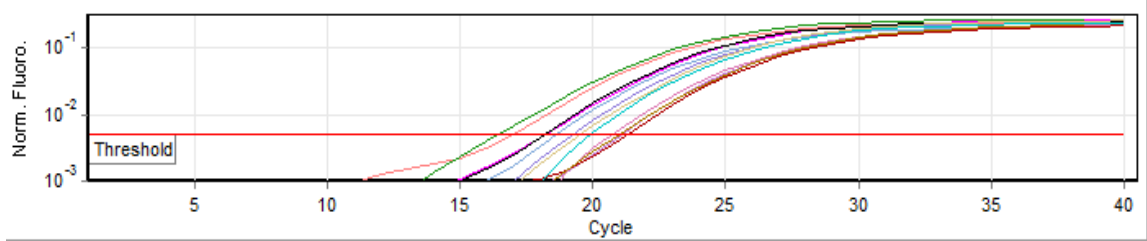Picture Amplification curves of GAPDH gene using quantitative polymerase chain reaction
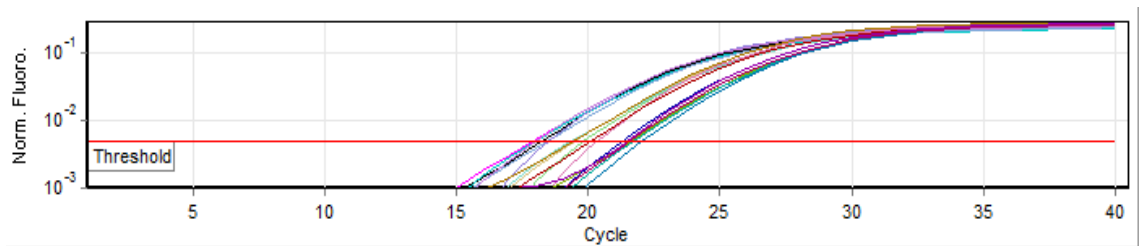
Picture Amplification curves of CDK2 and E2F genes using quantitative polymerase chain reaction
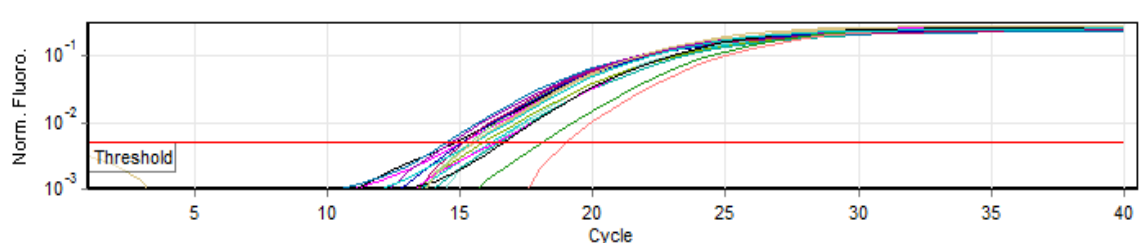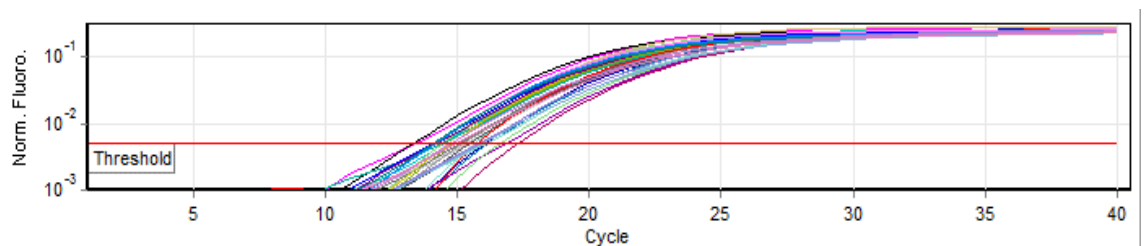

Picture Amplification curves of Bax, CDKN1A and GADD45A genes using quantitative polymerase chain reaction
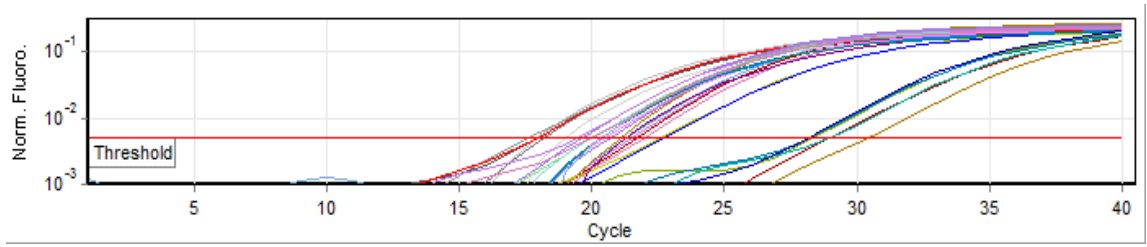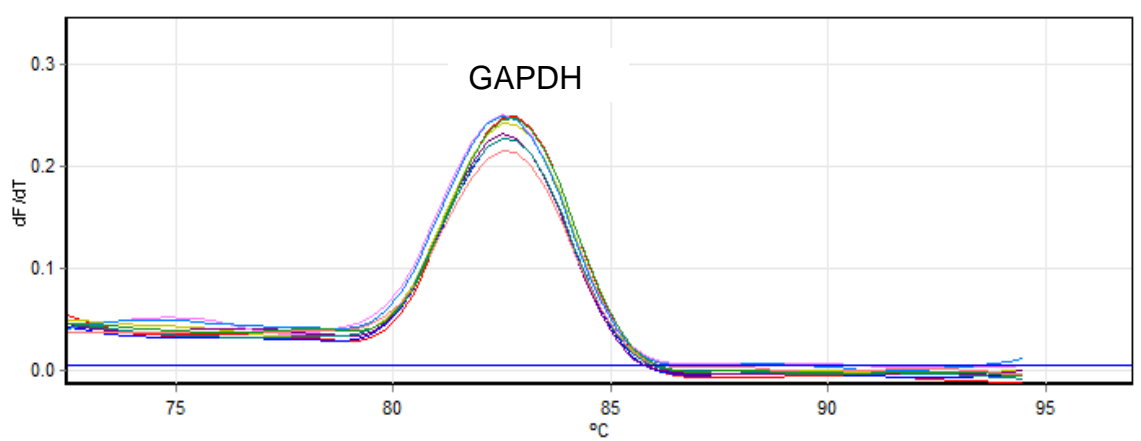
Picture Amplification curves of CASP8, DIABLO, FAS, MAPK8 and TNFSF10 genes using quantitative polymerase chain reaction
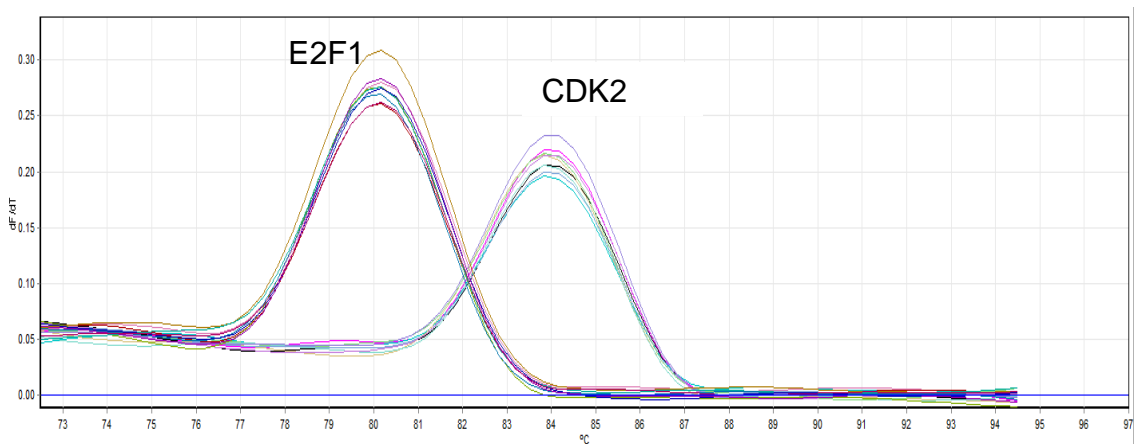

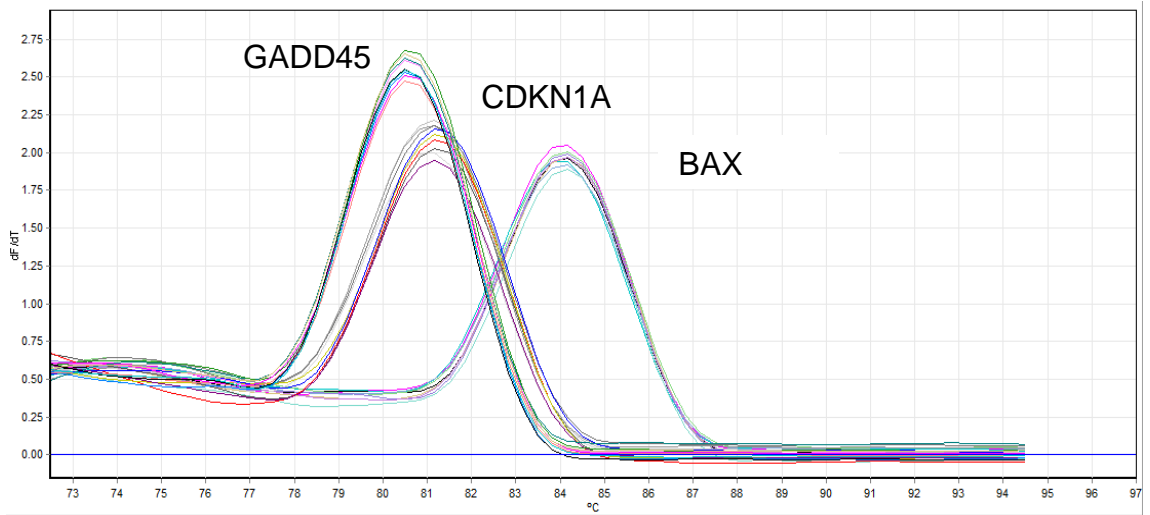Picture Amplification curves of BRCA1 and RAD51 genes using quantitative polymerase chain reaction

Picture Amplification curves of AKT, ESR1, GABARAPL2, MAP1LC3B and SQSTM1 genes using quantitative polymerase chain reaction
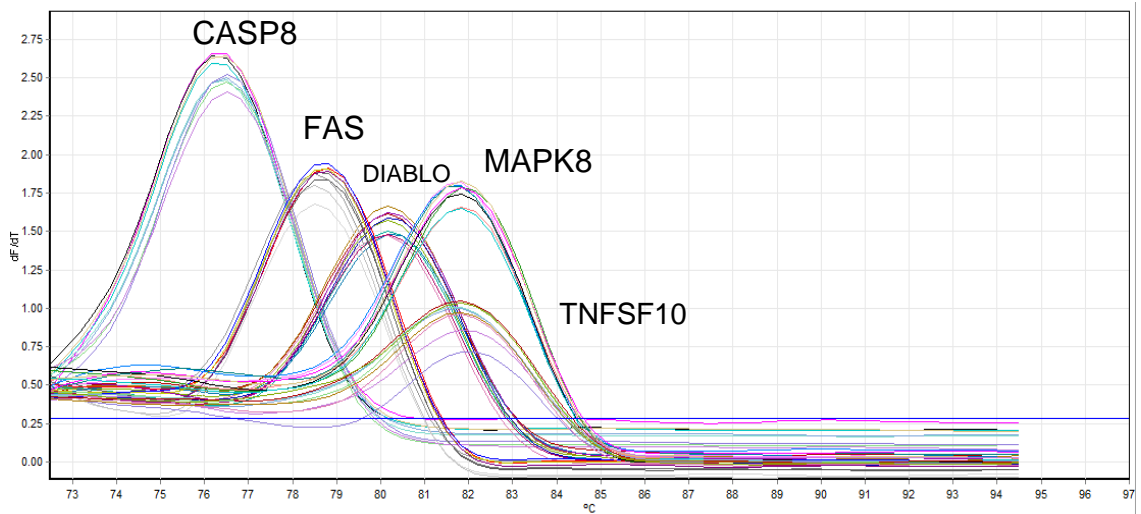
Picture Melting curves of GAPDH gene using quantitative polymerase chain reaction
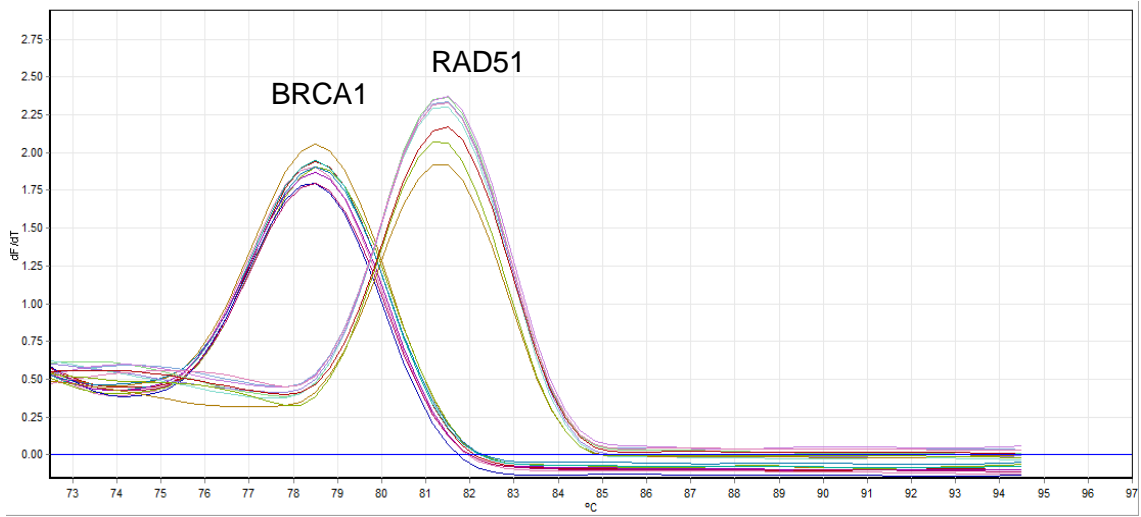

Picture Melting curves of CDK2 and E2F1 genes using quantitative polymerase chain reaction
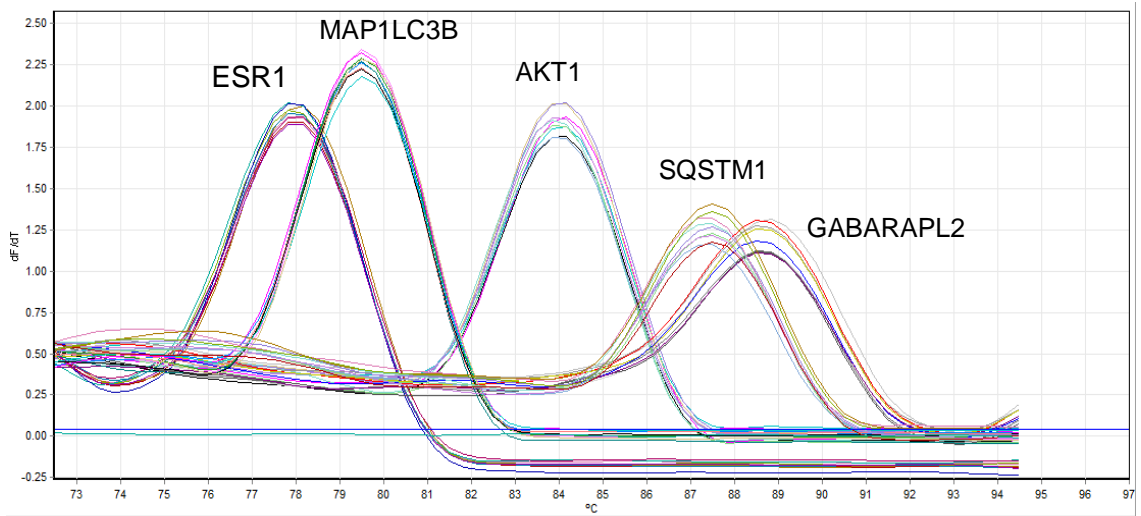
Picture Melting curves of Bax, CDKN1A and GADD45A genes using quantitative polymerase chain reaction

Picture Melting curves of CASP8, DIABLP, FAS, MAPK8 and TNFSF10 genes using quantitative polymerase chain reaction

Picture Melting curves of BRCA1 and RAD51 genes using quantitative polymerase chain reaction

Picture Melting curves of AKT1, ESR1, GABARAPL2, MAP1LC3B and SQSTM1

genes using quantitative polymerase chain reaction

Table concentrations and the absorbance values at 595 nm of bovine serum albumin (BSA) used for western blot analysis

Conc.	Absorbance at 595 nm			Average	SD
(µg/mL)	Replicate 1	Replicate 2	Replicate 3		
25.00	0.444	0.517	0.434	0.465	0.045
12.50	0.278	0.289	0.267	0.278	0.011
6.25	0.206	0.210	0.152	0.190	0.032
3.13	0.113	0.112	0.110	0.112	0.002
1.56	0.046	0.047	0.054	0.049	0.004
0.78	0.006	0.017	0.022	0.015	0.008
0.39	0.005	0.004	0.004	0.005	0.001
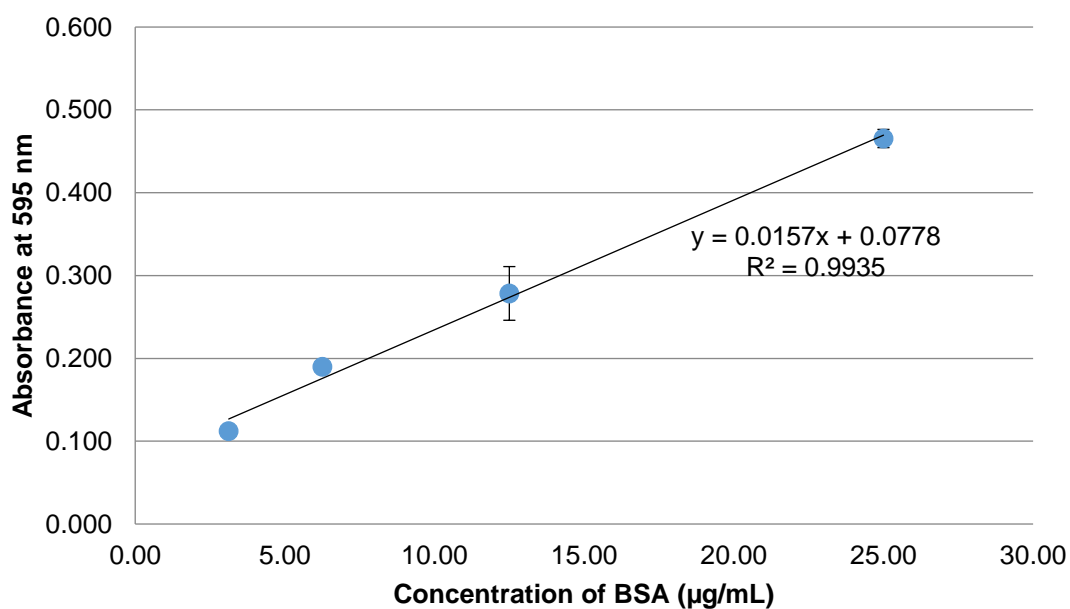
Picture Standard curve of bovine serum albumin (BSA) used for western blot analysis

APPENDIX II

Publication

1. **Radapong, S.;** Sarker, S.D.; Ritchie, K.J. OXY Possesses DNA Damaging Activity. Molecules 2020, 25, 2577.

Oral presentation

1. **Radapong, S**. (2019) OXY: Breast cancer killer. The faculty of science Three minutes Thesis competition, 2019, 6 March 2019, Lower James Parsons lecture theatre.

2. **Radapong, S.,** Sarker, S.D. & Ritchie, K.J. (2019) Anticancer properties of OXY In: Faculty of Science (eds.) Oral presentation in the Research seminar day, Proceedings of faculty of Science research seminar day, 11 June 2019, Liverpool John Moores University, Liverpool, UK, pp. 53.

3. **Radapong, S.,** Sarker, S.D. & Ritchie, K.J. (2020) Mechanisms of OXY toxicity in breast cancer cells In: Phytochemical society of Europe(PSE) (eds.) Oral presentation in T20 PSE Conference Liverpool 2020, Proceedings of T20 PSE Conference Liverpool 2020, 6 March 2020, Liverpool, UK, pp.

Poster presentation

1. **Radapong, S**., Sarker, S.D. & Ritchie, K.J. (2018) OXY and its pro-oxidant activity. Poster presentation in the Faculty of Science Research seminar day, Proceedings of faculty of Science research seminar day, 2018, 18 June 2018, Liverpool John Moores University, Liverpool, UK, pp. 75.

2. **Radapong, S**., Sarker, S.D. & Ritchie, K.J. (2018) Phytochemical analysis and pro-oxidant activity of *Artocarpus lakoocha* heartwood Poster presentation in the Phytochemical society of Europe(PSE)(eds.) PSE-YSM 2018 Liverpool, 2018, 2-5 July 2018, Liverpool, UK, pp. 62.

3. **Radapong, S**., Sarker, S.D. & Ritchie, K.J. (2018) Cytotoxicity of OXY. Poster presentation in the Phytochemical society of Europe (PSE)(eds.) The 3rd International symposium on natural products in cancer prevention and therapy. Trends in methods and modelling, 2018, 4-7 September 2018, Naples, Italy, pp.

4. **Radapong, S**. (2019) OXY: Breast cancer killer. The faculty of science Three minutes Thesis competition, 2019, 6 March 2019, Lower James Parsons lecture theatre.

5. **Radapong, S**., Sarker, S.D. & Ritchie, K.J. (2019) Gene expression profiles of MCF7 cells treated with OXY. Poster presentation in the Phytochemical society of Europe (PSE): Trends in Natural Product Research-PSE Young Scientists' Meeting on Biochemistry, Molecular Aspects and Pharmacology of Bioactive Natural Products, 19-22 June 2019, Budapest, Hungary, pp.